Mechanics of 3D Cell-Hydrogel Interactions: Experiments, Models, and Mechanisms

Franck J. Vernerey [1,2*], Shankar Lalitha Sridhar [1+], Archish Muralidharan [2+], Stephanie J. Bryant [2,3,4*]

[1]*Department of Mechanical Engineering, University of Colorado at Boulder, 1111 Engineering Drive, Boulder, CO USA 80309-0428.*

[2]*Materials Science and Engineering Program, University of Colorado at Boulder, 4001 Discovery Drive, Boulder, CO USA 80309-613.*

[3]*Department of Chemical and Biological Engineering, University of Colorado at Boulder, 3415 Colorado Ave, Boulder, CO USA 80309-0596*

[4]*BioFrontiers Institute, University of Colorado at Boulder, 3415 Colorado Ave, Boulder, CO USA 80309-0596*

Abstract. Hydrogels are highly water-swollen molecular networks that are ideal platforms to create tissue-mimetics owing to their vast and tunable properties. As such, hydrogels are promising cell-delivery vehicles for applications in tissue engineering and have also emerged as an important base for *ex vivo* models to study healthy and pathophysiological events in a carefully controlled three-dimensional environment. Cells are readily encapsulated in hydrogels resulting in a plethora of bio-chemical and mechanical communication mechanisms, which recapitulates the natural cell and extracellular matrix interaction in tissues. These interactions are complex with multiple events that are invariably coupled and spanning multiple length and time scales . To study and identify the underlying mechanisms involved, an integrated experimental and computational approach is ideally needed. This review discusses the state of our knowledge on cell-hydrogel interactions with a focus on mechanics and transport, and in this context, highlights recent advancements in experiments, mathematical and computational modeling. The review begins with a background on the thermodynamics and physics fundamentals that govern hydrogel mechanics and transport. The review focuses on two main classes of hydrogels, described as semi-flexible polymer networks that represent physically crosslinked fibrous hydrogels and flexible polymer networks representing the chemically crosslinked synthetic and natural hydrogels. In this review, we highlight five main cell-hydrogel interactions that involve key cellular functions related to communication, mechano-sensing, migration, growth, and tissue deposition and elaboration. For each of these cellular functions, recent experiments and the most up to date modeling strategies are discussed and then followed by a summary of how to tune hydrogel properties to achieve a desired functional cellular outcome. We conclude with a summary linking these advancements and make the case for the need to integrate experiments and modeling to advance our fundamental understanding of cell-matrix interactions that will ultimately help identify new therapeutic approaches and enable successful tissue engineering.

CONTENTS

9.

1. INTRODUCTION

Many cells that reside in tissues and organs are surrounded by an extracellular matrix or ECM. The ECM provides a physical scaffold for cells, endowing them with structural support and protection. Moreover, the ECM provides essential cues that direct cell differentiation during development and that helps support homeostasis of healthy tissue throughout adulthood. However, damage to tissues and/or organs by traumatic injury or by disease disrupts the ECM, which can have a significant impact on human health . Therapies that are capable of regenerating new tissue to replace the damaged tissue or that are capable of reversing disease and restoring the ECM are needed. A significant hurdle to developing such therapies is understanding how cells sense and respond to their environment under normal and pathophysiological conditions. While animal models have been paramount to uncovering pathways involved in development and disease, the role of the extracellular environment and in particular the matrix is difficult to parse due to the many confounding factors in the *in vivo* environment. To overcome this shortcoming, three-dimensional (3D) matrices, such as hydrogels, have been developed as an alternative to create *ex vivo* tissue-mimetics whose chemistry and properties can be tightly controlled. In conjunction, computational models are becoming increasingly important, which when combined with experiments can further decouple cues that act on cells providing additional mechanistic insights. Computational models can also be used in optimization studies to narrow the experimental design space. Therefore, strategies that combine experiments and computational models to study interactions between cells and hydrogel tissue mimetics are important to advancing tissue engineering and our fundamental understanding of cell and ECM biology in health and disease in *ex vivo* models. Figure 1 summarizes the overview of this review.

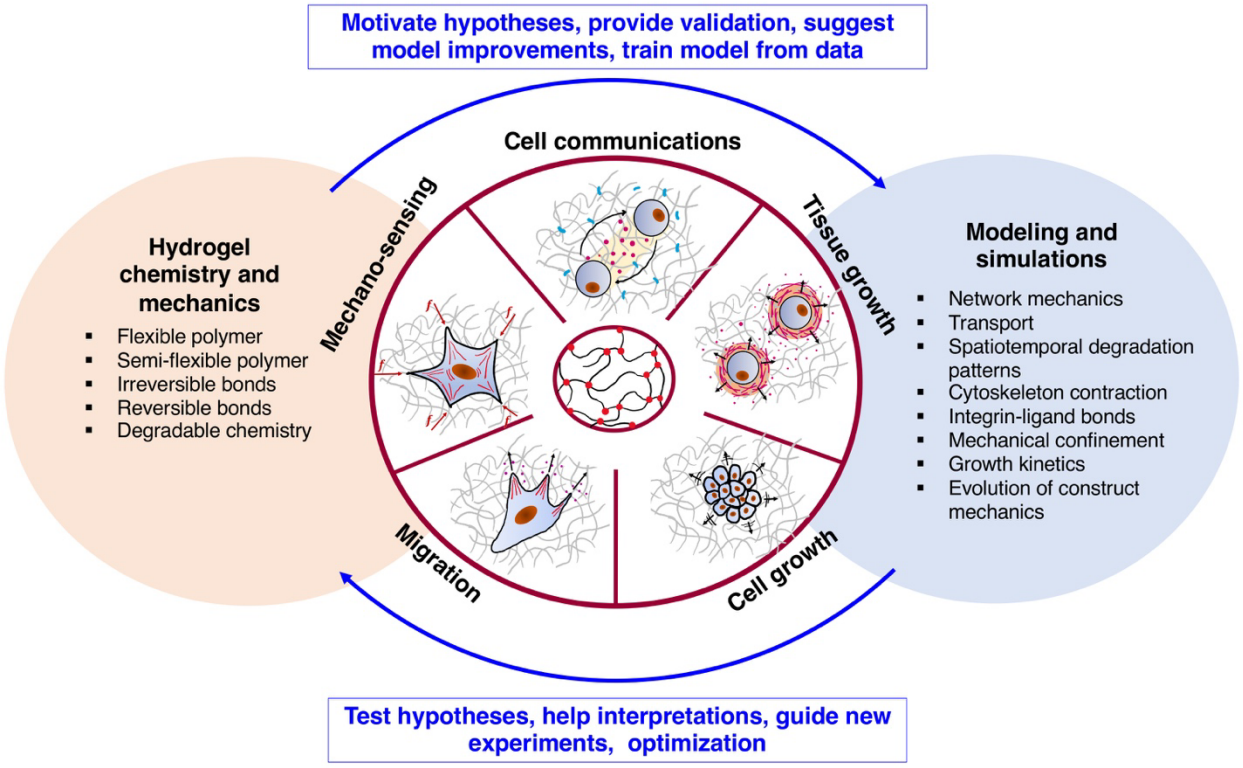

Figure 1. Overview of the main cell-hydrogel interactions that occur when cells are encapsulated in hydrogels: (1) cell communication with other cells and the hydrogel, (2) mechano-sensing of the hydrogel through matrix stiffness and integrin-ligand interactions, (3) mechanisms of cellular migration through hydrogels, (4) cellular expansion, cellular proliferation, and multi-cellular aggregates that can self-organized into organoids, and (5) tissue growth in hydrogels. An integrated experimental and computational approach can lead to novel mechanistic insights that are driven by hypothesis development and testing.

The objective for this review is to provide a comprehensive overview on the current state-of-the-field for physical models and their integration with experiments with a focus on mechanics and transport of cell -hydrogel interactions and their use as tissue-mimetics in cell biology and tissue engineering. Hydrogels are ideal materials to re-create the ECM for applications in tissue engineering and for use as 3D models to study development and disease. The review is limited to hydrogels that serve as ECM-mimetics with encapsulated cells. We begin with an introduction of the theory of hydrogels. This background lays the foundation for how the mechanics and transport mechanisms of cell-ECM interactions are recapitulated in hydrogels. We summarize the physical models that are employed across different length scales to understand the mechanisms of (a) cellular communication with other cells and the hydrogel through transport-mediated mechanisms, (b) mechano-sensing in hydrogels that drives contraction of the

cytoskeleton and re-organization of stress fibers and its impact on cell morphology, (c) cell migration as a function of hydrogel properties, (d) cellular growth, proliferation, and spheroid/organoid formation as a function of hydrogel properties, and (e) the coupled processes of hydrogel degradation and ECM assembly and neo-tissue growth. For each section, we provide the biological relevance, a summary of recent experimental advancements, highlighting knowledge gaps, the physical models that are used to address these gaps, and the future outlook for tuning hydrogels to control the desired cellular function. We end this review with a summary and broader future outlook for using physical models in combination with experiments in cell biology and tissue engineering.

2. MECHANICS OF MOLECULAR NETWORKS: FROM ECM TO HYDROGEL

Synthetic and biological polymers that can reproduce the physical principles of native ECM from a fundamental level, and therefore have a potential to not only reproduce the functions of the ECM, but also to provide a smooth transition and means of communication between the living cell and the synthetic or semi-synthetic polymers. To mimic these environments, hydrogel structures similarly possess a network structure that may or may not be close to their biological counterpart. Biopolymer-derived hydrogels can be classified as semi-flexible polymers that assemble into fibers to produce fibrous hydrogels with a strain-stiffening response, similar to that of the natural ECM. Purely synthetic, semi-synthetic, or non-fibrous forming biopolymers on the other hand, are flexible polymers that are structurally further from the biological ECM. The semi-flexible polymers however can be modified with covalent crosslinking moieties that reduces their ability to form fibers and creates a structure that more closely resembles a flexible polymer network. An advantage of synthetic and semi-synthetic polymers is that they are more controllable and easily functionalized. Figure 2 summarizes these two major classifications of polymer networks which will be discussed in this review , flexible and semi-flexible, along with specialized sub-categories of these networks that produce degradable hydrogels, networks with reversible bonds, and viscoelastic networks afforded by sliding bonds. This section discusses the physical mechanisms and the emerging macroscopic response of these different molecular networks, with an emphasis on the polymer physics of hydrogels. We also summarize current modeling approaches to link these physics to macroscopic behavior, concentrating on mechanics and transport, both of which are essential mediators to the cell-hydrogel interactions.

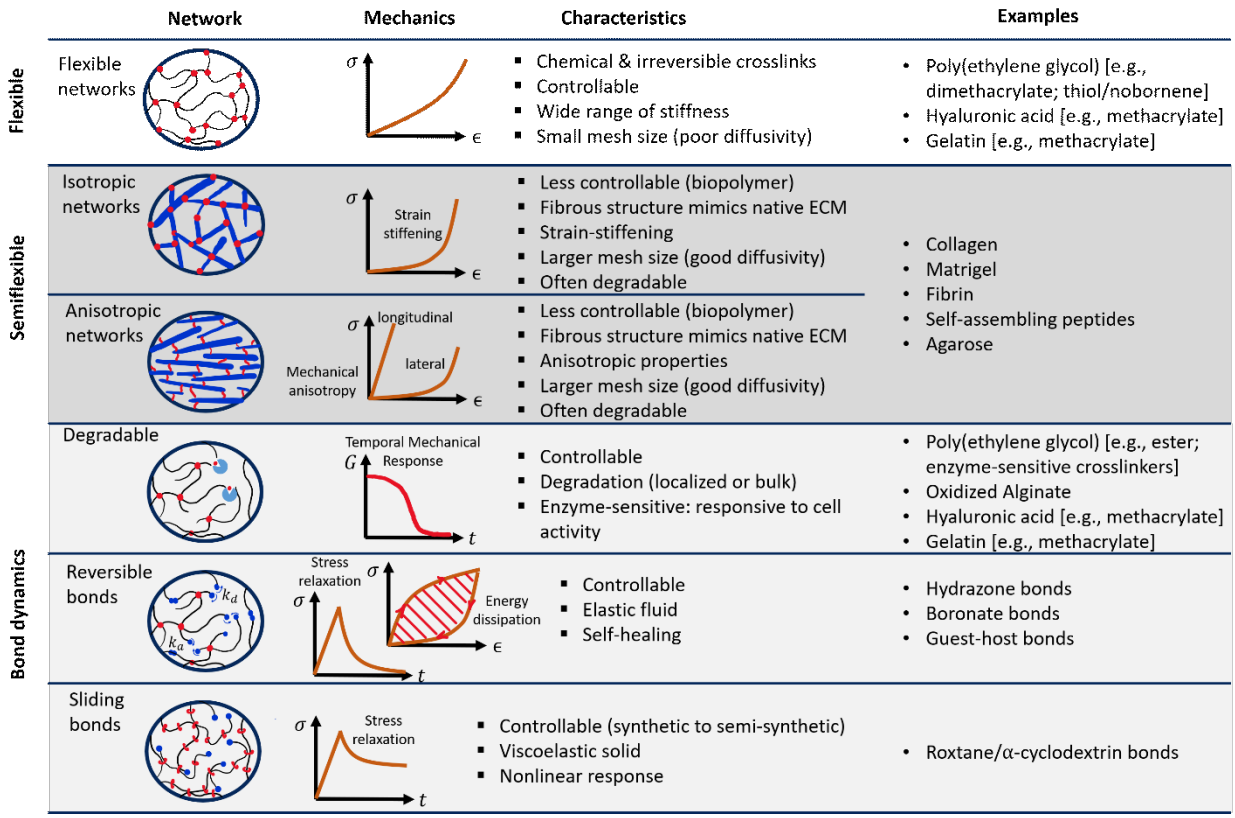

Figure 2. Types of molecular networks that are being investigated to study cell-hydrogel interactions in tissue mimetics and examples thereof.

2.1. Flexible and Semi-flexible Networks

The elasticity of a polymer network starts from the force-extension response of its underlying polymer chains or fibers, depending on the type of network. These molecules can roughly be distinguished into three categories: flexible, semi-flexible, and athermal. [1] What drives these distinctions is the persistence length $= \zeta /$ of the chain (where ζ is its bending energy and kT its thermal energy) which defines the distance over which correlations in the orientation of small chain segment are lost. The response of a chain then depends on the ratio of this persistence length and the contour length L, such that when $/ \mathcal{L} \gg 1$ the molecules are athermal and insensitive to thermal noise while when $/ \mathcal{L} \ll 1$ the molecules become very sensitive to thermal fluctuations. In this case, molecular collisions tend to bring them to a coiled configuration as shown in Figure 3a. The competition between this recoiling force and the molecule's bending resistance sets both its equilibrium end-to-end distance and mechanical response. [2]

2.1.1. Flexible Polymers. Most synthetic hydrogels are comprised of polymer chains that belong to the family of flexible chains, i.e., $l/L \ll 1$. In this case, the polymer chains are flexible and dominated by thermal fluctuations, which favor a completely recoiled conformation in a force-free state. An unfolding of the chain would however decrease the polymer's entropy and give rise to a thermodynamical tensional force as shown in Figure 3a. The resulting force-extension response exhibits a nearly linear regime for moderate extensions and a sharp stiffening when the chain is stretched near its contour length. This trend is well predicted by the Langevin chain model, [3] while the moderate stretch regimes can be approximated by the Gaussian chain model. For a chain with N Kuhn segments of length b, the force-displacement relation of such a Gaussian chain is given by:

$$f = \frac{3kT}{Nb^2} r \tag{1}$$

where k is Boltzmann constant and T is the absolute temperature. This model therefore predicts that longer chains are softer, while they stiffen with temperature. A hydrogel is made of a polymer network that consists of a complex organization of chains controlled by topology (number of chains per crosslinks) and the diversity in its chain length. An average measure of the chain stretch (direction and magnitude) in a network is described by the conformation tensor of the form:

(2)

where r^0 is the average end-to-end distance of the chains in a stress-free network while the terms r_i represents the ith components of the end-to-end vector of a chain in a cartesian coordinate system. [4] Finally, the operation $\langle\rangle$ is an average over all chains in the network. A representation of the conformation tensor is given in Figure 3b,c for an undeformed and deformed network. In this illustration, the principal directions of the tensor are shown by the axes of the ellipse (or ellipsoid in 3D), while the magnitude of the stretch in these directions are represented by the lengths of the semiminor and semimajor axes.

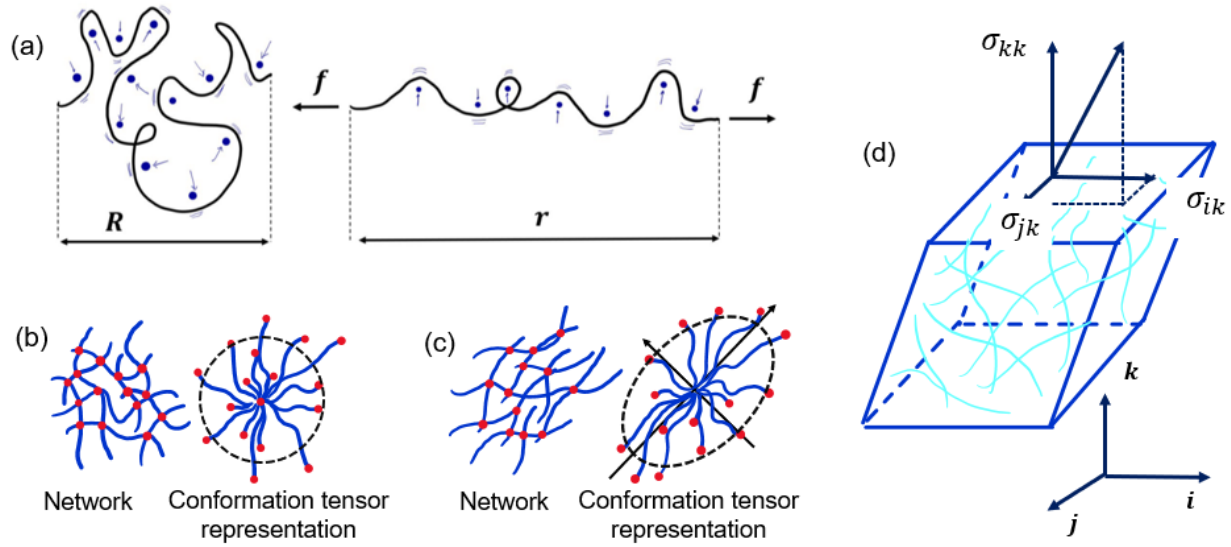

Figure 3. (a) Entropic origin of the elastic response of the flexible chain. While the force-stretch response of the chain stiffens dramatically near its contour length, its behavior can be approximated as a linear spring with zero rest length, when the end-to-end distance, denoted as R or r in the schematic, is significantly smaller than the contour length $L = N \times b$. Here N and b represent the number and length of Kuhn segments in the chain, respectively (not shown). [3] (b) Graphical illustration of the conformation tensor. When a flexible network is not subjected to external forces, it takes an isotropic conformation, represented by the conformation tensor $\boldsymbol{\mu} = I$. (c) When subjected to a macroscopic deformation, the chains in the network become stretched and aligned in a specific direction, and the tensor $\boldsymbol{\mu}$ deviates from the identity tensor I. (d) The stress is represented by a tensor whose components indicate the internal forces per unit area on the faces of a material volume.

The applied deformation of a network of polymer chains can be measured by the deformation gradient F, that is represented by a matrix that maps an infinitesimal segment from its undeformed configuration R to its deformed configuration r through $r = F \cdot R$ as shown in Figure 3a. The strain of the network can then be decomposed into a volumetric component $J = \det(F)$ (often denoted as the swelling ratio) and a deviatoric component that represents the amount of shear deformation. The former can be measured as the ratio of the swollen (V) to dry polymer (V_d) volume $J = V / V_d$. The latter, on the other hand, measures the hydrogel's distortion without volume change and may be calculated as:

$$\bar{} = J^{2/3} F \cdot F^T \tag{3}$$

Where the tensor multiplication $F \cdot F^T$ is known as the left Cauchy-Green deformation tensor. The response of the network to a macroscopic deformation is given by the stress tensor whose component σ_{ij} represents the elastic force in the i-th direction, applied onto a unit cross-section whose normal vector points in the j-th direction (Figure 3d). Using statistical mechanics, [5] it can be shown that a network of flexible chains whose response is linear (as shown in eq 1) behaves as a compressible neo-Hookean solid. While there are many versions of such a model, a commonly used version predicts a stress tensor of the form:

$$= (1 - 2/_f) \quad _{kT}[\bar{} - I^1 I] + \quad (J - 1) + p \qquad (4)$$

where $\bar{I}^1 = trace(\bar{\ })$ is the first invariant of the deformation tensor and ρ is the cross-link density. One can see that the stress originates from three sources: (a) the resistance of the gel to shear deformation with modulus $G = (1 - 2/f)\rho kT$, which is provided by the Phantom network theory, (b) the hydrogel's bulk modulus κ that resists volume changes, and finally (c) the osmotic pressure p of the interstitial fluid that represents the attractive interactions between the polymer and its interstitial solvent. When the network connectivity is high, i.e., the number f of polymer chains attached to a single crosslink is large ($f \to \infty$), the modulus reduces to $G = CkT$. However, for hydrogels discussed in this review, network connectivity is typically small and finite, for example, $f = 4$ for 4-arm poly(ethylene glycol) (PEG) macromolecular monomer. For these hydrogels, the network exhibits non-affine deformation [6] and results in a softer macroscopic response.

2.1.2. Polymer-solvent Interactions. Some tissue, like cartilage, must work in compression and thus cannot rely on the strength of the network itself. In this case, the molecular structure is complemented by a loose network of charged and hydrophilic molecules, such as sulfated glycosaminoglycans, that comprise proteoglycan molecules like aggrecan. Aggrecan in particular is brush-like molecule that can efficiently attract and retain water within the network, providing an internal pressure that resists compressive loads. It also triggers tensile forces on the surrounding network (of collagen for instance) that acts to stiffen the overall tissue, a phenomenon that is akin to the stiffening of a soccer ball with inflation. In most hydrogels, the osmotic pressure arises from two main contributions: the

mixing entropy of the solvent and the polymer, that promotes gel swelling and their physical interactions. An inverse relationship is observed with swelling ratio J and osmotic pressure or elastic stress (Figure 4a). The physical interactions can be either attractive or repulsive, depending on the nature of the environment. According to the Flory-Rehner theory,[7] the osmotic pressure depends on the volume fraction of the solvent, or alternatively on the swelling ratio J by:

$$p = -\frac{kT}{v}\left[\ln\left(1-\frac{1}{J}\right)+\frac{1}{J}+\frac{\chi}{J^2}\right] \quad (5)$$

where the first two terms on the right end side are from purely entropic origin, while the last term depends on the so-called polymer-solvent interaction parameter χ. When this parameter is positive, solvent and polymers are repulsive, while they become attractive as it becomes more and more negative. Hydrogel swelling is then controlled by the balance between the osmotic pressure and the elastic stress that resists the volumetric expansion of the polymer network, as shown in Figure 4a. The magnitude of the polymer-solvent parameter therefore has a large influence on swelling, where a negative value promotes swelling. By contrast, the network's bulk modulus κ provides an elastic resistance to volume expansion and thus exhibits an inverse relationship with the swelling ratio J (Figure 4b).

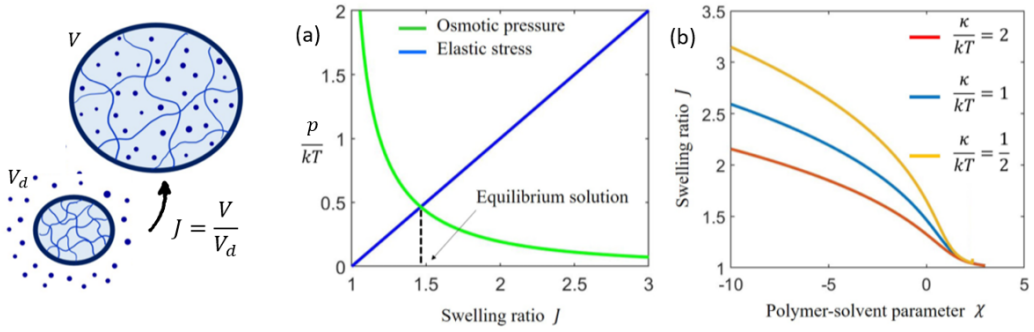

Figure 4. (a) The swelling equilibrium of a hydrogel depends on the balance between the osmotic pressure and the (bulk) elastic stress of the network. (b) Role of the bulk modulus and polymer-solvent interaction parameter χ.

2.1.3. Semi-flexible Polymers. Most hydrogels derived from biopolymers, including collagen, fibrin, and agarose belong to the family of semi-flexible polymers (Figure 5). For example, collagen [8,9] and agarose[10,11] hydrogels represent two distinctly different biopolymers. Collagen hydro gels are made of long crosslinked fibers of 1-10 microns in diameter while agarose consists of thick bundles of helical chain structure. As a polysaccharide, the chains of agarose are strongly attractive because of hydrogen bonding. At low temperature, hydrogen bonds induce the chains to intertwine with one-another in a double helix,

which further aggregate into bundles of diameter around 20 nm with significant bending stiffness. These bundles tend to not recoil onto themselves, which make them support compressive forces, but are prone to buckling instabilities.[12] Semi-flexible networks are especially known to exhibit a pronounced strain-stiffening, i.e., a sharp increase in their elastic modulus with strain. This peculiar response originates from an interplay between the bending stiffness of the chains and the network topology. A network of semi-flexible chains possesses a critical connectivity, known as the central-force isostatic point, [13] where the network transitions from stiff (for high connectivity) to floppy (for low connectivity). In the former, the main deformation mode is stretch, while in the latter, it is bending. For floppy networks however, the soft bending-dominated mode only occurs at small deformation, while larger strains involve a reorientation of the filaments and a switch to a stiff, stretch-dominated mode. Strain stiffening is then explained by the acute realignment of fibers at the transition. Both collagen [14] and agarose[15] exhibit this response. A thorough review of modeling work in this area is provided by Brodersz and MacKintosh [16] and Meng and Terentjev.[17]

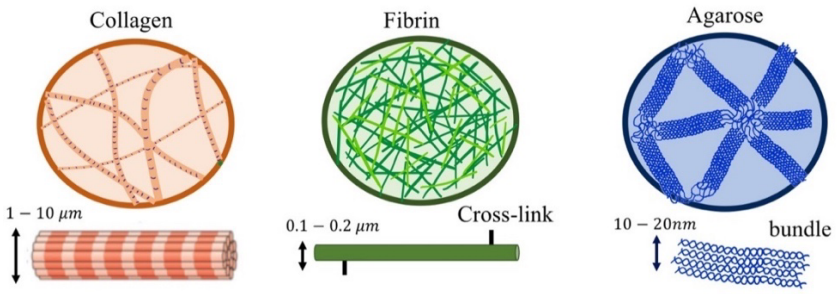

Figure 5. Three examples of semi-flexible hydrogels, derived from biopolymers used in cell encapsulation: collagen, fibrin, and agarose.

2.2. Hydrogels with Dynamic Crosslinks

The native ECM of essentially all tissues exhibit a time-dependent response under an applied stress. This response varies from tissue to tissue, spanning less than a second for brain tissue to 1000 seconds for skin to reach half-maximum stress.[18] While all polymers exhibit viscoelasticity, most chemically crosslinked hydrogels behave predominantly as elastic materials, especially when compared to the time-scale of the viscoelastic response of native ECM. To better mimic the native ECM, hydrogels engineered with dynamic bonds are gaining increasing interest. Here we describe dynamic crosslinks in the context of reversible bonds and irreversible degradable bonds.

2.2.1. Reversible Crosslinks. Several types of dynamic networks with varying levels of complexities have been developed and used to explore cellular behavior in 3D. Several examples are

highlighted, which are based on non-covalent bonds that re-arrange and include alginate via its ionic crosslinks and guest-host interactions and based on covalent bonds, such as those described as covalent adaptable networks (CANs) and networks with sliding bonds in their crosslinks. Of these networks, alginate hydrogels have been the most widely studied in cell encapsulation and tissue engineering. [19] Alginate hydrogels are traditionally formed from high molecular weight alginate that is crosslinked with divalent cations (e.g., Ca^{2+}) and often described by the egg-box model (Figure 6a). [20] Rich mechanical characteristics like nonlinear viscoelasticity (time-dependent response) in these networks have been widely reported in the literature. Particularly, the relaxation behavior is stress dependent, where the gel behaves exclusively elastic under small loads, i.e., the material holds stress under deformation, but displays a substantial increase in relaxation dynamics as the load increases. [21] While their relaxation times are considerably longer than that of native ECM, [22] they can be controlled by adjusting divalent ion concentration and the strength of the ionic bonds. To create alginate networks that relax at rates more similar to the ECM, Chaudhuri *et al.*[23] explored modification of the alginate hydrogel by decreasing its molecular weight (i.e., from 280 to 35 kDa) and introducing a covalent PEG crosslinker that created steric hindrance of the Ca^{2+} crosslinking. These changes to the network structure led to stress relaxing hydrogels that could achieve much faster relaxation times from ~60 to ~1000 seconds. Another class of dynamic hydrogels are those formed with crosslinks of supramolecular chemistry, which have been referred to as guest-host interactions.[24] The interactions are based on a transient non-covalent bond and association between a guest and a host molecule. Examples include cucurbit[6]uril and polyamine that have been functionalized to hyaluronic acid polymers to enable crosslinking and cell encapsulation. [25] More recently, a new class of covalently crosslinked networks have emerged that are broadly described as CANs. [26] These networks have crosslinks that under a force covalent bonds are broken returning to their original pre-crosslinking chemistry; this process enables the covalent bond to reform. This network can therefore dynamically re-arrange its topology permanently in response to an applied strain (Figure 6b). Examples of CANs that have been used for cell encapsulations include hydraozone [27–29] diels-alder,[30] and the phototunable thioester exchange.[31] Another approach has been used to fabricate hydrogels with sliding covalent bonds that are made of rotaxane and ➳cyclodextrin molecules, which produce mobile rings as crosslink junctions[32] (Figure 6c). Thus, as opposed to detaching and reattaching over time, the crosslinks are able to slide along the chains until the hit the end-stopper, a point at which the material becomes elastic again.[33] This pulley-effect [34] gives slide-ring gels unique tensile properties, [35] that combine nonlinear elasticity and dissipative properties like stress relaxation that can be tuned via the gel design. Slide-ring hydrogels have shown promising results in cell encapsulation studies where the permeability was shown

to substantially increase nonlinearly with pressure. [36,37]

The aspect common to the hydrogels discuss above is the fact that they dissipate energy when deformed by molecular re-arrangement of the polymer network. The emerging time-dependent response of such hydrogels are typically measured through stress relaxation and creep experiments, which can be quantified and compared with biological timescales to understand how the relaxation properties of the hydrogel affect a cellular response. In stress relaxation experiments, a network is deformed at different rates to a particular maximum level of strain after which it is kept constant. The measured stress in the material, then relaxes (or decays) over time at rates that correspond to the molecular structure of the network. Many studies report a value for $\tau_{1/2}$, which is defined as the time required to reach half the value of the maximum stress. Creep experiments provide an alternate method to estimate the dissipative timescales of these hydrogels where a sample is loaded quickly to a state of constant stress and the deformation is measured over time. The rate of change of strain over time can be used to infer multiple relaxation timescales that are at play in the hydrogel. Under the conditions of small deformation, linear viscoelastic models such as the Maxwell model, the Kelvin-Voigt model, and the standard models, which use a combination of connected mechanical elements like springs and viscous dampers. However, the parameters of these mechanical components like the spring stiffness or the damper viscosity are empirical and not the result of any physical mechanism taking place in the polymer network. Nonetheless, these models can provide a good framework to describe the dynamical response of hydrogels.

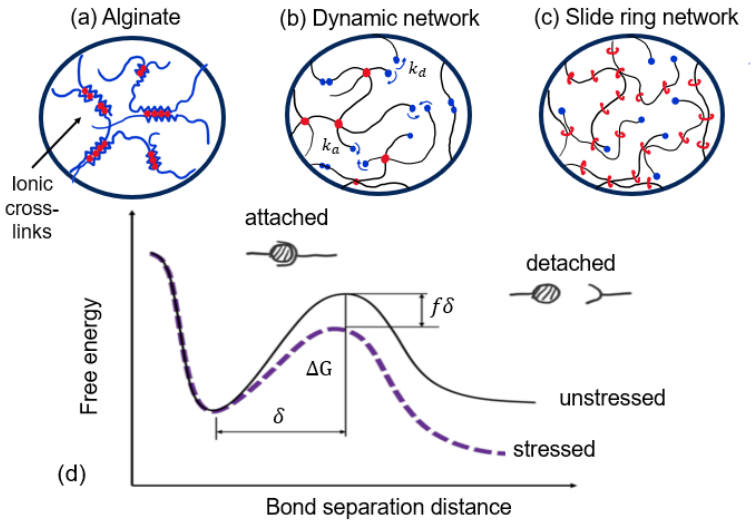

Figure 6. (a) Illustration of the dynamic structure of alginate, a hydrogel derived from biopolymers, (b) polymer network with dynamic bonds, (c) side-ring gel and (d) Energy landscape of a reversible bond. The strength of the bond is represented by the height of the energy barrier ΔG, a quantity that controls its rate

of dissociation. When a force f is applied to the bond, the energy barrier decreases by an amount $f\delta$ where δ is interpreted as the bond sensitivity. This mechanism eventually implies that the rate of bond dissociated is accelerated by tension.

Statistical mechanics of polymer networks is a growing field of study that offers a fundamental understanding of the origin of dissipative timescales to offer key insights into the nature of cellular responses within hydrogels. All crosslinked networks experience a viscoelastic response regardless of the type of crosslink. This time-dependent response arises due to the dissipative interactions between chains and the surrounding solvent that provides friction to oppose the quick deformation of the chains [3]. The friction gives rise to a characteristic time, the Rouse time, that is associated with the diffusion of chain segment over time. The presence of entanglement can also contribute to stress relaxation in covalent networks, by further increasing the diffusion time. The tube model [38] has provided an attractive framework to predict these phenomena. The relaxation times that result from these phenomena are much slower (e.g., >2000 seconds [39]) than that observed in ECM. On the contrary, for polymer networks with reversible cross-links, the viscoelastic behavior is dominated by relatively weak cross-links which gives them the ability to change topology over time and on time-scales that are more biologically relevant. The strength of a bond is characterized by its "binding energy" ΔG, or the free energy variation upon stretching the bond into its normal direction. This energy can be represented as the depth of the free energy well (in terms of bond stretch) as shown in Figure 6 d. For a macroscopic bond, such as Velcro, the breaking of a bond occurs if the force is sufficient to pull the bond out of the well. At the molecular scale, however, thermal fluctuations provide random kicks that could eventually pull a bond out of its energy well, provided that the energy ΔG is comparable to the thermal energy kT. In other words, if the ratio ΔG/kT is not negligible, there is a finite probability that a junction acquires sufficient energy to overcome the activation barrier ΔG and detach spontaneously. Green and Tobolsky [40] have shown that the exit rate (or inverse of the bond lifetime τ0) is a function of the natural thermal vibration frequency $\nu = 10^{10} - 10^{12}$ Hz and the depth of the energy barrier, thus introducing the relevant time scale describing debonding kinetics. From Eyring's kinetic theory, [41] Tanaka and Edwards [42] further postulated that the lifetime of a junction also depends on the force on the bond, that decreases the binding energy by an amount $f\delta$ (Figure 6d). The exit rate k_d of the bond can then be written:

$$k_d(f) = \nu \exp\left(\frac{-\Delta G + f\delta}{kT}\right) \quad (6)$$

where δ is the characteristic length scale at which the bond works (sometimes referred to as the bond sensitivity). A direct consequence of this theory is that stretched bonds have a higher dissociation rate than their force-free counterparts.

If a bond is reversible, it is possible for a pair of dissociated units to recombine under thermal fluctuations with an association rate k_a. This mechanism is usually not a function of force, as dissociated chains are typically found in a force-free configuration, but instead depend on the concentration of possible attachment sites within the hydrogel. [43] Taken together, the mechanisms of bond breaking and reformation is a stochastic process which occurs constantly in a network, implying that one can derive a first order kinetic equation for the nominal cross-link concentration $\boldsymbol{\rho}$ as:[4]

$$\frac{\partial}{\partial t}\boldsymbol{\rho} = -k_d\boldsymbol{\rho} + k_a(\bar{\boldsymbol{\rho}} - \boldsymbol{\rho}) \tag{7}$$

where $\bar{\boldsymbol{\rho}}$ is the total number of potential crosslinks in the network. We note here that all concentrations are nominal, i.e. they are expressed in terms of the reference polymer volume. The knowledge of crosslink density alone is however not sufficient to describe the viscoelasticity of polymer network. To illustrate this point, let us consider a "bond exchange" [44] situation during which a detachment event is immediately followed by an attachment event so that the total crosslink density $\boldsymbol{\rho}$ is preserved over time. In this case, the gel should be able to reorganize its topology overtime and relax its stress, despite the fact that the cross-link density remains constant ($\partial\boldsymbol{\rho}/\partial t = 0$). In this case, rather than crosslink depletion, the key mechanism is the reconfiguration of the polymer chains in the network, such that over time, a stretched chain detaches and reattaches in a relaxed state. The transient network theory [4,45–47] incorporates these mechanisms within a statistical framework where bond dynamics is described by a change of the chain's conformation over time. This theory predicts the conformation tensor evolves over time as: [48]

$$\dot{=} L\cdot + \cdot L^T + k_a(\bar{/} - 1)I - k_d \tag{8}$$

The first two terms describe the change of chain conformation with deformation, where L is related to the rate of deformation by $L = \dot{F}\cdot F^{-1}$. The last two terms describe, respectively, the effect of the association of new chains at rate $k_a(\bar{\boldsymbol{\rho}}/\boldsymbol{\rho} - 1)$ in a stress-free conformation (i.e., $0 = I$) and the dissociation of chains in their deformed conformation .

The mechanical response of these dynamic networks is sensitive to the competition between the loading rate $|L|$ and the dynamics of bond dissociation k_d, represented by the Weissenberg number $W = |L| / k_d$.[49] Thus, if a network is deformed fast, W is large and the last two terms in eq 8 can be neglected. In this case, the solution degenerates to the definition of the left Cauchy-Green deformation tensor $= F \cdot F^T$, a classical measure of deformation used for soft elastic solids. [4] By contrast, for a very slow deformation ($W \to 0$), the first two terms become negligible, and the solution predicts that $\approx I$ at all times. This corresponds to a situation where the deformation does not keep up with the network relaxation, and the polymer behaves like a viscous fluid that deforms permanently. At intermediate values of W, around 0.5, the hydrogel however exhibits a combination of elastic deformation and viscous flow. This can be seen for instance in a stress relaxation experiment, where a sample is quickly deformed and kept at a constant level of strain (Figure 7a). In this case, after responding elastically to fast loading, the gel relaxes over time with characteristic time $1 / k_d$ (Figure 7b). Experimentally, the relaxing time is often measured by the time $\tau_{1/2}$ it takes for the stress to reach half of its original value, which can now be related directly to the molecular timescale of bond lifetime as $\tau_{1/2} = \ln(2) / k_d$.

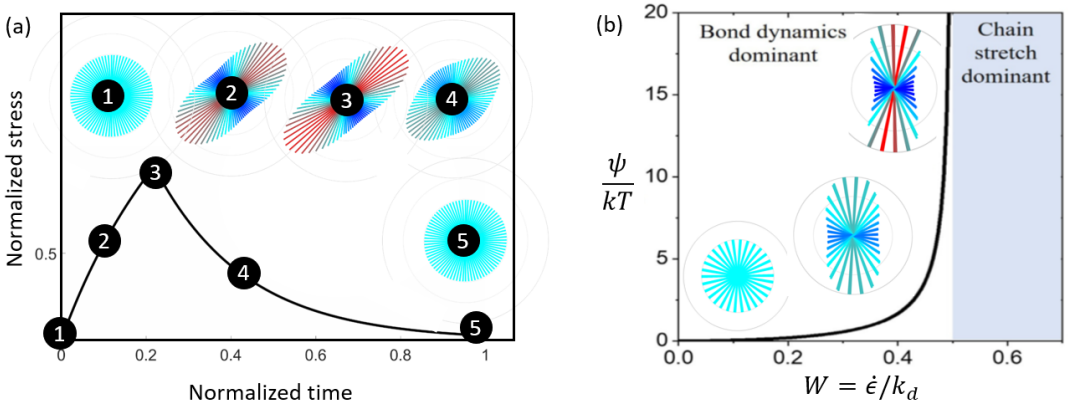

Figure 7. (a) Stress relaxation of a dynamic network over time, with the evolution of the chain conformation tensor. The diagrams show the average direction and stretch of polymer chains in the network during a shear deformation as indicated on the volume element of Figure 3d. We see that as bonds dissociate and reassociate over time, the average chain stretch decreases exponentially with time, until they reach their rest length. (b) Transition of a dynamic network from a viscous fluid ($W \ll 0.5$) to an elastic solid ($W \gg 0.5$). The elastic energy of a chain is here represented by ψ / kT (where kT is used for normalization purposes). We see that when a polymer network is subjected to a low Weissenberg number, bond dynamics dominate, and chains are subjected to very small elastic deformation. However,

as $W \to 0.5$, the strain rate becomes predominant compared to bond dynamics, and the network becomes highly stretched.

2.2.2. Degradable Crosslinks. For cell encapsulation and tissue engineering applications, hydrogel degradation is essential to allow cells to extend their processes, proliferate, and grow into multicellular spheroids, and for large ECM molecules to assemble into new tissue. Degradation of a hydrogel leads to chain scission that reduces the crosslink density, and thus can be thought of a dynamic hydrogel. As the crosslinks break, the size of the polymer mesh increases, which can then allow molecules previously trapped in the network to escape and diffuse through the hydrogel. The degradation process is mathematically described by the rate of change of crosslink density $\boldsymbol{\rho}$. We describe the two primary modes of hydrogel degradation: hydrolytic degradation and enzymatic degradation.

In hydrolytic degradation, hydrogels contain hydrolytically susceptible bonds, such as esters, [50] that are located within the backbone of the polymer chains or more commonly in the crosslinks. This hydrolysis reaction results in a progressive decrease in crosslink density over time, without recombination. This process can be reasonably approximated setting $k_a = 0$ in (eq 7), which gives:

$$\frac{\partial \boldsymbol{\rho}}{\partial t} = -k\boldsymbol{\rho} \tag{9}$$

where k is a pseudo-first order hydrolytic rate constant. After integration, one therefore finds that the crosslink density decreases in time exponentially according to the relation $\rho_x(t) = \rho^0_x e^{-kt}$. This simple relationship agrees well with experimental data for loosely crosslinked hydrogels. [51,52] However, more accurate models have been developed based on statistical models of network structure. [50,53,54] Since water is the solvent in hydrogels, the degradation process is spatially uniform and leads to a bulk decline in crosslink density that results in a macroscopic drop in mechanical stiffness over time (Figure 8a). The hydrogel remains structurally intact until a critical crosslink density is reached where the polymer network loses its mechanical integrity and transitions from a crosslinked network to a highly branched polymer that dissolves into the solvent. [55] This point of reverse gelation plays a critical role in designing degradable hydrogels which require transport of molecules (e.g., ECM macromolecules), extension of cellular processes like filopodia, and cell movement, all of which are larger than the largest mesh size achievable which occurs right before reverse gelation.

In enzymatic degradation, the progressive decrease in crosslink density has been modeled by Michaelis-Menten reaction kinetics as follows: [56]

$$\frac{\partial \rho}{\partial t} = -\left(\frac{k_{cat} c_e}{K_m + \rho}\right)\rho \tag{10}$$

where k_{cat} is the catalytic rate constant, c_e is the enzyme concentration, and K_M is a measure of affinity between the enzyme and the substrate. It is clear from the above equation that the presence of enzymes (via the concentration c_e) increases the effective rate constant for cross-link cleavage. Unlike water, enzymes do not have a global presence in the hydrogel but are transported from their source locations (e.g., cell boundary) by diffusion. This results in local degradation in the vicinity of the enzyme source as the reaction rate is higher in areas of higher enzyme concentration. This also implies that enzyme diffusion is faster in the locally degraded regions but is highly restricted through the undegraded regions of the hydrogel. Over time, degradation proceeds outwards from the source at a rate that is limited by the diffusion of enzymes through the polymer mesh of the hydrogel. [57,58]

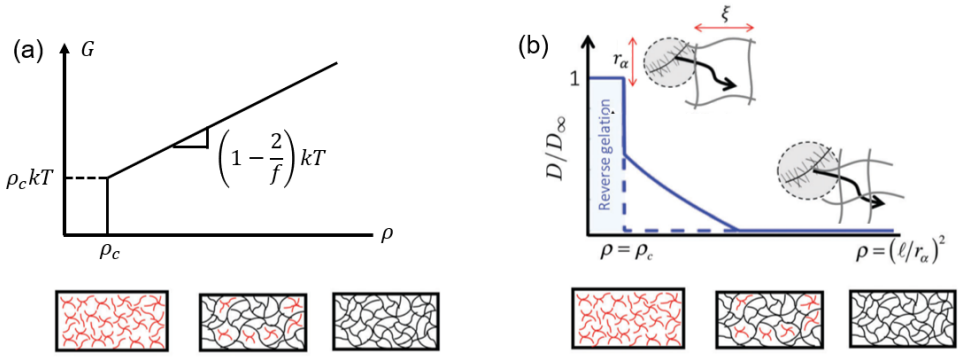

Figure 8. Change in hydrogel (a) stiffness and (b) diffusivity with crosslink density. The degradation process can be visualized by traveling from the right (large density) to the left (lower densities) of these graphs. We see that degradation induce an increase in hydrogel diffusivity and a linear drop of its stiffness until the network reaches its reverse percolation threshold. At this point, the hydrogel loses its stiffness and becomes permeable to molecules of arbitrary size. Adapted and reproduced from ref [58] with permission from the Royal Society of Chemistry. Copyright 2016 The Authors.

2.2.3. Secondary Reactive Crosslinking and/or Decrosslinking. In addition to the above methods to develop dynamic crosslinks using reversible or degradable bonds, there has been a substantial research effort focused on designing networks whose crosslink density can be altered by the user. These strategies leverage sequential or orthogonal crosslinking mechanisms that enable a secondary reactive crosslinking scheme to stiffen the network. On the contrary, strategies have also been developed to design crosslinks that can be degraded in response to a stimul us, leading to softening of the network. Sequential

crosslinking can occur by simply leaving some reactive groups (e.g., acrylates) behind after the initial hydrogel forms, which is the followed by a secondary reaction that consumes the remaining reactive groups. An example of orthogonal crosslinking uses a thiol-ene click reaction such as a maleimide and a thiol to form the initial hydrogel. The monomers are dually functionalized with acrylates in addition to the thiols or maleimide to enable a secondary light-initiated polymerization.[59] This approach allows the secondary reaction to begin at any time defined by the user. Light sensitive bonds have also been incorporated into networks that are formed by either a non-light activated polymerization reactions or using a photoinitator at a different wavelength. [60,61] This approach allows the user to cycle the light on and off to control the extent of degradation of the hydrogel. Strategies have also been developed that enable cycling between stiffening and softening of networks. For example, a reversible enzymatic reaction was developed using the SortaseA mediated reversible transpeptidation. In this approach, peptide crosslinkers are designed to react with this enzyme, leading to SortaseA-induced crosslinking. At the same time, this enzyme can also degrade the network. Through exogenous exposure to SortaseA researchers have shown the ability to reversibly stiffen and soften a hydrogel network. [62,63] The modeling approaches described in Section 2.2.1 can be easily employed to model networks with secondary crosslinking or decrosslinking as described here. Notably, eq 6 and eq 7 both have aspects of reduction in crosslinking due to dissociation of bonds and forming new bonds due to association. Taken together, these user-defined dynamic networks offer the unique ability to study cellular responses in time that result from changes in the mechanical environment.

2.3. Reaction and Diffusion Mechanisms in Degradable Hydrogels

The coupling of reaction and diffusion mechanisms in hydrogels can be observed in enzymatically degrading hydrogels and in the transport of biomolecules that can bind to the polymer chain via specific or non-specific interactions. For transport of molecules in a hydrogel, the polymer mesh can obstruct the path of large solute molecules, like enzymes, and slow down their transport. For example, the diffusion coefficient of enzymes is initially low in hydrogels with high cross-link density (i.e., smaller mesh size), but subsequently increases in time due to degradation before reaching its maximum value at reverse gelation (Figure 8b). Understanding the fundamental mechanism driving these coupled processes are important understanding cell-hydrogel interactions. The general mass balance equation for transport of solute species *i* has the form:

$$\frac{DC_i}{Dt} = -v_i \cdot \nabla C_i + \nabla \cdot (D_{g,i} \nabla C_i) + R_i \qquad (11)$$

where $D/_{Dt}$ is the material time derivative with respect to the solid polymer matrix and $\nabla(\cdot)$ is the spatial gradient operator. The quantity C_i is the concentration of the solute species i, v_i is its convective velocity vector relative to the polymer matrix, $D_{g,i}$ is its diffusivity constant in the hydrogel, and R_i is its reaction rate for consumption and/or production. In this review, species i could be growth factor (e.g., nutrient diffusing into the hydrogel or being released within the hydrogel), matrix-degrading enzyme (e.g., secreted by encapsulated cells that leads the hydrogel degradation), or ECM precursors (i.e., secreted by encapsulated cells that assemble into ECM and form tissue). We briefly review important concepts in the competing mechanisms of solute diffusion and reaction with the hydrated network that play a crucial role in predicting the evolving properties of the hydrogel that are important for transport and hydrogel degradation. Both convection and diffusion can be restricted by the crosslinked polymer chains of the ECM or hydrogel and depend on physical parameters such as size of solute molecule in relation to mesh size, polymer chain mobility, molecular shape of solute, and corresponding hydrodynamic drag. Charged groups that can result in binding between the polymer and the solute molecule can lead to a variety of different types of transport like sub and super diffusive behavior. Mechanical loading plays an important role in these transport mechanisms as they can influence the configuration of the underlying polymer network and the interstitial fluid pressure, both of which can significantly affect transport.

The diffusivity constant D_i of a solute species i freely moving in a dilute isotropic solution is typically estimated using the Stokes-Einstein relationship given by: [64]

$$D_i = \frac{k_B T}{6 \pi \mu r_{H,i}} \tag{12}$$

where k_B is the Boltzmann's constant, T is the temperature, μ is the viscosity of the solvent, and $r_{H,i}$ is the effective hydrodynamic radius of species i that is equivalent to the molecular radius for a spherical particle. Depending on the shape of the molecule (e.g., rod, disk), the hydrodynamic radius is corrected by multiplying with the corresponding shape factor. However, the estimate in eq 12 is not valid for molecules moving through the hydrogel as there are significant steric interactions from polymer chains that can reduce their diffusivity. Several models have been developed to relate the diffusion coefficient in a gel to that in free solution given in eq 12 based on the physical properties of the hydrogel such as mesh size. [65,66]

The free volume theory posits that the fluid phase of the solvent consists of voids that are formed by to a withdrawal of fluid molecules arising from random thermal motion (Figure 9a). [67] The solute molecules therefore diffuse by jumping between these voids or free volume where it is assumed that the free volume is distributed without any energy change. The rate of diffusion in a pure fluid solvent is

therefore determined by the jumping distance of the solute, its thermal velocity, and the probability of forming a void of sufficient volume to hold the solute molecule. Inside a hydrogel, the solute molecule not only needs to find a void due to free volume in the liquid solvent, but also an opening among polymer chains that is large enough to allow its movement. The solute diffusivity in a hydrogel is therefore given as a product of: (a) the probability of finding a free volume in the mesh of fluid solvent; and (b) given a hole in the mesh, the probability that the solute passes through the crosslinked polymer chains (also known as the sieving factor). The most prominent of diffusion models comes from Lustig and Peppas [68] who argued that the solute will pass only if the effective hydrodynamic radius $r_{H,i}$ is smaller than ξ, i.e., the sieving factor is assumed to be $(1 - r_{H,i}/\xi)$. While this approach provides a reasonable estimate for solutes with sizes that are of the same order as that of the solvent (water), it is found to underestimate the diffusion constant for larger solutes. [66]

In the obstruction theory framework, models assume that the path length for diffusive transport is increased by the presence of impenetrable polymer chains. Unlike the conceptual picture of the free volume theory, the solute is assumed to traverse through the fluid solvent following Langevin dynamics of Brownian motion where polymer chains are modeled as obstacles. The most prominent obstruction model considers the solute movement as a stochastic process where successful passage is achieved when the solute finds a succession of openings among the crosslinked polymer chains that are large enough to accommodate its hydrodynamic radius. Obstruction theory models are best applicable for large solutes in comparison to polymer mesh size which severely overestimating diffusion for small solutes. [66,69]

Recent work on solute diffusivity models in hydrogels points towards a hybrid multi-scale approach which combines the strengths of each approach into one comprehensive model. [66] The key idea is that diffusion by free volume dominates when the hydrodynamic radius is of the same size as the free volume voids (FV) ($r_{H,i} \sim r_{FV}$), while for solutes much larger the free volume voids, the mesh size is the limiting factor and is described through the obstruction theory model. A weighting factor A is introduced to combine these distinct diffusion mechanisms into the following:

$$\frac{D_g}{D_i} = A \exp\left(-\frac{V_i}{V_{FV}}\left(\frac{\varphi_p}{1-\varphi_p}\right)\right) + (1-A)\exp\left(-\pi\left(\frac{r_H + r_f}{\xi + 2r_f}\right)^2\right) \quad (13)$$

where V_i and V_{FV} are the volumes of the solute and free volume voids respectively, φ_p is the volume fraction of the polymer, and r_f is the cross-sectional radius of polymer chains. The weighting factor is taken to be a Gaussian error function of the form $A = \mathrm{erf}(r_{FV}/r_i)$ such that $A \to 1$ for solutes of the same size or

smaller than free voids, while $A \to 0$ when the solutes are much larger than the voids. The Gaussian form is motivated by the Gaussian distribution of an average void radius in polymer networks of diverse biological tissues and many hydrogels. [70–72]

The new so-called "Multi-Scale Diffusion Model (MSDM)" shows good agreement with experimental measurements on a series of hydrogels made of crosslinked PEG. As shown in Figure 9 , this model outperforms both free volume and obstruction theories over a wider range of solute sizes from which three distinct regimes are identified. At small solute sizes, the diffusion mechanism is primarily by free voids where diffusion decreases with increasing solute sizes due to lower probabilities of finding a free volume void. However, increasing the solute size also makes this mechanism of diffusion less likely, which results in an intermediate zone where the probability of the solute to diffuse by Langevin dynamics starts to become important. At solutes much larger than free voids, the mesh size drives the diffusion process, and the model converges to the obstruction theory predictions. Thus, when it comes to modeling transport through hydrogels or ECM, the size of the solute with respect to the solvent fluid ($r_{H,i} / r_{FV}$) and the mesh size ($r_{H,i} / \xi$) are important parameters to consider.

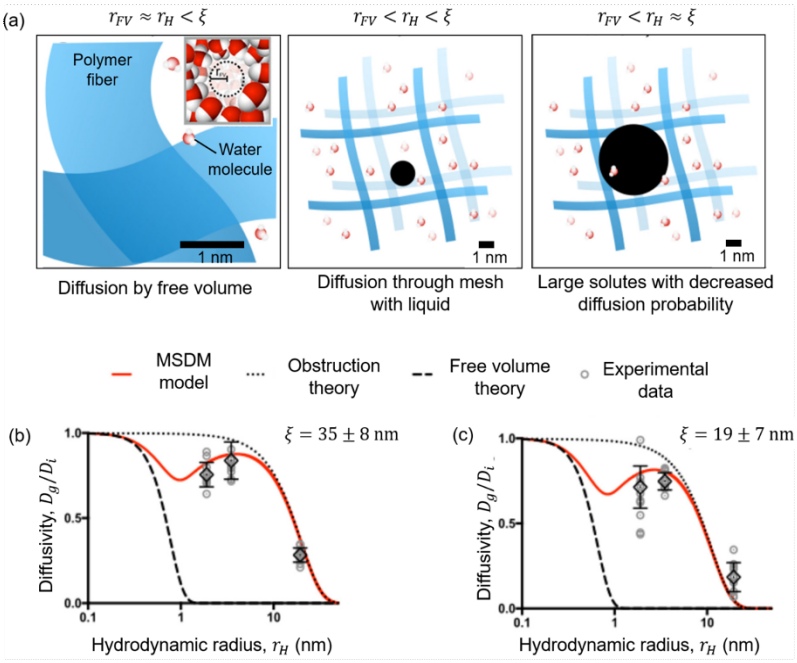

Figure 9. Multi-scale model of diffusivity of solutes through a polymeric mesh. (a) Regimes of different mechanisms of solute diffusion dependent on three length scales: radius free volume voids r_{FV}, hydrodynamic radius of the solute r_H, and hydrogel mesh size ξ. (b) Comparison of predictions of effective

solute diffusivity relative to free diffusivity D_g / D_i from different theories and experimental measurements. Adapted and reproduced with permission from [66]. Copyright 2019 American Chemical Society.

2.4. Poroelasticity

The flow of interstitial fluid in hydrogels is driven by osmotic and hydrostatic pressure gradients that can arise from mechanical deformation or boundary conditions. Fibrous hydrogels, like the ECM, are composed of semi-flexible chains that introduce bending modes to the chain deformation, which have significantly different mechanical characteristics such as strain stiffening compared to flexible polymer networks that are more rubber-like. [73] Fibrous hydrogels also tend to have a higher level of network heterogeneity and mesh sizes compared to flexible hydrogels. Regardless of their structure, ECM and hydrogels are considered porous media that allow solvent transport. From a modeling viewpoint, a hydrogel can be seen as a biphasic mixture made of a fluid and a solid constituent, whose volume fractions are $\boldsymbol{\phi}$ and $1-\boldsymbol{\phi}$ respectively. The relative solvent transport is characterized by its volume flux $q = (v_s - v)$ where v_s and v are the velocity vector of a solvent and solid particle occupying the same location at a given time. The mass balance can then be expressed as: [74,75]

$$\nabla \cdot q = -Trace(L) \tag{14}$$

This implies that the flow of solvent towards a particular location ($\nabla \cdot J$) induces an equivalent increase of volume of the hydrogel, described by the term $Trace(L)$ where L is a tensor that represents the velocity gradient (interpreted as a rate of strain) of the hydrogel. In most situations, interstitial fluid flows are slow and laminar (Reynolds number $\ll 1$) and the solvent's volumetric flux q (flow rate per area) is commonly described by Darcy's law as:

$$q = -\frac{\nabla \boldsymbol{\mu}}{\boldsymbol{\eta}} \tag{15}$$

where $\boldsymbol{\kappa}$ is the specific permeability of the gel, $\nabla \boldsymbol{\mu}$ is the gradient of chemical potential, and $\boldsymbol{\eta}$ is the viscosity of the solvent. The chemical potential can describe a variety of situation, where the flow is driven by pressure, chemical, and/or electrical gradients. For instance, osmotic pressure gradients can arise from spatial variations in the polymer or matrix composition as described in reference [76]. The above equations clearly show that solvent flow and deformation are intricately coupled such that a gradient in hydrostatic pressure can produce both solvent flow and solid deformation, and alternately deformation induces

pressure gradients and solvent flow. There are consequences of this mechanical coupling. First, for fast loading, the solvent does not have time to exit polymer network and the gel behaves as an incompressible medium. For slow loading however, the solvent can redistribute in the gel by flowing from high to low pressures. This further triggers a redistribution of stresses in the hydrogel that could affect cell response. [77] When dynamic loading is considered, this coupling may also speed-up the transport of molecules, [78] such as nutrients and growth factors, as was observed in agarose gels. [79] The time scale separating fast and slow loading is related to the characteristic time τ_s for swelling and deswelling. Scaling analysis [80] indicates that this time increases quadratically with specimen size as:

$$\tau_s = \frac{\eta}{\kappa}^2 \tag{16}$$

Because of the small permeability of hydrogels, however, this time is usually quite large (on the order of hours) even for specimen of a few millimeters in size.

The permeability κ depends on multiple factors such as pore size, polymer composition and geometry. It may also change over time, as a result of deformation, swelling, or change in the network's microstructure. In this context, significant differences in permeability have been reported for healthy and diseased (e.g., tumors) tissues and attributed to their distinct matrix composition and structural arrangement.[81] For an isotropic network, the general relationship between permeability κ and matrix properties is best captured by the Carman-Kozeny equation which has the general form: [82]

(17)

where ϕ_f is the volume fraction of voids, S is the wetted surface area per unit volume, G is the Kozeny factor that is related the shape of the pores and tortuosity, and $r_p = \phi_f / S$ is the hydraulic radius of the pores. The volume fraction of voids, $\phi_f = 1 - \phi_p$, can be calculated knowing the volume fraction of dry polymer in the solid phase which in turn depends on the molecular weight and molar volume of the polymer. For native ECM or fibrous hydrogels, which is composed mostly fibrillar structure, the above models can be a useful tool to further explore specific geometries. [83–85] For hydrogels of flexible polymer networks, the mesh size is small on the nanometer length scale and thus are typically thought of as non-porous. For these hydrogels, it is found that permeability is better described by substituting the pore hydraulic radius r_p in eq 17 with the mesh size ξ.[86] Furthermore, this implies that permeability can be enhanced with swelling ratio J as the mesh size increases under swollen conditions and is given in terms of the mesh size in the dry state as $\xi = J^{1/3}\xi_0$. The mesh size in the dry state ξ_0 is itself dependent on the

molecular weight and crosslink density of the polymer network. [87] This model implies that the effective permeability has a power law dependence on the swelling ratio as $\kappa \propto J^{2/3}$, with an exponent of $2/3$ which is within range of experimental findings that varies between 0.5 and 0.85. [88–90]

Because Darcy's law is a continuum approximation of the average flow in a network, it does not provide any information regarding the subtle flow profiles at the level of chains and fibers or near the cell membrane. The local microscopic flow behavior can be particularly important to understanding cellular response to interstitial flow such as stress-induced matrix production in cartilage, [91,92] cell-cell communication through morphogens, [93] fluid shear stress activated migration of endothelial and epithelial cells in tissue repair, [94,95] distribution, recruitment, and function of tumor-associated macrophages around highly invasive tumors, [96] and pressure-induced tumor proliferation. [97] In this case, detailed network-level simulations are necessary, where the discontinuous and inhomogeneous flow fields are described by the Navier-Stokes equation. [77,85]

3. BIOMOLECULAR TRANSPORT FOR CELL COMMUNICATION

The exchange of information among cells and between cells and their environment through soluble cues is essential for all multicellular organisms. Interstitial diffusive transport in the ECM, which can be augmented by flow, is critical for cell communication in development, growth, and homeostasis. It can drive cellular differentiation, stimulate production of cytokines, promote morphogenesis in perfused organ cultures, supply growth factors, and facilitate cell-cell signaling. [77,98] These cell-secreted soluble molecules include matrix-degrading enzymes, growth factors, cytokines, and chemokines. Recapitulation of the precise transport mechanisms *in vitro* provides crucial insights into *in vivo* cell behavior for translation of tissue engineering and for *in vitro* hydrogel models of development and disease. Importantly, the 3D environment adds a level of complexity. The soluble factors in 2D culture systems can undergo free diffusion and rapid convective transport in an aqueous medium, whereas in 3D matrices, the transport and distribution of soluble factors are usually affected by barrier and immobilization effects by the polymer chains of the hydrogel, leading to spatially graded cell responses. By tailoring the molecular structure, polymer networks can be programmed to interact with specific biomolecules that facilitate intercellular communication. At the same time, when cells are encapsulated in hydrogels that can be degraded by enzymes they secrete, this can be thought of a different kind of transport-mediated cell communication. In this scenario, cells secrete enzymes that degrade the crosslinks of the hydrogel, which in turn changes the hydrogel structure as it degrades. These different types of cell-cell and cell-hydrogel

communications require a fundamental understanding of the transport phenomena in the ECM and in the hydrogel, which is accomplished with the help of physical models that consider the microstructure of these materials. Particularly for cell-hydrogel interactions, three principal transport mechanisms are discussed in this section: (a) hindered transport due to steric interactions, (b) binding-mediated diffusion, and (c) diffusion coupled with cell-mediated degradation (Figure 10). The former two control transport of soluble biomolecules that influence cell-cell paracrine signaling, while the latter controls cell-hydrogel communication. In this section, we review the physical mechanisms related to transport of biomolecules, which include growth factors, cytokines, enzymes, and other morphogens in different hydrogel systems that play an important role in facilitating intercellular communication and accompanying mathematical models. We also review mechanisms of communication between cells and the hydrogel that is mediated through the combined processes of enzymatic degradation and diffusion, which produces specific spatiotemporal degradation patterns in the hydrogel. The mathematical models highlighted in this section utilize the fundamental transport equations that are described in Section 2.3 and thus are not included in this section. The section is concluded with an outlook on the development and design of hydrogels in which specific aspects of biomolecular transport can be facilitated and tuned.

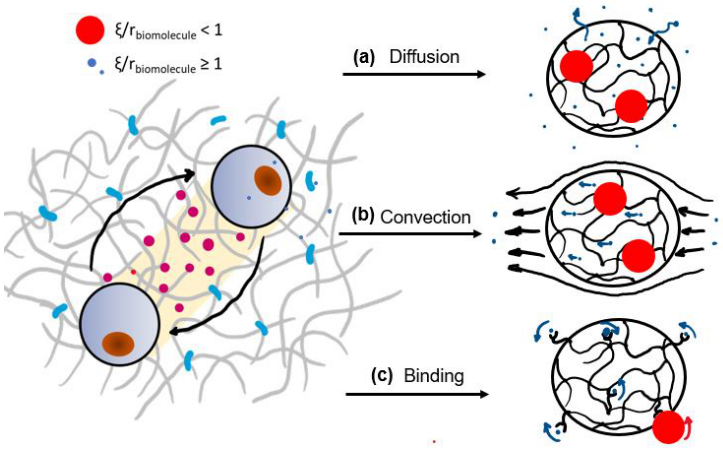

Figure 10. Overview biomolecular transport for cell-communication. The exchange of information between cells and their environment happens through three principal transport mechanisms: a) Passive diffusion, b) convection, and c) binding-mediated diffusion.

3.1 Non-reactive Hydrogels

3.1.1 Tortuosity-mediated Hindered Diffusion. The extracellular transport of biomolecules is strongly influenced by geometric obstacles in the surrounding environment of the cells which includes the

hydrogel structure (i.e., polymer mesh) and the presence of other cells. This makes the path of diffusing molecules increasingly tortuous and thereby increases the average time it takes a molecule to travel a given unit distance by a random walk process. The effective diffusivity of a particle in the extracellular environment depends on the relative sizes of the diffusing molecule and the mesh size of the hydrogel whose relationship is described in Section 2. Many studies have related protein size to release rates in hydrogels. For example, release rates of three model proteins, lysozyme, bovine serum albumin, and immunoglobulin G, ranging in hydrodynamic radii from 2 to 5.3 nm from a triblock copolymer hydrogel increased with decreasing protein size and increasing hydrogel mesh size, following Fickian diffusion. [99] When the biomolecule size approaches the mesh size $r_H \approx \xi$, the effect of steric hindrance becomes prominent and significantly reduces the effective diffusivity that can be quantified as shown in eq 13. [100] This mechanism of hindered transport of biomolecules has important consequences to autocrine and paracrine signaling in cells. For example, the hydrodynamic radii of typical growth factor is 2-6nm [101] and when multiple growth factors are tethered to a polymer chain, the conjugate can reach sizes up to 50-75nm.[102] This suggests that single growth factor molecules are able to diffuse through a hydrogel, but that once tethered to a soluble polymer chain, transport can be inhibited, but which will depend on the hydrogel structure. While the former supports diffusion, the polymer chains can induce frictional drag and diffusion will be slower for the single growth factors in the hydrogel than in the solvent alone. Mahadik *et al.*[103] demonstrated the role of diffusive transport in collagen hydrogels in regulating signaling between two cell types, hematopoietic stem cells (HSCs) and lineage positive niche cells, by varying cell concentration and hydrogel crosslink density. Autocrine feedback mechanisms in HSCs, where the cells respond to their own signals, promoted expansion of early hematopoietic progenitors. On the other hand, paracrine signaling, where communication is between two different cells, in this case between HSCs and niche cells, enhanced myeloid differentiation of HSCs. By tuning the cell density which mediates intercellular distances, and the hydrogel mesh size via crosslink density, the results of this study show that low cell density and small mesh size favored autocrine signaling while high cell density and large mesh size favors paracrine signaling (Figure 11a). A later study by Gilchrist *et al.*[104] reported similar findings in the signaling between HSCs and mesenchymal stem cells (MSCs) in methacrylamide-functionalized gelatin hydrogels. Specifically, the inclusion of MSCs promoted *in vitro* expansion of HSCs without loss of quiescent HSCs that is critical for hematopoiesis in the long-term. This study finds that a time-dependent balance can be achieved wherein an initially tight mesh results in autocrine signaling in HSCs which over time becomes dominated by paracrine signaling between HSCs and MSCs as the latter continuously

remodel gelatin hydrogels through enzymatic degradation.

One approach to improve the diffusivity of large particles through a hydrogel mesh is to increase the mesh size or lower the crosslink density though swelling. The swelling behavior of hydrogels is governed by the balance between forces in the chains that resist deformation and the osmotic pressure that leads to water absorption. [105,106] Altering one of these forces leads to an increase or decrease of swelling that can be engineered to alter the sensitivity to a variety of external conditions like temperature, glucose, pH, light, electric fields, or ionic strength. [107–110] An enlarged mesh can allow larger signaling molecules to diffuse longer distances through the gel in a shorter amount of time.

The presence of a hierarchy of mesh sizes also allows the passage of large solutes that are bigger than the average mesh size but within the distribution of mesh sizes available. [82,111,112] This type of diffusion is often seen in complex systems such as the cartilage or fibrous hydrogels. [113,114] In cartilage, for example, the average mesh size is estimated to be ~6nm but large molecules with sizes >7nm have been observed to diffuse through the dense network. This apparent discrepancy can be attributed to the fact that there is a heterogenous mesh size in the tissue ranging from 5 nm (spacing between glycosaminoglycan chains) to 50-100 nm (spacing between collagen fibrils). [82,111,112,115] Synthetic hydrogels that are formed through chain polymerization contain highly heterogeneous crosslink densities. For instance, polyacrylamide hydrogels at high crosslinker content have high-density polymer chain bundles that arise from the local enrichment of the hydrophobic crosslinker like N,N'–methylenebis(acrylamide).[116–119] Similar heterogeneities are also observed in hydrogels formed by polymerization of acrylate or methacrylate chain polymerizations. [120] While diffusion of solute particles in a homogeneous environment follows a Gaussian behavior, which is the basis of the models presented in Section 2, a heterogeneous environment can result in considerable deviations producing non-Gaussian behavior. This behavior is attributed to particles being intermittently confined in local tight mesh regions that act as cages. The particles are trapped for a time period before eventually escaping due to thermal fluctuations and either continue diffusive motion or get trapped again. The common approach to model such diffusion behavior is the continuous time random walk (CTRW) framework in which a random walker waits for a certain time ("caging" time) at any given site before jumping to a neighboring site. [116,121] While this formalism has been used to describe diffusion in different types of complex heterogeneous systems like desorption dynamics in porous activated carbon grains, [122] electronic transport in disordered solids, [123] and protein dynamics,[124] its application to heterogeneous hydrogels and ECM is still in its infancy. [116,118,125,126]

An alternative approach to improve diffusion of large solute molecules is through dynamic reconfiguration of the network using reversible crosslinking. As the crosslink junctions are subject to continuous breaking and reformation, it is possible for a large solute to escape out of their trapped cages. This scenario is likely to occur as long as the timescale of bond exchange τ_r is larger than the timescale of intrinsic free diffusivity of the particle in the solvent [127] (Figure 11b). Computational molecular dynamics simulations in 2D have shown the possibility of enhanced long-term diffusivity of trapped solute molecules due the re-arrangement of the crosslink junctions. [127] Lenzini *et al.*[128] investigated transport of extracellular vesicles (EVs) in a stress relaxing alginate hydrogel. EVs are important intercellular communicators (carrying cargoes including microRNA, proteins, or resistance genes) involved in many biological processes and diseases, making them promising therapeutic agents. [129,130] EVs can transfer information between cells in proximity and at distance. [131,132] EVs are composed of a phospholipid bilayer that incorporates several distinct surface and membrane proteins with size ranging from 50 to 500nm, [131] thus EVs are typically too large to diffuse through the mesh of most hydrogels. Interestingly, Lenzini *et al.* [128] demonstrated when MSC-derived EVs were encapsulated in stress relaxing alginate hydrogels, EVs were able to diffusion through stiffer hydrogels when compared to softer hydrogels and non-stress relaxing hydrogels (Figure 11 b). This counterintuitive result was attributed to the deformity of EVs, where a stiffer hydrogel along with vesicle specific surface proteins led to EV deformation and subsequently this change in geometry enabled diffusion of the EV through the hydrogel. It was noted by the authors that the increased stiffness in the alginate occurred without significantly altering the mesh size. Transport was limited in covalently crosslinked hydrogels and when non-deformable polystyrene beads of similar size were encapsulated. This shows that stress relaxing hydrogels can improve transport of large molecules and that the shape of the molecule (i.e., spherical to non-spherical) can also improve transport.

3.1.2. Convective flows. One limitation of cell-signaling molecules by diffusive transport is that it takes a long time for molecules to travel long distances. Diffusive transport is sufficient for paracrine signaling over short distances, whereas some long-range paracrine and most endocrine signals moving over longer distances require directional active transport such as fluid flow to shorten the transport time. Convective fluid flow could serve as the primary mode of transport for large solute molecules since solute convection is only weakly related to solute size provided that the particle is not larger than the mesh size. [77] Depending on the flow conditions, the time to transport a molecule over a defined distance can be decreased by several orders of magnitude. For example, neuropeptides are transported and regulated over multiple cell lengths through fluid flow convection in cerebrospinal fluid. [133] Several recent studies

have looked at perfusion for faster and efficient nutrient transport. For instance, a 3D perfusable capillary-like microchannel network was introduced into cell-laden gelatin [134] and PEG-based hydrogels [135] to enhance cell viability and nutrient exchange. Lee *et al.*[136] also reported that cell viability in perfused hydrogel networks was improved significantly compared to hydrogels that were not perfused, indicating that convective flow can be important particularly for larger solutes. Sawyer *et al.*[137] encapsulated Saos-2 osteoblast-like cells in methacrylated gelatin hydrogels along with 3D printed poly(vinyl alcohol) pipes as perfusable channels and reported enhanced oxygen and other nutrient transport. Negrini *et al.*[138] created a 3D printed pre-vascular channel made of sacrificial alginate within a crosslinked gelatin hydrogel and showed improved nutrient transport for adipogenic differentiation in MSCs. Using a parallel-plate bioreactor, Chen *et. al.*[139] observed that Poiseuille flow stimulation of chondrocyte-seeded agarose hydrogels led to an increase in glycosaminoglycan and type II collagen deposition on the surface region of the hydrogel exposed to flow. Collectively, convective transport of cell-signaling molecules in hydrogels improve a cell's ability to differentiate and proliferate.

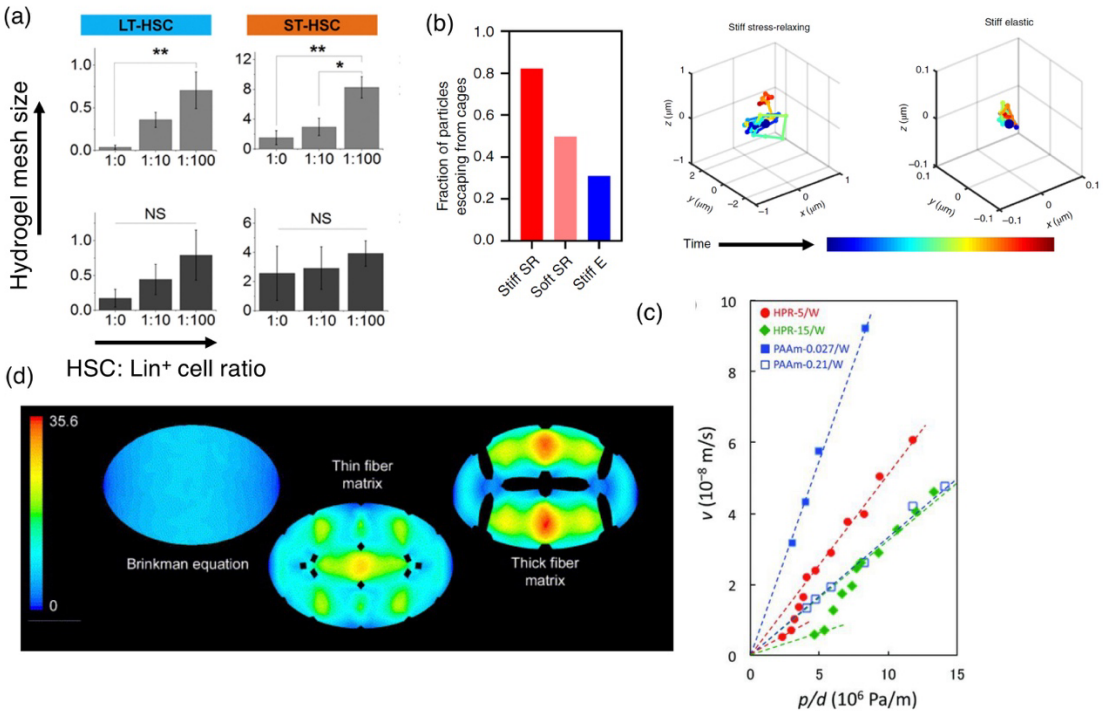

Figure 11. (a) Comparative analysis of hematopoietic progenitor populations via flow cytometry as a function of hydrogel mesh size and niche cell (Lin $^{+}$) co-culture density. Early hematopoietic progenitor populations of long term and short-term HSCs (LT-HSC, ST-HAS) are found to increase with increasing niche cell density. Reproduced with permission from ref [103]. Copyright 2017 Elsevier Inc. (b) Plot of number of extracellular vesicles (EVs) escaping from hydrogel "cages" in stiff and soft stress relaxing hydrogel comparing to a stiff elastic hydrogel. 3D particle tracks for EVs in a hydrogel. EVs in stiff stress-relaxing hydrogel exhibit a more diffusive ensemble-averaged transport relative to stiff elastic hydrogel.

Reproduced with permission from ref [128]. Copyright 2020 Springer Nature. (c) Velocity vs pressure normalized by gel membrane thickness d, shown for fluid flow through slide-ring gels with movable crosslinks. At sufficiently low pressures of $p < p_{c1}$, the network structure is homogenized by the active sliding motion of the crosslinked cyclodextrins. The dashed lines represent linear extrapolations that pass through the origin. The slide-ring crosslinks show unique behavior that has different permeabilities (slopes) at low and high pressures (denoted as HPR-X/W), whereas classical covalent crosslinked hydrogels (denoted by PAAm-X/W) have one unique slope for all pressure ranges. X denotes the crosslink concentration in wt% at preparation. Reproduced with permission from ref [140]. Copyright 2013 John Wiley & Sons Inc. (d) The result on the left was computed from the Brinkman equation, and the two on the right were calculated using the Navier Stokes equation, assuming explicit fiber sizing and spacing. In all three cases the permeability value was the same, but the Navier Stokes solutions reveals the range in shear stress on the cell surface and predicts much larger shear stresses than estimated by the Brinkman approximation. Reproduced with permission from ref [85]. Copyright 2007 Elsevier Inc.

Fluid flow can also be controlled through the deformation of the hydrogel by applying an external stimulant such as magnetic fields [141] or mechanical force. [142] In addition, cyclic loading can achieve high fluid flow at the edges of a hydrogel, but can also lead to deep fluid penetration, which can further enhance transport.[142,143] Several studies have shown that mechanical loading can increase fluid flow within tissues, and specifically for cartilage, which increased molecular transport for large molecules, such as large antibodies (>100kDa).[142,144] Oscillatory compression was reported to increase macromolecular transport in bone by 100x due to convective flow. [145] Interestingly, the extent of transport enhancement through convection from dynamic loading increases with the size of the solute of interest. Unlike static loading which constrains the motion of large solute by altering the mesh size and thereby the solute diffusivity, dynamic loading involves momentum exchange between the solid polymer matrix and solute. Solute molecules easily diffuse into the hydrogel during the unloading cycle when the mesh size is larger and solvent flow is directed inward. However, they are retained more strongly during the loading cycle when the mesh size reduces and the solvent flows out faster than the solute. The solute enters the hydrogel deeper with every cycle until a steady state is reached when the pumping and diffusion forces balance each other out. [79] Taken together, these studies indicate that unlike static compression that reduces diffusivity by shrinking the mesh size, dynamic loading can significantly improve transport of large molecules through the hydrogel that could potentially serve as a useful strategy to guide cell signaling.

Convective flow can arise not just from direct fluid pressure gradients but also through deformations of the gel driven by the mechanisms of poroelasticity discussed in Section 2. Using mixture theory where three phases are considered namely the solid matrix phase, the fluid solvent phase and the fluid solute phase, [143,146] the conditions for enhancing solute transport of neutral solutes under dynamic loading are found to be when: (a) solute diffusion is significantly hindered by the polymer matrix, i.e.,

solute size is comparable to the mesh size, (b) the characteristic rate of solvent flow is higher than the diffusivity of the solute in the gel, i.e., the permeability of the solvent is higher than the diffusivity of the solute, and (c) the loading frequency is higher than the rate of solvent flow, i.e., the rate of deformation of the solid matrix is higher than the solvent velocity. To understand the relative contributions from convective transport and diffusive transport, the non-dimensional Peclet number is often used. The Peclet number is defined by $Pe = Lv/D$,[147] where v is the bulk convective velocity of the solute, L is a characteristic length (e.g., thickness of the hydrogels sample during dynamic loading or cell diameter for slow convective flow around a cell that might be important for morphogenic events), and D is the diffusion constant of the solute. When $Pe \gg 1$, convective transport dominates. Moreover, the magnitude of Pe is enhanced by higher amplitudes of strain for the dynamic loading. [143] Typically, the role of convection can be safely ignored at low Pe, however, in instances like modeling morphogenetic events, concentration gradients as low as 1% can trigger cellular responses to guide morphogenesis. [148] For cellular processes that are highly sensitive to the concentration of soluble factors (e.g., morphogens), the increase in local concentration afforded by the convective contribution to transport, may be just enough to reach a threshold in cell signaling, and therefore cannot be ignored even under low Pe. The bulk convective velocity of the solute v_s is related to the convective velocity of the solvent v_f through the convection coefficient ϕ_v such that, $v_s = \phi_v v_f$.[77] The convective coefficient is influenced by factors such as mesh size distributions, charge interactions, and steric effects. If the network creates steric hindrances or the solute particles are attracted to the network, convective velocity of the solute can be slowed, [149] i.e., $\phi_v < 1$. Alternately, in situations where the crosslinked polymer repels the solute or the solute is large enough to only access larger sizes, size exclusion results in the solute travelling solely with faster fluid velocities, [150] thus producing $\phi_v > 1$. Studies have compared the effects of size, shape (linear vs globular), and charge on interstitial convection.[151,152] Mechanical hindrance slows transport of larger molecules and globular proteins compared to linear molecules of similar molecular weight and repelling charges increase convection through repulsive forces with the polymer. [152] The permeation properties in classical hydrogels can typically be described using Darcy's law. However, ring-sliding hydrogels have been recently shown to control the flow rate by varying the imposed fluid pressure through movable crosslinks (Figure 11c), deviating from Darcy's law.[140] For such network-level simulations, the discontinuous and inhomogeneous flow fields can be described by the Navier-Stokes equation. This approach is particularly crucial in describe the effect of surrounding polymer structure on the convective flow fields that arise in the proximity of cells

that induce shear stresses on the cells (Figure 11d).

3.2 Binding-mediated transport

In native tissues, the ECM regulates biomolecular transport with remarkable specificity using non-steric interactions like electrostatics and hydrophobicity. Often, thee interactions are used to distinguish between particles of similar size wherein the diffusion of particles smaller than mesh size can also significantly reduced by binding (Figure 12a). [153] Alternatively, transient binding mechanisms can also produce selective and enhanced diffusion of molecules larger than the mesh size. Notably, this mechanism is put to use in the nuclear pore complex, a large protein gel-like plug that regulates macromolecular transport between the cell nucleus and cytoplasm. [154–156] Signaling molecules that govern intercellular communication in the ECM, experience a heterogeneous environment with mixed attractive/repulsive interactions that greatly impact their transport properties. [157] It has been demonstrated that positive charges and hydrophobicity hinder diffusion, [158] but have a strong affinity for negatively charged cell-membrane, enhancing cellular uptake. [159–161] Understanding the transport mechanisms underlying binding-mediated motion of molecules through the ECM will provide key insights into designing hydrogels that have a superior control over biomolecular transport between cells. [162,163] Particularly, hydrogels with dynamic bonds can provide a lot of versatility in achieving specificity of molecular transport that transcends the constraint of mesh size discussed in Section 3.1.

3.2.1. The ECM. Morphogens, such as growth factors, chemokines, cytokines, are secreted by cells embedded within the ECM and must diffuse through the ECM to reach their target cells, specifying their fate and function. This process is mediated in large part by a group of heparan sulfate proteoglycans that are present on the cell surface and in the ECM. [164] For example, fibroblast growth factors contains amino acid residues that bind to the negatively charged sulfate and carboxyl groups of heparin sulfate through ionic and van der Waals forces. [165] A number of other growth factor families contain heparin-binding members, including platelet-derived growth factor (PDGF-BB), epidermal growth factor, and vascular endothelial growth factor (VEGF). [166,167] Modifications of heparan sulfate occurs through desulfation, which produces diverse heparan sulfate molecules. Because different degrees of sulfation and sulfation patterns differentially affect binding affinity of molecules and their subsequent release, these modifications lead to differences in how each growth factor interacts with the ECM and generates signals. [164] Furthermore, desulfation can be initiated by the local concentration of a morphogen, which leads to a feedback mechanism whereby changes in the local concentration of a morphogen can lead to changes in

how it interacts with the ECM; this process creates concentration gradients of distinct morphogens within a tissue. Cells may further cleave the cell-bound heparan sulfate with its bound growth factor, allowing the biochemical complex to diffuse into the ECM. Contrarily, heparan sulfate proteoglycans that are localized in the ECM trap and release growth factors, indicating that the ECM acts as a reservoir to store growth factors. These heparan sulfate proteoglycans also prevent long-range diffusion of growth factors, which ensures that growth factors remain in the vicinity of where they were produced. For example, collagen type II that is produced by immature chondrocytes contains a domain that binds transforming growth factor β1 (TGF-β1) and bone morphogenic protein 2 (BMP2), which retains these growth factors in the tissue, inhibits their signaling when bound. [168] The ECM can also potentiate growth factor signaling. For example, when VEGF is bound to fibronectin, both integrin and VEGF receptor are activated, and this signaling crosstalk within the cell enhances VEGF signaling. [169] ECM protein fragments and/or mechanical loading can expose cryptic sequences that bind growth factors. For example, epitopes that are not usually present in fibronectin are exposed after proteolytic degradation. These epitopes can bind to PDGF-BB and have been implicated in promoting fibroblast survival. [170] Growth factors containing "heparin-binding" members can interact with the glycosaminoglycans (GAGs) and heparin sulfate in ECM. Fibroblast growth factors (FGFs) and VEGFs are bounded to heparan sulfate proteoglycans (HSPG) and can, when needed, be released as soluble factors by the hydrolytic enzyme heparinase. [171] Taken together, these studies show that the ECM uses binding mechanisms to controls how growth factors are transported, stored, and released. The design of hydrogels that can perform similar functions would therefore greatly enhance their functionality and performance in mediating cell communication.

3.2.2. Interactive Filtering in Charged Hydrogels. Physical and chemical properties of the matrix, like crosslink density, hydrophobicity, and charge can be tailored to increase growth factor retention. [172] When additional intermolecular interactions, such as electrostatic forces and hydrophobic interactions, exist between the hydrogel and the biomolecule, longer biomolecule retention can be achieved. [173] A number of studies have utilized non-covalent interactions, such as incorporating heparin binding domains into networks,[162] to control transport of bioactive factors through a hydrogel. Yan *et al.*[174] showed that by controlling the charge of hyaluronic acid hydrogels through the pH of buffers, release of BMP-2 could be modulated by tuning the protonation state of carboxylic acid residues. At neutral pH, BMP-2 release is primarily governed by Fickian diffusion, whereas at acidic pH both diffusion and electrostatic interactions between hyaluronic acid chains and BMP-2 become important.

Lin *et al.*[175] developed hydrogels capable of retarding small chemokine molecules secreted from cells through an affinity peptide functionalized PEG hydrogel to sequester the chemokine, monocyte

chemotactic protein 1. Freudenberg *et al.*[176] demonstrated using PEG hydrogels that steric constraints hardly restrict the transport of cytokines (larger hydrodynamic radius than the star-shaped hydrogel mesh size) (Figure 12b). PEG hydrogels were conjugated with various amounts of heparin and sulfated glycosaminoglycans to tune both the number of ionizable sulfate groups per hydrogel volume and the charge density on the glycosaminoglycan. The binding of strongly acidic and basic cytokines correlated with the integral space charge density of the hydrogel, while the binding of weakly charged cytokines was governed by the GAG sulfation pattern. Acidic cytokines with no heparin-binding domain did not bind to the highly negatively charged gels. Atallah *et al.*[177] studied the release of platelet derived growth factor-BB PDGF-BB from glycosaminoglycan-based hydrogels with various sulfation patterns and concluded that transport of PDGF-BB within hydrogel is controlled by interaction of protein with negatively charged sulfate moieties on hydrogel. (Figure 12c,d). Lieleg *et al.*[178] showed that by tuning the strength of physical electrostatic interactions of the particles with the biopolymer matrix, the microscopic mobility of formerly trapped particles can be rescued on demand. Prokopová-Kubinová *et al.*[179] demonstrated using integrative optical imaging that l ong chains of poly[*N*-(2-hydroxypropyl)methacrylamide] conjugated with bovine serum albumin (BSA) to make a bulky polymer (molecular weight of 176kDa) was able to diffuse through the extracellular space in rat neocortical slices at a similar rate as BSA or dextran alone, which has a molecular weight of 66 kDa or 70kDa, respectively. Olsen and co-workers[180,181] used forced Rayleigh scattering to measure diffusion of terpyridine end-functionalized PEG polymers transiently linked to zinc ions in an organic solvent across a wide range of length and time scales. They found that due to the interplay between chain dissociation and diffusion, the mean squared displacement of particles followed a power law scaling with time such that $\langle x^2 \rangle \propto t^{\alpha}$, where the exponent α was greater than one suggesting super-diffusion behavior, in comparison to classical diffusion where α is 1. Other studies on diffusion of nanoparticles with strong binding affinity to specific groups in a hydrogel have found sub-diffusion behavior (α<1).[158,182,183] Taken together, these findings indicate that binding affinities of molecules traveling through a charged hydrogel can significantly impact the speed and extent of their spread and is likely to have important implications for cell communication that impacts paracrine signaling, growth and immune response.

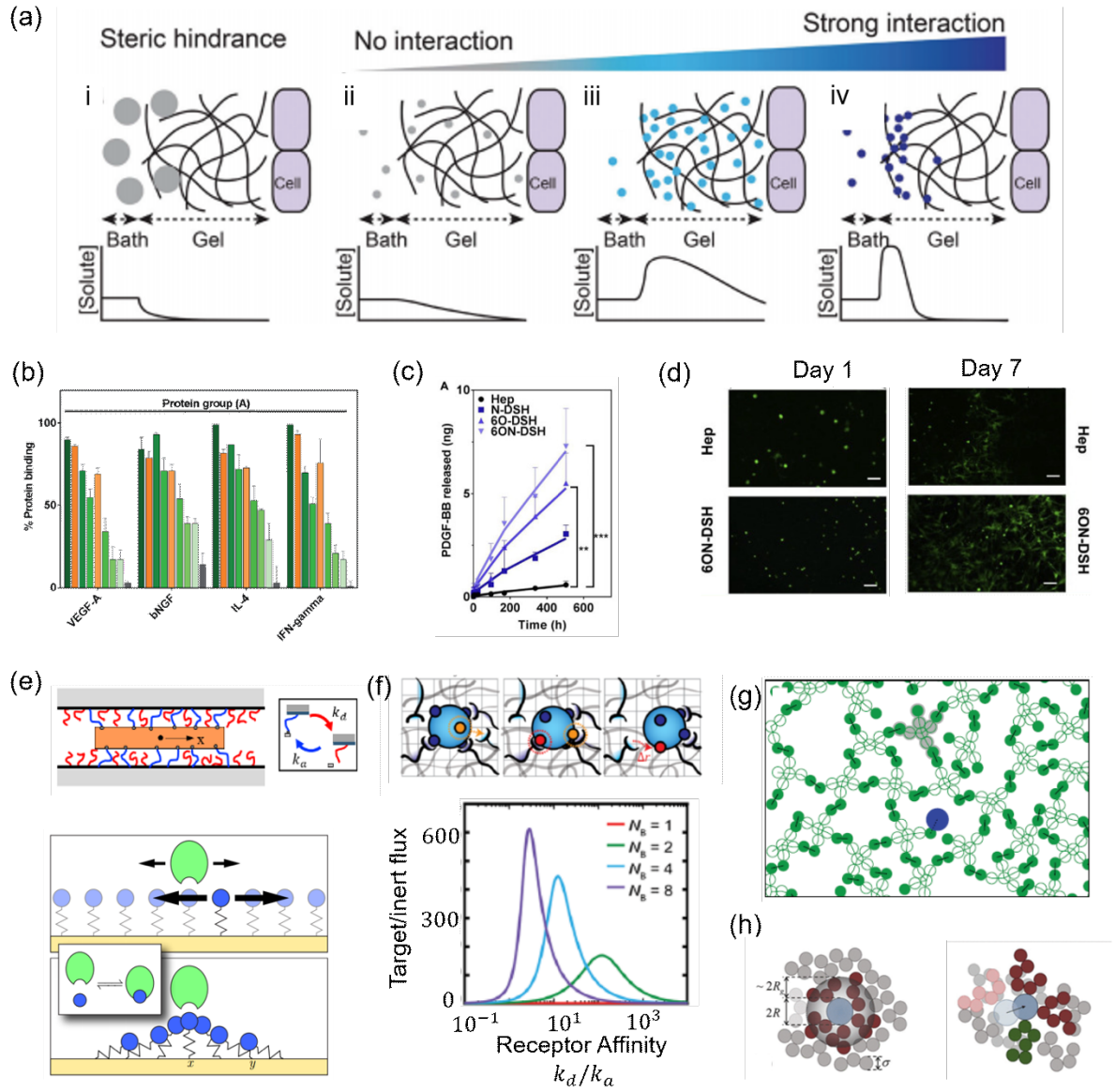

Figure 12. (a) Effect of steric hindrance and physical/chemical interactions on transport. Reproduced with permission from ref [184]. Copyright 2017 The Royal Society of Chemistry. (b) Sequestered percentage of cytokines into a PEG hydrogel with various glycosaminoglycan content and sulfation. Reproduced with permission from ref [176]. Copyright 2019 The Royal Society of Chemistry. (c) Tunable growth factor release from a PEG-glycosaminoglycan hydrogel with various sulfation degrees. Reproduced with permission from ref [177]. Copyright 2018 Elsevier Inc. (d) Representative confocal microscopy images of fluorescently labeled mesenchymal stem cells at day 1 and day 7 of culture. Cellular proliferation measure was enhanced with higher PDGF-BB case in 6ON-DSH. Reproduced with permission from ref [177]. Copyright 2018 Elsevier Inc. (e) One dimensional models of binding mediated transport with multivalent binding (top) and monovalent binding (bottom). Bottom schematic reproduced with permission from ref [185]. Copyright 2018 Elsevier Inc. (f) Model of walking diffusion of multivalent molecules in nucleopore inspired hydrogels. Schematic (top) of sequential binding (orange) and unbinding (red) events of a multi-receptor protein MNB in an interacting polymer network. In the bottom panel, plot of target biomolecular solute flux relative to inert flux is shown with respect to the equilibrium binding constant for different number of

receptors N_B showing that the target flux greatly exceeds inert flux. Reproduced with permission from ref [186]. Copyright 2018 American Chemical Society. (g) A diffusing particle (blue) and the surrounding gel (green) simulated as a 2D network of star-shaped polymers. The polymer strand ends (solid circles) can be in one of three states: free, crosslinked with another strand end, or bound to a particle. Reproduced with permission from ref [127]. Copyright 2018 The Authors. (h) Model of sticky nanoparticle in a polymer melt where matrix chain segments (gray and red circles) are adsorbed onto a nanoparticle bead (blue). The "core" mechanism (left) is suppressed, and the particle moves with a higher effective size that includes the chains, while the "vehicle" mechanism (right) is faster and involves binding and unbinding from chain segments. Reproduced with permission from ref [187]. Copyright 2018 American Chemical Society.

3.2.3 Mechanisms for Diffusion While Bound. Unlike neutral hydrogels where molecular diffusion is hindered primarily by a tortuous path created by the polymer network, charged hydrogels typically affect diffusivity by intermittently pausing or producing motion through binding events. While strong binding affinities effectively immobilize molecules at the hydrogel binding location, weaker affinities provide the possibility for optimal transient binding conditions that promotes transport in an otherwise impenetrable mesh. Diffusion models for binding-mediated transport in biology have primarily focused on the mucus membranes and the nuclear pore complex, both of which employ strikingly similar binding-mediated transport mechanisms as the ECM. [153] The existing models for this type of transport are predominantly one-dimensional approximations, partly due to the polymer brush view of the nuclear pore complex and mucus membranes.[188,189] These models provide useful insights into the diffusive process by drawing attention to scaling laws and qualitative dependency on physical parameters that govern diffusive behavior such as chain length and stiffness, binding rates, strength, and number of available binding sites. To model this kind of transport, first a set of coupled reaction-diffusion equations are constructed (eq 11) that describes the time evolution of concentration of free and bound particles, c_F and c_B respectively. The reaction terms R_F and R_B for free and bound particles in eq 11 have the general form:

$$R_F = -k_a c_p c_F + k_d c_B \tag{18}$$

$$R_B = k_a c_p c_F - k_d c_B \tag{19}$$

where c_p is the concentration of binding sites of the polymer, k_a and k_d are the binding and unbinding rates, respectively. Assuming a negligible convective flow, the transport of solutes is driven by the corresponding diffusion coefficients of free and bound particles, D_F and D_B that need to be determined from the geometry and interaction of the particles with the polymeric matrix. Taking a one-dimensional approximation of the physical problem, Fogelson *et al.*,[185,190] introduced a model which predicts that diffusion is enhanced or hindered based on three time scales namely binding kinetics, elastic relaxation and solvent diffusion (Figure 12e). Other models have further explored the sub-diffusive transport of a

particle constrained in an energy well by its closest neighbors, modeled as rigid walls. [189] More recently, models that predict long-time diffusivity of the particle in terms of molecular parameters have been introduced. These models relate the bound diffusivity D_B to the following physical parameters: [186,191,192] particle size r_p, persistence length of the binding polymer l_p, average spacing between binding sites l_b, the valency of the binding particle N, and the binding/unbinding rates k_a and k_d. Maguire *et al.*[191] assumed that the polymer chains bind to the particle at constant rates to estimate bound diffusivity as:

$$D_B = D_F \frac{L_c l_p k_d}{L_c l_p k_d + 3 D_F} \tag{20}$$

where L_c is the contour length of the polymer chain. The model by Lalitha Sridhar *et al.*[192] was also extended to active polymer chains that are powered by an additional energy source like ATP and showed that enhanced diffusion is possible under optimum conditions of active energy and binding/unbinding rates. Yang *et al.*[186] developed a molecular transport theory using similar principles of affinity-mediated diffusion of multi-receptor molecules through walking and hopping mechanism (Figure 12f). They also showed that entropic repulsion of non-interacting molecules can enhance selectivity of transport, a feature relevant for the extracellular matrix that filters based on electrostatic charges. [178] We note that the one-dimensional model in Yang *et al.*[186] is used to make scaling arguments for diffusion in a dynamic polymer network that make good qualitative agreement with experimental findings in PEG hydrogels containing antibody-binding oligopeptides (affinity domains).

Using Brownian dynamics simulations of 2D particle diffusion in reversible hydrogels, Goodrich *et al.*[127] showed that particles larger than a hydrogel's characteristic mesh size can facilitate their own diffusion through the network by binding to crosslink junctions (Figure 12 g). At optimum conditions, the binding events lead to local reorganization of the gel structure such that interacting particles diffuse while non-interacting particles remain caged. The mechanism proposed by this model considers two key features: (a) competitive binding that arises from the crosslink junctions being unable to remain bound to the particle and crosslinking chains at the same time, and (b) direct bond exchange, i.e., crosslink binding sites transition directly from being bound to the particle to the crosslinked state or vice-versa without going through a free state. Yamamoto *et al.*[187] present a combination of coarse-grained molecular dynamics simulations and theoretical framework based on dynamic percolation theory to model the diffusive motion of sticky nanoparticles in entangled polymer melts (Figure 12 h). The model provides a conceptual picture that sheds light on the influence of chain length, degree of entanglement, nanoparticle size, and particle-polymer strength. It predicts that with increasing chain length there is a cross-over from

a microscopic "core-shell" to "vehicle" mechanisms. The first mechanism describes an effective particle with size that includes the nanoparticle core and a shell of adsorbed polymer chain segment diffusing through the viscous polymer melt. The second mechanism is proposed for particles smaller than the chains such that the particle moves along with the adsorbed chain using it as a carrier or vehicle. Experimental measurements on diffusion of silica nanoparticles in poly(propylene glycol) melts are shown to agree well with this model. [193] The emergence of anomalous sub-diffusive behavior of strongly binding particles in a polymer network has been well studied through both experiments and models and arise due to intermittent trapping of the particles in polymeric cages. [194–197] These findings could be particularly important in modeling binding-mediated transport through reversible gels like alginates that have similar mechanical characteristics as viscous polymer melts. [198]

An important consideration for modeling transport in charged hydrogels is the spatial distribution of charges across the network and their effect on either binding to or repelling the particle. Coarse-grained models of diffusion through polymeric hydrogels with both attractive and repulsive interactions find that charged particles of either sign are immobilized in mixed cationic/anionic gels while neutral particles diffuse rapidly.[157,199] Diffusion models of charged particles through the ECM reveal similar findings indicating the importance of considering the effect of electrostatic interactions for binding mediated transport.[178,200,201] In essence, computational models provide a valuable tool that can assist in the design of distribution of charges and binding motifs in hydrogels that can best support intercellular communication to achieve the functions of the ECM. Future work on modeling biomolecular transport in cell-laden dynamic hydrogels needs to incorporate binding-mediated transport models to obtain improved predictions of growth factor retention and paracrine signaling.

3.3 Cell-gel Communication: Enzymatic Degradation

In the native ECM, cells are responsible for remodeling the ECM as part of tissue development, enabling the tissue composition and structure to evolve during growth, and throughout adulthood as part of homeostasis.[202] ECM is degraded by specific matrix-degrading proteinases that are secreted by cells including matrix metalloproteinases (MMPs), adamalysins, and cathepsins. Consequently, cell-mediated enzyme degradation of hydrogels takes importance in mechano-sensing that involves cell spreading (see Section 4), cellular migration (see Section 5), cellular growth (see Section 6), and in tissue engineering applications to promote ECM growth and remodeling (see Section 7). Features of native ECM can be engineered into hydrogels, in the form of protease cleavable crosslinkers or sequences that are present

within the hydrogel backbone.[203–205] The spatiotemporal characteristics of degradation are driven to a large extent by enzyme transport mechanisms. As discussed in Section 2, diffusion of macromolecules in a hydrogel network depends on the relative size of enzyme to that of hydrogel mesh size. Cell secreted enzymes have hydrodynamic radius of 1-10nm (i.e., MMP-8 has hydrodynamic radius of ~3nm [206]), which are on the order of a typical hydrogel mesh size (1-100nm). Enzyme diffusion though hydrogels is therefore hindered by the mesh and is slower than free diffusion in a fluid medium. At the same time, the enzyme cleaves the enzyme-labile bonds in the hydrogel, resulting in a competition between enzyme diffusion and reaction. The reaction rate of the enzymes can be controlled through amino acid sequence of the peptides,[207] while the diffusion rate can be controlled through the hydrogel mesh size. Different scenarios of spatiotemporal degradation that arise from the reaction-diffusion patterns in enzymatic degradation, which have been summarized by Bryant and Vernerey, [52] and are reviewed below.

The degradation of enzyme-sensitive hydrogels is mediated by the encapsulated cells and exhibits complex behavior. Because cells are the source of enzymes, a concentration gradient forms near the cell surface that can lead to spatiotemporal degradation patterns in the hydrogel. Mathematical models can therefore provide valuable insights into the coupled processes of enzyme transport and hydrogel degradation. A unique feature of enzyme-sensitive hydrogels is the localized degradation that develops in the region immediate neighborhood to the cell. This process depends on two competing mechanisms: (a) the transport of enzyme through the polymer mesh that depends on the ratio r_e/ξ of the enzyme size and the polymer mesh and (b) the degradation rate k (refer to Section 2). This yields a reaction-diffusion system, where the enzyme diffusion is represented by a diffusion equation for its concentration $C(x,t)$ (shown in eq 11). As enzymes diffuse through the hydrogel, they act as catalysts for polymer degradation, hence reducing the crosslink density. The degradation results in an expansion of the mesh that eventually dissolves away when the reverse gelation point is reached. [55] As the rates of diffusion and degradation compete with each other, reverse gelation is reached locally resulting in a degradation front that advances away from the cell surface which can be characterized by a width w and speed v (Figure 13a). Experimentally, Skaalure *et al.*[208] studied degradation front velocities as a function of hydrogel crosslink density in a one-dimensional setup that has an enzyme (collagenase) source and sink on either side of a cylindrical sample of PEG hydrogel with enzyme-sensitive peptide cross-links (Figure 13 b). Hydrogels with the fewest crosslinks exhibited the fastest front velocity and underwent reverse gelation. However, the front has a large width that resulted in an apparent decrease in crosslink density. On the contrary, in higher crosslinked hydrogels, a sharp front (low w) is observed. This represents a reaction-dominated

regime where enzymes cleave polymer chains in the region immediately near the source leading to localized reverse gelation of the hydrogel. The former represents the scenario where both diffusion and reaction mechanisms are equally dominant, a concentration gradient of enzymes forms at the boundary of the cell as enzymes diffuse, while at the same time, the crosslink density in the bulk hydrogel decreases. This is indicative of a wide degradation front that travels over time and in space, but concomitant with an overall decrease in the bulk cross-link density. Extending this analysis to 3D, Skaalure *et al.*[208] also encapsulated spherical poly(lactic-co-glycolic acid) microparticles loaded with collagenase to act as cell mimics into a hydrogel sample (but without other cell-secreted molecules). Similar findings were reported where a weakly crosslinked hydrogel underwent rapid degradation and overall decrease in crosslink density across the hydrogel. By contrast, a tightly crosslinked hydrogel displayed local degradation dynamics where the network remained intact at distances far from the microparticle, while the closer regions are fully degraded (Figure 13c). It is important to note that cell-secreted molecules can also lead to competitive inhibition reactions with the enzymes resulting in very different degradation patterns. Notably, endogenous tissue inhibitors like tissue inhibitors of metalloproteinases (TIMPs) can prevent the degradation of ECM through MMPs by inhibiting the activity of MMPs. [209,210]

Numerical[74] and theoretical[211] models for a spherical 3D cell geometry have shown that the reaction-diffusion process of cell-secreted enzymes is driven by two competing time scales: the enzyme transport time $\tau_t = L^2 / D_g$ and the degradation time $\tau_d = \ln\beta / \kappa c_0$. Here D_g is the diffusivity of the enzyme in the hydrogel and is a direct function of the hydrogel mesh size (see Section 2), L is a characteristic length scale (e.g., intercellular distance), β is a measure of the reverse gelation point, and c_0 is the enzyme concentration at the cell surface. This interplay gives rise to a degradation front of effective width w, that propagates outward from the enzyme source at speed v, predicted as:

(21-22)

This scaling law predicts that diffusion-dominated systems ($\tau_t \ll \tau_d$) are characterized by wider transitions from fluid to intact solid polymer. By contrast, reaction-dominated systems ($\tau_t \gg \tau_d$) display sharper transitions (Figure 13d). The models therefore suggest that it is possible to tune the polymer mesh size, crosslink density, and the enzymatic reaction rate constant to individually control the front width and speed. As discussed in the next section, a fine control over the degradation process is a crucial step in designing hydrogels to support ECM growth, deposition, and tissue regeneration. It is also important to support cell migration in dense hydrogel as discussed in Section 5.

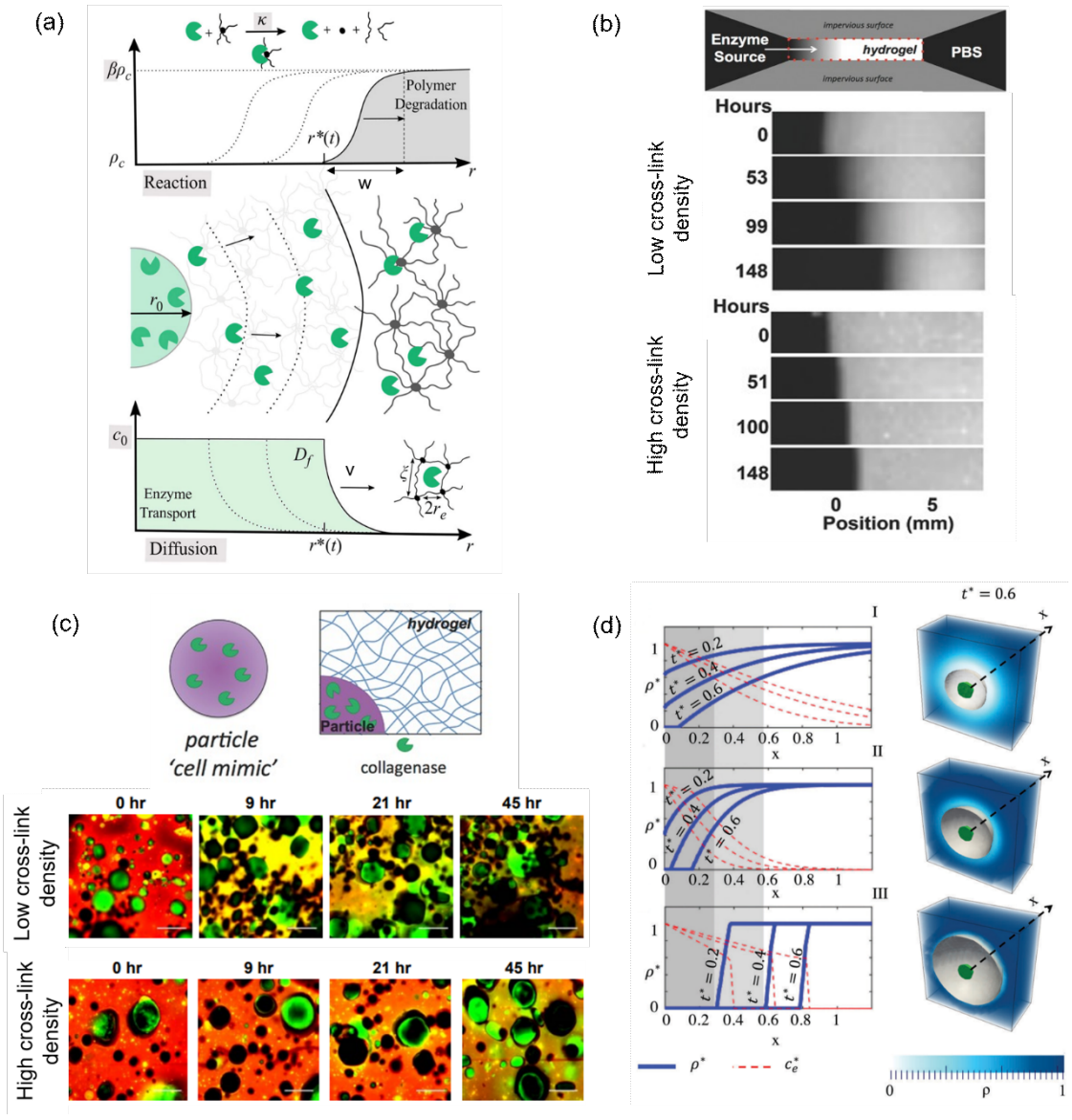

Figure 13. (a) Schematic illustrating the propagation of a fuzzy interface due to enzyme diffusion and degradation reaction in an enzyme-sensitive hydrogel. The evolution of crosslink density ρ (ρ $_c$ corresponds to the crosslink density at reverse gelation) and enzyme concentration c are illustrated. The highlighted parameters κ, c_0, and D_g are the key features of the model. Reproduced with permission from ref [211]. Copyright 2018 American Physical Society. (b) One-dimensional experimental setup to study the enzyme-mediated hydrogel degradation front over time for an enzyme-sensitive, covalently crosslinked PEG hydrogel. For a low and high crosslink density, the degradation front was observed through a fluorescently labeled hydrogel. Position "0mm" corresponds to the edge of the hydrogel prior to degradation, with a reservoir of enzyme to the left. Over time, enzymes diffuse into the hydrogel and degrade the crosslinks resulting in reduced fluorescence in hydrogel. A wide front is observed in the low crosslinked hydrogel

evident by a diffuse hydrogel boundary and a sharp front is observed in the high crosslinked hydrogel evident by a sharp contrast between reservoir (black) and hydrogel (white). Reproduced with permission from ref [208]. Copyright 2016 John Wiley & Sons Inc. (c) Confocal microscopy images of the spatiotemporal degradation patterns of a hydrogel containing collagenase loaded microparticles encapsulated in an enzyme-sensitive, covalently crosslinked PEG hydrogel [Collagenase (green) and PEG hydrogel (red)]. Reproduced with permission from ref [208]. Copyright 2016 John Wiley & Sons Inc. (d) Characteristics of 3D degradation dynamics in a hydrogel degrading by enzymes, as a function of the normalized enzyme size r_e and degradation rate constant k_{cat}*. The crosslink density is plotted as a function of distance x from the cell surface for three specific conditions. One observes a transition from a diffusion-like profile (in plot I) to a narrow moving degradation front as r_e*and k_{cat}* increase from plots II to III. Reproduced from ref [58] with permission from the Royal Society of Chemistry. Copyright 2016 The Authors.

3.4 Outlook: Tuning Hydrogels for Directed Communication

Extracellular transport of biomolecules like growth factors, chemokines, cytokines, other morphogens, and antibodies is critical to development, homeostasis, and disease progression, but is highly dependent on the cellular microenvironment. In hydrogels, molecular transport is heavily hindered by a tightly crosslinked network, whereby autocrine signaling is favored. However, when molecular transport is possible, paracrine signaling is enabled. This can be further controlled through hydrogel degradation, where a switch in signaling from autocrine to paracrine can occur. There are several strategies that can be used to overcome the size-based constraints for transport of large molecules in a tight mesh, one of which is leveraging the hydrogel chemistry to produce networks that have a heterogeneous crosslinking. Another strategy is to use hydrogels with polymer chains of a dynamically reconfiguring network, such as covalently adaptable networks, which offer a path for large molecules to find their way through the hydrogel. Introducing convective flow can be particularly useful when long range cell communication is needed. Furthermore, the coupling of mechanical and transport properties in hydrogel designs can be utilized to enhance transport against concentration gradients, such as in the case of improved solute transport when hydrogels are subjected to dynamic loading.

Unlike neutral/static hydrogels which only produce steric hindrance to molecular transport, charged/dynamic hydrogels can produce complex diffusion phenomena due to binding from electrostatic or hydrophobic interactions or from reversible crosslinks. This provides the unique opportunity to achieve selective filtering of biomolecules based on their specific interaction and to overcome the constraints of size-based filtering. A strongly binding particle can be significantly slowed down or even immobilized even if its size is much smaller than the mesh size. This can help achieve concentration gradients in a hydrogel to

provide important signaling feedback for specific cell signaling events. Alternately, a weakly binding particle can move through the gel due to transient binding and dynamic reconfiguration of the hydrogel network even if the particle size is much larger than the mesh. Hydrogel designs that not only involve tuning of the structural properties, but also consider distribution of specific molecular moieties and charges are an important next step for controlling cell-hydrogel interactions . Mathematical and computational models are important tools in decoding the relationship between the physical properties of a polymer network such as the chain size and shapes, distribution of mesh size, and cross-linker concentration to the diffusive properties of cell signaling molecules. With these tools, the performance of hydrogels for a range of applications, such as for tissue engineering or molecular delivery can be designed with unprecedented control. While, this review was limited to interactions associated with cells and ECM and the hydrogel, a number of studies have examined binding-mediated transport in the context of drugs release and similar approaches could be used to control transport of ECM molecules. [163,212,213]

Cell-mediated degradation is a key mechanism of cell communication with the hydrogel that mimics how cells naturally interact with the surrounding matrix. This creates a unique degradation pattern in the hydrogel, whereby the hydrogel disappears in regions immediately around cells, creating space where transport of large molecules is no longer hindered, nor are larger features of the cell such as cell processes (e.g., filopodia) and the cell body itself transport . Combined experimental and computational studies have enabled the degradation front to be fully characterized, showing that it advances outward from the cell. The characteristics of the front speed and width can then be controlled through the hydrogel design by tuning the competition between diffusion and reaction rates. In diffusion-dominated regimes, the degradation is global while in the reaction dominated regime the degradation is local. Mathematical models are particularly beneficial for tuning spatiotemporal degradation patterns, which are difficult to quantify experimentally and become more complex when cells are active in other functions (e.g., cell spreading, depositing an ECM). The guidance of mathematical models will be necessary to decouple these complex events, occurring across multiple length and time scales. Less studied is the potential for cell-mediated hydrogel crosslinking. One example is lysyl oxidase, which is an amine oxidase secreted by cells, which catalyzes the oxidative deamination of lysine in proteins such as collagen and elastin. [214] Synthetic and natural hydrogels containing primary amines could see increases and spatial variations in crosslinking due to cell-secreted enzymes that would whose transport would also mediated by reaction-diffusion mechanisms. Mathematical models could help identify the relative contributions of enzyme-mediated degradation and enzyme-mediated crosslinking and how these two competing factors could affect temporal changes in network properties.

4. MECHANO-SENSING IN 3D HYDROGELS

Cells receive cues by sensing the 3D mechanical environment of a hydrogel using cell-surface receptors called integrins that mediate mechanotransduction pathways. These cues can lead to adaptation of the actin cytoskeleton by actin polymerization, re-organization, and contraction, which manifest through changes in cellular morphology. These adaptations have a direct impact on intracellular signaling pathways that ultimately influence cellular fate and function. A unique characteristic of cells embedded within a hydrogel matrix is that at the time of encapsulation, all cells exhibit a spherical morphology. Depending on the hydrogel stiffness, cell adhesivity, and degradability, cells adapt to this new environment, which can lead to morphological changes. However, the type and density of hydrogel crosslinks will dictate whether a cell can extend its processes and further spread. These cellular processes are typically around 1 micrometer [215] in diameter while the mesh size of a typical covalent flexible hydrogel is in the range of 10-100 nanometers. This means that the cell must forcibly deform and/or degrade the hydrogel in order to extend its processes and begin to change shape. [216] At the same time, cells exert a force on the hydrogel when integrins directly bind to cell adhesivity sites on a polymer chain in the hydrogel. The force is generated through focal adhesions that are connected to the actin cytoskeleton. The extent of these traction forces depends in part on the stiffness of the hydrogel matrix, the density of cell adhesion sites, and the specific integrin-ligand bond. [217,218] Figure 14 summarizes the key elements involved in cell mechano-sensing and spreading in a 3D hydrogel. Below, we describe recent experimental findings that use different types of hydrogels to study the mechano-sensing capabilities of cells in 3D culture and highlight examples of the effect that the mechanical signals have on cellular fate. We then describe advancements in mathematical models and how they are aiding to uncover the mechanistic link between cellular traction forces and cellular morphology in mechano-sensing. Although cellular traction and spreading are strongly coupled through the actin cytoskeleton, they involve different mechanisms at a fundamental level. We therefore discuss them separately. We end this section with a future outlook of how to tune hydrogels to control cell mechano-sensing.

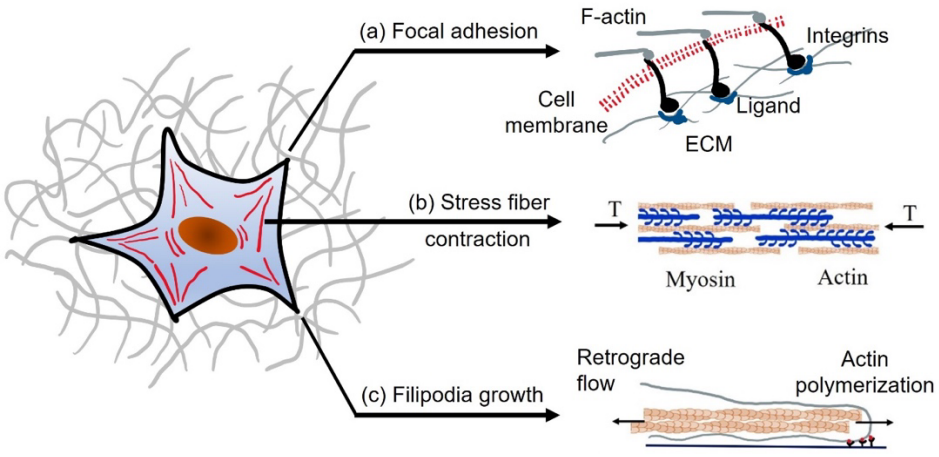

Figure 14. (a) Principal components and mechanisms of cell mechano-sensing. (a) The adhesion between a cell and its environment is established by the integrin-ligand complex, whose lifetime is mediated by force. Under an appropriate mechanical environment, integrins can cluster into large focal adhesion complexes. (b) Stress fibers are large contractile acto -myosin assemblies that can span the length of the cells between two focal adhesion complexes. Their association and dissociation are conditioned by the internal tension they can sustain. (c) In 3D, cell spreading is generally ensured by the extension of filopodia whose dynamic relies on a balance between actin polymerization at the leading edge and the retrograde flow powered by actomyosin contraction.

4.1. Cell Spreading in Hydrogels

4.1.1. Semi-flexible Isotropic Networks. Isotropic networks with semi-flexible polymers produce fibrous hydrogels that most closely resemble cell adhesion observed in 2D culture, as long as the density of the fibers remains low. Collagen hydrogels are the most widely studied fibrous hydrogels that lead to rapid cell spreading of encapsulated cells, followed by remodeling of the collagen fibers via matrix degrading enzymes and then contraction of the hydrogel. [219,220] Self-assembling peptide hydrogels are also fibrous hydrogels that are engineered with specific peptide sequences designed to induce fiber formation in response to a stimulant (e.g., temperature); an example is shown in Figure 15a. [221] The peptides are also often engineered with sequences such as RGD to endow cell adhesivity. Hogrebe *et al.*[222] showed that human MSCs encapsulated in a self-assembling peptide hydrogel containing RGD rapidly adopted a spread morphology within 24 hours for stiffnesses between 1.25 to 5 kPa, as measured by the shear modulus, *G*. These findings were comparable to cells seeded on the same hydrogels and cultured in 2D. However, in softer hydrogels of 250 Pa (*G*), cells were unable to spread and instead retained a spherical morphology. Longer culture times did not lead to cell spreading; a finding that agreed with 2D culture. This finding indicates that similar to 2D cultures, cells must generate a sufficient level of force on the hydrogels (referred to as traction force) to induce cell spreading. The authors also reported that if the hydrogel was

too stiff, at 10 kPa (G), MSCs retained a spherical morphology at 24 hours; a finding contrary to 2D culture, where cells readily spread. However, by day 26, cells spreading was evident in the 3D hydrogel. Select results are shown in Figure 15b. This finding indicates that if the density of the fibers is too high, cell spreading is delayed as the cells must degrade and remodel more of the fibrous matrix to create space before they can spread. Buitrago *et al.*[223] observed similar trends. In this work, the authors developed a fibrous hydrogel with tunable modulus that was comprised of collagen for its cell adhesivity and silk for its mechanical properties (silk lacks cell adhesivity). Three days post-encapsulation, MSCs retained a spherical morphology, but by day 7, cell protrusions were evident indicating that the cells were beginning to spread in the hydrogels. This finding was observed over a range of moduli from 280 Pa to 1.5 kPa (G). In a direct comparison to 2D culture on the same hydrogels, the authors showed that cells rapidly spread in 2D within 24 hours, suggesting that adaptation in cell morphology was slower in 3D. These findings, when compared to the results from Hogrebe *et al.*[222] with self-assembling peptide hydrogels, suggesting that the introduction of silk led to slower rate of cell spreading likely due to differences in the fibrous architecture (i.e., nanofibrous vs a globular microstructure) and reduced degradability.

While cell contraction is generated by traction forces that can drive cell spreading in 3D, cells can undergo adaptations in the cytoskeleton without changing cell morphology. For instance, Di Caprio *et al.*[224] encapsulated adipogenically differentiated MSCs in collagen hydrogels whose stiffness was increased from 100 to 300 Pa (G) by the addition of a poly(ethylene glycol) (PEG) crosslinker. [224] Adipocytes in their native tissue have a circular morphology, which is important for their ability to maximize lipid storage. In this study, the adipocytes retained a circular morphology regardless of hydrogel stiffness. However, an increase in hydrogel stiffness was sufficient to cause a dysregulated pro-fibrotic phenotype in the adipocytes. This response was caused by an increase in actin contractility as a result of the stiffer hydrogel. Collectively, these studies indicate that in 3D fibrous hydrogels, cell spreading requires a sufficient level of stiffness; however, the mechano-sensing capabilities of cells may be more sensitive than what emerges with cell spreading.

4.1.2 Covalent Flexible Networks. Cell spreading is generally more restricted in chemically crosslinked flexible networks owing to their smaller mesh size when compared to the more open networks afforded by fibrous hydrogels. This observation is particularly evident in semi-interpenetrating networks that introduce a covalent flexible network into a fibrous hydrogel. For example, Liu *et al.*[225] demonstrated that if an alginate hydrogel, crosslinked with Ca^{2+}, was introduced into a collagen hydrogel, encapsulated cardiac fibroblasts retained a spherical morphology. However, when alginate was introduced on day 2, after cell spreading was achieved in the collagen gel, it was possible to lock in a spread morphology in the

3D hydrogel. The addition of alginate, however, led to an increase in hydrogel stiffness, which in turn led to positive expression for ↣smooth muscle actin (↣SMA), indicating a fibroblast to myofibroblast transition. This phenotypic change was not observed in the collagen-only gels or in stiffness-matched collagen+alginate gels with spherical cells. This finding suggests that the change in phenotype was mediated by a combination of cell spreading and increased hydrogel stiffness. Cao *et al.*[226] reported similar findings when cancer-associated fibroblasts (CAFs) were encapsulated in a collagen-alginate interpenetrating network. The difference in this study was that at the time of encapsulation the gels were either exposed to extracellular Ca^{2+}ion to induce alginate crosslinking or not. In the absence of exogenous alginate crosslinking, weak ionic crosslinking from divalent cations in the media is possible. Cell spreading was possible in the softer hydrogel without exogenous alginate crosslinking owing to the ability of cells to remodel the collagen. However, this was not the case when alginate was crosslinked with exogenous cations as the mesh size was considerably smaller . The encapsulated CAFs were cultured in these two hydrogels and in a transwell culture system with an invasive breast cancer cell line MDA-MB-231 that was separately encapsulated in a collagen-only gel. The CAFs exhibiting a spread morphology induced a greater invasive response in the cancer cells compared to CAFs encapsulated in the stiffer hydrogel that retained a spherical morphology. This study illustrates that the 3D culture environment through changes in cell morphology and/or cell sensing of stiffness directly affect the secretome, which in turned influences its paracrine signaling on other cells.

When cells are encapsulated in purely covalent flexible networks, cell spreading requires degradation of the hydrogel and extended culture times. For example, Zhang *et al.*[227] showed that MSCs encapsulated in a methacrylated gelatin hydrogel were spherical at day 1 in hydrogels with initial moduli ranged from 120 Pa to 4 kPa (G), but by day 7, cells were spreading in 80-120 Pa (G) soft hydrogels. However, there was minimal spreading in stiffer >120 Pa (G) hydrogels. Scott *et al.*[228] encapsulated adventitial fibroblasts in a covalently crosslinked enzyme-sensitive PEG hydrogel containing RGD that had an initial stiffness which varied from 300 Pa to 2.9 kPa (G). The cells retained a circular shape during the first 7 days, but by 14 days cells began spreading and the degree of spreading further increased with longer culture times. The increase in spreading was most pronounced in the 300 Pa and 1.4 kPa (G) hydrogels and to a lesser extent in the 2.9 kPa (G) hydrogels. An interesting observation from this study was that over time the modulus converged to similar levels by day 42. However, the cellular behavior was distinctly different in the softest hydrogels leading to a myofibroblast transdifferentation over time, while the stiffer hydrogel supported a myofibroblast phenotype from the onset. Schweller *et al.*[229] encapsulated HUVEC and human brain pericyte cells (HBVPs) together in a covalently crosslinked enzyme-sensitive PEG

hydrogel with RGD, but which a peptide crosslinker sequence that contained an internal vinyl group that allowed for control over stiffness without altering polymer density. The hydrogel modulus was varied from 0.7 to 15 kPa, as measured by compressive modulus, E. The HUVEC-HBVPs were able to spread in the soft hydrogel within 24 hours, while it took 6 days to see significant spreading in the stiff gels. By four weeks, the two environments were indistinguishable, suggesting that the stiffer hydrogels eventually caught up to achieve the same degree of cell spreading. This finding can be attributed to the stiffer hydrogels requiring more degradation before cell spreading can occur. Arkenberg *et al.*[62] showed that MSCs encapsulated in a covalently crosslinked PEG hydrogel of 4 kPa (G) containing two enzyme-sensitive sequences [one sensitive to matrix-degrading enzymes and one sensitive to the exogenous enzyme, soratseA (srtA)] retained a spherical morphology. However, when softened to 1 kPa (G) by exogenous delivery of SrtA, cells were able to spread, indicating that the cell-mediated degradation was much slower (Figure 15c). Wang *et al.*[230] reported on patient-derived glioblastoma xenograft cells encapsulated in an enzyme-sensitive PEG hydrogel with RGD and hyaluronic acid with varying moduli from 40 Pa to 27 kPa (E). Cells retained their spherical shape at day 1, but cell spreading was evident in the softer hydrogels of 40-240 Pa (E) by day 7 and in the 550 Pa (E) gels by day 14, although not to the same extent. This study reported that cells cultured in the highest stiffness hydrogel of 27 kPa (E), which retained a spherical shape were most resistant to a chemotherapeutic drug. It is worth pointing out that cell spreading was possible in very low modulus hydrogels of 40 Pa, which is contrary to studies in very soft fibrous hydrogels [222] that are unable to promote cell spreading due to limited cell traction forces. This implies that the minimum cell traction forces required to induce cell spreading could be dependent on the crosslink mechanism.

4.1.3 Stress Relaxing Hydrogels. Viscoelastic hydrogels have gained increasing interest due to their ability to mimic the time-dependent responses of native ECM. [63,231–233] While fibrous-forming hydrogels exhibit stress relaxation behaviors, we focus here on hydrogels formed from synthetic polymers or modified biopolymers that result in flexible polymer networks for their ability to offer control over the time-dependent properties of stress relaxation. Herein, we provide the values for $\tau_{1/2}$, the time to reach half maximum stress, if this parameter was reported, and can be used a comparator of the stress relaxing capabilities between different types of hydrogels (see also Section 2).

Several studies have shown that fast stress relaxing hydrogels are required to achieve rapid cell spreading in chemically (i.e., ionic or covalent) crosslinked hydrogels. For example, Ma *et al.*[234] encapsulated quiescent valvular interstitial cells (VICs) in a stress relaxing PEG hydrogel consisting of reversible boronate-triazole crosslinks and studied how the maximum amount of stress relaxation influenced cell morphology (Figure 15d). The elastic modulus was held constant at 1.6 kPa (G) across

different formulations and the degree of stress relaxation was varied from ~0 to 90% of the maximum applied stress ($\tau_{1/2}$ was not reported). Cell spreading occurred within 24 hours in gels that relaxed 70 to 90%, while cells remained spherical in hydrogels that relaxed from ~0 to 40%. The higher relaxing hydrogels led to elevated expression of myofibroblast activation in the VICs. This study demonstrates that a rapid increase in cell spreading can accelerate activation of quiescent VICs. Liu *et al.*[235] incorporated dynamic imine crosslinks into collagen hydrogels that resulted in $\tau_{1/2}$ of less than 10 s. When MC3T3-E1 pre-osteoblasts were encapsulated in this hydrogel with an initial modulus of 3 kPa (E), cell spreading was substantial in 24 hours in hydrogels with $\tau_{1/2}$ of ~1s, but minimal cell spreading was observed in hydrogels with a $\tau_{1/2}$ of 5-10 s. However, by day 5 cells spreading was similar across all hydrogels. The time-dependent response, however, had a pronounced effect on osteogenesis of the MC3T3-E1 cells. In the fast-relaxing hydrogels, there was increased expression in the osteogenic genes *Runx1*, *Alp*, and *Ocn* at day 5 despite similar morphologies. The authors identified activation of Trpv4, a calcium ion channel, as a mediator for the time-dependent enhancement of osteogenesis. These findings indicate that stress relaxing hydrogels independently affect cellular morphology and ion channels, complicating the interpretation of mechanical effects of the hydrogel on cellular spreading. Brown *et al.*[31] encapsulated MSCs in PEG hydrogels with RGD and containing thioester bonds in the crosslinks and compared to MSCs encapsulated in control hydrogels with non-thioester bonds. By controlling the stoichiometry at the time of hydrogel formation with increasing excess thiol but maintaining a constant modulus (1.5 kPa, G), hydrogels with the thioester bonds exhibited stress relaxation in a pH-dependent manner. Cell spreading was evident in some of the cells in the stress relaxing hydrogels and was greater in gels with faster relaxation times (i.e., excess thiols) by day 3. Interestingly, the relaxation times were much longer, with $\tau_{1/2}$ of 10^5 s for the excess thiol and 10^7 s at stoichiometry at pH 7, than other studies, which may explain why only a few cells were showing signs of spreading. Silva *et al.*[236] reported on an alginate-silk hydrogel consisting of Ca^{2+} ionic crosslinking and physical crosslinking of the silk biopolymer that resulted in relatively high moduli (100-600 kPa, G). While silk enhanced the viscoelastic response of the hydrogel, encapsulated human umbilical vein endothelial cells (HUVECs) retained a spherical morphology. This result is likely due to a combination of the high modulus, slow viscoelastic response (i.e., days), and the lack of cell adhesivity. Collectively, these recent findings in conjunction with earlier studies indicate that rapid stress relaxation (i.e., shorter $\tau_{1/2}$) is necessary to support cell spreading, but that the specific time-dependent response may depend on the cell type. If the relaxation is too slow, cell spreading is inhibited and is more similar to permanently bonded flexible networks. However, mechano-sensing due to rapid changes in hydrogel stress may enhance other cellular functions beyond cellular spreading.

Several studies have pointed to integrin clustering as a key driver to cell response in dynamic hydrogels. For example, Chaudhuri *et al.*[23] reported on a Ca^{2+} crosslinked alginate hydrogel whose viscoelasticity was varied through manipulation of the alginate molecular weight and addition of PEG crosslinkers. The viscoelastic response for $\tau_{1/2}$ ranged from ~1 min to ~1 hour. With an initial modulus of 9 kPa (*G*), NIH/3T3 fibroblasts extended their processes (e.g., filopodia) into the hydrogel and spread after 7 days in hydrogel with a $\tau_{1/2}$ of 70s. Longer relaxation times of $\geq$170s forced a circular shape. The degree of cell spreading was further improved by introduction 10x RGD sites for the fast-relaxing hydrogels. This study also investigated encapsulated MSCs to determine the time-dependent response on differentiation. Soft hydrogels (9 kPa, G) supported adipogenesis while stiffer hydrogels (17 kPa, G) supported osteogenesis. Moreover, soft and slow relaxing hydrogels supported adipogenesis, while stiff and fast relaxing hydrogels supported osteogenesis. The latter was determined to be due to clustering of RGD ligands enabled by the viscoelastic properties of the hydrogel. This in turn led to integrin clustering which mediated actomyosin contractility and enhanced osteogenesis. In a different study, Wei *et al.*[237] investigated vascular morphogenesis of endothelial cells encapsulated in gelatin and dextran based hydrogels with dynamic crosslinks compared to non-dynamic crosslinks at two different hydrogel stiffness (~200 Pa and ~600 Pa, *G*). Cell spreading and actomyosin contraction was significantly greater in the dynamic and softer (200 Pa) hydrogels. The authors confirmed that cell spreading was mediated by integrin clustering and the formation of focal adhesions. Interestingly, the dynamic hydrogel also induced higher expressions of MMPs, which was necessary for cell spreading and vascular sprouting. The authors further showed that FAK phosphorylation was required for focal adhesion stability, integrin clustering and up-regulation of MMPs. Tong and Yang[36] reported on a PEG hydrogel containing sliding bonds that allowed for dynamic movement of the crosslinks and cell adhesive RGD sites. MSCs were encapsulated in these hydrogels with a modulus of 10 kPa (*E*) and although the cells retained a spherical morphology, extension of thin cellular processes were observed in hydrogels with sliding bonds, but not in statically crosslinked PEG hydrogels of the same stiffness. This result can be attributed to the relatively short distance over which the bonds can slide. The sliding distance is limited to the length of the crosslink. Nonetheless differentiation was enhanced by the sliding hydrogel, which was attributed to integrin clustering afforded by the chain mobility. Taken together, these studies indicate that viscoelastic hydrogels enable cells to aggregate cell adhesive ligands in their environment, which has been shown to lead to recruitment of additional integrins and increases the force that cells can bear and remain attached to their surrounding matrix.[238] Integrin clustering has been shown to have a positive effect on osteogenic

differentiation.[239] Collectively, these findings point to the importance of cells being able to re-arrange their local environment which then guides their fate.

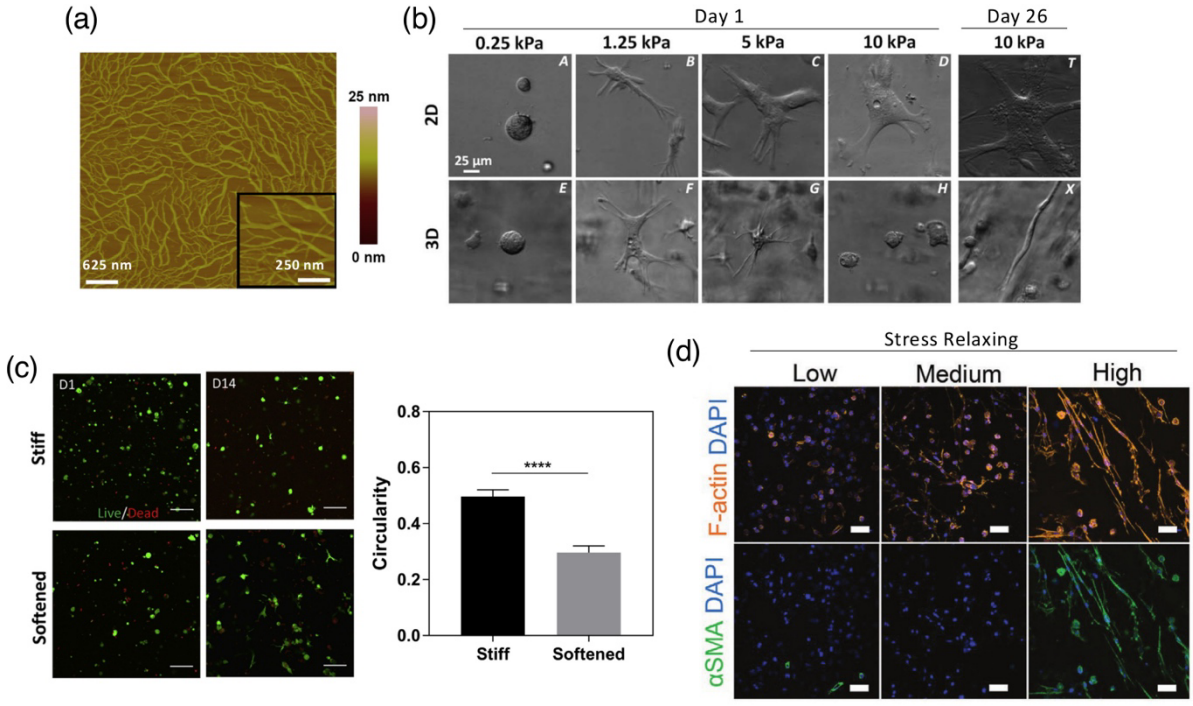

Figure 15. (a) Self-assembling fibrous hydrogels of a KFE-8-RGD peptide shown by atomic force microscopy image; legend is height ranging from 0 to 25 nm. Reproduced with permission from ref [221]. Copyright 2018 John Wiley & Sons Inc. (b) MSCs cultured in 2D or 3D on KFE-8-RGD self-assembling fibrous hydrogels for 1 or 26 days. Reproduced with permission from ref [222]. Copyright 2016 John Wiley & Sons Inc. (c) Morphology of MSCs encapsulated in covalently crosslinked, flexible polymer network containing matrix metalloproteinase-sensitive Sortase A-sensitive crosslinks. Softening was achieved by exogenous exposure to the enzyme Sortase A. Reproduced with permission from ref [62]. Copyright 2019 Elsevier Inc. (d) Morphology of valvular interstitial cells encapsulated in a stress relaxing covalent adaptable hydrogel after five days. Cell spreading is evident in high relaxing gels, which correlated with increased ↣smooth muscle actin. Reproduced with permission from ref [234]. Copyright 2020 John Wiley & Sons Inc.

4.2. Mechano-sensory Mechanisms

The mechanical interactions between a cell and its surrounding hydrogel involve a sequence of well-orchestrated mechanisms occurring at the cell membrane and within the cytoskeleton. We here discuss three of the key mechanisms and their associated sensing elements: the focal adhesion complex, the stress fibers, and the filipodia (Figure 14). Force sensing starts in adhesion complexes, where mechano-sensitive integrins can self-organize in larger complexes depending on the forces applied (or resisted) by the environment. In turn, cells are able to generate traction forces, [240,241] that induce deformation and structural changes in the hydrogel. Studies have demonstrated that cell contraction and architecture are

strongly dependent on the stiffness of their environment, [242–245] where increasing rigidity leads to the generation of significant traction forces. In addition, actin staining procedures have shown that fibroblast contraction is associated with the formation of highly aligned stress-fibers within the cell's cytoskeleton that anchor at the point of cell-substrate adhesion and often span the entire length of the cell. Finally, in 3D networks, cell spreading primarily occurs by the local extension of thin cell processes, known as filipodia.[246] These dynamic structures are constituted of actin filaments that polymerize at the leading edge, while at the same time are pulled towards the cell by actin retrograde flow. We have seen earlier that cell spreading dynamics are mediated by contractile forces, which themselves rely on cell adhesion. This emphasizes a strong coupling between each mechanism, a dynamic that can be explored by the models disused below.

4.2.1 Cell Adhesion and Sensing. Mechano-sensing starts at the cell membrane and its interactions with the hydrogel through adhesion. Specific adhesion usually occurs when integrins establish a physical bond with ligands present in the hydrogel. [247] Integrins have been identified as mechano-sensitive molecules that exhibit a catch bond response, [248] which occurs when a bond's life time is increased by the presence of tension. Models suggest that this behavior is likely responsible for the integrin's capacity to form a strong adhesion complex depending on the stiffness of the microenvironment. To explore the mechanical behavior of integrins, Paszek *et al.*[249] developed a model that describes the integrin-ligand adhesion kinetics and its relation with mechanical forces. The local cell/gel deformation occurring during adhesion was simulated by considering the cell membrane, the glycocalyx, and the hydrogel as networks of elastic springs with different mechanical properties. Integrins on the cell membranes were then assumed to attach stochastically with the hydrogel, thereby triggering elastic deformation, and tensile forces as shown in Figure 16 . To capture the catch bond response of integrin-ligand complexes, the authors considered force-sensitive rates of integrin association k_a and dissociation k_d of the form:

(23,24)

where and are the force-free rate constant, kT is the thermal energy, γ measures the bond's force sensitivity and ΔE is the change of energy that results from bond formation. A binding event triggers the deformation of the cell-glycocalyx-gel assembly, which mediates the force in the integrin and the lifetime of the complex. Simulations involving large numbers of integrins showed that integrand-ligand interactions could become highly cooperative, which resulted in integrin clustering under a proper combination of model parameters. More specifically, this model suggests that the formation of strong adhesion complex is favored by stiff gels and high ligand density, while it may be impaired otherwise.

Studies by Deshpande *et al.*[250] similarly used this idea within a continuum framework. In this case, integrin stability was expressed by their chemical potential, which was reduced by the presence of a force (Figure 16b,c). The authors similarly found that integrin clustering gives rise to strong focal adhesion complex on stiff substrates. The model was also able to reproduce a number of experimental features such as the distribution of adhesion complex at the periphery of cells or the positive feedback between cell contractility and the strength of focal adhesion complexes. [251]

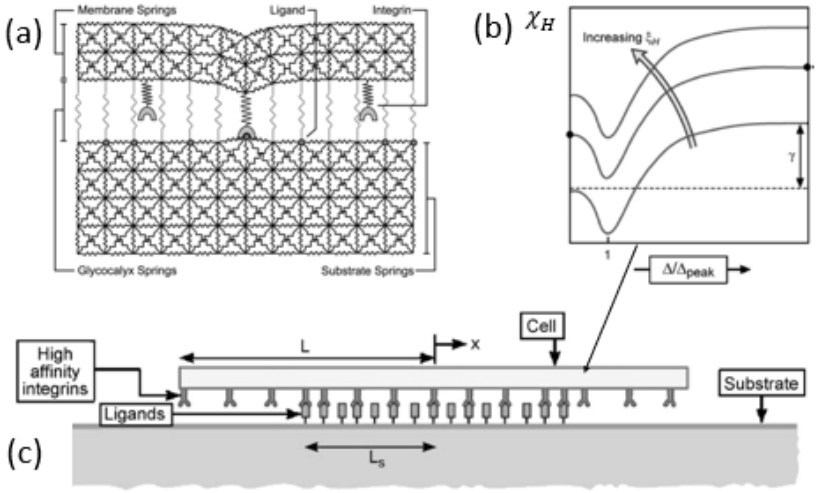

Figure 16. (a) Stochastic model of Paszek *et al.*[252] that considers the random association and dissociation of integrin to surface ligands according to force-dependent kinetics. Integrin stability and clustering then depends on the elasticity of the substrate, glycocalyx and cell membrane. Reproduced with permission from ref [252]. Copyright 2009 The Authors. (b,c) Continuum model of Deshpande *et al.*[253] that simulates the diffusion and force-dependent adhesion of integrins to surface ligands. In this model, the chemical potential χ_H of high affinity integrins is reduced (and therefore integrins are stabilized) when the tension on the integrin-ligand complex reaches an optimal value. Reproduced with permission from ref [253]. Copyright 2008 Elsevier Inc.

4.2.2 Cell Contraction. Once a cell has developed its adhesion complexes, the actomyosin cytoskeleton becomes a central player in the way by which cells sense and respond to their mechanical environment. Several experimental approaches have been developed to quantify the cell traction forces that are generated on the surrounding environment. [254] We highlight two approaches here: elastomeric micropillar arrays and traction force microscopy. Because of the difficulty in measuring precisely the mechanical forces generated in 3D, cells seeded on arrays of micropillars have been used. [255] Cells attach to pillars through focal adhesions as a result of integrins recognizing and binding to adhesive ligands on the

pillars. This engagement leads to cytoskeletal re-arrangement and stress fiber formation, which eventually generate traction forces and cause the pillars to bend. The force generated is dependent on the shape, density, and mechanical properties of the pillars. A seminal paper by Tan *et al.*[217] showed that cells generate force within a few minutes of attaching to substrates, indicating that this process of cell adaptation can occur rapidly. Moreover, the authors found that the average force applied to each pillar, increases with increasing cell spreading area. [217] Other studies have shown that increasing pillar stiffness can increase the average force applied to each pillar for a given cell spread area. [218] This means that cells can generate greater traction forces in response to a stiff substrate, but cell morphology does not necessarily have to change. Traction force microscopy has been used to assess local deformation of a hydrogels as cells pull on the matrix during cell spreading in 3D in hydrogels. [59] In this approach, fluorescent microspheres are embedded into the hydrogel along with cells and movement of the beads is tracked during cell spreading. Using this approach, bead displacement in a covalently crosslinked degrading hydrogel was greatest in the immediate area surrounding cell protrusions. While bead displacement was significantly reduced around spherical cells in a non-degrading covalently crosslinked hydrogel, the displacement was non-zero suggesting that even spherical cells may cause some deformation in the hydrogel. While this method enables assessment of hydrogel deformation, it is difficult to quantify the absolute traction forces generated by the cells.

To better understand the mechanisms underlying cell contraction and cytoskeletal organization, a number of theoretical and computational have been developed. An important feature of these models is that they are based on simple hypotheses but are able to predict complex cell behaviors. They can therefore be used to interpret experimental data, test hypotheses, and explore situations that would be challenging to investigate with experiments alone. Despite the variety of approaches, all of them are based on a similar concept: the contraction of a cell is dictated by its stress-fiber cytoskeleton, whose direction and level of tension aim to reach a targeted homeostatic state mediated by mechanics. In this context, one of the earlier models was developed by Zemel *et al.*,[256,257] where cells are represented as contractile force dipoles embedded in an elastic medium (Figure 17a). The moment generated by cells is captured by the tensor $P_{ij} = f_i$ where f_i indicates the average direction and magnitude of contractile forces while specify the distance over which this contraction acts. The presence of this dipole induces an elastic deformation in the hydrogel which induces cells to reorient in order to maintain an optimal level of tension within their cytoskeleton. This minimal model could predict that the average orientation and contraction of cells as a function of the elastic properties of the matrix. This model was also extended to

predict the effect of applied forces on the gel, as well as the effects of boundary conditions, such as the shape of the gel and the application of prescribed displacement on its boundaries. To explore the origin of mechano-sensitivity within the cytoskeleton, Vernerey and Akalp [258] presented a structural (network) model of a cell, where each strand was representative of a stress-fiber. Starting from the sliding filament theory,[259] they explored the role of a mechano-sensitive element within the actin-myosin bond, that increases its life-time under tension [260,261] (therefore characterized as catch-bonds). The authors simulated the contraction of this stress-fiber network against a substrate of micropillar whose stiffness could be modulated. They found that when a stress-fiber contracted against a stiff-substrate, it could develop the appropriate level of tension to stabilize the acto -myosin bond and the overall fibrous assembly. This in turn, generated a higher level of contraction along stiff directions in agreement with experimental observations that contraction increases with gel rigidity. Despite its simplicity, this model could reproduce the overall organization and density of stress-fibers in a cell for various pillar stiffnesses [258,262] (Figure 17b).

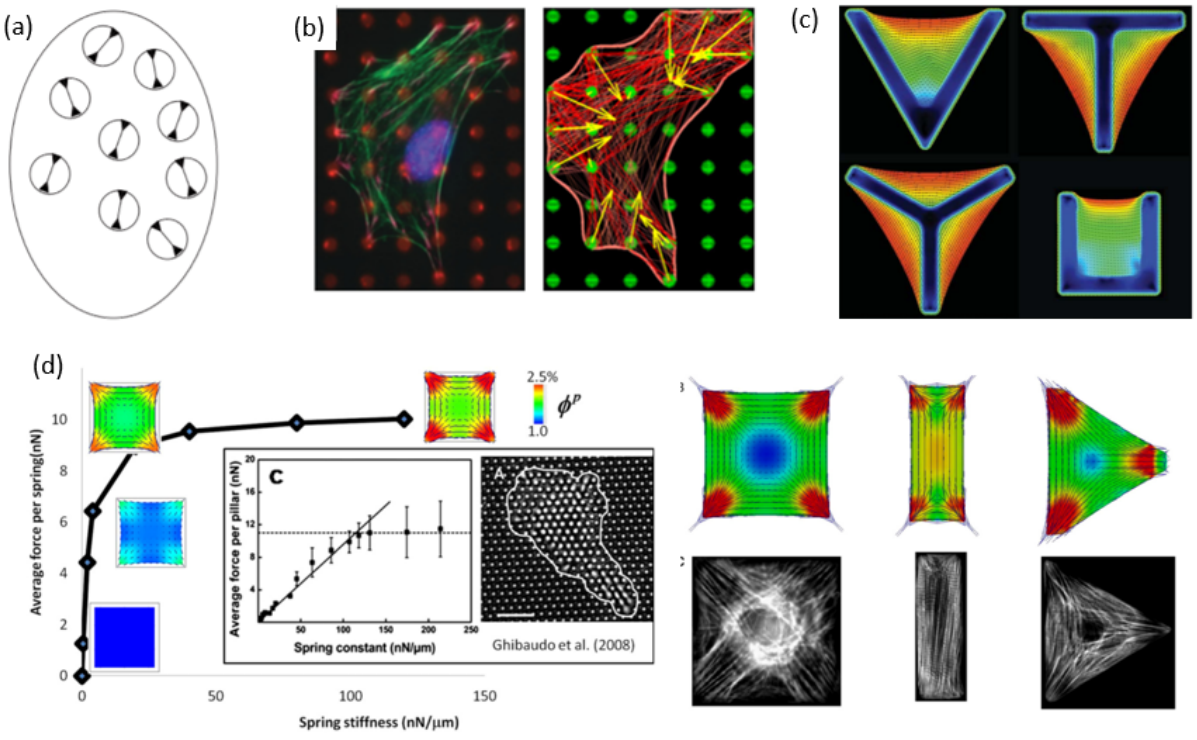

Figure 17. Illustration of the cellular-scale models of mechano-sensitivity. (a) The active dipole model predicts the alignment of cells from a positive feedback mechanism with their elastic environment. Reproduced with permission from ref [256]. Copyright 2007 American Physical Society. (b) Prediction of the model on the effect of catch bonds on the stabilization of the cytoskeleton in a contractile cell with the rigidity of its substrate. Reproduced with permission from ref [258]. Copyright 2016 American Physical

Society. (c) The bio-chemo-mechanical model predicts the local stress-fiber organization and contraction depending on its mechanical and geometrical environment, by postulating a tension dependent degradation of the stress-fibers. Data are reproduced with permission from ref [253]. Copyright 2008 Elsevier Inc. (d) The constrained mixture model is based on a similar hypothesis, but also consider the limited quantity of actin in the cytoskeleton. Simulations can predict the increase in stress-fiber activation and contraction as a function of substrate stiffness (as observed by Ghibaudo *et al.*[263]), and the stress-fiber organization in different geometrical environments. Reproduced with permission from ref [264]. Copyright 2011 Elsevier Inc.

Despite its fibrous nature, the cytoskeleton has also been described as a continuum, where the presence of stress-fibers and other filament are represented by the density and orientational distribution. The advantage of this class of models is that fundamental laws, such as momentum and mass conservation can be enforced, while specific constitutive relations can be explored to capture the feedback interactions between stress-fiber polymerization, dissociation, and their contraction against an elastic microenvironment. In this context, the constrained mixture model [264,265] (and its extentions [266]) and bio-chemo-mechanical models[267] are based on two main mechanisms: (a) a stress fiber exerts a contractile force that is described by the Hill model [268] in the form $T = T^0(1 + k_v/\eta(\dot{\epsilon}/\dot{\epsilon}^0))$ where T^0 is the isometric tension, $\dot{\epsilon}$ is the strain rate, and other symbols are model parameters. (b) The presence of stress fiber in a specific direction is promoted by tension. In the mixture model, this was expressed by writing the rate of stress-fiber polymerization Γ as a first order kinetic equation, that depends on the level of fiber tension T:

$$\Gamma = k_a(1 + \frac{T}{T^0})c^m - k_d c^p \tag{25}$$

where c^m and c^p are the concentration of actin in its monomer and polymer form, respectively, while k_a, k_d are binding/unbinding rate constants and T^0 is a material parameter. In the bio-chemo-mechanical model,[269] force-dependent stress-fiber assembly was enforced by stating that the rate of stress-fiber activation η was reduced with tension:

$$\frac{d\eta}{dt} = Ck_a(1 - \eta) - k_d(1 - \frac{T}{T^0})\eta \tag{26}$$

where C is an activation signal that decays over time. Both models therefore postulate that if a stress-fiber is able to generate an appropriate level of internal tension (by contracting against a stiff substrate for instance), new filaments will be recruited in this direction. This is represented by an increase in association rate in eq 25, but a decrease in the dissociation rate in eq 26 . Finite element implementation of both the

mixture and the bio-chemo-mechanical were developed to explore mechano-sensitivity in various situations as shown in Figure 17c,d. Generally, simulations could predict the local organization of stress fiber in a cell, as well as its local contraction when adhering to an elastic substrate. For instance, it could explain the rise in cell contraction when a cell adhered to micropillars of increasing stiffness [264,267] (Figure 17d) or the correlation between boundary conditions, cell shape, and stress-fiber organization and contraction (Figure 17c).[264,270] Taken together, these models point towards the existence of a positive feedback mechanisms where the contraction of stress-fibers may or may not promote their stabilization, depending on their ability to maintain a "healthy" level of tension. Simulations show that the stiffness of the microenvironment, together with the presence of adhesion molecules, are key players to maintaining this tension.

One explanation for the differences in the mechano-sensing capabilities between cells cultured in 2D versus 3D environments is the microtubule cytoskeleton, which is considered the core of the cell structure. In 2D cultures, cells respond to their environment by remodeling the actomyosin cytoskeleton while the microtubule cytoskeleton is largely insensitive to the underlying substrate. [271] Remodeling of the actomyosin cytoskeleton may be dominated by cell spreading events, while microtubules may help the cell to sense the mechanical environment in the absence of cell spreading. [272] Studies have reported that microtubule polymerization in 3D hydrogels affects differentiation of MSCs encapsulated in hydrogels that limit cell spreading. Notably, inhibiting microtubule polymerization eliminated the stiffness dependence that promoted osteogenesis and suppressed adipogenesis of MSCs encapsulated in covalently crosslinked PEG-hyaluronic acid hydrogels (modulus 0.5-12 kPa). [273] From a modeling view point, this is consistent with the tensegrity model [274] of the cytoskeletal network, which describes the mechanical equilibrium between actin filaments (in tension) and microtubules (in compression). In this model, microtubules can hold a large portion of the contractile stresses generated by actin and can therefore determine the stability and mechanical properties of the cytoskeleton. A recent model [275] indeed suggests that microtubules can act as force sensors in plant cells, and may thus be implicated in the force-sensitive element expressed in eq 25 and eq 26.

4.2.3. Cell Contraction Induces Cell Spreading. Cell spreading starts from the extension of lamellopodia (in 2D) or filipodia (3D) that are dynamical processes driven by the balance between two competing processes: (a) the polymerization of actin and microtubules to generate protrusion forces that push the cell membrane forward and (b) the actin retrograde flow which resists growth by pulling the actin filaments towards the center of the cell. To understand the mechano-sensitivity of protrusion growth observed experimentally, two classes of models were introduced. On the one hand, the motor-clutch

model concentrates on retrograde flow and its dependence on mechanics. On the other hand, the Brownian ratchet model focuses on the process of actin polymerization.

The motor-clutch model[276] is based on the idea that retrograde flow is itself controlled by two competing processes. On the one hand, the contraction of F-actin bundles at a given rate $v_{filament}$ pull actin towards the cell center. On the other hand, the adhesion of the F-actin filaments to the substrate (at the leading edge,) is controlled by dynamic molecular clutches that periodically associate and dissociate with turn-over rates k_a and k_d (Figure 18a). When a clutch adheres to the substrate, it can elastically resist the retrograde flow while inducing a local strain x_{sub} of the cell substrate. This resistance is however mediated by substrate stiffness if the clutches are force sensitive, such that its dissociation rate k_d is accelerated with force according to Bell's law:

(27)

where , γ and kT are the force-free dissociation rate, force sensitivity and thermal energy, respectively. Simulations show (Figure 18b) that when the substrate is soft, the clutches exhibit a "load-and-fail" dynamics, which results in slow retrograde flow. By contrast, a stiff substrate is associated with "frictional slippage," and high retrograde flow. Taken together, this model shows that these clutches can create a frictional slippage adhesive region allowing actin polymerization to advance filopodial protrusion at the leading edge. The motor-clutch model was recently extended to explore the role of the substrate viscoelasticity[277] by replacing the elastic spring with a Zener model comprised of two elastic springs and a dashpot. It was found that viscosity does not play a major role on stiff substrate but can become a major player in soft substrates. Indeed, in the low stiffness regime, the model predicts that when the relaxation time of the substrate is on the order of the time scale of clutch dynamics, viscous substrates appear stiffer to the clutches, and promote cell spreading. This is consistent with experimental observations showing that cell spreading is only sensitive to the hydrogel viscosity if the relaxation time is short enough.

In contrast to the motor-clutch model, the elastic Brownian Ratchet model aims to provide a physical explanation for the change in protrusion velocity under external forces. [278,279] At the tip of a filipodium, the polymerization of actin filaments operate against the elastic force f of the membrane (Figure 18c), such that protrusion velocity V decreases exponentially with f as:[278]

$$V = k_p \delta \exp\left(-\frac{\alpha f \delta}{kT}\right) \tag{28}$$

where δ is the half monomer size, k_p the force free polymerization rate and α a model parameter. When the contraction of the F-actin filaments are considered however, we see the appearance of a new force

that effectively reduces the membrane's resistance. [280] Therefore, the model predicts an acceleration of cell spreading with contraction. This effect was observed in simulations that combined the cell mixture model and the Brownian ratchet model [280] (and other models [281,282] based on a similar idea) providing a rational explanation of the relationship between cell spreading area and the substrate stiffness observed experimentally in 2D cultures using micropillars [263] (Figure 18d). One limitation of studying cell spreading in 2D using micropillars is that they contain homogeneously coated substrates, which do not capture the heterogeneous 3D geometry of fibrous scaffolds or spatial heterogeneities in cell adhesive sites in degrading crosslinked hydrogels. Important insights to cellular behavior in wound healing, development and cancer metastasis, and regenerative medicine require a better understanding of cellular behavior on 3D environments whose direct observation is hindered by challenges with quantifying high resolution images. More recently, one solution to this problem has been to design adhesive micropatterns with specific geometries that incorporate corners and gaps to recapitulate *in vivo* cell spreading behavior like turning of corners and matrix bridging using high-resolution 2D matrices. [283] Kassianidou *et al.*,[283] used a combination of adhesive micropatterns and stress-fiber time lapse imaging to link cell spreading to ECM geometry and initial cell position with respect to the adhesion sites. The authors found that corners considerably slowed spreading due to cell rotation that is often observed in the fibrous hydrogels. The authors also found that stress fibers locally align in the direction of the advancing edge of the cell as it spreads, indicating that the memory of spreading in a given direction can be encoded within their stress-fiber architecture. These findings were further supported by prediction of the spreading trajectories and shape dynamics using computations from the Cellular Potts Model, [284] where cells are represented as deformable objects mapped onto a lattice and each lattice point can either belong to the cell or the surroundings, which have the option to be adhesive. The model considers the combined effects of (a) surface tension due to the action the plasma membrane and the underlying actin cortex wrapped around the cell body which draws the cell periphery inward, (b) line tension due to the effect of accumulated actin filament bundles at the edges that drives to straighten the cell periphery, and (c) adhesion energy of the environment. Cell spreading is simulated by using a Metropolis algorithm to change randomly a lattice site at cell peripheries and whose acceptance probability is given from the energy functional:

(29)

where σ_{st} is the surface tension which scales linearly with the cell area A and the simple line tension λ_l is proportional to the cell perimeter l. The third term accounts for an additional elastic line tension arising in free curved arcs of length L_i with an associated elastic modulus E_a and rest length $L^0_{,i}$. Lastly, the adhesion

energy E^0 in adhered area A_{ad} reduces the energy penalty to allow spreading, i.e., the cell prefers to adhere than spread. The mechanistic insights on the interplay between gain in adhesion energy and cell tension was found to reasonably predict the experimentally observed spreading trajectories. Particularly, the study showed good agreement with experiments where low concentrations of blebbistatin that support cell spreading and stress-fiber formation decreased the line tension of spreading edges but had no measurable effect on the actin bundle rigidity and surface tension. Taken together, these models indicate that cell contraction, cytoskeletal rearrangement and spreading are tightly coupled mechanisms. We also note that regardless of the model, there is a general agreement that the mechanosensing elements are based on force-sensitive bond association and dissociation at some level. All models also tend to agree that stiffness promotes cell adhesion, stress-fiber contraction, and cell spreading through positive feedback mechanisms.

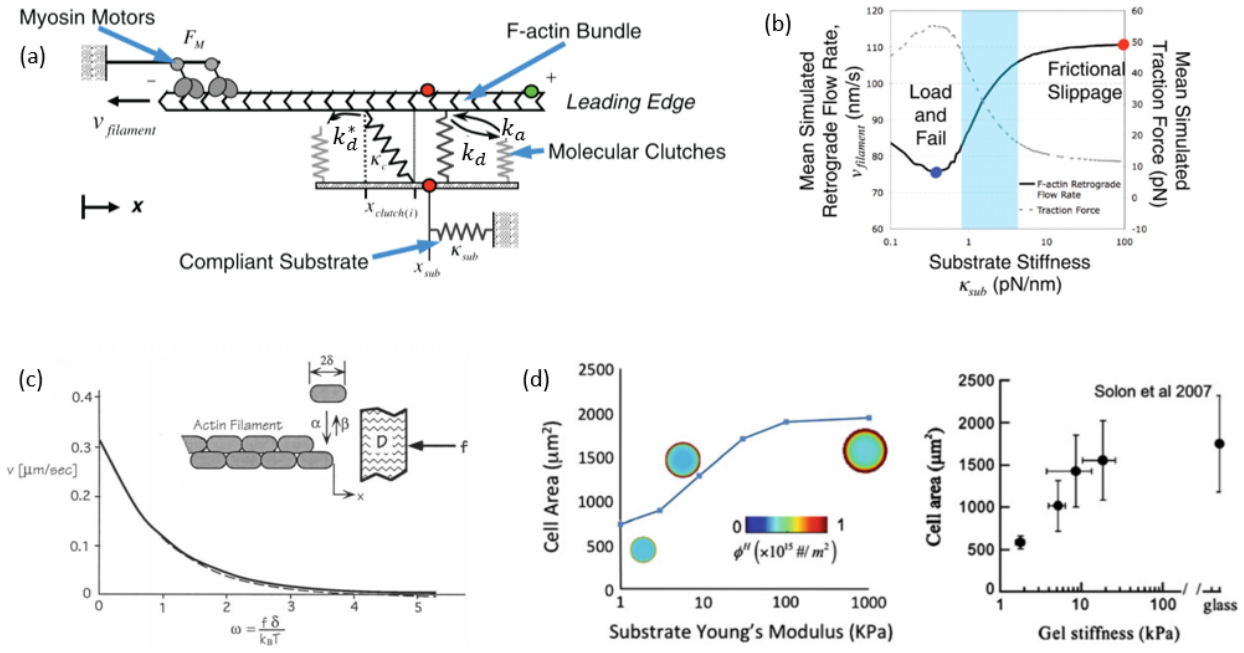

Figure 18. (a) The motor-clutch model couples F-actin contraction, cell adhesion through molecular clutches and substrate elasticity. Reproduced with permission from [276]. Copyright 2008 The American Association for the Advancement of Science. (b) It predicts a load and fail clutch dynamics and slow retrograde flow at low substrate stiffness and a frictional slippage mechanism with fast retrograde flow at large substrate stiffness. Reproduced with permission from ref [276]. Copyright 2008 The American Association for the Advancement of Science. (c) The Brownian ratchet model predicts that velocity of protrusion growth from a force dependent actin polymerization process. Reproduced with permission from ref [278]. Copyright 1993 Elsevier Inc. (d) When this concept is integrated with the above models of cell contractility, it can predict the stiffness-dependent dynamics of cell spreading [280] observed experimentally for fibroblasts.[245] Reproduced with permission from ref [280]. Copyright 2013 Springer Nature.

4.2.4. Mechanical Confinement Restricts Cell Spreading. Another major factor that influences cell spreading in 3D environment is mechanical confinement. In biological ECM and fibrous tissues, cells often need to squeeze their processes through very small pores and tight fiber networks in order to spread.[285,286] When encapsulated in a dense chemically crosslinked network, the mesh size is however too restrictive for cells to extend their processes. In this case, cell spreading can occur in two conditions. First, if the gel is physically weak or if it consists of reversible bonds, it may yield under the effects of protrusion forces and enable some amount of spreading. Second, if the gel can be locally degraded by cell-mediated enzymes, this provides additional space for protrusion growth. Computational models of these processes that describe mechanical confinement have been developed with a focus on cell migration; they are therefore described in Section 5. The idea of mechanical confinement can also be used to guide anisotropic cell contraction and spreading. Reconstituted networks of aligned and well-organized semi-flexible polymers can provide topographies that influence and control cell spreading. Computational models[287] have shown that cells are indeed sensitive to topography and curvature of local structural features, such as fibers and channels. This is confirmed by experimental work where hydrogels were infused with aligned nanofibers which dictated cell spreading alignment. [288]

4.3. Outlook: Tuning Hydrogels to Drive Mechano-sensing and Cell Fate

Hydrogels are a powerful model system to study the mechanisms by which cells sense their mechanical environment in 3D owing to their vast tunability. For example, the architecture of the hydrogels can be tuned to mimic the fibrous structure of native ECM using semi-flexible polymers, but these often have a limited range of material properties. On the other hand, chemically crosslinked hydrogels formed from flexible polymers offer a vast range of possible properties such as hydrogel stiffness, stress relaxation behaviors, and controlled cell adhesivity, but tend to create a tighter mesh surrounding the encapsulated cells. One of the major responses of a cell to its mechanical environment is changes in cellular morphology (i.e., cell spreading). A common finding amongst all types of hydrogels is that cell spreading is permitted in soft hydrogels, with many studies employing hydrogels that have a stiffness are in the range of 100's Pa to 1's kPa (G). In soft fibrous hydrogels, it is clear that cell spreading is rapid, often occurring within one day owing to the open network and the physical crosslinks that allow cells to re-arrange the hydrogel network. At the same time if the hydrogel is too soft, the cells are unable to generate enough traction force to induce the molecular events that lead to actin polymerization and cell contraction. Interestingly, this

observation appears to be limited to the fibrous hydrogels, as cell spreading in soft flexible hydrogels has been observed. On the contrary, when cells are encapsulated in conventional hydrogels, the mesh size presents a significant barrier, requiring much longer (i.e., days) for cells to begin to spread. Cell spreading, however, is limited to hydrogels that are degradable or have reversible bonds; irreversible and stable bonds prevent cell spreading due to the tight mesh irrespective of the stiffness of the hydrogel. This observation can be attributed to the fact that the mesh size even in the softest hydrogels remains too small for filopodia to infiltrate. While spreading can occur in stiffer hydrogels ~>1's kPa, cells require much longer times to degrade the crosslinks of the hydrogel and/or to remodel more of the fibrous network.

Cell sensing requires that cells engage their integrins with ligands in the hydrogel. Mathematical models have provided key insights into the force-sensing mechanisms, identifying for example the role of catch-bonds in the integrin-ligand bond and the importance of integrin clustering to enhance cell contraction. It is important to note that the majority of the mathematical models that describe focal adhesions, cell contraction and cell spreading have utilized 2D experiments. While the mechanisms would be similar in a 3D environment, mechanical confinement will be a confounding factor that limits the degree to which cell spreading occurs. Direct comparisons between 2D and 3D environments show that cells encapsulated in soft fibrous hydrogels show largely similar cell spreading behaviors. On the contrary, cell spreading in conventional, chemical crosslinked hydrogels is significantly reduced by mechanical confinement. An alternative mechanism for mechano-sensing in 3D hydrogels with mechanical confinement may rely more on the microtubule cytoskeleton rather than on stress fibers. Therefore, an important focus for future mathematical models is to consider mechano-sensing capabilities when mechanical confinement restricts the number and length of filopodia that can be produced by a cell. Despite a lack of obvious cell spreading in stiffer (i.e., ~1kPa) hydrogels, cells are highly responsive to the hydrogel stiffness that affect downstream pathways and cellular fate.

5. CELL MIGRATION IN HYDROGELS

Cell migration through the ECM occurs as part of development and homeostasis, in response to an injury, and during the progression of disease. Single cells will polarize in response to a chemical gradient (chemotaxis) and/or to a mechanical gradient (durotaxis) that leads to directional migration. Cells may also migrate in mass, which is referred to as collective migration. Here, cell-cell interactions remain intact and chemical and mechanical signals between cells contribute to migration. Collective migration is an important part of development and is observed in for example, branching morphogenesis and vascular

sprouting, and contributes to cancer and wound healing. [289] A significant amount of research in both experimental and computational modeling studies have investigated cell migration in 2D, focusing on the role of substrate mechanics. While these efforts have been critical to understand the direction, speed and nature of cell motion as a function of the substrate, cells in a 3D microenvironment are subjected to very different cues and importantly must operate under mechanical confinement. [290] There is mounting evidence that the mode of migration in a 3D matrix is distinctly different than in 2D. [291,292] These observations affirm that 3D models are paramount to translating knowledge learned *in vitro* to *in vivo*.

There are two distinct modes of cell migration that have been identified, namely mesenchymal and amoeboid migration (Figure 19). Mesenchymal migration is traction-dependent where cells pull on the ECM to create a directional pulling force. In this mode, cells rely on strong adhesive interactions with the surrounding matrix and induce proteolytic degradation and remodeling of the ECM in order to migrate through tissues. In amoeboid migration, cells utilize contractility-driven propulsion, where cells polarize with a leading edge of actin-rich cell protrusions. Actomyosin-mediated contraction occurs in the mid-body of the cell that enables the posterior tail to propel the cell in the direction of the leading edge. [293] This mode of migration utilizes weak adhesive interactions with cells and ECM and is independent of proteolytic degradation. Because this mode relies primarily on force and does not require ECM degradation, ameboid migration is rapid (e.g., up to 1800 m/h in leukocytes [294]) compared to mesenchymal migration (typically less than 60 m/h [295]). For a cell to migrate through a hydrogel, it must therefore be able to deform the polymer matrix in the hydrogel or disrupt the hydrogel crosslinks (Figure 19). The mode of migration will therefore be in part dictated by the hydrogel and its crosslink type. This means that hydrogels with irreversible covalent crosslinks are only permissible to mesenchymal migration as they require local degradation. On the contrary, hydrogels that are formed with physical crosslinks (e.g., semi-flexible networks) and reversible crosslinks (e.g., dynamic bonds) have the potential to support either mesenchymal or amoeboid migration depending on cell adhesivity and traction forces. To understand the role of 3D mechanics on the migration of embedded cells, mathematical models must be able to describe physical interactions occurring not only within the cytoskeleton, but also, how they are influenced by the complex architecture and mechanics of their surroundings (i.e., the hydrogel). For instance, during mesenchymal migration, cells form protrusions that adhere to the polymer network. These protrusions, called filopodia use actomyosin motors to contract in order for a cell to probe the local stiffness of the hydrogel, information that is then utilized to instruct cell motion. These phases of cell migration integrate a variety of mechanisms such as signaling, chemical reaction, and mechanics, [296] making them challenging to model mathematically. In this section, we describe recent experimental

findings with an emphasis on the types of hydrogels employed for mesenchymal migration, amoeboid migration, and instances of their combination. We also summarize key approaches and findings from mathematical modeling studies with a focus on mechanics. Due to the complexity of the models, we refer the reader to the cited references for the details of the model.

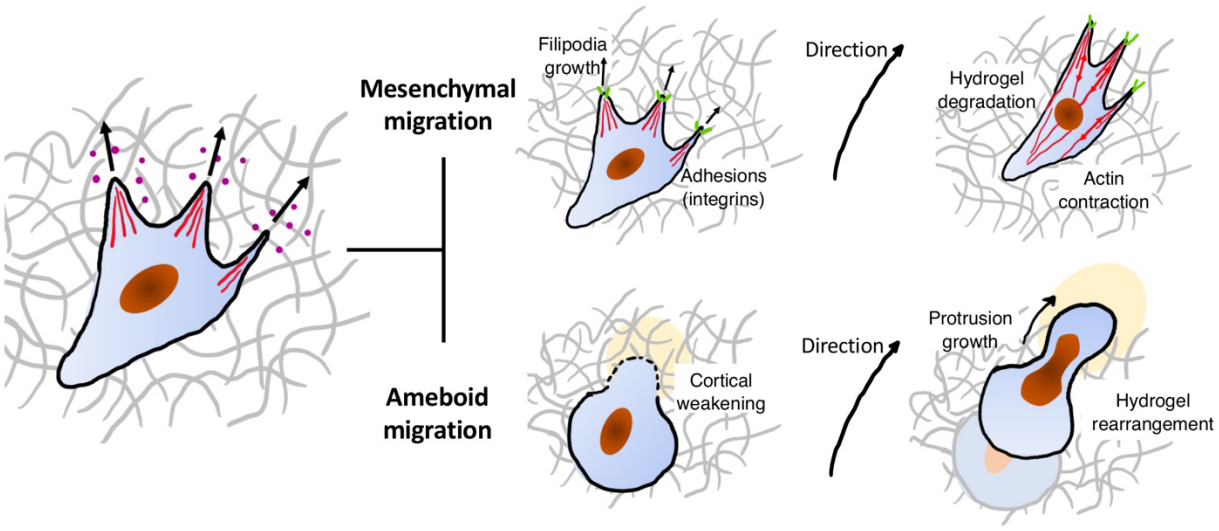

Figure 19. Overview of the two main modes of cell migration in a 3D hydrogel: Mesenchymal migration and Amoeboid migration.

5.1. Mesenchymal Migration

5.1.1. Hydrogel Stiffness. The stiffness of a hydrogel influences two competing processes in mesenchymal migration. The cell must be able to attach to and pull on the matrix of the hydrogel in order to migrate. As such, cells require a certain level of matrix stiffness to generate the traction forces required to initiate migration.[297] At the same time, increasing the stiffness of a hydrogel, through polymer and/or crosslink density, creates a tighter mesh that requires more of the polymer and/or its crosslinks to be degraded in order for a cell to physically be able to move through the polymer network. Proteolytic degradation of the hydrogel can be described by the speed and width of the advancing degradation front, which depend on the susceptibility of the crosslink to its enzyme, rate of enzyme production by the cell, and enzyme transport through the hydrogel (Section 3). Therefore, stiffer hydrogels with a higher cross-link density will produce highly localized degradation and therefore require more proteases to be secreted for a cell to be able to migrate long distances through a hydrogel.

A number of studies have shown that cell migration is indeed inhibited with increasing hydrogel stiffness. For example, Wang *et al.*[298] encapsulated highly invasive MDA-MB-231 breast cancer cells, which are known migrate primarily by the mesenchymal mode, [299] in a collagen-alginate hydrogel. The stiffness was independently controlled through the Ca^{2+} ion concentration (via alginate crosslinking) while the same level of cell adhesion sites could be maintained by the collagen. Using this hydrogel, cell migration was in soft hydrogels (300 Pa, *E*) resulted in speeds of 20 m/h. Cell migration was possible in stiffer hydrogels (20 kPa, *E*), but the migration speeds were slower at 10 m/h. Because the ionic crosslinks in the alginate produce networks with a mesh size that is much smaller than the size of a cell, it is likely that MDA-MB-231 cell migration occurred by a combination of cell-mediated degradation of the collagen and of cells forcibly disrupting the Ca^{2+} crosslinks. The latter would be possible in softer hydrogels. Dubbin *et al.*[300] reported that collective migration outwards from tumor spheroids (i.e., aggregates of cells) that were encapsulated in covalently crosslinked fibrinogen-gelatin hydrogels was inhibited in 1 kPa (*G*), but not in softer hydrogels (~400-500 Pa) hydrogels. The stiffer hydrogel exhibited the slowest degradation by proteases. This result supports the idea that a denser, more crosslinked network, which degrades more slowly, will retard migration. Daviran *et al.*[301] also reported a stiffness dependence on MSC migration in a covalently crosslinked, enzyme-sensitive, PEG hydrogel containing the cell adhesive peptide RGD (Figure 20a). Cell migration speeds in soft hydrogels with an initial modulus of 80 Pa (*G*) increased from ~30 m/h at day 3 to 300 m/h at days 5-6, which can be attributed to cell-mediated degradation of the hydrogel occurring both locally and globally in the hydrogel. Soft hydrogels with low crosslink density will lead to bulk diffusion of matrix-degrading enzymes that results in a wide degradation front and reduces the crosslink density more globally in the hydrogel (Section 3). In turn, as the hydrogel degrades there are fewer crosslinks the cell needs to cleave in order to migrate, hence resulting in faster migration speeds over time. Contrarily, migration speeds in stiffer hydrogels (2.4 kPa, *G*) were significantly slower at ~3 m/h and did not change over the six days, suggesting over this time-frame local hydrogel degradation may have dominated due to the effect of a more tightly crosslinked network on transport. Vasudevan *et al.*[299] encapsulated MDA-MB-231 cells in a covalently crosslinked methacrylated gelatin hydrogel. In this study, the stiffness was varied through the degree of methacrylation, which enabled the concentration of gelatin to remain constant. Cell migration speeds decreased from ~3 to ~1 m/h with increasing stiffness from 1 to 5 kPa (*G*) due to the higher degree of crosslinking. Taken together, these and other studies demonstrate that when cells are encapsulated in hydrogels with cell adhesivity, an increase in matrix stiffness, due to increased hydrogel crosslinking or polymer density, slows cell

migration. While stiffer substrates in 2D also slow migration, this occurs due to stronger and more stable focal adhesions to stiffer substrates. [302] These observations indicate that mesenchymal migration in 3D hydrogels is dominated by the degradability of the hydrogel.

5.1.2. Cell Adhesivity. Mesenchymal migration requires that cells interact with a hydrogel through integrin-ligand bonds. The type and density of cell adhesion ligands in a hydrogel will influence cell migratory behavior. For example, Ruud *et al.*[303] investigated invasion of MDA-MB-231 cells through different types of natural fibrous hydrogels and found that a laminin-rich matrix promoted greater invasion compared to a fibrillar collagen I-rich matrix. Interestingly, the number of cellular protrusions was significantly lower in laminin-rich matrix when compared to collagen-rich matrix. One possible explanation is that the cell adhesion was stronger with collagen, [304] and therefore favored cell spreading over cell migration. Anguiano *et al.*[305] showed similar results for H1299 lung cancer cells that were encapsulated in collagen hydrogels with and without Matrigel (Figure 20 b). Migration was slower in collagen gels when compared to collagen gels prepared with Matrigel, which contains laminin among other proteins. However, too much Matrigel hindered migration. The authors further showed greater contraction of the hydrogel containing Matrigel indicating that while cells created greater traction forces with Matrigel, higher concentrations of Matrigel led to fewer, but larger focal adhesions that hindered cell migration. Ho *et al.*[306] showed that the extent of MSC migration from encapsulated spheroids in an alginate hydrogel crosslinked with Ca^{2+} ions was greater with decreasing RGD concentration (comparing 4 to 0.8 mM) while keeping hydrogel stiffness constant at ~12 kPa (*G*); although cell migration speeds were not determined. However, He *et al.*[307] created a gradient in RGD within a covalently crosslinked, enzyme-sensitive PEG hydrogel (from 0.5 to 1 mM) while maintaining a constant hydrogel stiffness (600 Pa, *E*). When endothelial cell spheroids were encapsulated in this hydrogel, the length of vascular sprouts (arising from endothelial migration) after seven days was greater in the direction of increasing RGD. However, the authors did not assess the rate of vascular sprouting over the course of seven days. It is possible that tethered RGD ligands in the hydrogel provided a haptotaxis cue to drive migration in the direction of increasing ligand concentration. Here, haptotaxis is defined as directional cell migration typically up a gradient in cellular adhesion sites. An alternative explanation is that the lower concentrations of RGD permitted faster migration initially, as suggested by the study by Ho *et al.*,[306] but that cell migration could have slowed as the cells reached higher RGD concentrations. Nonetheless, these studies indicate that cell migration is influenced by both overall ligand concentration and gradients in ligand concentration. Hung *et al.*[308] encapsulated MSC spheroids in ionically crosslinked alginate hydrogels of varying stiffness and RGD concentrations and examined collective migration. The authors found that in the absence of RGD, there

was no migration observed outward from the spheroids regardless of hydrogel stiffness (1 to 15 kPa, G), which is consistent with the need for cells to attach to a matrix in mesenchymal migration. However, the authors found that stiff hydrogels (15 kPa, G) with high RGD supported collective migration, while migration was inhibited in low stiffness (1 kPa, G) hydrogels regardless of RGD concentration. These findings appear to be in contrast to other studies. Mesenchymal migration is clearly involved owing to the requirement of RGD. However, the ionic crosslinks of alginate result in mesh sizes that have been shown to restrict cell spreading; thus, one would expect that it would also inhibit cell migration. Alginate does not degrade by proteolysis, but its viscoelastic response enables the ionic crosslinks to be disrupted if under a sufficient force. Collective migration has been shown to generate greater force on the surrounding matrix compared to a single protrusion emerging from a cell, [309] which could have enabled cell migration. In the low 1 kPa hydrogels that did not support migration, it is possible that the cells were unable to generate sufficient traction forces to induce cell migration, despite the fewer crosslinks that need to be disrupted. Taken together, these studies point to the type of cell adhesivity as playing a significant role in migratory capabilities and a biphasic role of adhesivity where too low or too much can hinder migration.

5.1.3. Combined Role of Adhesivity and Stiffness. Mathematical models can offer insights into the dependence on mechano-sensing through hydrogel cell adhesivity and stiffness when cultured in a confined environment. Most reduced models of mesenchymal migration represent the cell as a single particle whose speed depends on the balance between protrusive forces, traction forces, and drag from the environment.[296,310,311] In these models, the protrusion force arises from two distinct phenomena: (a) the polymerization of actin, that occurs at the front of the cell (i.e., in the direction the cell is migrating) and (b) the adhesive forces between the cell and the hydrogel at the tip of the new protrusion. Opposing traction forces are exerted on the front and back of the cell, which depend on both hydrogel stiffness and ligand density. Finally, the drag force is expressed by a pseudo-viscosity coefficient, that depends on cell shape. This model could predict the random walk nature of a cell migrating in 3D and the non-monotonic relationship between cell speed, ligand density and matrix stiffness. More specifically, the model showed that cell migration exhibits a biphasic relationship with adhesivity, wherein extreme adhesion (whether high or low) will restrict cell motion, suggesting that there is an optimal level of adhesion that maximizes migration speed. This finding was attributed to the balance of pulling forces at the cell front and detachment forces at the back, necessary for migration. A low ligand concentration does not allow the cell to exert enough pulling force for motion, while too high of a concentration inhibits detachment at the back. The authors further found that stiffness plays a significant role in this process where low stiffness induce lower traction forces and decrease migration speed, while high stiffness enable more stable

adhesion and prohibit cell detachment at the back. In agreement with the above experiments, the model therefore predicts that there is an optimal stiffness for cell to achieve an efficient migration speed. Taken together, this class of models allow for a quantitative understanding of how cell adhesivity and stiffness play inter-dependent roles in mesenchymal migration.

5.1.4. Durotaxis. Cell migration in the direction of an increasing stiffness gradient is termed as durotaxis. In 2D culture, cells typically move along the gradient from a soft to a stiff environment. [312] While studies have shown that durotaxis occurs *in vitro*, there is no evidence as of yet of cellular durotaxis *in vivo*. There are, however, examples of stiffness gradients that form during development and in disease and therefore durotaxis is thought to have a role. [313] A complicating factor for durotaxis during mesenchymal migration in 3D is that cell migration requires proteolytic degradation. In addition to the experiments described previously, He *et al.*[307] also encapsulated a spheroid of endothelial cells in a covalently crosslinked, enzyme-sensitive, PEG hydrogel containing a constant concentration of RGD, but with a stiffness gradient. The study found that vascular sprouts of migrating endothelial cells were longer in the direction of decreasing stiffness, suggesting reverse durotaxis. [314] This finding is consistent with prior work which showed that neurite outgrowth in 3D collagen hydrogels occurred down a gradient of stiffness. [315] Mason *et al.*[316] developed a strategy to decouple the effect of collagen density and collagen stiffness on cell migration in 3D. Using this same approach, Bordeleau *et al.*[317] showed that an increase in collagen density decreased cell migration speed in 3D for both single cells and for cell outgrowth from spheroids. However, increasing collagen crosslinking without altering collagen density showed that migration occurred in the direction of increasing stiffness (i.e., durotaxis), a finding that is consistent with 2D observations. This study therefore demonstrates that durotaxis can indeed occur in 3D. Taken together, these findings suggest that if an increase in crosslinking (and stiffness) does not affect the cell's ability to degrade the hydrogel, then cells will migrate up a gradient in stiffness under durotaxis. However, if an increase in stiffness is accompanied by an increase in the need for a cell to produce more enzymes to degrade the matrix, then the cell will choose to move down a gradient in stiffness under reverse durotaxis.

Computational models[318,319] have been developed to understand the detailed microscopic mechanisms responsible for cell sensing and migration, and their consequences on migration. These models specifically highlight the connection between filipodia mechanics and durotaxis. Stiffness sensing occurs at the level of the filopodium, that can grow through the gel, adhere to it, and probe its stiffness by applying traction forces. As shown in Figure 20 c, the model considers a 3D cell embedded in a discrete network of elastic fibers, whose length and density can be varied. By contrast, the model of Heck *et al.*[319] considered a continuous model for the viscoelastic matrix, and protrusion growth was associated with an

instantaneous degradation of its surroundings (Figure 20 d). In both models, the rules for cell migration are based on the polymerization-driven protrusion of a filipodium through the fiber network (or through a hydrogel), its adhesion to the fibers and a tugging phase, where the cell can sense the local stiffness of the network. This sensing phase is then used to update the next direction of cell migration and the cell polarization. These models provide a fundamental understanding of the meaning of "local stiffness," that stems from both force and displacement felt by the tip of the filipodium. They could predict how this stiffness regulates the number, lifetime, and length of protrusions, and their consequences on migration efficiency. They may also be used to guide experimental effort in developing "structured hydrogels" to optimize the cell-hydrogel interactions for controlled migration. For instance, Kim *et al.*[318] could predict complex situations where cells migrate near sharp (stiff-soft) interfaces and where able to reproduce experimental observation of durotaxis . More specifically, the model could show that a cell will move away from an interface when starting from the stiff side, while it will cross the interface when starting from the soft side. It was also used to explore the role of the number and size of filipodia on cell migration, where many filipodia, characterizing the phenotype of aggressive cancer cells, would promote faster migration. Despite the potential of these models in exploring the role of cell activity and gel structure on migration, they have not yet been combined with models that account for mechanical confinement, which are known to also contribute to the direction and speed of cell migration.

5.1.5. Plithotaxis. Several studies have observed that the application of a constant strain on a hydrogel construct induces embedded cells to move towards the direction of maximum stretch (plithotaxis). For instance, Dietrich *et al.*[320] encapsulated HT-1080 fibrosarcoma cells in a covalently crosslinked PEG hydrogel with RGD and controlled degradation by varying the ratio of enzyme-sensitive crosslinks to non-degradable crosslinks. The authors showed that the effect of stretch is non-monotonic, i.e., it has an significant effect on cell migration when the strains are small, but tend to disappear as the deformation becomes more significant. These results were further explored with the use of a computational model where the gel was represented as a lattice of elastic springs, that could be locally deformed and degraded by a cell whose location when concentrated at a lattice site and its immediate neighbors (Figure 20e).[320] The direction of migration was determined by the concept of durotaxis, i.e., the cell location was moved to a direction that had the strongest local stiffnesses felt by the cell. This model showed that matrix fibers tend to provide a stiffer environment in the stretch direction for lower strains, but that this effect vanished at larger strains, as the perpendicular direction became stiffer as well. This finding therefore suggests that the plithotaxis and durotaxis stem from the same origin, which lays in the nonlinear mechanics of the network.

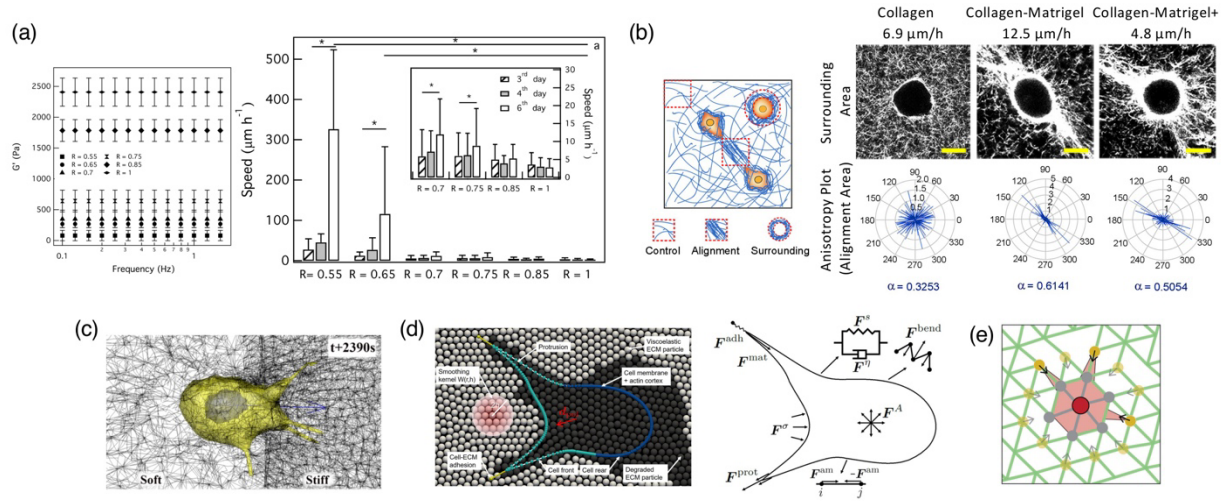

Figure 20. Mesenchymal Migration in 3D. (a) Mesenchymal stem cell migration in a covalently crosslinked, enzyme-sensitive, PEG hydrogel with RGD of varying stiffness. Migration speeds are shown as a function of time after encapsulation. Reproduced with permission from ref [301]. Copyright 2020 American Chemical Society. (b) H1299 lung cancer cell migration in collagen, collagen-Matrigel, and collagen-Matrigel+ (i.e., high concentrations of Matrigel) hydrogels. Migration speeds are reported along with images of cells (black circle) and surrounding fibrous hydrogel (white) in regions surrounding the cell. Direction of the fibers are shown in the anisotropy plot for regions in between cells (i.e., alignment area). Reproduced with permission from ref [305]. Copyright 2020 The Authors. (c-e) Computational models of mesenchymal migration. (c) Migration of a cell in a fibrous environment under durotaxis. Reproduced with permission from ref [321]. (d) Model of the combined migration and degradation of a viscoelastic medium. Reproduced by permission from ref [319]. Copyright 2020 The Authors. (e) Lattice model of cell sensing and migration. Reproduced by permission from ref [320]. Copyright 2018. The Authors.

5.2. Amoeboid Migration

5.2.1. Hydrogel Stiffness. Amoeboid migration is independent of cell adhesivity, but highly dependent on matrix stiffness. Mechanical confinement has been shown to cause a switch from mesenchymal to amoeboid mode of migration, enabling faster migration speeds in 3D. [322] Depending on the crosslink density, the polymer network can apply substantial forces on the encapsulated cells through mechanical confinement. For example, Lin *et al.*[323] showed that encapsulated MSCs in an alginate hydrogel containing RGD and crosslinked with Ca^{2+} ions exhibited a switch in migration mode from mesenchymal to amoeboid. The authors varied the molecular weight of the alginate and the divalent ion concentration to independently control stress relaxing behavior and stiffness. In low stiffness (1.2 kPa, G) hydrogels, MSCs were able to spread, which increased the stiffness of the cell's nucleus and led to lower cell migration speeds. However, when matrix stiffness was increased to 14 and 20 kPa (G), cell spreading

was reduced, nuclear stiffness was lower, and migration was faster, suggesting a uniquely different mode of migration compared to mesenchymal mode (Figure 21a). This study suggests that the viscoelasticity of the alginate hydrogels enabled the cells to forcibly disrupt the Ca^{2+} crosslinks promoting amoeboid migration. Duan *et al.*[324] showed that MSCs encapsulated in a hyaluronic acid hydrogel crosslinked using a mix of reversible and irreversible bonds, but lacking any cell adhesion ligands led to faster migration in hydrogels of 16 kPa compared to 5 kPa hydrogels. Taken together, these studies demonstrate that for amoeboid migration, cell adhesivity is not required and stiffer hydrogels lead to higher migration speeds; the latter, however, depends on the ability of the crosslinks to be broken and/or re-arranged.

5.2.2. Mechanisms. In amoeboid migration, cells randomly grow pseudopods, that are finger-like protrusion that extend, and retract over time. Modeling the pseudopod dynamics is therefore critical to any computational model that aims to understand this mode of locomotion, especially when cells are embedded in a 3D environment and exposed to external gradients. [325] Moure *et al.*[326] proposed a model where pseudopods were generated spontaneously by solving a reaction-diffusion equation for a membrane-bound species, known as inhibitor and activator. This equation is well-known for its capacity to generate spontaneous pattern formation, as observed on cells undergoing ameboid migration. The activation of these species then interacts with actin and myosin present in the cell and initiate internal flows that produced physical forces that subsequently initiated protrusion that could grow, retract, and bifurcate in time. This approach could reproduce many features of ameboid motion as depicted in Figure 21b, even when no chemical gradients were applied. Campbell *et al.*[327] used a similar approach to model locomotion through a fibrous matrix by considering the presence of rigid obstacles (Figure 21 c). The model predicts that unlike in an unconfined medium, the presence of obstacle forces cells to frequently initiate and retract new pseudopod, and to exhibit zig-zag trajectories. Thus, increasing confinement in an already confined environment decreases migration speed by forcing the cell to constantly change direction and may even prevent locomotion if the cell is not sufficiently deformable to squeeze through the pores. The effect of confinement on ameboid migration was also explored with a computational model for the initiation, growth, and retraction of a surface bleb resulting from the dissociation of the actin cortex. [328] Limiting their study to locomotion in a straight channel, Lim *et al.*[329] showed that in this case, adhesion was not necessary for locomotion and that confinement by a microchannel, if not too strong, could increase cell speed. Similar results were found when studying the locomotion of hydrogel particles in confined channels.[330] These findings could help explain faster migration speeds of cells encapsulated in a more tightly crosslinked, stiffer hydrogel, which creates significant mechanical confinement.

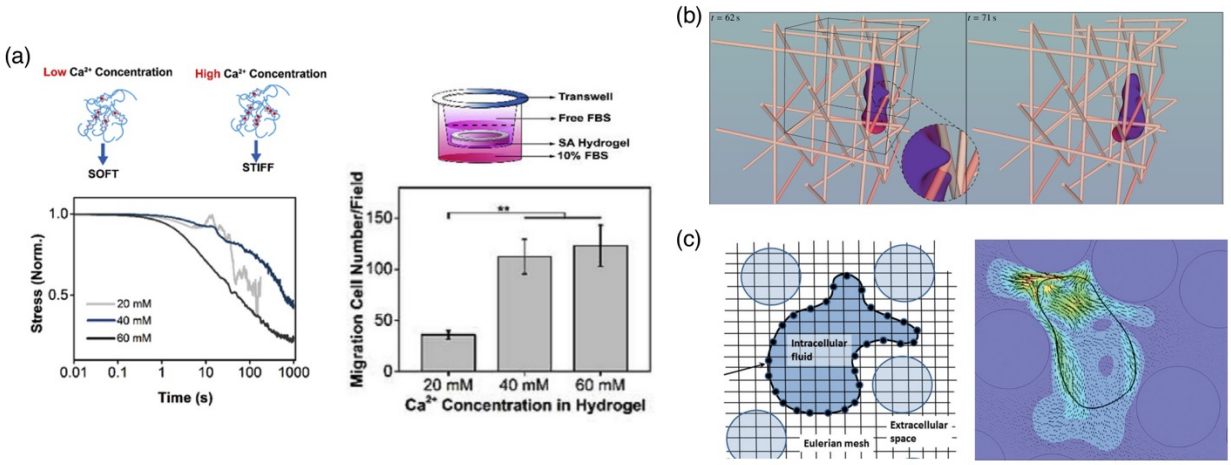

Figure 21. Amoeboid Migration in 3D. (a) Migration of MSCs in an alginate hydrogel containing RGD and crosslinked with increasing concentration of Ca^{2+} ions showed that more cells migrated through the hydrogel in stiffer hydrogels, indicating a switch in migration mode from mesenchymal to amoeboid. Reproduced with permission from ref [323]. Copyright 2019 Elsevier Inc. (b) Simulation of ameboid migration in 3D fibrous networks. Reproduced with permission from ref [326]. Copyright 2017 Elsevier Inc. (c) Amoeboid migration modeled by reaction-diffusion. Reproduced with permission from ref [327]. Copyright 2018 The Royal Society of Chemistry.

5.3. Combined Migration

Depending on the 3D environment, cells can switch from one mode of migration to another, for example between mesenchymal and amoeboid or between single cells and collective cells. An example was already highlighted in the previous section, where MSCs switched from mesenchymal to amoeboid. One of the most well-known phenomena that involves changes in cellular migratory behavior is in the progression of invasive cancers. For instance, the epithelial-to-mesenchymal transition or EMT occurs when epithelial cells undergo a phenotypic change, losing their polarization and cell-cell contacts, and adopting a mesenchymal stem cell phenotype that is characterized by high invasiveness. [331] In EMT, cell migration switches from collective migration to single cell migration and is characterized by increased migratory capacity. As tumors develop and grow, an increase in matrix stiffness is observed. To understand the effects of a dynamically changing environment, studies have utilized hydrogels that undergo a softening or stiffening process *in situ* after cells have been encapsulated. These *ex vivo* models allow one to probe changes in cellular migratory behavior in an environment that mimics the dynamically changing ECM during the progression of disease. For example, Allen *et al.*[332] encapsulated mammary epithelial cells isolated from tumors in an alginate-Matrigel hydrogel that was stiffened by UV-triggered release of calcium chloride ($CaCl_2$) after a pre-defined culture period in the soft environment. Stiffening from 150 Pa

to 1.2 kPa produced an invasive phenotype in encapsulated epithelial cells, which was characteristic of the EMT, and led to increased migration. This behavior is opposite to what was described earlier for mesenchymal migration in 3D hydrogels, which is typically slower with increasing hydrogel stiffness. This study by Allen suggests that mechano-sensory mechanisms may be contributing to the cellular phenotype that leads to cellular changes in migratory speeds.

Several recent reviews have highlighted that cells may exhibit both mesenchymal and amoeboid migration modes, referred to as lobopodial migration.[333,334] In lobopodial migration, cells utilize asymmetric intracellular pressure to generate protrusions on the leading edge similar to amoeboid migration and simultaneously utilize cell traction forces to augment migration. Zuo *et al.*[335] studied collective migration from spheroids of endothelial cells (ECs), smooth muscle cells (SMCs), and their combination when encapsulated in a dual crosslinked hydrogel formed of fibrin and methacrylated hyaluronic acid prepared at different ratios. The EC-SMC spheroids showed the greatest migration over EC -only and SMC-only spheroids. Migration depended on both the interaction with fibrinogen via RGD and with hyaluronic acid via CD44, where equal ratios of fibrin and hyaluronic acid led to the greatest migration when compared to fibrin-dominated or hyaluronic acid-dominated hydrogels. There did not appear to be strong dependence on the matrix stiffness, which ranged from 4-8 kPa. Interestingly, migration required both the cell adhesivity and interaction with hyaluronic acid.[335] Cell adhesivity is required for mesenchymal migration, however CD44 is insufficient at generating traction forces, but is involved in amoeboid migration.[336–338] These findings suggest that the mode of migration may have been lobopodial, a combination of mesenchymal and amoeboid.

5.4. Outlook: Tuning Hydrogels to Control 3D Migration

When cells are encapsulated in 3D within a hydrogel, their ability to migrate, the speed of migration, and the mode of migration depends on a number of factors. Fibrous hydrogels offer a more open polymer network that can enable cells to move through the hydrogel similar to that of native ECM. However to restrict migration to the mesenchymal mode, hydrogels with irreversible bonds are required, but which contain cell adhesivity and enzyme-sensitive sequences found either in the crosslinks or within the polymer backbone (e.g., biopolymers). The speed of migration is dependent on the ability of cells to secrete enough enzymes to degrade the hydrogel such that it reaches its point of reverse gelation locally. If the crosslink density is too high or if the polymer is too dense, cell migration can be prevented. Speed of migration also depends on cell adhesion to the hydrogel matrix. If cell attachment is too strong, cells will

be unable to migrate and instead will remain in place adopting a spread morphology. However, if the cell attachment is too weak, cells will not be able to generate sufficient traction force to pull themselves through the hydrogel and migration does not occur. In most 3D studies, it is difficult to decouple the role of stiffness from the role of degradability, as increased stiffness usually means slower degradability. Most studies point to degradability as the defining parameter of whether cells can migrate and how fast they migrate. Computational models of cell migration, when coupled with models of cell-mediated gel degradation discussed in Section 3 can provide insight into the balance between these competing factors. While modeling efforts in 3D have been limited, the results confirm the importance of cell traction forces in cell migration. However, these models to date have been limited in their ability to address mechanical confinement and the coupled processes of hydrogel degradation.

Tuning hydrogels to restrict the mode of migration to amoeboid is more complicated. For amoeboid migration to be possible, cells need to be in 3D hydrogel where they can push their way through the crosslinks. This means that the hydrogel should be formed from dynamic bonds, such as physical bonds, reversible covalent bonds, or ionic bonds, which can undergo stress relaxation under forces that are equivalent to those generated by cells during amoeboid migration. While limiting cell adhesivity is one mechanism to initially design for exclusive amoeboid migration, many cells can secrete their own matrix (see Section 7) that could introduce cell adhesivity through local interactions. Many of the natural hydrogels or biopolymers inherently have cell adhesivity and therefore could promote either migration mode. A further complicating factor is that many cells can switch their phenotype between amoeboid and mesenchymal migration modes. Here, computational models can play a pivotal role in understanding the mechanisms by which the mechanical environment controls cell migration mode. For example, a stiffer hydrogel with limited cell adhesivity sites would favor amoeboid migration. However, an increase in cell adhesion could favor focal adhesion engagement, actin polymerization, and induce mesenchymal migration over amoeboid migration. Elucidating these mechanisms will be important to understand how cells adapt to their environment during development and disease, such as EMT that occurs during cancer. Moreover, hydrogels can be purposely designed such that only one mode of migration (e.g., amoeboid vs mesenchymal migration or single vs collective migration) is possible, which would allow for deeper studies into how migration mode and cellular phenotype are coupled.

6. CELL GROWTH IN HYROGELS

Hydrogels have emerged as an important *in vitro* model to study cell proliferation and multi-cellular aggregate formation in 3D. A major difference between 2D and 3D environments relates to the concept of confinement. In order to expand, proliferate, or organize into multi-cellular aggregates, cells often need to undergo changes in dimensions. When these changes are physically or geometrically resisted by their environment, cells are said to be mechanically confined. The division or expansion of cells in elastically confined environments indicates that stress may act as inhibitor. As cells embedded within their native ECM will be subjected to mechanical confinement, the 3D hydrogel environment is critical to understanding biological processes and cell signaling that are involved in normal and pathological cell growth. In this section, we first discuss cell growth as single cells when encapsulated in hydrogels as it relates to cell volume expansion and cell division. We then discuss multi-cellular aggregate formation with a large focus on tumor spheroids given the wealth of studies in this area. Finally, we end by discussing new and emerging areas in organoid growth and development in hydrogels. We limit our focus primarily to describing the mechanical effects of the hydrogel on growth, division, multi-cellular aggregate and organoid formation. A summary of the cellular events that lead to cell growth is shown in Figure 22.

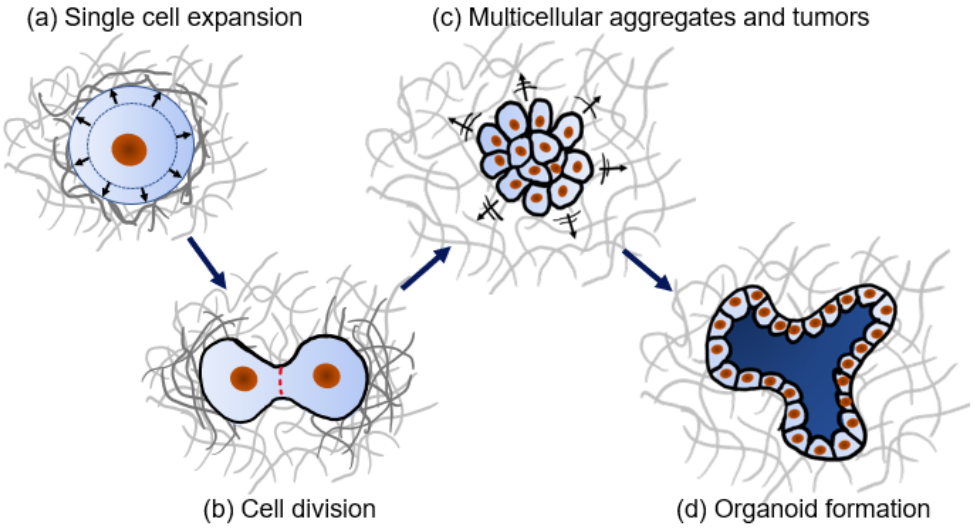

Figure 22. The (a) Expansion and (b) division of a single cell are controlled by the mechanics of the hydrogel in 3D (c) Multicellular aggregates and tumor must overcome the pressure from the hydrogel to expand (d) Hydrogel mechanics and adhesion influences the development of organoids.

6.1. Single Cells

6.1.1 Cell expansion. Cell growth and cell proliferation are tightly regulated processes that involve changes in cell volume [339–341] and are therefore influenced by the surrounding mechanical environment [342]

(Figure 22a). Studies have shown that 2D culture on stiff hydrogels can lead to increases in cell volume, while 3D stiff hydrogels can cause a decrease in cell volume. For instance, Wang *et al.*[298] reported decreased cell volume of MDA-MB-231 cells encapsulated in collagen-alginate hydrogels with increasing stiffness from 0.3 to 20 kPa (E). Changes in cell volume can have pronounced effects on its fate and function. Caliari *et al.*[343] reported non-monotonic cell volume changes of MSCs encapsulated in covalently crosslinked hyaluronic acid hydrogels containing the cell adhesion peptide RGD, where cell volume increased with increasing hydrogel stiffness from 1 to 5 kPa (E), but then decreased in 20 kPa gels (E) (Figure 23a). However, the observed changes in cell volume were accompanied by changes in cell spreading due to the presence of RGD. YAP/TAZ signaling, which is involved in transducing mechanical signals into intracellular signals (i.e., mechanotransduction), [344,345] correlated with both cell volume and cell spreading, but to a greater degree with the latter (Figure 23b). This suggests that cell volume could be contributing to mechanotransduction signaling, but it is difficult to decouple from cell spreading. Major *et al.*[346] encapsulated adipose derived stem cells in a covalently crosslinked methacrylated gelatin hydrogel and demonstrated an inverse relationship between cell volume and hydrogel stiffness. Cell volume expansion strongly correlated with nuclear localization of YAP. Further analysis identified that actomyosin contractile forces, which were inhibited either by blebbistatin or by a small molecule inhibitor of ROCK, were required for cell volume expansion. However, this study also could not decouple cell volume from cell spreading due to the cell adhesivity of gelatin. In an effort to tease out these effects on MSC fate, Lee *et al.*[347] investigated MSCs encapsulated in a viscoelastic and cell adhesive alginate hydrogel and externally altered cell volume by changing the osmotic pressure. The latter was achieved by adding of 400 Da PEG to the solution to create hyperosmotic conditions that decrease cell volume or by diluting the osmolyte concentration of the medium through water to increase cell volume. This enabled decoupling of changes in cell volume from that of cell spreading. The authors identified that cell volume expansion correlates strongly with osteogenesis and was mediated through Trpv4 ion channels and nuclear translocation of the transcription factor Runx2, but not through YAP/TAZ signaling. As studies have linked YAP/TAZ to osteogenesis[348] and other studies have found that YAP/TAZ regulates focal adhesion assembly,[349] these findings suggest that osteogenesis may be induced through distinctly different pathways: one that is integrin-dependent and one that is integrin-independent. However, the extent of the effects on differentiation remains to be determined. This observation is supported by a recent review, which highlighted conflicting reports on the role of YAP/TAZ in osteogenic differentiation. [350] Collectively, these studies suggest that changes in cell volume, which is dependent on the hydrogel stiffness, contributes to mechano-sensing of hydrogels through cell spreading, but also influences other mechano-

sensitive signaling pathways in cells (e.g., ion channels). In other studies on cell expansion, Lee *et al.*[351] encapsulated articular chondrocytes in a stress relaxing alginate hydrogel (3 kPa, *E*) that did not contain cell adhesivity. Within two days post-encapsulation, cell volume was greater in hydrogels with increasing stress relaxation with values of $\tau_{1/2}$ that ranged from 2,114 s (slow relaxing) to 63 s (fast relaxing) (Figure 23c). Cell volume expansion was connected to cell division, which was evident in the fastest relaxing hydrogels. To further study the contribution due to cell volume on cell response, cells in the fast-relaxing hydrogel were exposed to increasing osmotic pressure to prevent cell volume expansion (Figure23 d). The authors could correlate cell volume expansion in the fast relaxing hydrogels and independently in hydrogels under osmotic pressure with decreased catabolic markers, improved cell survivability, and increased ECM deposition (Figure 23e), providing more direct evidence that changes in cell volume affect cell response. In further support of these findings, Lee *et al.*[352] showed an inverse correlation with solution viscosity of hydrogel and cell proliferation, but a positive correlation with cell phenotype. Collectively, these studies and others demonstrate that for a wide range of cell types cultured in 3D hydrogels, the stiffness of the hydrogel is inversely related to cell volume. Since cell volume influences intracellular signaling pathways, hydrogel stiffness affects cells through mechano-sensory mechanisms as described in Section 4 as well as cell volume described in this section.

6.1.2. Cell division. The process of cell division in hydrogels requires that cells either push and deform the hydrogel matrix in order to undergo the initial cell expansion during cell division or degrade the hydrogel to create space for two daughter cells (Figure 22b). Lee *et al.*[351] showed that chondrocyte volume changes (described in Section 6.1.1) were coupled with proliferation in the stress-relaxing alginate hydrogels. The authors showed a strong correlation between an increase in cell volume and increased proliferation (Figure 23f). Wei *et al.*[353] demonstrated that proliferation of MSCs encapsulated in a covalently crosslinked PEG hydrogel depended on the crosslinker type and stiffness. Cell proliferation was minimal with stable crosslinks (0.5 kPa, *G*) and with enzyme-sensitive crosslinks in high stiffness hydrogels (3 kPa, *G*). However, cell proliferation increased by ~2-fold in degrading hydrogels that showed a decrease in stiffness from 3 to 0.5 kPa (*G*). Tan *et al.*[354] encapsulated chondrocytes in PEG hydrogels containing covalent and physical crosslinks that permitted stress relaxation ($\tau_{1/2}$ = 100-300 min). Chondrocyte proliferation was reported in stiff hydrogels of 2.5-8 kPa (*E*). However, a comparison of cell proliferation in softer hydrogels (1.5 kPa, *E*) was not possible due to lower cell viability. Nonetheless, this finding suggests that stress relaxing hydrogels can support proliferation in stiffer hydrogels. Chowdhuri *et al.*[355] reported rapid cell proliferation by ~4.5-fold and ~5.5-fold in 72 hours of macrophages and monocytes, respectively, that were encapsulated in a self-assembling peptide hydrogel with a stiffness of ~2 kPa (*G*).

Interestingly, proliferation was higher in the 3D fibrous hydrogels compared to cells cultured on the same hydrogels in 2D. This finding is contrary to other 3D studies with chemically crosslinked, flexible polymer networks, suggesting that the hydrogel architecture and crosslinking mechanism influence the ability of a cell to divide and proliferate. These findings can be attributed to a more open network afforded by the semi-flexible polymer networks and physical crosslinks that can be more easily disrupted. Boddupalli and Bratlie[356] compared proliferation of NIH/3T3 fibroblasts in a methacrylated alginate hydrogel formed through different crosslinking mechanisms (e.g., step growth, chain growth, ionic, and mixed mode), which led to a range of hydrogel stiffness from 9 to 22 kPa (E). Interestingly, cell proliferation did not correlate with hydrogel stiffness. Cell proliferation was lowest in step-growth hydrogels (9 kPa, E) and comparably higher in all other conditions ($\geq$13 kPa, E). Although the exact mechanism was not identified, these results imply that the structure of the crosslinked network can impact cell proliferation. It is known that step-growth mechanisms tend to lead to more homogeneous crosslinking, while chain-growth mechanisms tend to lead to more heterogeneous crosslinking. [357] Thus it is reasonable to postulate that network heterogeneity may enable some cells to proliferate, while other cells in the same network may be surrounded by a tighter mesh. [358] Taken together, these studies suggest that the proliferative capabilities of cells in hydrogels is highly sensitive to hydrogel crosslinking, crosslink bond dynamics, and hydrogel architecture.

6.1.3. Mechanical Confinement. In 2D culture, cells can expand and divide in an unrestricted manner. By contrast, when encapsulated in 3D elastic hydrogels (e.g., chemically crosslinked), any change of volume is resisted by the elastic deformation of the surrounded matrix. To understand the mechanical resistance to volumetric expansion (such as that triggered by cell expansion) in a hydrogel, a mechanical test known as cavitation rheology was recently developed. [359] This approach involves growing a cavity in the material using a syringe needle and measuring the relationship between cavity expansion and resisting pressure over time (Figure 23g). For an incompressible Neo-Hookean polymer ($\kappa \gg G$ in eq 4), this relation is given by: [360]

$$p = 3G\left(\frac{5}{6} - \frac{2}{3\lambda} - \frac{1}{6\lambda^4}\right) \tag{30}$$

where $\lambda = R/R_0$, with R and R_0 the radius of the cavity before and after expansion, respectively. This expression indicates that the pressure increases monotonically and reaches an asymptote at $p = 5G/2$ for large deformations. In other words, if the pressure generated by cells can reach this critical value,

expansion may occur without elastic penalty (Figure 23g). However, if a cell cannot generate enough pressure such as the case for a stiff chemically crosslinked hydrogel, cell volume expansion may not carry on. On the contrary, when the hydrogel is viscoelastic (eq 7), the pressure reaches a maximum value lower than $5G/2$ after which the cavity expands without bounds (Figure 23h). [361] The energy barrier for a cell, or a cellular aggregate, to overcome the critical pressure is therefore dictated by the ratio $k_d/\dot{\lambda}$, where $1/k_d$ is the relaxation time of the hydrogel and $\dot{\lambda}$ is the cavity's expansion rate. These results imply that a viscoelastic medium with fast relaxation times is likely to decrease the confinement effects of a cell and support its expansion.

The ability of a cell to divide and ultimately proliferate under mechanical confinement relies on a competition between the protruding forces exerted by cells and the deformation imposed by the gel. Studies of unrestricted cells has provided useful information regarding the intracellular forces during division.[362] In eukaryotes, mitosis occurs under the effect of a bipolar assembly of microtubules called the mitotic spindle. These structures are made of a network of oppositely oriented microtubules that can produce axial forces through polymerization and depolymerization and by sliding with respect to one-another in an anti-parallel fashion. The magnitude of these forces largely depends on the power generated by molecular motors, kinesin and dynein, that convert ATP hydrolysis energy into a sliding movement. When those forces are opposed by the elastic forces of a cell's environment, the division process may cease. To understand this, Nam and Chaudhuri [363] studied constrained division on a tumor cell line encapsulated in an alginate hydrogel. This hydrogel was characterized by a stiffness of 3 kPa, fast stress relaxation, and no cell-adhesion ligands so that division was only resisted by elastic deformation. The study showed that during the division process, the gel was significantly deformed along the mitotic axis of the cells, due to the existence of protrusive forces (Figure 23 i). These forces have two origins: the elongation of the interpolar spindles and cytokinetic ring contraction. While the former relies on the action of kinesin motors transmitted through microtubules, the second induces a lateral contraction that produces longitudinal protrusive forces, relying on the cell's volume conservation. Depending on the mechanical response of the hydrogel, these forces can be insufficient to generate enough elongation in the mitotic axis, and cell division is ended during the metaphase. He *et al.*[364] showed that the 3D environment could dictate the orientation of cell division. Specifically, MDA-MB-312 breast cancer cells encapsulated in a collagen hydrogel were observed to undergo mitosis in an elongated configuration. Interestingly, the direction of the major axis of the mitotic cells was found to be determined by the cell's

local confinement, rather that the density of the surrounding matrix. Indeed, the properties of the local environment induced cells to grow integrin-mediated protrusions in the least confined directions. This cell -matrix interaction controlled cell elongation, which then controlled subsequent division of the cell.

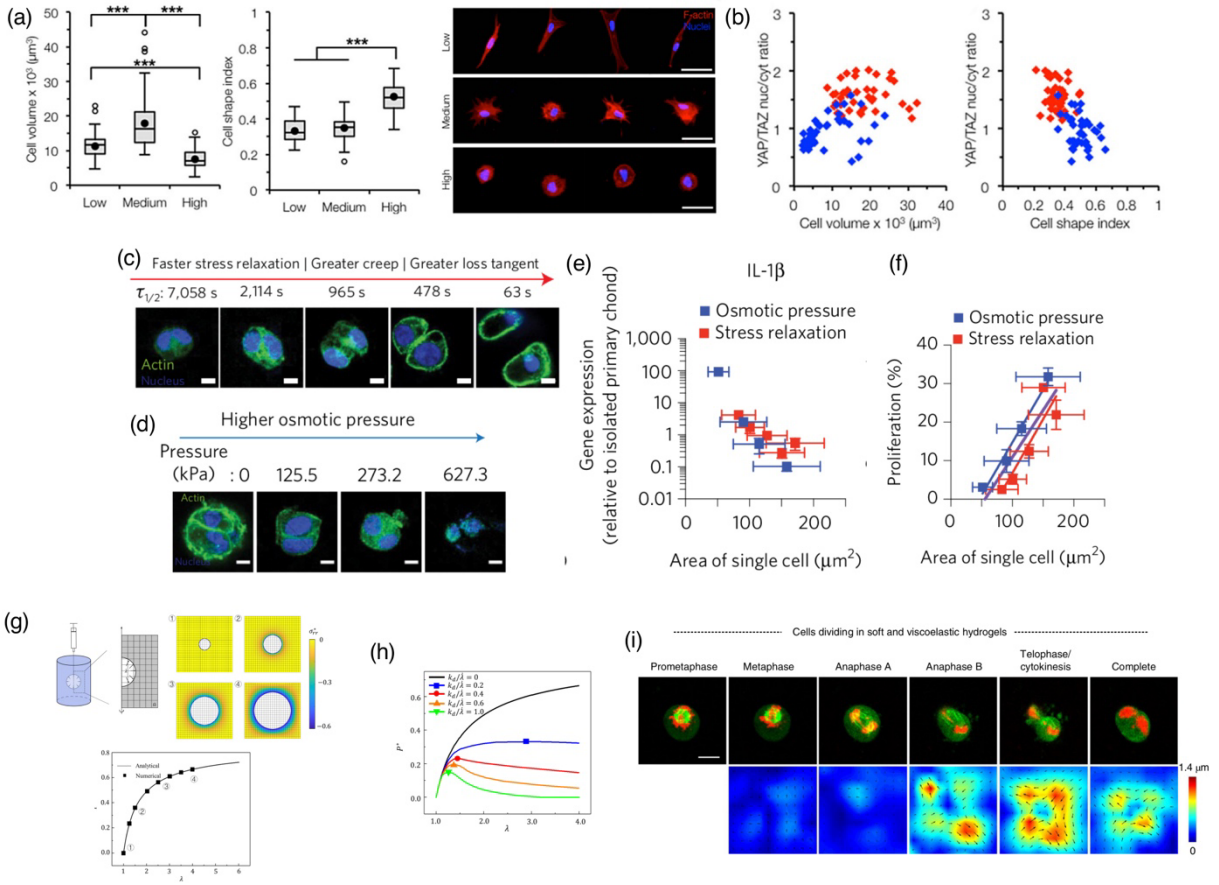

Figure 23. (a) Cell volume and cell spreading as a function of hydrogel stiffness (low, medium and high) and corresponding confocal microscopy images stained for F-actin (red) and nuclei (blue) (scale bar is 50 m). Reproduced with permission from ref [343]. Copyright 2016 Elsevier Inc. (b) Correlations of cell volume and cell spreading to YAP/TAZ signaling. Reproduced with permission from ref [343]. Copyright 2016 Elsevier Inc. (c) Cell volume expansion and cell proliferation in stress relaxing hydrogels with faster stress relaxation. Reproduced with permission from ref [351]. Copyright 2017 Springer Nature. (d) Cell volume expansion in a fast relaxing hydrogel, but with increasing osmotic pressure. Reproduced with permission from ref [351]. Copyright 2017 Springer Nature. (e) Correlation of catabolic response of interleukin-1 β (IL-1β) with decreasing cell volume (indicated by area of single cells). Reproduced with permission from ref [351]. Copyright 2017 Springer Nature. (f) Correlation of cell proliferation with decreasing cell volume (indicated by area of single cells). Reproduced with permission from ref [351]. Copyright 2017 Springer Nature. (g,h) Expansion of a cavity in an elastic network (g) and a viscoelastic network. Reproduced with permission from ref [361]. Copyright 2018 Springer Nature. (i) Confocal microscopy of a cell dividing at different stages of cell division and corresponding deformation of the hydrogel. Reproduced with permission from ref [364]. Copyright 2015 The Authors.

6.2. Cellular Aggregates and Tumors

A significant amount of research has focused on developing 3D hydrogel cultures to study tumor growth.[365] By encapsulating individual cancer cells in hydrogels that grow into multicellular aggregates or spheroids (Figure 22c), rate of tumor growth can be studied. These hydrogel platforms containing tumor spheroids can then be used to test the effectiveness of chemotherapeutic drugs as a function of the tumor microenvironment.[366] The vast majority of these studies have focused on breast cancer cells, and therefore much of the examples provided are with these cell types. When possible, we highlight recent findings from cells derived from other cancers.

6.2.1. Hydrogel Effects. As with single cells, the growth and proliferation of cellular spheroids when encapsulated in hydrogels will be significantly impacted by the hydrogel mechanical environment. For example, Jiang *et al.*[367] encapsulated the invasive MDA-MB-231 breast cancer cells in alginate-gelatin hydrogels that contained ionic and physical crosslinks. The alginate and gelatin concentrations were varied to produce hydrogels with stiffness that ranged from ~5 to 23 kPa (*E*). Spheroid growth was faster in hydrogels with lower concentrations of alginate (comparing 8 kPa to 13 kPa (*E*) hydrogels), but was inhibited in hydrogels with a higher stiffness. Taubenberger *et* al.[368] encapsulated MCF-7 breast cancer cells in covalently crosslinked, enzyme-sensitive, PEG-heparin hydrogels of varying stiffness from 2 to 20 kPa (*E*). An increase in hydrogel stiffness reduced spheroid growth (Figure 24a). The authors encapsulated elastic polyacrylamide beads (15 m φ; 4 kPa) as a stress sensor to investigate the local stress within the hydrogel. On day 14, deformed beads were observed within ~50 m of the tumor spheroid in the stiff hydrogel, but not in the soft hydrogel (Figure 24b). However, deformed beads were observed in control hydrogels that were non-degradable, suggesting that the lack of radial stress in the soft enzyme-sensitive hydrogel was due to degradation of the hydrogel. Interestingly, inhibiting cytoskeleton organization (by inhibiting ROCK signaling) in the stiffest 20 kPa (*E*) hydrogel led to increased spheroid growth. This finding suggests that both mechanical confinement and mechano-sensory mechanisms control tumor growth. Dubbin *et al.*[300] encapsulated 4T1 mammary gland carcinoma cells in covalently crosslinked fibrinogen-gelatin hydrogels and showed that spheroids were the smallest in the stiffest hydrogel (1 kPa, *G*). Spheroid growth, however, could be abrogated with an MMP-inhibitor, which suggests the degradation of the hydrogel, which was also confirmed through fluorescent imaging, was necessary for growth. The authors

correlated reduced transport of growth factors as a result of increased crosslink density with decreased spheroid size, suggesting that nutrient transport is another contributing factor to tumor growth in stiffer hydrogels. Li *et al.*[369] encapsulated MCF-7 breast cancer cells in a collagen-alginate hydrogel crosslinked by physical and/or ionic bonds, producing a predominantly fibrous structure. Spheroids developed and grew in the hydrogels with moduli that varied from 47 to 900 Pa (controlled by Ca^{2+} concentration). Interestingly the rate of growth was similar through day 12, but on day 16, differences emerged. The spheroids were largest in the softest hydrogel and smallest in the stiffest hydrogel. Larger spheroids were more resistant to doxorubicin when comparing day 7 to day 16 for the same hydrogel stiffness and also when comparing softest to stiffest hydrogels at day 16. This study also confirms that hydrogel stiffness restricts spheroid growth, but has a significant effect on the chemotherapeutic response. Another contributing factor could be the physical size of the individual cells in the spheroids, which could be influenced by the stiffness of the hydrogel and could alter the phenotype of the cells. Lu *et al.*[370] encapsulated tumor cells in Matrigel followed by a second encapsulation in an alginate hydrogel that produced a stiff outer shell. This stiff outer shell induced cellular proliferation in the Matrigel (Figure 24c), which correlated to phenotypic changes in the cells, increased invasion, and increased tumorigenicity *in vivo*. This study allowed for decoupling of direct mechano-sensory mechanisms as the cells were not in contact with a stiff hydrogel. In agreement with Taubenberger *et* al.[368], it also showed that physical confinement can enhance tumor growth, further implying that cells can sense stiffness from a distance and that this mechanical cue induces cell growth. Furthermore, Liu *et al.*[371] developed a gelatin-hyaluronic acid hydrogel with enzyme-responsive crosslinks that upon dynamic stiffening induced cell migration from tumor spheroids containing pancreatic ductal adenocarcinoma cells that were encapsulated in the hydrogel. Sivakumar *et al.*[372] encapsulated multiple and differentially labeled cell types in a covalently crosslinked PEG-hyaluronic acid-gelatin hydrogel to create a glioblastoma tumor organoid. This study showed that cell proliferation rates differ by cell type within the organoid, which then affects the chemotherapeutic response. Ashworth *et al.*[373] utilized self-assembling peptide hydrogels and showed that soft hydrogels (~500 Pa, *G*) supported spheroid formation of a pre-invasive ductal carcinoma cell line (MCF10DCIS.com) and of an invasive breast cancer cell line (MCF7). However, increasing the hydrogel stiffness to ~5 kPa (*G*) led to cell death of the MCF10DCIS.com cells, but supported spheroid formation and viable cells with the MCF7 cell line. This finding indicates that the effects of mechanical confinement on spheroid formation is highly dependent on the cell type, where more invasive or aggressive tumor cells can either generate greater forces to induce spheroid growth or produce more matrix degrading enzymes that allows for local cellular growth. Taken together, these studies support the

notion that hydrogel stiffness regulates spheroid growth rate in 3D through mechanical confinement, but that other cues involving direct and/or indirect mechano-sensory mechanisms and nutrient transport affect the growth rate and that these effects are highly dependent on cell type.

While tumor spheroid growth in hydrogels has received the most attention, studies have investigated cell aggregation and spheroid growth of other types of cells in 3D hydrogels and reported similar findings that mechanical confinement through increased hydrogel stiffness inhibits spheroid growth. For instance, Unal *et al.*[374] encapsulated oligodendrocyte progenitor cells (OPCs), which are key in the central nervous system, in covalently crosslinked hyaluronic acid hydrogels and reported stiffer hydrogels restricted spheroid growth (2 kPa vs 170 Pa, G). Wu *et al.*[375] encapsulated induced pluripotent stem cell-derived neural progenitor cells (iPSC-NPCs) in methacrylated hyaluronic acid hydrogels. Soft hydrogels (0.5 kPa, E) better supported cell proliferation, spheroid formation, and neurite outgrowth over stiff hydrogels (1.5 kPa, E), while the stiff hydrogels were able to maintain the progenitor phenotype. This study suggests that the soft hydrogels enhanced differentiation, while stiff hydrogels preserved stemness.

6.2.2. Mechano-sensory Mechanisms. Mathematical modeling is an important asset to separate the effect of various factors during the expansion of multicellular aggregates. Depending on the question asked, different modeling strategies can be invoked. For instance, Shirinifard *et al.*[376] undertook a study that aimed to understand the relationship between cell division and growth locally, and the confinement pressure exerted by their surrounding environment. In this case, a discrete approach, that models each single cell as a particle within a multi-cellular spheroid, can be invoked where stochastic rules for cell division can be tested and compared with experimental observations. An integrated experimental-modeling approach may then be devised to identify the local rules that dictate cell mechano-sensitivity. Using this approach, Van Liedekerke *et al.*[377] established a set of rules that replicated the growth dynamics of a cellular aggregate in an elastic medium. First, they found that the spheroid growth rate depends on volumetric strain in a nonlinear fashion, with the existence of a threshold strain below which cells became quiescent and their growth rate dropped significantly. Second, the model indicated that cell division occurred on the condition that their mass had doubled during the division cycle. This new knowledge, which can uniquely be created with computational models, has a great potential to guide experimental efforts in controlling both the geometry and dynamics of multicellular aggregates.

When the emphasis is on the role of the mechanical behavior of the hydrogel, rather than the cell-cell interactions, continuum mechanics [378] provides an attractive modeling strategy. In this case, one does not model individual cells, but instead considers them in an average fashion through their concentrations.

In these formulations, growth is often treated as a volumetric expansion λ^3 of the cellular spheroid, where λ represents the stretch ratio in each direction due to combined expansion and division in the cell aggregate. The corresponding deformation gradient F can then be expressed by decomposing it into an elastic (F_e) and a cellular growth (F_g) contribution as:

$$F = F_e F_g \quad \text{where} \quad F_g = I \tag{31}$$

with $I = Diag(1,1,1)$ is the identity tensor, expressing the fact that cell growth is isotropic. [379] But growth also relies on the transport of nutrients and building blocks that are used to make up the added mass. Mixture theories, that consider a "material" as a combination of solid and fluid phases constitute a good framework to couple mechanics, transport, and growth. [76] Simulations [380] of tumor growth within fibrous networks show a reorientation of the fibers in the circumferential direction, which is consistent with the idea of network compression during growth. The model also predicted anisotropic tumor growth when the network was aligned. The continuum approach has also been used to explain the dependence of tumor morphology on the mechanical properties of the hydrogel in which it is encapsulated. [381,382] Experimental studies indeed show that when the hydrogel is stiffer than the tumor, the latter tends to take an oblate ellipsoidal shape (Figure 24f), while then the hydrogel is softer, the tumor remains spherical.[383] Assuming a purely elastic gel, the continuum model was used to estimate the total free energy of the tumor-hydrogel system and could show that, out of a variety of possible tumor shapes, the oblate ellipsoid was the one that minimizes the free energy (Figure 24g) of the cell-hydrogel system.

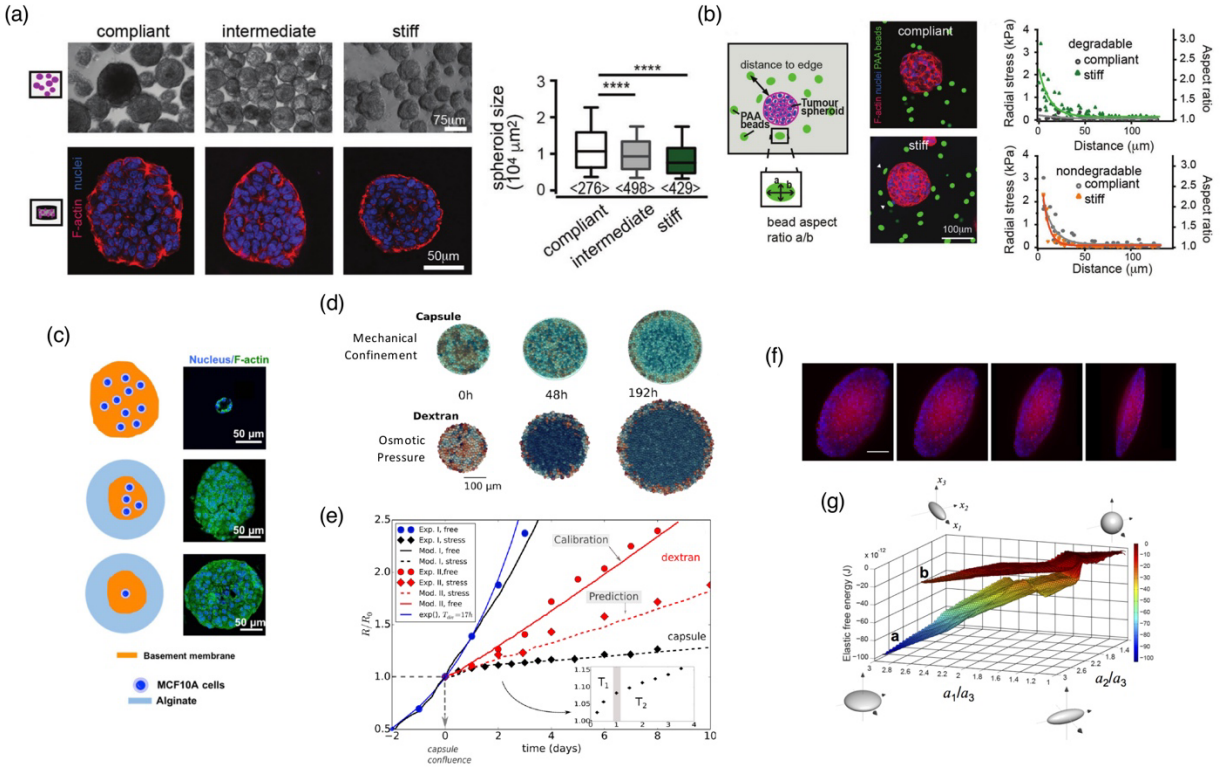

Figure 24. (a) MCF-7 breast cancer cell spheroid growth in an enzyme-sensitive PEG-heparin hydrogel with a stiffness of 2.5 (compliant), 7 (intermediate), and 17 (stiff) hydrogels and cultured for 14 days. Brightfield and confocal microscopy images stained for F-actin (red) and nuclei (blue) are shown along with quantification of spheroid size. Reproduced with permission from ref [368]. Copyright 2019 John Wiley & Sons. (b) Similar spheroids from panel a, but with elastic polyacrylamide beads (15 m φ; 4 kPa). Deformation of the bead was visualized after 14 days in culture and quantified by aspect ratio and radial stress as a function of distance from the spheroid. Reproduced with permission from ref [368]. Copyright 2019 John Wiley & Sons. (c) Mammary epithelial MCF10A cells that were cultured in Matrigel (basement membrane) and then encapsulated in a stiff alginate hydrogel shell led to a malignant transformation and spheroid growth after 21 days. Reproduced with permission from ref [370]. Copyright 2019 Elsevier Inc. (d) Simulation results of spheroid growth under mechanical confinement using a capsule or under osmotic pressure using dextran. Reproduced with permission from [377]. Copyright 2019 The Authors. (e) Radial growth curves of tumor spheroids under mechanical confinement (red), osmotic pressure (black), or free growth (blue). Modeling results are shown by solid line. Reproduced with permission from ref [377]. Copyright 2019 The Authors. (f) Light sheet microscopy images of a tumor spheroid that is rotated about its vertical axis, stained for E-cadherin (red) and nuclei (blue); scale bare is 90 m. Reproduced with permission from ref [381]. Copyright 2014 The Authors. (g) The elastic free energy landscape of a tumor spheroid morphology along its ellipsoidal axes ratios (a 1/a3 and a 2/a3). Reproduced with permission from ref [381]. Copyright 2014 The Authors.

6.3. Organoid Growth

Directed organoid formation using 3D hydrogels is gaining increasing attention. [384–386] Organoids are defined as multi-lineage progenitor cells that self-organize into a 3D multicellular structure exhibiting physiological functions consistent with organs (Figure 22d). [387,388] Early work investigated formation of embryoid bodies (EBs), which are multicellular aggregates of pluripotent stem cells that spontaneously aggregate in 3D culture, [387] while more recent work has focused on self-organization of multiple cellular types, for example intestinal organoid development and growth.

6.3.1. Hydrogel Effects. There are relatively few studies investigating EBs in hydrogels, which have been limited to natural hydrogels such as fibrin and hyaluronic acid. These studies demonstrate improved reproducibility of EB differentiation in 3D hydrogels, but the efficiency of EB formation is low. [389] In support of this observation, Li *et al.*[390] used a self-assembling peptide hydrogel to induce EB formation for neuronal differentiation. While the 3D environment supported differentiation, it did not support neuron morphology and instead required removal of the EBs from the hydrogel followed by dissociation into single cells and then 2D culture. With recent attention on organoid development, which relies on differentiation and self-organization, hydrogels have emerged as an important 3D platform to guide organogenesis. Gjorevski *et al.*[391] investigated intestinal organoid development from intestinal stem cells (ISCs) encapsulated in covalently crosslinked, enzyme-sensitive, PEG hydrogels. ISC expansion and formation of colonies required stiffer hydrogels (i.e., 1.7 kPa vs 300 Pa), which was mediated through YAP/TAZ signaling, suggesting a mechano-sensing effect. Once formed, the colonies polarized leading to the columnar epithelial cells surrounding a lumen. However, during differentiation to form the organoid, the mechanical forces applied by the hydrogel led to buckling of the developing organoid. This was overcome by softening of the hydrogel through hydrolytic degradation. This study highlighted the importance of a mechanical confinement on cell proliferation to form cell aggregates, but the need for a soft matrix to support differentiation and organoid formation. Cruz-Acuña *et al.*[392] encapsulated human intestinal organoids (HIOs) in a covalently crosslinked PEG hydrogels with varying stiffness (50 to 400 Pa, G) and with different cell adhesive ligands. Soft hydrogels (400 Pa, G) supported organoid growth, while stiffer hydrogels led to apoptosis. Cell adhesive ligands of RGD (fibronectin) retained the greatest number of viable cells over GFOGER (collagen) and IKVAV (laminin). This study indicated that both stiffness and the type of integrin-ligand interaction are important for organoid development and survival. Lancaster *et al.*[393] reported on a forebrain organoid and described that increasing surface area to volume led to more reproducible neural induction of pluripotent stem cells while a structured environment with patterned microfiber polymers embedded in Matrigel was needed for self-organization and organoid development.

Broguiere *et al.*[394] investigated epithelial organoid development in a fibrin-laminin hydrogel. Utilizing tethered fluorescent nanoparticles, the authors were able to spatially measure traction forces in the hydrogel (Figure 25a). They reported an internal pressure in the crypt-like budding regions which led to forces exerted on the hydrogel. These forces were counterbalanced by increased contractility in regions that retained stemness. These findings demonstrate that hydrogel stiffness is a major factor in the ability of cells to form crypt-like structures. Nowak *et al.*[395] reported on mammary epithelial cell (MEC) morphogenesis in covalently crosslinked, degradable, PEG-heparin hydrogels that were soft (~200 Pa, G) or stiff (~1.5 kPa, G). Achieving morphogenesis to a MEC acini, which consists of a small lumen surrounded by polarized cells, required a soft hydrogel (~200 Pa, G) (Figure 25b). The authors identified that hydrogel degradation was required for luminal clearance, which is necessary to form the acini, and that heparin was necessary to achieve differentiation and morphogenesis in the soft hydrogels. The authors hypothesized cell-secreted laminin, LN-332, into the pericellular space acted as a link to connect cell surface receptors to heparin, both of which bind LN-332. Thus, the heparin in the hydrogel may have served as a mechanism for cells to sense matrix stiffness in addition to its well-known role for binding growth factors. On the contrary, while the stiff hydrogel supported proliferation and spheroid formation, this environment induced an invasive cellular phenotype evident by a lack of self-organization and cell migration out from the spheroids. Yavitt *et al.*[396] encapsulated intestinal stem cells in a PEG hydrogel containing photodegradable allyl sulfide bonds and RGD for cell adhesivity. A hydrogel stiffness of 1.5 kPa (G) promoted colony and organoid formation where lower (~250 Pa, G) or higher (~2 kPa, G) stiffness retarded colony formation. The author utilized the photodegradable crosslinks as a means to expand the number of organoids. This was achieved by releasing the organoids, dissociating the cells into single cells, and encapsulating the single cells, which went on to produce new organoids. Hushka *et al.*[397] utilized this same photodegradable hydrogel as a means to culture and differentiate intestinal stem cells in stiffer hydrogels and then soften the hydrogel to enable crypt formation (Figure 25 c). Taken together, these studies indicate that organoid development requires a temporal mechanical response to achieve cell proliferation and spheroid formation in a relatively stiff hydrogel, but that differentiation and self-organization during morphogenesis requires a softer matrix where cells can deform the hydrogel to create crypt-like budding structures.

6.3.2. Mechanisms of Growth. Mathematical models enable the study of multiscale dynamics of organoids,[398] with most till date focused on numerical models of intestinal organoids; the first computational model of a full intestinal organoid was developed in 2012 by Buske *et al.*[399] using an individual cell-based model. Because organoid growth and subsequent crypt formation depend spatially

on proliferation and cellular fate (maintaining differentiated and undifferentiated cells) for self-renewal, such models consider cell type, cell location, and intercellular signaling. In Buske *et al.*,[399] the model defines an organoid surface as a semi-flexible polymer network that can bend in response to cells that are attached to the polymer. In essence, this polymer network resembles the basement membrane to which an epithelial monolayer of cells is attached. Moreover, the model effectively captures the idea of cell-cell and cell-matrix interactions. The model also considers a positive feedback loop between neighboring cells, which depend on cell specification. The polymer network is modelled as a dynamic triangulated mesh of stiff polymers, where each triangle undergoes deformation during growth until a maximum threshold is reached at which point new triangles of stress-free polymers are synthesized (Figure 25d). The polymer network has a bending modulus (denoted as K_c in Figure 25e), which depends on the stiffness of the basement membrane (which in turn depends on the cell type) as well as the surrounding matrix. The value of the bending modulus is critical to crypt formation during organoid differentiation. In the case of network compression due to folding of the membrane, a critical minimum triangle area is used to delete triangles. The model finds that shape changes and local buckling arise from dynamic instabilities produced by cell proliferation in the cell monolayer. This arises from competing timescales of cell proliferation and network relaxation. The authors modeled the evolution of cell specifications as a function of time and for increasing bending moduli to simulate stiffening of the surrounding matrix during development. The simulations showed that initial proliferation was independent of bending modulus, but once a critical size was reached, there was a loss of undifferentiated cells, which further corresponded to a loss in differentiated cells that are responsible for crypt formation (Figure 25e). These simulations suggest that stiffening the surrounding environment inhibits differentiation and self-renewal of the organoid. Collectively, this model identified that stem cell proliferation and crypt formation in an organoid depends on the mechanical constraint arising from the cell monolayer and mechanical confinement owing to the surrounding hydrogel. Thalheim *et al.*[400] modified this model to further explore the interdependencies of cell signaling in cell specification and cell biomechanics that consequently impacts the organization of the intestinal organoid. This model showed that cyst-like growth patterns in organoids arose as a result of differentiation. This was further mediated by changes in cell biomechanics that occurred during differentiation. Collectively, these models demonstrate that mechanical cues arising from the surrounding matrix (i.e., hydrogel) and the cells themselves drives organoid growth.

Other models of intestinal organoids described by Langlands *et al.*[401] and Almet *et al.*[402] use a two-dimensional agent-based approach to explore the biomechanical aspects of organoid crypt fission with the primary goal of investigating the role of cell specification. The model considered two cell populations

of soft and hard cells that could correspond to undifferentiated and differentiated cells, respectively. With the ability to modify different properties like adhesiveness of hard cells to the basement membrane and stiffness and cell population ratios, these models allowed exploration of different hypotheses regarding the link between cell mechanics and crypt generation. For example, areas that contain more undifferentiated cells, which are flanked by differentiated cells (that are stiffer), create regions of lower mechanical stiffness that are more likely to undergo buckling. Buckling initiates crypt fission that leads to branching and formation of two new crypts. Although, this formalism is in 2D and does not account for molecular signaling, it provides broad physical insights into the typical morphologies of intestinal organoids arising from specific biomechanical properties. Yan *et al.*[403] took a different approach to simulate 3D growth of a colon cancer organoid using multispecies mixture theory [404,405] to explicitly model the dynamics of progenitor, stem and terminally differentiated cell populations. The mechanical interactions between cells and hard membrane are modelled through an adhesive energy governed by volume fractions of solid tumor cells and host gel. The other parameters of this model include general properties like cell mobility, cellular mitosis rate, and apoptosis rate as one of the cellular environment parameters obtained from the literature. [404,406] The system dynamics illustrated by this model show diverse growth patterns, and suggests that stable organoid growth patterns are caused by stem cell control of self-renewal capacity. Overall, this model points towards a connection between changes in the microenvironment of a tumor and cancer metastasis.

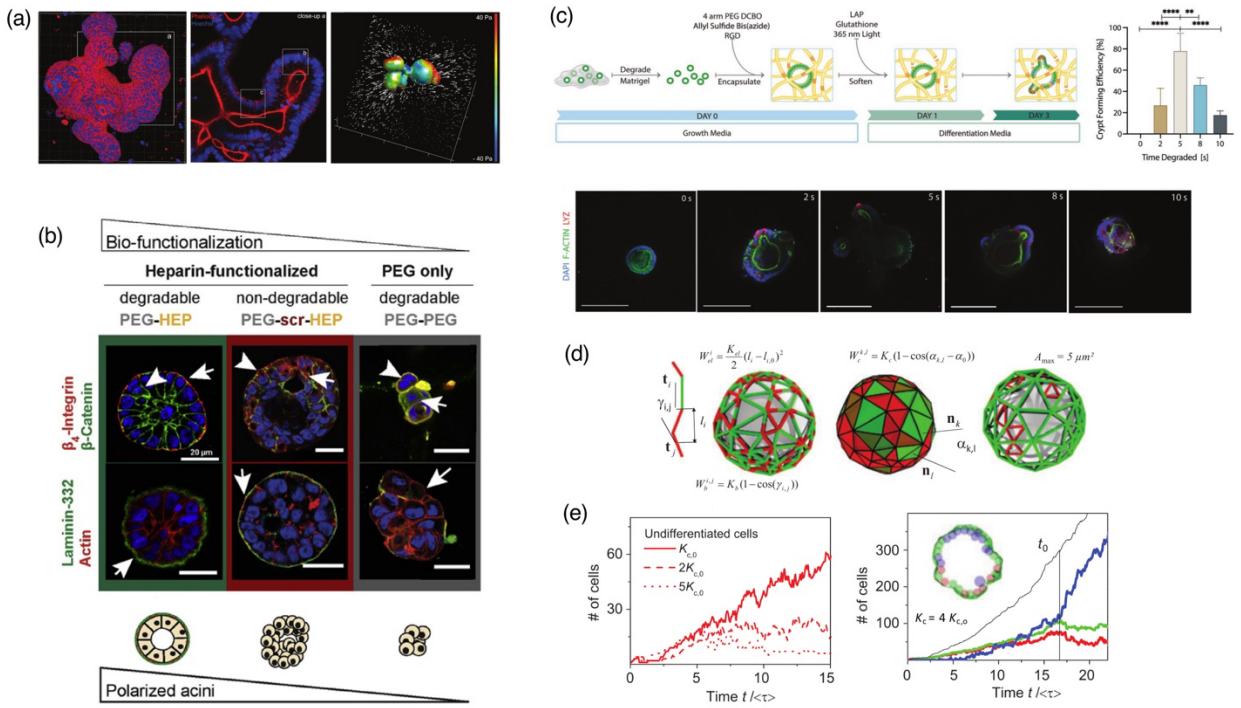

Figure 25 (a) Epithelial organoid growth in a fibrin-laminin hydrogel stained for F-actin (red) and nuclei (blue). A 3D traction force microscopy image shows normal pressures at the surface of the organoid and arrows show local displacement of the hydrogel. Reproduced with permission from ref [394]. Copyright 2018 John Wiley & Sons. (b) Mammary epithelial cell (MEC) morphogenesis requires both hydrogel degradability and bio-functionalization with heparin to form a polarized acini. Reproduced with permission from ref [395]. Copyright 2017 Elsevier Inc. (c) Intestinal organoid growth in a photodegradable hydrogel. Intestinal stem cells were encapsulated in a stiff hydrogel to allow colony formation. After which the hydrogel was softened by light-induced hydrogel degradation for different amounts of time and then exposed to differentiation medium. Crypt formation was dependent on the light exposure, which correlates to the extent of hydrogel degradation. Reproduced with permission from ref [397]. Copyright 2020 John Wiley & Sons. (d) An individual cell-based model of an intestinal organoid using a bending modulus network. The network defines stretching and compressing polymers (left), bending between polymers represented as triangles (middle), and the mesh size (right). Reproduced with permission from ref [399]. Copyright 2012 John Wiley & Sons. (e) Simulation results of organoid growth and cell specification as a function of bending modulus (K_c), where $K_{c,o}$ is the initial bending modulus of the network: number of undifferentiated cells for different values of K_c (left) and number of cells in the organoid that are undifferentiated (red), differentiated (green, i.e., Paneth cells), and enterocytes (blue). Paneth cells are differentiated cells responsible for guiding crypt formation. Enterocytes are nutrient-absorbing cells. Reproduced with permission from ref [399]. Copyright 2012 John Wiley & Sons.

6.4. Outlook: Tuning Hydrogels to Control Growth

Cell growth in 3D hydrogels involves cell expansion and proliferation, both of which require additional space for cells and daughter cells to occupy within the hydrogel. The forces generated by the cell during these processes must therefore be sufficient to deform the surrounding hydrogel matrix. Otherwise, if the hydrogel is too stiff, cell expansion is limited and proliferation is prevented. To support these cellular processes, soft hydrogels must be employed or hydrogels must be degradable so that they soften over time. Alternatively, stress relaxing hydrogels offer the advantage that the forces generated by the cell could break crosslinks in the immediate vicinity of the cell, allowing for cell expansion and division, but which can then re-form around the cells in a new state. Such dynamic networks enable stiffer hydrogels to be used as long as the stress relaxing properties are appropriately tuned. When single cells encapsulated in a hydrogel have the capacity to undergo extensive proliferation (e.g., cancer cells) and form cellular aggregates or spheroids, the cumulative force generated by the cells will be greater than that of a single cell. This means that as cell aggregates form within a hydrogel, there is the potential for the rate of growth to increase. However, as with single cells, if the hydrogel is too stiff, growth can be significantly slowed. Computational models can play an important role by quantifying the forces generated by single cells and/or aggregates of cells during cell expansion and division and how these forces are then resisted by the surrounding hydrogel matrix. To date, however, computational models of cell expansion in 3D have been scarce. Computational modeling is a critical area of need as this information can then be used to design hydrogels that enable or prevent cell division, depending on the application. For instance, the latter may be desired when differentiation is the primary goal.

A confounding factor is that the stiffness of the hydrogel not only contributes to mechanical confinement that physically restricts cell expansion and division, but can induce mechano-sensory mechanisms in the cell as described in Section 4. Indeed, in the absence of a mechanical constraint, a stiffer matrix through mechano-sensory mechanisms can inhibit invadopodia, which are the actin-rich cellular protrusions found on cancer cells and which are involved in cell invasion. [407] Several studies highlighted above demonstrate that it is possible to overcome some of the effects of mechanical confinement by altering the cells. This means that the state of the cell influences the amount of force that it can generate during cell expansion and cell division. Decoupling the effects of mechanical confinement and mechano-sensory mechanisms is challenging to do experimentally, although a few studies have provided evidence that both are important. Combining the computational models of mechano-sensory with models of mechanical confinement will be an important next step to determine how cells through mechano-sensing of the hydrogel, can generate greater forces to overcome mechanical confinement.

An exciting new area of research is in organoid growth and development. Experimental studies have clearly demonstrated the importance of a 3D hydrogel culture environment with temporally tunable stiffness. Stiffer hydrogels are necessary to induce cell proliferation and colony formation. However, these events will be limited by the stiffness of the hydrogel. Interestingly, differentiation of the organoid and crypt formation requires a much softer environment. One possible explanation is that forces generated by the crypt forming cells is much lower than the forces generated during cell division. To date, computational models have largely been limited to understanding how organoids grow and form crypts through the self-organization of differentiated and undifferentiated cell types. The role of biomechanics has been largely limited to the cells, where differentiated cells are considered stiffer than undifferentiated, which is thought to be in part from cell-matrix interactions with their basement membrane. The models have yet to include the effects of surrounding hydrogel matrix, which will serve as an important cue that can influence both the stiffness of the cell through cell-matrix interactions and through mechanical confinement, which will impact whether a crypt can physically form in the hydrogel.

7. GROWTH AND DEVELOPMENT OF NEO-TISSUE IN DEGRADING HYDROGELS

One of the most promising functions of hydrogels is that of a mechanical scaffold that can encapsulate cells in 3D and direct them to grow into functional tissues comprised of an ECM. More than a temporary structure, these hydrogels must act as the conductor driving a population of cells to differentiate appropriately and/or maintain a tissue-specific phenotype and grow an engineered tissue that is as close as possible to the native tissue. As such, the hydrogel should perform three main functions: (a) provide a 3D structural support for cells as it transitions from polymer to tissue, (b) provide appropriate physical cues to cells so that they develop the targeted functional tissue, and (c) possess adequate degradation kinetics to enable a successful transition between the hydrogel construct and tissue. Figure 26 provides an overview of the coupled processes of ECM growth and hydrogel degradation.

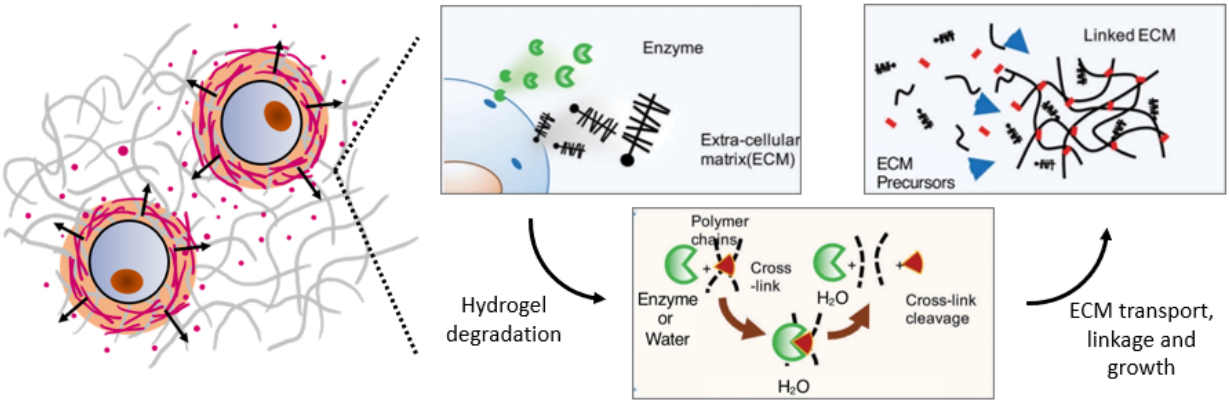

Figure. 26. Cell-mediated tissue growth in a hydrogel with encapsulated cells. The hydrogel may be designed with bonds that are susceptible to hydrolysis or enzyme-mediated hydrolysis. The approach starts with the encapsulation of cells in a hydrogel. The cells synthesize and release a variety of biomolecules, which include precursors to the ECM (such as procollagen molecules and aggrecan monomers) and matrix-degrading enzymes. Over time, the hydrogel can be induced to degrade, either locally or globally, via the action of cell-mediated enzymes or simply by the presence of water molecules. Under proper conditions, the ECM precursors can be transported away from cells and assembled into larger ECM molecules in the pericellular space, that will become the neo-tissue. Figure is adapted and reproduced from ref [58] with permission from the Royal Society of Chemistry. Copyright 2016 The Authors.

As already alluded to in the previous sections, a key challenge to the use of hydrogels with encapsulated cells is that the mesh size of the hydrogel is much smaller than most ECM macromolecules. As a result, neo-tissue growth in hydrogels is closely coupled to hydrogel degradation. In this section, we highlight advancements in experiments and mathematical models that describe neo-tissue growth in hydrogels with encapsulated cells. We focus on three key mechanisms in this process: (a) growth that arises from the assembly of ECM precursors into macromolecules within the interstitial space of the hydrogel, (b) temporal changes in the hydrogel structure that may occur by degradation through hydrolysis or enzyme-mediated hydrolysis, and/or by stress relaxing hydrogels, and (c) the evolution in construct mechanics owing to the concurrent hydrogel disappearance and appearance of a neo-tissue. Much of the research efforts connecting ECM growth to hydrogel degradation have involved cartilage tissue engineering. The reason for this is that cartilage is an avascular and aneural tissue whose solid content is primarily made of an ECM with cells occupying only about 2% of the volume. As chondrocytes (or cartilage cells) secrete copious amounts of ECM, chondrocytes encapsulated in degrading hydrogels offers a unique system to study the coupled processes of tissue growth and hydrogel degradation. To this end, most of the work described herein this section focuses on cartilage. Where possible, we also highlight ECM deposition from other cell types.

7.1. ECM Assembly and Deposition

7.1.1. Interstitial ECM Assembly. Deposition of ECM requires cells to secrete precursors that subsequently undergo a coordinated series of events involving the post-processing of these molecule by MMPs and aggrecanases to facilitate their direct assembly in the pericellular space (the interstitial region immediately adjacent to the cell). Several studies have evaluated cartilage ECM assembly and deposition in non-degrading hydrogels, which has provided direct insight into how the hydrogel structure through its crosslink density affects ECM deposition. The most abundant protein found across all tissues is fibrillar collagen, a very large protein that is assembled from cell-secreted pro-collagen molecules. These cell-secreted precursors of the ECM are smaller molecules that can be transported through the hydrogel (see Section 3). For example the diameter of procollagen molecules has been reported to be ~10 nm. [408] Indeed, proteomic analysis identified procollagen molecules in the culture medium of chondrocytes that are encapsulated in stably crosslinked hydrogels of varying stiffness (i.e., 8-46 kPa), confirming that the precursors of a collagen macromolecule can be transported through a hydrogel. [409] Although it is difficult to differentiate between precursor and degraded ECM, the fact that collagen macromolecules are large, even their degraded sequence are unlikely to be able to diffuse, especially in more tightly crosslinked hydrogels. Aggrecan is another large ECM macromolecule that is abundant in cartilage. It is comprised of brush-like proteoglycan monomers that assemble along a hyaluronic acid polymer chain to create very large aggregate macromolecules. Each aggrecan monomer consists of a core protein containing chains of sulfated glycosaminoglycan (sGAG) that extend from the protein to create a brush structure as shown in Figure 26. The proteoglycans are processed inside the cell, secreted, and then assembled extracellularly onto hyaluronic acid chains that are bound to the cell membrane. [410] Once assembled, the hyaluronic acid is cleaved off the cell membrane. The role of hydrogel structure on ECM assembly is striking when comparing the spatial distribution of chondroitin sulfate and aggrecan in hydrogels encapsulated with chondrocytes. For instance, chondroitin sulfate was detected throughout a 60 kPa (E) stably crosslinked PEG hydrogel, but was restricted to the pericellular space in higher stiffness (320-590 kPa, E) hydrogels.[411] On the contrary, positive staining for aggrecan was only detected pericellularly regardless of hydrogel stiffness and co-localized with collagen type II. Interestingly, link protein and decorin, which are much smaller molecules (and hence could diffuse through the hydrogel) were localized pericellularly. These molecules are required for ECM assembly whereby link protein connects aggrecan to hyaluronic acid and

decorin is required for collagen fibrillogenesis.[412] Moreover aggrecan and collagen type II are linked through complexes with matrilin-1 and biglycan or decorin.[413] Once fully linked, these assembled macromolecules make up the deposited tissue, which can be considered as a solid matrix that can no longer diffuse.

More recently, the mechanisms of ECM assembly in the pericellular space have been a subject of deeper investigation. Loebel *et al.*[414] encapsulated chondrocytes and fluorescent beads in stably crosslinked hyaluronic acid hydrogels, where the beads were used to track the location of the hydrogel. The hydrogels were cultured in a medium supplemented with either azide-methionine (a non-canonical amino acid) or azide-mannose, to probe for newly synthesized proteins and proteoglycans. The authors demonstrated that neo-tissue assembles in the pericellular space (Figure 27 a). The deposition of the matrix exerts a force on the hydrogel that causes deformation as the nascent tissue grows around the cell. A stiffer hydrogel resists these forces leading to a thinner pericellular matrix. Within one day after cell encapsulation, the distance over which the nascent secreted molecules were deposited was 1.1 m for nascent proteins and 4.7 m for nascent proteoglycans. The distance increased to 3.7 and 7.9 m, respectively, by day 7. Interestingly, there was some overlap of the beads and the neo-tissue suggesting that there may be interpenetration of the ECM and the hydrogel. These results indicate that some of the ECM precursors, notably the proteoglycans, can diffuse and potentially assemble within the mesh network of the hydrogel. This agrees well with previous results which reported glycosaminoglycans were present throughout the hydrogel, suggesting that these molecules can readily diffuse in the hydrogel.[411,415] However, larger proteins and proteoglycans (i.e., aggrecan) were unable to diffuse. Schneider *et al.*[409] encapsulated chondrocytes in stably crosslinked PEG hydrogels and showed a pericellular matrix rich in aggrecan, collagen II, and collagen VI, but which was much thinner in stiffer hydrogels (46 kPa, E) compared to softer hydrogels (8 kPa, E). This finding also agrees with previous studies in stable PEG hydrogels, which have shown that the pericellular matrix is thicker in softer hydrogels.[416] Tan *et al.*[354] encapsulated chondrocytes cells in a stable PEG hydrogel that was formed from the copper-free click reaction between dibenzocyclooctyne (DBCO) and azide. The authors formed hydrogels off stoichiometry with excess DBCO, which induced physical crosslinking owing to the hydrophobicity of DBCO. This allowed the authors to control for the viscoelastic response, whereby the half-time for relaxation, $\tau_{1/2}$ ranged from 100 to 300 min. They showed that ECM elaboration was greater in the gels that had lower $\tau_{1/2}$. Taken together these studies, indicate that precursors can readily diffuse through hydrogels, but that once the large ECM macromolecules assemble and deposit into a solid matrix, they are restricted to the pericellular space, located between the cell membrane and the hydrogel. As cells secrete and assemble more matrix,

this matrix exerts a force on the hydrogel and depending on the hydrogel properties such as stiffness and viscoelastic response, the evolving matrix can either grow or be restricted by the hydrogel.

7.1.2. Models of Hydrogel-Based Tissue Growth. Theoretical and computational models provide unique opportunities to explore how the hydrogel structure and its corresponding properties control the coupled processes of hydrogel degradation and neo-tissue growth. Such an approach has the potential, in the long term, to replicate the growth process "in-silico" and predict hydrogel structures that would lead to optimal tissue development for a specific patient. A challenge in this endeavor is that the hydrogel is not just a temporary host for the encapsulated cells; it is the medium that will nurture cells to differentiate appropriately and enable neo-tissue growth with properties close to its biological counterpart. Thus, in addition to providing cells with the appropriate mechanical and biochemical cues discussed earlier, a hydrogel must provide a continuous structural support for cells as they transition from being encapsulated in a hydrogel to being part of a tissue. If not, the hydrogel would undergo dissolution releasing cells into the surrounding medium. This implies that the hydrogel must possess well-tuned degradation kinetics to ensure tissue growth and maintain mechanical integrity during the hydrogel-to-tissue transition. To fundamentally understand this problem, an interdisciplinary approach must be taken, where theoretical models of tissue growth, accounting for mass transport and reaction kinetics are integrated with the physical model of hydrogels described in Section 2 . Such models must also consider processes occurring at different length-scales, from the molecular mechanisms in hydrogels (nanometer) to the cellular scale (micron) and to the tissue scale (millimeter). Last but not least, these models must constantly be validated and integrated with experimental observations due to the complexity, nonlinearity, and coupling of the processes involved. While the literature on tissue growth is vast,[417–420] models are often phenomenological and rarely discuss growth in a tissue engineering context. Recent experimental work in tissue engineering has however been accompanied with a new class of models that do integrate growth at the cell-hydrogel level. For instance, Sengers *et al.*[421] used a computational homogenization approach to explore the transport and deposition of cell-secreted ECM through a hydrogel. By changing the ECM diffusivity through the hydrogel , they showed that the construct stiffness and permeability were governed by the total amount of ECM and were only weakly affected by their local distribution in the hydrogel. However, this model is limited by the fact that it is 2D and does not consider the effects of a degrading hydrogel in tandem with a growing matrix. Additionally, later studies have shown that heterogeneity in the cell distribution promotes local gel degradation and ECM deposition that can be a key factor in maintaining construct integrity and the success of a hydrogel as a tissue construct,[422] an aspect that is discussed further in Section 7.3. Trewenack *et al.*[423] proposed a multispecies formulation of cell-

mediated growth in cartilage constructs, pointing out the distinct roles of advective and diffusive fluxes at the microscopic level. The model indicated that both transportation modes are important for cartilage growth, and further predicted the chondrocyte density that is necessary to grow a functional cartilage tissue. Haider *et al.*[424] extended the phenomenological model of Wilson *et al.*[425] to incorporate experimentally measurable quantities and the presence of inhibitory mechanisms in the deposition of ECM. The model was used to identify the role of parameters on the density of new cartilage, which correlated with the construct modulus. Finally, Dhote *et al.*[51,426] built a single cell model under the centro-symmetry assumption and showed that localized degradation of the encapsulating scaffold helps maintain the mechanical integrity of the construct.

7.1.3. Predicting Mechanical Properties. Before we discuss the role of transport, degradation, and growth on the development of a new tissue, it is first useful to define the methodology by which one can assess and predict the evolving mechanical properties of a hydrogel construct. During the initial stages of ECM growth, a hydrogel construct consists of a spatially heterogeneous mixture of hydrogel and nascently deposited ECM (Figure 27b) whose overall properties may be predicted by computational homogenization methods.[427] This approach consists of simulating the deformation of a representative volume element and estimating its overall stress response based on an accurate knowledge of the spatial distribution and properties of its constituents. The mechanics of this composite material structure has been described under the assumption that hydrogel and ECM are interpenetrating networks that do not strongly interact with one another. [58] This implied that the mechanical response of a point within the construct can be expressed with an additive rule for mixtures, i.e., the stress is written as: $= {}_{g} + {}_{m}$, where subscripts g and m are used for gel and matrix, respectively. Each contribution is thus weighted by its own chain and crosslink densities as provided in Section 2, eq 4, such that ${}_{g}$ vanishes when the gel is degraded, while the relative role of ${}_{m}$ increases as new matrix is deposited and linked together. [76,426] Because the mechanical properties of the neo-tissue are still poorly understood, a generic isotropic model was used in the literature. Nevertheless, this approach can be used to perform "numerical experiments" of the tissue growth process in a hydrogel and explore the effect of various types of hydrogel designs and degradation kinetics as discussed next. [52]

7.2. Tissue Growth in Hydrogels

7.2.1. Hydrolytically Degradable Hydrogels. Many studies have focused on designing synthetic hydrogels engineered with hydrolytically-labile bonds into the crosslinks to enable hydrogel degradation and promote neo-tissue growth.[428] More recently, Neumann *et al.*[429] encapsulated chondrocytes in a PEG hydrogel that was synthesized with caprolactone moieties containing a hydrolytically-susceptible ester linkage into each crosslink and assessed ECM growth over time (Figure 27c). The hydrogel alone (i.e., without cells) readily degraded in an aqueous environment, dropping in modulus from 60 kPa to 3 kPa (E) over 33 days. The cells secreted collagen type II and aggrecan which assembled pericellularly as seen on day 7, but by day 28 the deposited ECM surrounding each cell was connecting and forming a neo-tissue. This correlated with an increase in the construct modulus from 5 kPa(E) at day 7 to 50 kPa (E) at day 28. This indicates that the ECM is contributing mechanically to the overall properties, since the acellular hydrogels were 3 kPa on day 33. Schneider *et al.*[430] utilized the same hydrogel design and showed that increasing the cell density at the time of encapsulation accelerated the overall neo-tissue growth in the hydrogels. Peng *et al.*[431] encapsulated chondrocytes in a PEG hydrogel comprised of crosslinks with varying ratios of a fast degrading lactic acid moiety and a slow degrading caprolactone moiety. Hydrogels with faster degrading crosslinks supported higher sGAG deposition, while hydrogels with more slower degrading crosslinks supported higher collagen deposition. However, the effect on degradation is complicated by the fact that the initial modulus varied from 11 kPa to 46 kPa (E) for hydrogels containing only lactic acid or only caprolactone, respectively. Nonetheless, findings from this study suggest that collagen deposition may have been compromised in fast degrading hydrogels. This could be due to a greater loss of procollagen precursors, which diffuse away prior to being assembled into collagen fibers. On the contrary, sGAGs which are secreted as part of aggrecan monomers, can often diffuse through a hydrogel but whose diffusion is improved with decreasing crosslinking. The differences between sGAG and collagen may therefore be due to the differences in size where procollagen molecules are smaller than aggrecan monomers or could be due to how the ECM is assembled where aggrecan aggregates are assembled directly at the cell membrane, while collagen requires multiple processing steps and additional cell-secreted molecules.

There have been several recent advancements to develop hydrolytically degradable hydrogels that afford greater control over degradation that is independent of mechanical properties, although their effect on neo-tissue growth remains to be determined. Cereceres *et al.*[432] synthesized a degradable PEG hydrogel that would allow for decoupling of hydrogel stiffness and hydrogel degradation. To this end, the authors synthesized a PEG hydrogel where the concentration of the hydrolytically susceptible β-thioesters

could be varied while maintaining the same macromer molecular weight. By co-polymerizing with a stable macromer, the degradability of the hydrogel could be tuned from weeks to months. The authors also demonstrated that the rate of hydrolysis was accelerated *in vivo*, which will need to be considered when translating such hydrogels *in vivo*. Lueckgen *et al.*[433] synthesized a hydrolytically degradable alginate hydrogel that could be crosslinked via a norbornene-tetrazine click chemistry. The authors demonstrated that degradation could be decoupled from the initial mechanical properties. Kroger *et al.*[434] showed that for hydrogels crosslinked via thiol-acrylate Michael-type reaction, the degradation rate could be controlled by modifying the chemistry adjacent to the carbonyl carbon in the crosslink without substantially changing the initial mechanical properties. The authors showed that that these modifications led to degradation times that ranged from hours to weeks. These new advancements will help to design hydrogels whereby the initial mechanical properties can be tuned to control cellular phenotype, while the rate of degradation can be independently tuned for neo-tissue growth. This control will be helpful when considering personalized tissue engineering strategies.

Hydrolytically degradable hydrogels present several challenges for supporting neo-tissue growth. ECM assembly and deposition can only occur in regions where the hydrogel has reached its point of reverse gelation. Because hydrogels that degrade by hydrolysis lead to bulk degradation, the rate of hydrogel degradation must be closely coupled to the rate of neotissue growth. However, de-coupling these two processes is difficult to do experimentally and as a result mathematical models have served as a valuable tool for understanding this coupled relationship. Hydrolytic degradation arises from the cleavage of crosslinks initiated by hydrolysis. Due to the highly swollen nature of hydrogels, typically >80% in cell encapsulation and tissue engineering studies, degradation will occur on a bulk scale as described in Section 3. During degradation, a critical point is reached when the polymer network loses its connectivity and undergoes a transition from a solid-like to fluid-like medium at the reverse gelation point. Mathematically, this point can be described when the crosslink density $\rho(r,t)$ at any spatial point r drops from an initial value of $\rho^0 = \rho(r,0)$ to a critical value of where $1/\beta \leq 1$ measures the point of minimum network connections needed for structural integrity.[435] The parameter β can be determined experimentally by relating crosslink density to shear modulus at reverse gelation. Experimentally, the reverse gelation point at degradation is equivalent to the point of gelation, which can be determined using the Winter-Chambon criterion or modifications thereof [436] that define gelation at the crossover point of the storage and loss modulus. Reverse gelation plays an important role in the transport of the ECM within the gel since a sharp increase in macromolecular diffusivity occurs at this threshold. By combining

experiments with modelling, studies have identified network heterogeneities that enable neo-tissue to grow in hydrolytically degradable hydrogels [422,430]. We describe these novel characteristics in the following section.

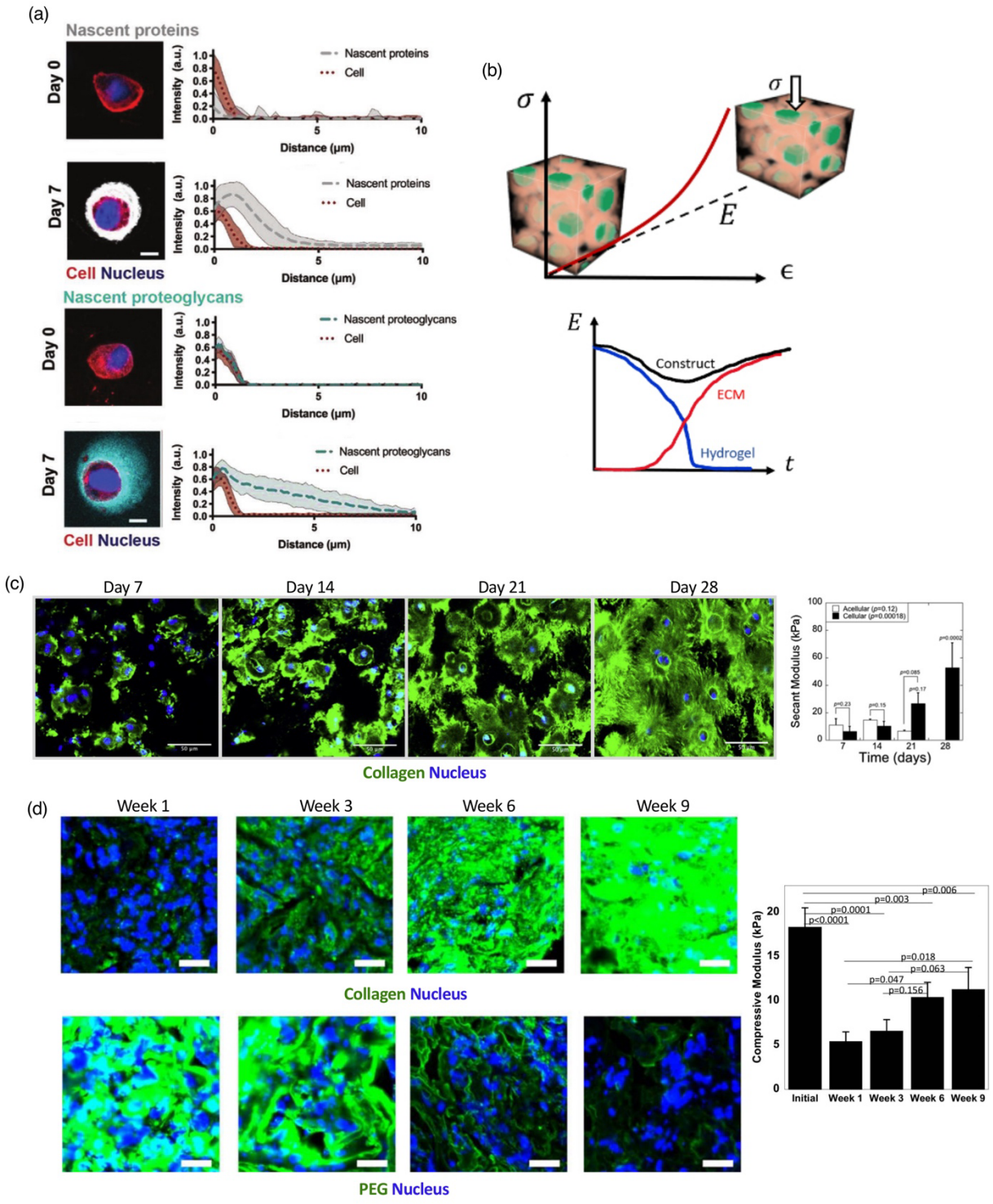

Figure 27. Cartilage ECM growth in hydrogels. (a) ECM assembly in nascent secreted proteins and proteoglycans in the pericellular space around chondrocytes encapsulated in a stably crosslinked hyaluronic acid hydrogel. Reproduced with permission from ref [414]. Copyright 2020 John Wiley & Sons. (b) Computational homogenization technique to determine the construct's properties (i.e., of hydrogel and ECM) over time. Left: The linearized compressive modulus was used to estimate its mechanical integrity over time. Right: Using computational methods, it is possible to evaluate the properties of the construct over time and further estimate the contributions of each of its constituting phases. (c) ECM growth in a hydrolytically degradable PEG hydrogel and corresponding construct modulus over the course of 28 days. Scale bar is 50 m. Reproduced with permission from ref [429]. Copyright 2016 Elsevier Inc. (d) ECM growth in an enzyme-sensitive PEG hydrogel, disappearance of PEG polymer, and corresponding construct modulus over the course of 9 weeks. Scale bar is 20 m. Reproduced with permission from ref [437]. Copyright 2018 John Wiley & Sons.

7.2.2. Enzymatically Degradable Hydrogels. Hydrogels that degrade by cell-secreted enzymes offer many advantages over hydrolytically degradable hydrogels. Several natural biopolymers (e.g., collagen, Matrigel, gelatin, and hyaluronic acid) that form hydrogels on their own via physical crosslinking or which are modified to produce covalent crosslinks are inherently sensitive to enzymes secreted by cells. Contrarily, synthetic hydrogels can be designed with peptide sequences that are susceptible to cell-secreted enzymes, where the sequence can be further tailored to a specific cell type and/or can be tweaked (e.g., exchanging one amino acid for another) to speed up or slow down the rate of degradation.[438] Several studies have shown that enzyme-sensitive hydrogels support ECM growth and are promising for cartilage tissue engineering. For instance, Aisenbrey *et al.*[437] encapsulated MSCs in a covalently crosslinked enzyme-sensitive PEG hydrogel and assessed ECM growth and hydrogel degradation (Figure 27d). After nine weeks, the MSCs had differentiated into chondrocytes and deposited a neocartilaginous tissue that was rich in aggrecan and collagen type II, the main matrix molecules of cartilage, with minimal PEG hydrogel remaining. Rogen *et al.*[439] encapsulated MSCs in covalently crosslinked hydrogels made by co-polymerizing methacrylated chondroitin sulfate and PEG diacrylate. The authors compared differentiation and tissue growth when MSCs were encapsulated either as single cells or as aggregates from pre-formed micro-pellets while maintaining the same overall cell density. Interestingly, single cells outperformed the micro-pellets, depositing more collagen type II and leading to a higher overall construct modulus. Collagen appeared to be abundant throughout the construct with single cells, which would indicate that the hydrogel had largely degraded. However, newly deposited ECM was restricted to the regions around the encapsulated pellets, with no evidence of ECM connecting between pellets. This finding could be attributed to a difference in the biosynthesis of matrix-degrading enzymes and/or the spacing between aggregates, which was greater than between single cells. The latter could dilute the concentration of enzymes in the hydrogel and therefore limit hydrogel degradation. Kim *et al.*[440] isolated

MSCs from different human donors that were either healthy or had been diagnosed with osteoarthritis and encapsulated them in methacrylated hyaluronic acid hydrogels. The authors reported that tissue growth was highly dependent on the donor, with several, but not all, of the osteoarthritic donors leading to rapid hydrogel degradation and minimal ECM deposition, resulting in complete mechanical failure of the hydrogel. This study highlights the importance of balancing ECM deposition and matrix-degrading enzyme production to achieve a seamless transfer from hydrogel to tissue. Schneider *et al.*[441] encapsulated chondrocytes in a PEG-chondroitin sulfate hydrogel crosslinked with enzyme-sensitive peptides and studied the effects of dynamic compressive loading on tissue growth. The authors noted that chondrocyte aggregation occurred at the time of encapsulation, which led to regions of high cell density and regions of low cell density. While both culture environments supported tissue growth, ECM accumulation was greatest in regions of high density and more so in the absence of dynamic loading. The effect of the loading environment was not readily explained by transport and was instead attributed to load-induced changes in biosynthesis rates.

Enzyme-sensitive hydrogels have also been used for other tissue engineering applications. For instance, Carles-Carner *et al.*[442] encapsulated MC3T3-E1 pre-osteoblasts in an enzyme-sensitive PEG hydrogel with RGD and hydroxyapatite nanoparticles that were cultured under osteogenic conditions. After 28 days, localized degradation was evident by interconnected regions consisting of collagen type I deposits that spanned multiple cells. Stevens *et al.*[443] encapsulated hepatocytes in a covalently crosslinked, enzyme-sensitive PEG hydrogels containing RGD, which supported liver cell function and was measured by albumin and urea secretion. However, the addition of J2-3T3 fibroblasts and liver endothelial TMNK-1 cells at the time of encapsulation produced an interconnected cellular network within three weeks suggesting that hydrogel degradation was mediated by the fibroblast and/or endothelial cells, although ECM deposition was not assessed.

As discussed in Section 3, enzyme sensitive hydrogels offer the unique feature of achieving localized degradation in the immediate vicinity of the cell. As enzymes diffuse away from the cell, i.e., their source, a degradation front advances from the cell surface. The sharpness (a measure of localization) and speed of this front depend on the competing time scales of degradation rate (see eq 10) and enzyme transport as described by eq 21 and eq 22 . When the enzyme diffusion is fast relative to enzyme reaction, degradation behavior will be on a macroscopic scale and similar to hydrolytic degradation. However, when the enzymatic degradation front is localized, this leaves substantial space for ECM precursors to transport, assemble, and deposit around cells, while preserving the mechanical integrity of the hydrogel further away from this interstitial (degraded) space. The combined synthesis, transport, and deposition of ECM

precursor molecules in the interstitial space has been described by a diffusion-reaction equation. This equation assumes that once ECM precursors are secreted by a cell, they are immediately assembled into the large ECM macromolecules. Therefore, the ECM transport can be modeled by assuming: (a) the diffusivity of ECM molecules vanishes when the gel is still connected ($\rho / \rho^0 > 1/\beta$) and (b) the diffusivity is maximal when the gel reaches reversed gelation ($\rho / \rho^0 < 1/\beta$). Furthermore, the rate of matrix deposition was assumed to follow the relation: [58]

(32)

where k_m is the intrinsic degradation rate while c_m and $\tilde{c}_m$ are the concentration of unbound (i.e., ECM precursor) and bound (i.e., assembled, solid) matrix, respectively. This equation was motivated by the concept of product inhibition hypothesis [444] that states that the ECM will deposit until it reaches a homeostatic target concentration . Numerical simulations [58,426] show that the mechanical integrity of the construct can be maintained if two conditions are met (Figure 28). First, the degradation front must be localized in order to allow for a local ECM deposition around the cells during the degradation process. Second, the rate of ECM deposition must be relatively fast compared to the rate of hydrogel degradation. This enables the development of a neo-tissue with mechanical integrity that can compensate for the loss of hydrogel from degradation.

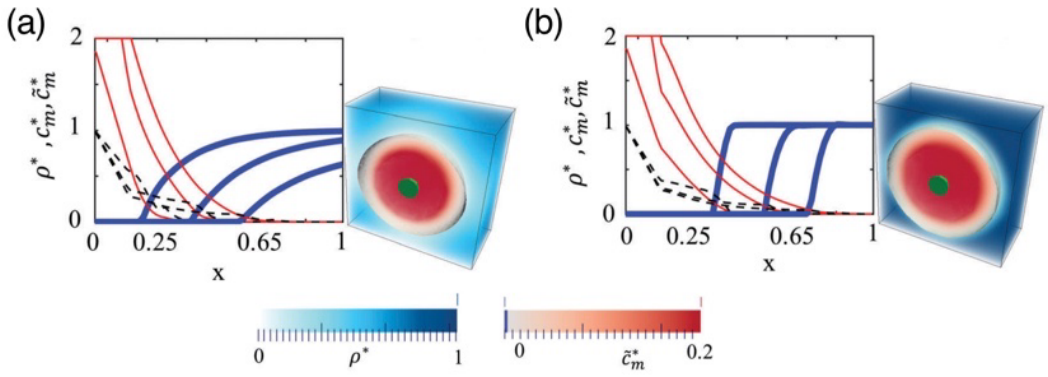

Figure 28. Profile of polymer cross-link density (solid blue lines), unbound ECM concentration (dashed black lines) and linked ECM concentration (red lines) as a function of distance from the cell surface. (a) Slow ECM deposition in a hydrogel scaffold with a wide and slow degradation front and (b) fast ECM deposition in a hydrogel scaffold with a sharp and fast degradation front. Reproduced from ref [58] with permission from the Royal Society of Chemistry. Copyright 2016 The Authors.

7.2.3. Stress Relaxing Hydrogels. While there has been a number of studies investigating the mechano-sensing in stress relaxing synthetic hydrogels as described in Section 4, there have been only a few studies that have investigated tissue growth in such hydrogels. Lee *et al.*[351] encapsulated chondrocytes in a stress relaxing, but otherwise stable, alginate hydrogels and showed that the amount of matrix deposited pericellularly was highly dependent on $\tau_{1/2}$. Hydrogels with $\tau_{1/2}$ values of 63-478 s led to the most elaborate ECM and was corroborated by quantitative measurements of collagen and sulfated glycosaminoglycan contents. Interestingly, the effect of hydrogel stiffness (3 *vs* 20 kPa, *G*) on ECM deposition was less pronounced in fast relaxing hydrogels ($\tau_{1/2}$ = 63 s). This indicates that the restricted matrix assembly and deposition due to the hydrogel structure could largely be overcome by the ability of the hydrogel to relax under the stress applied by the deposited ECM. Moreover, there was evidence that the growing pericellular matrix was connecting between cells, indicating that these forces could push out the hydrogel by viscoelastic flow, despite a lack of chemically (i.e., hydrolytic or enzymatic) degradable bonds. Richardson *et al.*[29] encapsulated chondrocytes in a covalently adaptable PEG-hydrazone network formed with varying ratios of aliphatic (alkyl-aldehyde) and aromatic (benzaldehyde) functional groups, which yielded fast and slow stress relaxing crosslinks, respectively. In addition, the hydrazone bond is susceptible to hydrolysis over time, with alkyl-aldehyde forming hydrazone bonds showing 50% mass loss within four weeks and minimal mass loss with the benzaldehyde forming hydrazone bond. Balancing viscous-to-elastic response, the authors identified an optimal average relaxation time of 3 days, where higher or lower relaxation times led to inferior ECM deposition. Histologically, there was evidence of ECM connecting between cells in the optimal hydrogel formulation. Taken together, these studies demonstrate that as ECM is secreted, assembled, and deposited, a stress relaxing hydrogel affords greater elaboration of the matrix in the interstitial space prior to hydrogel degradation and that hydrogel degradation can augment expansion of ECM to ensure that eventually the hydrogel is completely degraded.

7.3. Hydrogel-to-Tissue Transition

7.3.1. Mechanical Properties. The evolution of the construct properties has been studied by combining the above models of gel degradation and ECM growth with computational homogenization techniques discussed in Section 7.1.2. For a bulk (e.g., hydrolytically) degrading system, the model predicts a slow degradation of the gel, with little to no tissue growth until the polymer reaches its point of reverse gelation. When this occurs, the construct consists of cells embedded in a fluid-like degraded gel, with no

elastic modulus (Figure 28). By contrast, a localized (e.g., enzymatically) degrading system shows the development of a very different structure, with the appearance of a double connected network of ECM and hydrogel (Figure 29). This eventually allows a smooth transition between hydrogel and tissue and continuous mechanical integrity.

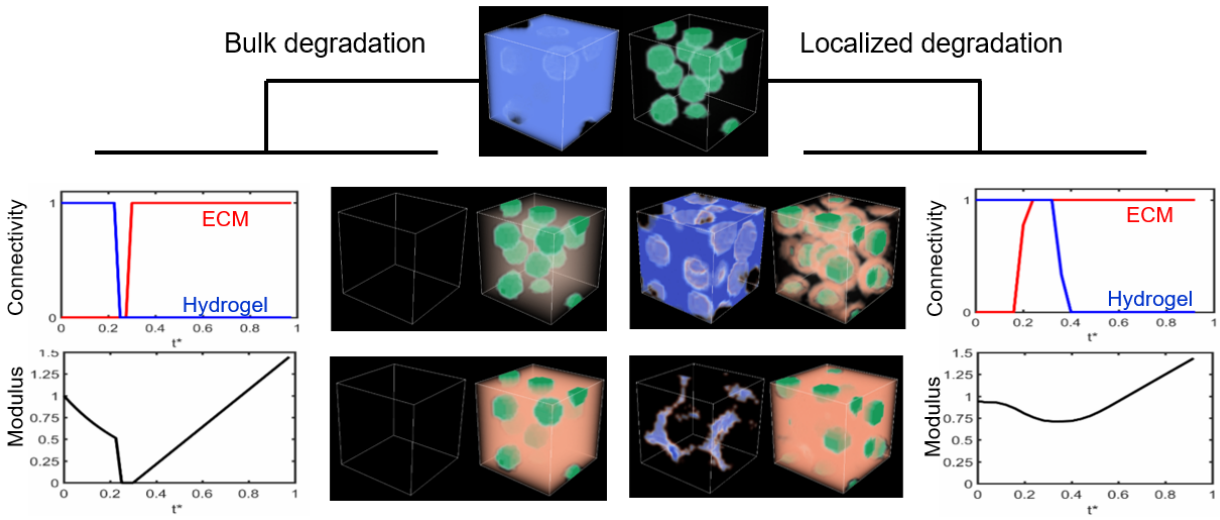

Figure 29. Evolution of the construct's constitution during its transition from hydrogel to tissue. The dark panels show hydrogel (blue) and ECM (red) concentrations and the chondrocytes (green). For hydrolytic degradation, the hydrogel degrades uniformly, and growth only occurs after complete hydrogel disappearance. This yields a discontinuity of the general connectivity of the construct, associated with a sudden drop of the elastic modulus to zero. The modulus is normalized to its initial value. For localized, enzymatic degradation (with a slow and sharp front), we observed the appearance of voids around cells where the new matrix can deposit and grow. This scenario enables a maintenance of the construct's connectivity in time, which manifest itself by a continuous mechanical integrity during the transition.

Experimental studies have shown that the evolution of construct modulus over time in different types of degrading hydrogels is highly variable. This variability can be attributed to a number of factors such as the hydrogel crosslinking and degradation mechanism, loading vs free swelling, the cell type (i.e., differentiated vs stem cell), donor variability, cell density, and spatial distribution of cells. In Aisenbrey *et al.*,[437] the modulus in the enzyme-sensitive PEG Hydrogels dropped by 70% after one week (18 to 5 kPa, E), but increased to 10 kPa (E) by week 9 shown in Figure 27d, capturing the trend in modulus predicted by the computational model in Figure 29. In Rogen *et al.*[439] the modulus of chondroitin sulfate/PEG hydrogel increased from 4 kPa (E) at day one to 211 kPa (E) at day 21, although the modulus during the transition from hydrogel-to-tissue was not captured. In Schneider *et al.*,[441] the modulus of the PEG/Chondroitin sulfate hydrogel with enzyme-sensitive peptide crosslinkers dropped from 40 kPa to 11 kPa at day 15, but

recovered to 100 kPa by day 43. In the dynamic loading environment, the modulus dropped from 40 kPa to 2.5 kPa at day 15 and only recovered to 26 kPa. The computational model described above was used in this study and was able to predict the temporal evolution of modulus by accounting for the combination of ECM deposition and enzyme synthesis rates. These findings indicate that the sensitivity of the cellular response to its environment is an important factor to consider in the transition from hydrogel-to-tissue.

The mathematical model of tissue growth in bulk degrading, hydrolytic hydrogels predicts that there is a narrow window where one can achieve a transition from hydrogel to tissue. From an experimental perspective, achieving success would therefore be nearly impossible. However, successes have been reported in using hydrolytically degradable hydrogels in cartilage tissue engineering. In Neumann *et al.*,[429] the modulus increased 8-fold from 7 kPa on day 7 to 55 kPa (E) on day 28 as shown in Figure 27c. On the contrary, a previous study by Roberts *et al.*[445] reported a decrease in modulus from 20 kPa initially to 1 kPa on day 14 and which remained similarly low on day 28 for chondrocytes encapsulated in a PEG-poly(lactic acid) hydrogel. A lower cell density and a faster degrading hydrogel could have led to the inferior outcomes reported in Roberts *et al.*[445] compared to Neumann *et al.*[429] Chu *et al.*[446] recently identified spatial heterogeneities in hydrogel crosslinking that occur at the time of encapsulation in free-radical polymerized hydrogels. These heterogeneities arise from cells interfering with the polymerization that causes a reduction in the hydrogel crosslinking in a region immediately adjacent to the cell. As a result, the hydrogel can reach reverse gelation in the interstitial region creating space for ECM to assemble and deposit, while the bulk hydrogel remains intact. This creates a front that is similar to that predicted for enzyme-sensitive hydrogels. When cells are in close proximity such as aggregates or clusters, these regions of reduced crosslinking overlap. This study also showed that spatial heterogeneity was observed in enzyme-sensitive PEG hydrogels formed through free-radical polymerization. When diffusion dominates in enzyme-sensitive hydrogels, degradation would be akin to bulk degradation. However, these spatial heterogeneities will create a degradation front that can support tissue growth. This concept has been applied to in the aforementioned mathematical model and could explain tissue growth in hydrolytic [422,430] and enzyme-sensitive PEG hydrogels.[441,447] Heterogeneities can also form as a result of the method of hydrogel formation. For example, differences between chain growth and step growth polymerizations have been described, where the former leads to greater network heterogeneities. [357,358] PEG hydrogels formed from chain growth produced more ECM than PEG hydrogels formed from step growth, which may be attributed at least in part to the greater network heterogeneities in the former. [448] Taken together, these findings suggest that heterogeneities across multiple length scales have a significant impact on the growth of ECM in hydrogels.

7.3.2. Percolation Theory. During hydrogel-to-tissue transition, the change in a construct's stiffness has been conceptualized as a double percolation problem. [422,449] Simple percolfation[450] describes the emergence of a connected network (i.e., mechanically stable) from a set of nodes between which links are randomly created. A cell-hydrogel construct may similarly be thought of as an interpenetrating network made of the polymer network and the new ECM. On the one hand, the hydrogel, which is originally connected, loses its connectivity with degradation until the point where the network is no longer percolated. On the other hand, the ECM, which is originally absent, is slowly synthesized and deposited by encapsulated cells until it forms a percolated network. The total mechanical integrity of the construct is then assessed by the time t_g at which the gel loses its connectivity and is no longer a percolated network, and the time t_m at which the ECM gains percolation. The latter can only be achieved once the voids that represent regions where the hydrogel has reached its reverse gelation are able to percolate, which can be assessed by the time t_v. Figure 30 depicts two scenarios. Generally, if $t_m > t_g$, the construct loses its overall percolation and fails during growth, losing all mechanical integrity. Therefore, $t_g > t_m$ is a necessary condition for a successful hydrogel design. In the second scenario, a successful transition from hydrogel-to-tissue is achieved because the neo-tissue reaches percolation before the hydrogel loses its percolated network. Numerical simulations have shown that this can be achieved in various ways: (a) by using localized (e.g., enzymatic) degradation that exhibits a sharp front that propagates slowly [58] (relative to tissue growth), or (b) by using hydrolytic degradation and a cell population that is heterogeneously distributed throughout the hydrogels. [422,441] The latter case is made possible due to the spatial heterogeneities in hydrogel crosslinking and a heterogeneous cell distibution. In this case, the model suggested the presence of dense and interconnected cell clusters.

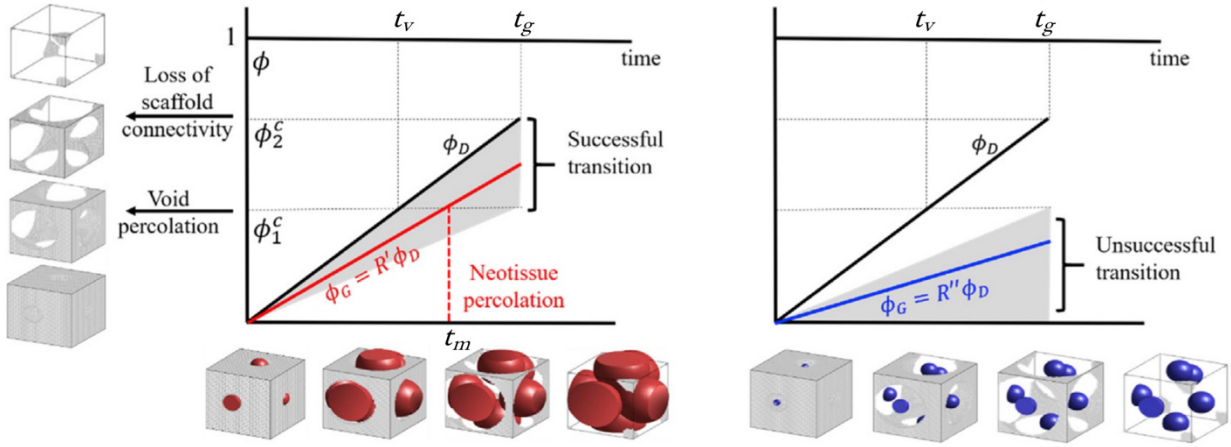

Figure 30. A linear model based on percolation theory was developed to determine the conditions that yield a smooth hydrogel-to-tissue transition. Here, the symbol ϕ_v denotes the volume fraction of the voids created by degradation around the cells while ϕ_g is the volume fraction of the new matrix filling those voids. Two hydrogel percolation thresholds are defined: (1) is the threshold when the voids, representing regions of the hydrogel that have reached reverse gelation, reach percolation corresponding to the time t_v and (2) is the threshold when the crosslinked polymer loses its connectivity corresponding to the time t_g. Left: A successful transition is achieved when the time t_m that ECM (i.e., neotissue) reaches percolation occurs before t_g. Right: An unsuccessful transition occurs when $t_m > t_g$. Adapted and reproduced with permission from ref [449]. Copyright 2020 Elsevier Inc.

7.4. Outlook: Tuning Hydrogels to Engineer Tissue

The integration of experiments and computational models has helped identify key mechanisms that are necessary to achieve tissue growth when cells are encapsulated in a hydrogel. One of the underlying mechanisms that is absolutely critical to tissue growth is the presence of spatial heterogeneities in hydrogel crosslink density. Mathematical models were able to show that if the hydrogel crosslink density is uniform, then it is impossible to achieve a successful hydrogel-to-tissue transition, as the hydrogel must reach its reverse gelation before ECM is able to assemble. This led to the identification that heterogeneities must exist within experimental cell-laden hydrogels. Indeed, studies were able to identify that during encapsulation, cells can interact with monomers (or macromolecular monomers) and propagating radicals to alter the crosslink density near the cell. Heterogeneities are likely to exist in other hydrogel systems as well. For example, biopolymers have the potential to interact with cell surface receptors, which could influence their ability to form crosslinks. [451] Understanding these heterogeneities and the mechanisms that lead to them offers a powerful approach to allow ECM to grow and increase the probability of achieving a percolated ECM network. While enzyme-sensitive hydrogels naturally create a gradient in enzyme concentration emanating from the cell membrane, most of the hydrogels that are used in tissue engineering are soft, leading to a large mesh size relative to the size of cell-secreted enzymes. As a result, these hydrogel systems often will degrade by bulk degradation. One way to overcome this shortcoming is to engineer peptide sequence that have fast degradation kinetics. This would allow for reaction mechanisms to dominate over diffusion and achieve a sharp degrading front without needing to control diffusion through mesh size. The ability to tune degradation with respect to reverse gelation, void formation, and percolation is critical to achieving degradation rates that match ECM synthesis, assembly, and deposition. This becomes even more challenging, yet important, when considering cells isolated from

different donors, where ECM and enzyme synthesis rates can vary dramatically. Another way to overcome the above shortcoming is to use relative stable hydrogels with fast relaxation rates; this would allow the cell to push on the hydrogel and create space as it is depositing its ECM. Another factor that could be important, but which has not received much attention, is the geometry of the hydrogel construct. While geometry is unlikely to have an effect on the hydrogel-to-tissue transition if cells remain uniformly distributed, if geometry alters the spatial distribution of cells, it could have a significant effect on tissue growth. As the size of the construct increases, nutrient transport becomes limiting and can affect the health and phenotype of the encapsulated cells. Computational models will need to not only aid in understanding the coupled processes of hydrogel degradation and ECM growth, but will also need to be able to predict optimal designs that are suitable for each patient. Future models will need to begin considering how to personalize hydrogel design for tissue growth.

Although most of the work described in this section focused on cartilage, there are other cell types that produce large amounts of ECM, such as cancer-associated cells. The hydrogels and coupled mathematical models described in this section could serve as a valuable 3D model to study the role of the ECM in cancer progression and how the surrounding environment such as mechanical forces or other cues could impact ECM growth.[452,453] Such studies could help identify mechanisms that prevent the spread of tumors and which could also serve as test beds for cancer therapeutics.

8. SUMMARY AND OVERALL OUTLOOK

A cell encapsulated in a hydrogel receives local physical cues that depend on the nature of the polymer, as well as the density and dynamical nature of its crosslinks. Cell-hydrogel interactions are indeed mediated by transport mechanisms, that depend on mesh size, and mechanical sensing that rely on a combination of stiffness, stress-relaxation, and degradability of the surrounding polymer. Through this review covering a multitude of recent studies on cell-hydrogel interactions involving experiments, mathematical and computational models, and their combination, we have identified two defining mechanical characteristics of the hydrogel that have the most significant impact on cellular functions. These are: (a) the size of the polymer mesh that acts as a physical barrier to biomolecular transport and to cells and (b) mechanical confinement that applies forces onto the cell membrane. While these characteristics are inherent to every hydrogel, they can be controlled through the properties of the hydrogel to achieve a targeted cellular fate.

The mesh size affects several important cellular functions in a cell-laden hydrogel. The polymer network can act as a barrier to hinder the transport of large biomolecules required for both cell to cell signaling and cell-secreted ECM precursors that subsequently assemble into an ECM. The mesh size also limits the extent to which cells can probe the hydrogel environment or migrate through the hydrogel. For instance, polymer networks with physically crosslinked semi-flexible chains can afford a greater ability for intercellular interaction through a large mesh that arises due to fiber geometry. They can also provide a mechanism for the cells to explore their environment by navigating the fibrous network using cellular forces that can reconfigure the network. On the contrary, flexible polymer networks with stable covalent bonds are essentially inhibitory to cellular process extension due to their small mesh sizes; even in the softest hydrogels of 10's Pa, cell spreading is generally prohibited. Hydrogels must therefore be engineered with either bonds that are degradable by solute molecules (e.g., water or enzymes) diffusing through the polymer network or with dynamic bonds whose reversible binding kinetics are fast enough to enable network reconfiguration and allow cells to both probe their environment and secrete and assemble ECM. Thus, to enable key cellular functions such as cell spreading, cell growth, cell migration, and ECM growth in flexible polymer networks, cells must be able to degrade the hydrogel or remodel it through the application of forces. Moreover, for these functions to occur, the hydrogel has to have reached its point of reverse gelation, as there is no large enough mesh size that can allow these events to occur. These observations demonstrate that there are distinct differences in how cells interact with semiflexible (i.e., fibrous) and flexible polymer networks.

An interesting finding, discovered by the integration between experiments and modeling, is that heterogeneities in the crosslink density especially for flexible polymer networks are key to achieving many of these cellular functions (e.g., cell communication, cell spreading, and ECM growth). For example, diffusion of molecules larger than the average mesh size is possible in a heterogeneous network if a solute can navigate a pathway through the larger openings in the polymer mesh. In enzyme-sensitive hydrogels where cells are the source of the enzyme, a concentration gradient forms where enzymes can degrade the hydrogel faster in regions near the cell than afar. Recent findings have also identified that cells can inhibit the polymerization reaction during cell encapsulation, leading to a heterogeneous crosslink density in the vicinity of the cell. This in turn leads to faster degradation rates, where reverse gelation occurs quickly around cells. Taken together, these studies suggest that heterogenous networks may in fact be more supportive of cellular interactions with hydrogels, which may also better mimic the heterogenous nature of native ECM.

The second defining characteristic of the cell's 3D environment is mechanical confinement, which plays a key role in many of the cellular functions discussed in this review. Mechanical confinement is particularly important when cells are encapsulated in a hydrogel and the polymer network completely surrounds the cell – a stark contrast to 2D cultures and 3D cultures in porous scaffolds. Under this scenario, cells experience a force that is exerted on the cell membrane, providing cells with a direct mechanical cue that can alter its behavior. While mechanical confinement is often exacerbated by stiffer hydrogels, which means a smaller mesh size, the effects of mechanical confinement can lead to cellular behavior that is opposing to that of a physical barrier. For instance, mechanical confinement can induce amoeboid migration of cells in a 3D hydrogel. This force can also cause a phenotypic switch in the cells, where they change their mode of migration from mesenchymal to amoeboid. Mechanical confinement can lead to cell proliferation and a more aggressive cellular phenotype, such as that observed in cancer. These findings are possible in hydrogels that contain reversible bonds or degradable bonds due to their dynamic nature. With advancements in hydrogel designs, the ability to probe new and different types of cellular behavior in 3D is helping to advance our understanding of how cells interact with their surroundings.

Understanding and deciphering the cell-hydrogel interactions is challenging in a 3D hydrogel environment due to the difficulty of isolating one property from the rest. For example, it is challenging to control mesh size independent of mechanical confinement. While some studies, as discussed in this review, have been able to partially decouple these two hydrogel characteristics by using natural hydrogels, such as fibrous hydrogels or ionically crosslinked alginate, a true decoupling is nearly impossible and is even more difficult in flexible polymer networks. Mathematical models have been instrumental in identifying novel mechanisms through experiment-informed directed hypotheses. However, the results from modeling rely on their validation with experiments. This means that an integrated experimental and computational campaign is critical to confirming the mechanistic insights revealed by the models. Once validated, the models offer optimization strategies that can be leveraged to narrow the experimental design space for testing fundamentally important questions.

In summary, there have been major recent advancements identifying how cells interact with and respond to their surrounding environment in 3D, which can be in large part attributed to the advancement of new hydrogels, more sophisticated analysis techniques, and computational models. This knowledge has provided key insights into the design of advanced hydrogels that can control specific cellular functions. With this knowledge, the field is now at a turning point where we can extend this information to

personalized medicine. Computational models and their potential for improvement through data mining and machine learning techniques can accelerate the progress towards design of hydrogels that will support tissue growth unique to an individual, regardless of their demographics or health status, and to develop *ex vivo* model systems for testing therapeutics for personalized medicine.

AUTHOR INFORMATION

Corresponding Authors

Stephanie J. Bryant – *Department of Chemical and Biological Engineering, Materials Science and Engineering Program, BioFrontiers Institute, University of Colorado at Boulder, 3415 Colorado Ave, Boulder, CO USA 80309-0596*

Orcid.org/ 0000-0003-1907-5216; Email: sbryant@colorado.edu

Franck J. Vernerey – *Department of Mechanical Engineering, Materials Science and Engineering Program, University of Colorado at Boulder, 1111 Engineering Drive, Boulder, CO USA 80309-0428.*

Orcid.org/ 0000-0001-6138-1431; Email: franck.vernerey@colorado.edu

Authors

Shankar Lalitha Sridhar – *Department of Mechanical Engineering, Materials Science and Engineering Program, University of Colorado at Boulder, 1111 Engineering Drive, Boulder, CO USA 80309-0428.*

Orcid.org/ 0000-0003-4226-4779

Archish Muralidharan – *Materials Science and Engineering Program, University of Colorado at Boulder, 3415 Colorado Ave, Boulder, CO USA 80309-0596.*

Author Contributions

[+]S.L. and A.M. contributed equally

Notes

The authors declare no competing financial interests.

Biographies

Dr. Stephanie J. Bryant is a Professor in the Department of Chemical and Biological Engineering and the Associate Director of the Materials Science and Engineering Program at the University of Colorado at Boulder. She received her Ph.D. from the University of Colorado in Chemical Engineering and was a post-doctoral fellow in the Department of Bioengineering at the University of Washington. Since joining the University of Colorado in 2005, her research group has focused on engineering biomimetic and biodegradable hydrogels as model systems for mechanobiology and as cell delivery vehicles for *in vitro* and *in vivo* tissue engineering applications. Dr. Bryant is the recipient of the NSF Career Award, NIH K-Award, the Daniel I.C. Wang Award from *Biotechnology and Bioengineering*, and is a fellow of the American Institute of Medical and Biological Engineering.

Dr. Franck J. Vernerey is a Professor in the Department of Mechanical Engineering and Faculty Fellow in the Materials Science and Engineering Program at the University of Colorado at Boulder. He received his Ph.D. from Northwestern University in 2006 in the field of theoretical and applied mechanics, where he worked on the development of micro-continuum theories for fracture, under W.K Liu and B. Moran. Since joining the University of Colorado in 2007, his research group has focused on developing theoretical and numerical approaches to elucidate the physical mechanisms that drive the emerging mechanical response of molecular networks. These include polymers, hydrogels, biopolymers and active biological matter. Dr. Vernerey is the recipient of the NSF Career Award in 2014 and the Presidential Early Career Award for Scientists and Engineers (PECASE) in 2017.

Dr. Shankar Lalitha Sridhar is a postdoctoral researcher in the BioFrontiers Institute at the University of Colorado Boulder. He received his PhD in 2020 from the department of mechanical engineering at the University of Colorado Boulder with a research focus on developing theoretical and computational models describing the mechanics of complex soft materials with an emphasis on biological and bio-inspired systems. He was awarded the Outstanding Dissertation and Distinguished Dissertation Awards from the University of Colorado Boulder for his PhD dissertation given to one student whose dissertation is of extremely high quality and contributes significantly to the understanding of the subject matter. His research interests include complex soft materials and its applications in polymer science and biomaterials,

developing theory and modeling to bridge local interactions and global emergent properties of materials with evolving micro-structures.

Archish Muralidharan is a PhD student at the University of Colorado Boulder. He got his B.S. degree in Polymer Engineering at Institute of Chemical Technology, Mumbai. In 2018, he received his M.S. degree in Materials Science and Engineering. He received Dick Aubin Distinguished Paper Award from the Society of Manufacturing Engineers in 2020. His current research interests include applications of fundamental polymer science and engineering towards additive manufacturing, optics and biomaterials.

ACKNOWLEDGMENTS

The authors would like to acknowledge support from the National Institute of Arthritis and Musculoskeletal and Skin Diseases (R01 AR069060-A1), the National Institute of Child Health and Human Development (R33HD090696), and the National Heart, Lung and Blood Institute (R01HL119371-A1). The content is solely the responsibility of the authors and does not necessarily represent the official views of the National Institutes of Health. The authors would also like to acknowledge support from the National Science Foundation from the Division of Civil, Mechanical and Manufacturing under Award numbers 1761918, 1825692, and 2023179 and from the Division of Molecular and Cellular Biosciences under Award number 1943488.

REFERENCES

ADDIN ZOTERO_BIBL {"uncited":[],"omitted":[],"custom":[]} CSL_BIBLIOGRAPHY (1) Picu, R. C. Mechanics of Random Fiber Networks—a Review. *Soft Matter* **2011**, *7*, 6768–6785.

(2) Blundell, J. R.; Terentjev, E. M. Stretching Semiflexible Filaments and Their Networks. *Macromolecules* **2009**, *42*, 5388–5394.

(3) Rubinstein, M.; Colby, R. H. *Polymer Physics*; OUP Oxford, 2003.

(4) Vernerey, F. J.; Long, R.; Brighenti, R. A Statistically-Based Continuum Theory for Polymers with Transient Networks. *J. Mech. Phys. Solids* **2017**, *107*, 1–20.

(5) Doi, M. *Soft Matter Physics*; Oxford University Press.

(6) Rubinstein, M.; Panyukov, S. Nonaffine Deformation and Elasticity of Polymer Networks. *Macromolecules* **1997**, *30*, 8036–8044.

(7) Flory, P. J.; Rehner, R., Jr. Statistical Mechanics of Crosslinked Polymer Networks. I. Rubberlike Elasticity. *J. Chem. Phys.* **1943**, *11*, 521–526.

(8) Ibusuki, S.; Halbesma, G. J.; Randolph, M. A.; Redmond, R. W.; Kochevar, I. E.; Gill, T. J. Photochemically Cross-Linked Collagen Gels as Three-Dimensional Scaffolds for Tissue Engineering. *Tissue Eng.* **2007**, *13*, 1995–2001.

(9) Meghezi, S.; Seifu, D. G.; Bono, N.; Unsworth, L.; Mequanint, K.; Mantovani, D. Engineering 3D Cellularized Collagen Gels for Vascular Tissue Regeneration. *J. Vis. Exp.* **2015**, No. 100, 52812.

(10) López-Marcial, G. R.; Zeng, A. Y.; Osuna, C.; Dennis, J.; García, J. M.; O'Connell, G. D. Agarose-Based Hydrogels as Suitable Bioprinting Materials for Tissue Engineering. *ACS Biomater. Sci. Eng.* **2018**, *4*, 3610–3616.

(11) Varoni, E.; Tschon, M.; Palazzo, B.; Nitti, P.; Martini, L.; Rimondini, L. Agarose Gel as Biomaterial or Scaffold for Implantation Surgery: Characterization, Histological and Histomorphometric Study on Soft Tissue Response. *Connect. Tissue Res.* **2012**, *53*, 548–554.

(12) Blundell, J. R.; Terentjev, E. M. Buckling of Semiflexible Filaments under Compression. *Soft Matter* **2009**, *5*, 4015.

(13) Broedersz, C. P.; Mao, X.; Lubensky, T. C.; MacKintosh, F. C. Criticality and Isostaticity in Fibre Networks. *Nat. Phys.* **2011**, *7*, 983–988.

(14) Jansen, K. A.; Licup, A. J.; Sharma, A.; Rens, R.; MacKintosh, F. C.; Koenderink, G. H. The Role of Network Architecture in Collagen Mechanics. *Biophys. J.* **2018**, *114*, 2665–2678.

(15) Bertula, K.; Martikainen, L.; Munne, P.; Hietala, S.; Klefström, J.; Ikkala, O.; Nonappa. Strain-Stiffening of Agarose Gels. *ACS Macro Lett.* **2019**, *8*, 670–675.

(16) Broedersz, C. P.; MacKintosh, F. C. Modeling Semiflexible Polymer Networks. *Rev. Mod. Phys.* **2014**, *86*, 995–1036.

(17) Meng, F.; Terentjev, E. M. Theory of Semiflexible Filaments and Networks. *Polymers* **2017**, *9*, 52.

(18) Chaudhuri, O.; Cooper-White, J.; Janmey, P. A.; Mooney, D. J.; Shenoy, V. B. Effects of Extracellular Matrix Viscoelasticity on Cellular Behaviour. *Nature* **2020**, *584*, 535–546.

(19) Lee, K. Y.; Mooney, D. J. Alginate: Properties and Biomedical Applications. *Progress in Polymer Science* **2012**, *37*, 106–126.

(20) Li, L.; Fang, Y.; Vreeker, R.; Appelqvist, I.; Mendes, E. Reexamining the Egg-Box Model in Calcium−Alginate Gels with X-Ray Diffraction. *Biomacromolecules* **2007**, *8*, 464–468.

(21) Lee, K. Y.; Mooney, D. J. Alginate: Properties and Biomedical Applications. *Prog. Polym. Sci.* **2012**, *37*, 106–126.
(22) Yonese, M.; Baba, K.; Kishimoto, H. Stress-Relaxation of Alginate Gels Crosslinked by Various Divalent Metal-Ions. *Bull. Chem. Soc. Jpn.* **1988**, *61*, 1857–1863.
(23) Chaudhuri, O.; Gu, L.; Klumpers, D.; Darnell, M.; Bencherif, S. A.; Weaver, J. C.; Huebsch, N.; Lee, H.; Lippens, E.; Duda, G. N.; et al. Hydrogels with Tunable Stress Relaxation Regulate Stem Cell Fate and Activity. *Nat. Mater.* **2016**, *15*, 326–334.
(24) Rodell, C. B.; Mealy, J. E.; Burdick, J. A. Supramolecular Guest–Host Interactions for the Preparation of Biomedical Materials. *Bioconjug. Chem.* **2015**, *26*, 2279–2289.
(25) Park, K. M.; Yang, J.-A.; Jung, H.; Yeom, J.; Park, J. S.; Park, K.-H.; Hoffman, A. S.; Hahn, S. K.; Kim, K. *In Situ* Supramolecular Assembly and Modular Modification of Hyaluronic Acid Hydrogels for 3D Cellular Engineering. *ACS Nano* **2012**, *6*, 2960–2968.
(26) McBride, M. K.; Worrell, B. T.; Brown, T.; Cox, L. M.; Sowan, N.; Wang, C.; Podgorski, M.; Martinez, A. M.; Bowman, C. N. Enabling Applications of Covalent Adaptable Networks. *Annu. Rev. Chem. Biomol. Eng.* **2019**, *10*, 175–198.
(27) McKinnon, D. D.; Domaille, D. W.; Cha, J. N.; Anseth, K. S. Biophysically Defined and Cytocompatible Covalently Adaptable Networks as Viscoelastic 3D Cell Culture Systems. *Adv. Mater.* **2014**, *26*, 865–872.
(28) Hafeez, S.; Ooi, H.; Morgan, F.; Mota, C.; Dettin, M.; van Blitterswijk, C.; Moroni, L.; Baker, M. Viscoelastic Oxidized Alginates with Reversible Imine Type Crosslinks: Self-Healing, Injectable, and Bioprintable Hydrogels. *Gels* **2018**, *4*, 85.
(29) Richardson, B. M.; Wilcox, D. G.; Randolph, M. A.; Anseth, K. S. Hydrazone Covalent Adaptable Networks Modulate Extracellular Matrix Deposition for Cartilage Tissue Engineering. *Acta Biomater.* **2019**, *83*, 71–82.
(30) Madl, C. M.; Heilshorn, S. C. Rapid Diels–Alder Cross-Linking of Cell Encapsulating Hydrogels. *Chem. Mater.* **2019**, *31*, 8035–8043.
(31) Brown, T. E.; Carberry, B. J.; Worrell, B. T.; Dudaryeva, O. Y.; McBride, M. K.; Bowman, C. N.; Anseth, K. S. Photopolymerized Dynamic Hydrogels with Tunable Viscoelastic Properties through Thioester Exchange. *Biomaterials* **2018**, *178*, 496–503.
(32) Okumura, Y.; Ito, K. The Polyrotaxane Gel: A Topological Gel by Figure-of-Eight Cross-Links. *Adv. Mater.* **2001**, *13*, 485–487.
(33) Vernerey, F. J.; Lamont, S. Transient Mechanics of Slide-Ring Networks: A Continuum Model. *J. Mech. Phys. Solids* **2021**, *146*, 104212.
(34) Ito, K. Novel Cross-Linking Concept of Polymer Network: Synthesis, Structure, and Properties of Slide-Ring Gels with Freely Movable Junctions. *Polym. J.* **2007**, *39*, 489–499.
(35) Bitoh, Y.; Akuzawa, N.; Urayama, K.; Takigawa, T.; Kidowaki, M.; Ito, K. Peculiar Nonlinear Elasticity of Polyrotaxane Gels with Movable Cross-Links Revealed by Multiaxial Stretching. *Macromolecules* **2011**, *44*, 8661–8667.
(36) Tong, X.; Yang, F. Sliding Hydrogels with Mobile Molecular Ligands and Crosslinks as 3D Stem Cell Niche. *Adv. Mater.* **2016**, *28*, 7257–7263.
(37) Cho, I. S.; Ooya, T. Cell-Encapsulating Hydrogel Puzzle: Polyrotaxane-Based Self-Healing Hydrogels. *Chem. Eur. J.* **2020**, *26*, 913–920.

(38) McLeish, T. C. B. Tube Theory of Entangled Polymer Dynamics. *Adv. Phys.* **2002**, *51*, 1379–1527.
(39) Roberts, J. J.; Earnshaw, A.; Ferguson, V. L.; Bryant, S. J. Comparative Study of the Viscoelastic Mechanical Behavior of Agarose and Poly(Ethylene Glycol) Hydrogels. *J. Biomed. Mater. Res. Part B Appl. Biomater.* **2011**, *99*, 158–169.
(40) Green, M. S.; Tobolsky, A. V. A New Approach to the Theory of Relaxing Polymeric Media. *J. Chem. Phys.* **1946**, *14*, 80–92.
(41) Eyring, H. Viscosity, Plasticity, and Diffusion as Examples of Absolute Reaction Rates. *J. Chem. Phys.* **1936**, *4*, 283–291.
(42) Tanaka, F.; Edwards, S. F. Viscoelastic Properties of Physically Crosslinked Networks. 1. Transient Network Theory. *Macromolecules* **1992**, *25*, 1516–1523.
(43) Stukalin, E. B.; Cai, L.-H.; Kumar, N. A.; Leibler, L.; Rubinstein, M. Self-Healing of Unentangled Polymer Networks with Reversible Bonds. *Macromolecules* **2013**, *46*, 7525–7541.
(44) Long, R.; Qi, H. J.; Dunn, M. L. Modeling the Mechanics of Covalently Adaptable Polymer Networks with Temperature-Dependent Bond Exchange Reactions. *Soft Matter* **2013**, *9*, 4083–4096.
(45) Tanaka, F.; Edwards, S. F. Viscoelastic Properties of Physically Crosslinked Networks. 1. Transient Network Theory. *Macromolecules* **1992**, *25*, 1516–1523.
(46) Jongschaap, R. J. J.; Wientjes, R. H. W.; Duits, M. H. G.; Mellema, J. A Generalized Transient Network Model for Associative Polymer Networks. *Macromolecules* **2001**, *34*, 1031–1038.
(47) Thien, N. P.; Tanner, R. I. A New Constitutive Equation Derived from Network Theory. *J. Non-Newton. Fluid Mech.* **1977**, *2*, 353–365.
(48) Vernerey, F. J. Transient Response of Nonlinear Polymer Networks: A Kinetic Theory. *J. Mech. Phys. Solids* **2018**, *115*, 230–247.
(49) Sing, M. K.; Wang, Z.-G.; McKinley, G. H.; Olsen, B. D. Celebrating Soft Matter's 10th Anniversary: Chain Configuration and Rate-Dependent Mechanical Properties in Transient Networks. *Soft Matter* **2015**, *11*, 2085–2096.
(50) Metters, A. T.; Bowman, C. N.; Anseth, K. S. A Statistical Kinetic Model for the Bulk Degradation of PLA-b-PEG-b-PLA Hydrogel Networks. *J. Phys. Chem. B* **2000**, *104*, 7043–7049.
(51) Dhote, V.; Skaalure, S. C.; Akalp, U.; Roberts, J. J.; Bryant, S. J.; Vernerey, F. J. On the Role of Hydrogel Structure and Degradation in Controlling the Transport of Cell-Secreted Matrix Molecules for Engineered Cartilage. *J. Mech. Behav. Biomed. Mater.* **2013**, *19*, 61–74.
(52) Bryant, S. J.; Vernerey, F. J. Programmable Hydrogels for Cell Encapsulation and Neo-Tissue Growth to Enable Personalized Tissue Engineering. *Adv. Healthc. Mater.* **2018**, *7*, 1–13.
(53) Rydholm, A. E.; Reddy, S. K.; Anseth, K. S.; Bowman, C. N. Development and Characterization of Degradable Thiol-Allyl Ether Photopolymers. *Polymer* **2007**, *48*, 4589–4600.
(54) Metters, A. T.; Anseth, K. S.; Bowman, C. N. A Statistical Kinetic Model for the Bulk Degradation of PLA-b- PEG-b-PLA Hydrogel Networks: Incorporating Network Non-

Idealities. *J. Phys. Chem. B* **2001**, *105*, 8069–8076.
(55) Miller, D. R.; Macosko, C. W. A New Derivation of Postgel Properties of Network Polymers. *Rubber Chem. Technol.* **1976**, *49*, 1219–1231.
(56) Leskovac, V. *Comprehensive Enzyme Kinetics*; Springer Science & Business Media, 2003.
(57) Skaalure, S. C.; Akalp, U.; Vernerey, F. J.; Bryant, S. J. Tuning Reaction and Diffusion Mediated Degradation of Enzyme-Sensitive Hydrogels. *Adv. Healthcare Mater.* **2016**, *5*, 432–438.
(58) Akalp, U.; Bryant, S. J.; Vernerey, F. J. Tuning Tissue Growth with Scaffold Degradation in Enzyme-Sensitive Hydrogels: A Mathematical Model. *Soft Matter* **2016**, *12*, 7505–7520.
(59) Khetan, S.; Guvendiren, M.; Legant, W. R.; Cohen, D. M.; Chen, C. S.; Burdick, J. A. Degradation-Mediated Cellular Traction Directs Stem Cell Fate in Covalently Crosslinked Three-Dimensional Hydrogels. *Nat. Mater.* **2013**, *12*, 458–465.
(60) Kloxin, A. M.; Kasko, A. M.; Salinas, C. N.; Anseth, K. S. Photodegradable Hydrogels for Dynamic Tuning of Physical and Chemical Properties. *Science* **2009**, *324*, 59.
(61) Norris, S. C. P.; Delgado, S. M.; Kasko, A. M. Mechanically Robust Photodegradable Gelatin Hydrogels for 3D Cell Culture and *in Situ* Mechanical Modification. *Polym. Chem.* **2019**, *10*, 3180–3193.
(62) Arkenberg, M. R.; Moore, D. M.; Lin, C.-C. Dynamic Control of Hydrogel Crosslinking via Sortase-Mediated Reversible Transpeptidation. *Acta Biomater.* **2019**, *83*, 83–95.
(63) Arkenberg, M. R.; Nguyen, H. D.; Lin, C.-C. Recent Advances in Bio-Orthogonal and Dynamic Crosslinking of Biomimetic Hydrogels. *J. Mater. Chem. B* **2020**, *8*, 7835–7855.
(64) Einstein, A. On the Motion of Small Particles Suspended in Liquids at Rest Required by the Molecular-Kinetic Theory of Heat. *Ann. Phys.* **1905**, *322*, 549560.
(65) Amsden, B. Solute Diffusion within Hydrogels. Mechanisms and Models. *Macromolecules* **1998**, *31*, 8382–8395.
(66) Axpe, E.; Chan, D.; Offeddu, G. S.; Chang, Y.; Merida, D.; Hernandez, H. L.; Appel, E. A. A Multiscale Model for Solute Diffusion in Hydrogels. *Macromolecules* **2019**, *52*, 6889–6897.
(67) Cohen, M. H.; Turnbull, D. Molecular Transport in Liquids and Glasses. *J. Chem. Phys.* **1959**, *31*, 1164–1169.
(68) Lustig, S. R.; Peppas, N. A. Solute Diffusion in Swollen Membranes. IX. Scaling Laws for Solute Diffusion in Gels. *J. Appl. Polym. Sci.* **1988**, *36*, 735–747.
(69) Hadjiev, N. A.; Amsden, B. G. An Assessment of the Ability of the Obstruction-Scaling Model to Estimate Solute Diffusion Coefficients in Hydrogels. *J. Control. Release* **2015**, *199*, 10–16.
(70) Axpe, E.; Lopez-Euba, T.; Castellanos-Rubio, A.; Merida, D.; Garcia, J. A.; Plaza-Izurieta, L.; Fernandez-Jimenez, N.; Plazaola, F.; Bilbao, J. R. Detection of Atomic Scale Changes in the Free Volume Void Size of Three-Dimensional Colorectal Cancer Cell Culture Using Positron Annihilation Lifetime Spectroscopy. *PLOS ONE* **2014**, *9*, e83838.
(71) García-Arribas, A. B.; Axpe, E.; Mujika, J. I.; Mérida, D.; Busto, J. V.; Sot, J.; Alonso, A.; Lopez, X.; García, J. Á.; Ugalde, J. M.; et al. Cholesterol–Ceramide Interactions in Phospholipid and Sphingolipid Bilayers As Observed by Positron Annihilation Lifetime Spectroscopy and Molecular Dynamics Simulations. *Langmuir* **2016**, *32*, 5434–5444.

(72) Axpe, E.; Bugnicourt, L.; Merida, D.; Goiriena-Goikoetxea, M.; Unzueta, I.; Sanchez-Eugenia, R.; Garcia, J. A.; Plazaola, F.; Contera, S. Sub-Nanoscale Free Volume and Local Elastic Modulus of Chitosan–Carbon Nanotube Biomimetic Nanocomposite Scaffold-Materials. *J. Mater. Chem. B* **2015**, *3*, 3169–3176.

(73) Wen, Q.; Basu, A.; A. Janmey, P.; G. Yodh, A. Non-Affine Deformations in Polymer Hydrogels. *Soft Matter* **2012**, *8*, 8039–8049.

(74) Vernerey, F. J.; Greenwald, E. C.; Bryant, S. J. Triphasic Mixture Model of Cell-Mediated Enzymatic Degradation of Hydrogels. *Comput. Methods Biomech. Biomed. Engin.* **2012**, *15*, 1197–1210.

(75) Chester, S. A.; Anand, L. A Coupled Theory of Fluid Permeation and Large Deformations for Elastomeric Materials. *J. Mech. Phys. Solids* **2010**, *58*, 1879–1906.

(76) Vernerey, F. J. A Mixture Approach to Investigate Interstitial Growth in Engineering Scaffolds. *Biomech. Model Mechanobiol.* **2016**, *15*, 259–278.

(77) Swartz, M. A.; Fleury, M. E. Interstitial Flow and Its Effects in Soft Tissues. *Annu. Rev. Biomed. Eng.* **2007**, *9*, 229–256.

(78) Coussy, O. *Poromechanics*; John Wiley & Sons, 2004.

(79) Chahine, N. O.; Albro, M. B.; Lima, E. G.; Wei, V. I.; Dubois, C. R.; Hung, C. T.; Ateshian, G. A. Effect of Dynamic Loading on the Transport of Solutes into Agarose Hydrogels. *Biophys. J.* **2009**, *97*, 968–975.

(80) Bertrand, T.; Peixinho, J.; Mukhopadhyay, S.; MacMinn, C. W. Dynamics of Swelling and Drying in a Spherical Gel. *Phys. Rev. Applied* **2016**, *6*, 064010.

(81) Guyton, A. C.; Hall, J. E. Textbook of Medical Physiology. WB Saunders Company. *Philadelphia PA* **1991**, *8*, 801–815.

(82) Levick, J. R. Flow through Interstitium and Other Fibrous Matrices. *Q. J. Exp. Physiol.* **1987**, *72*, 409–437.

(83) Nabovati, A.; Llewellin, E. W.; Sousa, A. C. M. A General Model for the Permeability of Fibrous Porous Media Based on Fluid Flow Simulations Using the Lattice Boltzmann Method. *Compos. Part A Appl. Sci. Manuf.* **2009**, *40*, 860–869.

(84) Netti, P. A.; Berk, D. A.; Swartz, M. A.; Grodzinsky, A. J.; Jain, R. K. Role of Extracellular Matrix Assembly in Interstitial Transport in Solid Tumors. *Cancer Res.* **2000**, *60*, 2497–2503.

(85) Pedersen, J. A.; Boschetti, F.; Swartz, M. A. Effects of Extracellular Fiber Architecture on Cell Membrane Shear Stress in a 3D Fibrous Matrix. *J. Biomech.* **2007**, *40*, 1484–1492.

(86) Scherer, G. W. Hydraulic Radius and Mesh Size of Gels. *J. Sol-Gel Sci. Technol.* **1994**, *1*, 285–291.

(87) Peppas, N. A.; Bures, P.; Leobandung, W.; Ichikawa, H. Hydrogels in Pharmaceutical Formulations. *Eur. J. Pharm. Biopharm.* **2000**, *50*, 27–46.

(88) Tokita, M.; Tanaka, T. Friction Coefficient of Polymer Networks of Gels. *J. Chem. Phys.* **1991**, *95*, 4613–4619.

(89) Engelsberg, M.; Barros, W. Free-Evolution Kinetics in a High-Swelling Polymeric Hydrogel. *Phys. Rev. E* **2013**, *88*, 062602.

(90) Grattoni, C. A.; Al-Sharji, H. H.; Yang, C.; Muggeridge, A. H.; Zimmerman, R. W. Rheology and Permeability of Crosslinked Polyacrylamide Gel. *J. Colloid Interface Sci.* **2001**, *240*, 601–607.

(91) Fitzgerald, J. B.; Jin, M.; Grodzinsky, A. J. Shear and Compression Differentially Regulate Clusters of Functionally Related Temporal Transcription Patterns in Cartilage Tissue. *J. Biol. Chem.* **2006**, *281*, 24095–24103.
(92) Albro, M. B.; Chahine, N. O.; Li, R.; Yeager, K.; Hung, C. T.; Ateshian, G. A. Dynamic Loading of Deformable Porous Media Can Induce Active Solute Transport. *J. Biomech.* **2008**, *41*, 3152–3157.
(93) Müller, P.; Rogers, K. W.; Yu, S. R.; Brand, M.; Schier, A. F. Morphogen Transport. *Development* **2013**, *140*, 1621–1638.
(94) Albuquerque, M. L.; Waters, C. M.; Savla, U.; Schnaper, H. W.; Flozak, A. S. Shear Stress Enhances Human Endothelial Cell Wound Closure in Vitro. *Am. J. Physiol. - Heart Circ. Physiol.* **2000**, *279*, H293-302.
(95) Li, S.; Huang, N. F.; Hsu, S. Mechanotransduction in Endothelial Cell Migration. *J. Cell. Biochem.* **2005**, *96*, 1110–1126.
(96) Skobe, M.; Hamberg, L. M.; Hawighorst, T.; Schirner, M.; Wolf, G. L.; Alitalo, K.; Detmar, M. Concurrent Induction of Lymphangiogenesis, Angiogenesis, and Macrophage Recruitment by Vascular Endothelial Growth Factor-C in Melanoma. *Am. J. Pathol.* **2001**, *159*, 893–903.
(97) Hofmann, M.; Guschel, M.; Bernd, A.; Bereiter-Hahn, J.; Kaufmann, R.; Tandi, C.; Wiig, H.; Kippenberger, S. Lowering of Tumor Interstitial Fluid Pressure Reduces Tumor Cell Proliferation in a Xenograft Tumor Model. *Neoplasia* **2006**, *8*, 89–95.
(98) Rutkowski, J. M.; Swartz, M. A. A Driving Force for Change: Interstitial Flow as a Morphoregulator. *Trends Cell Biol.* **2007**, *17*, 44–50.
(99) Censi, R.; Vermonden, T. Photopolymerized Thermosensitive Hydrogels for Tailorable Diffusion-Controlled Protein Delivery. *J. Control. Release* **2009**, *140*, 230–236.
(100) Muralidharan, A.; Uzcategui, A. C.; McLeod, R. R.; Bryant, S. J. Stereolithographic 3D Printing for Deterministic Control over Integration in Dual-Material Composites. *Adv. Mater. Technol.* **2019**, *4*, 1900592.
(101) DiDomenico, C. D.; Bonassar, L. J. How Can 50 Years of Solute Transport Data in Articular Cartilage Inform the Design of Arthritis Therapeutics? *Osteoarthr. Cartil.* **2018**, *26*, 1438–1446.
(102) Zbinden, A.; Browne, S.; Altiok, E. I.; Svedlund, F. L.; Jackson, W. M.; Healy, K. E. Multivalent Conjugates of Basic Fibroblast Growth Factor Enhance *in Vitro* Proliferation and Migration of Endothelial Cells. *Biomater. Sci.* **2018**, *6*, 1076–1083.
(103) Mahadik, B. P.; Bharadwaj, N. A. K.; Ewoldt, R. H.; Harley, B. A. C. Regulating Dynamic Signaling between Hematopoietic Stem Cells and Niche Cells via a Hydrogel Matrix. *Biomaterials* **2017**, *125*, 54–64.
(104) Gilchrist, A. E.; Lee, S.; Hu, Y.; Harley, B. A. C. Soluble Signals and Remodeling in a Synthetic Gelatin-Based Hematopoietic Stem Cell Niche. *Adv. Healthc. Mater.* **2019**, *8*, e1900751.
(105) Hong, W.; Zhao, X.; Zhou, J.; Suo, Z. A Theory of Coupled Diffusion and Large Deformation in Polymeric Gels. *J. Mech. Phys. Solids* **2008**, *56*, 1779–1793.
(106) Brannon-Peppas, L.; Peppas, N. A. Equilibrium Swelling Behavior of PH-Sensitive Hydrogels. *Chem. Eng. Sci.* **1991**, *46*, 715–722.

(107) Obaidat, A. A.; Park, K. Characterization of Protein Release through Glucose-Sensitive Hydrogel Membranes. *Biomaterials* **1997**, *18*, 801–806.
(108) Ohmine, I.; Tanaka, T. Salt Effects on the Phase Transition of Ionic Gels. *J. Chem. Phys.* **1982**, *77*, 5725–5729.
(109) Hirokawa, Y.; Tanaka, T. Volume Phase Transition in a Nonionic Gel. *J. Chem. Phys.* **1984**, *81*, 6379–6380.
(110) Zhang, S.; Bellinger, A. M.; Glettig, D. L.; Barman, R.; Lee, Y.-A. L.; Zhu, J.; Cleveland, C.; Montgomery, V. A.; Gu, L.; Nash, L. D.; et al. A PH-Responsive Supramolecular Polymer Gel as an Enteric Elastomer for Use in Gastric Devices. *Nat. Mater.* **2015**, *14*, 1065–1071.
(111) Leddy, H. A.; Guilak, F. Site-Specific Molecular Diffusion in Articular Cartilage Measured Using Fluorescence Recovery after Photobleaching. *Ann. Biomed. Eng.* **2003**, *31*, 753–760.
(112) DiDomenico, C. D.; Lintz, M.; Bonassar, L. J. Molecular Transport in Articular Cartilage — What Have We Learned from the Past 50 Years? *Nat. Rev. Rheumatol.* **2018**, *14*, 393–403.
(113) Grady, M. E.; Parrish, E.; Caporizzo, M. A.; Seeger, S. C.; Composto, R. J.; Eckmann, D. M. Intracellular Nanoparticle Dynamics Affected by Cytoskeletal Integrity. *Soft Matter* **2017**, *13*, 1873–1880.
(114) Wang, B.; Anthony, S. M.; Bae, S. C.; Granick, S. Anomalous yet Brownian. *Proc. Natl. Acad. Sci. U. S. A.* **2009**, *106*, 15160.
(115) Maroudas, A. Biophysical Chemistry of Cartilaginous Tissues with Special Reference to Solute and Fluid Transport. *Biorheology* **1975**, *12*, 233–248.
(116) Lee, C. H.; Crosby, A. J.; Emrick, T.; Hayward, R. C. Characterization of Heterogeneous Polyacrylamide Hydrogels by Tracking of Single Quantum Dots. *Macromolecules* **2014**, *47*, 741–749.
(117) Hecht, A. M.; Duplessix, R.; Geissler, E. Structural Inhomogeneities in the Range 2.5-2500 .ANG. in Polyacrylamide Gels. *Macromolecules* **1985**, *18*, 2167–2173.
(118) Parrish, E.; Caporizzo, M. A.; Composto, R. J. Network Confinement and Heterogeneity Slows Nanoparticle Diffusion in Polymer Gels. *J. Chem. Phys.* **2017**, *146*, 203318.
(119) Fawcett, J. S.; Morris, C. J. O. R. Molecular-Sieve Chromatography of Proteins on Granulated Polyacrylamide Gels. *Sep. Sci.* **1966**, *1*, 9–26.
(120) Lin-Gibson, S.; Jones, R. L.; Washburn, N. R.; Horkay, F. Structure-Property Relationships of Photopolymerizable Poly(Ethylene Glycol) Dimethacrylate Hydrogels. *Macromolecules* **2005**, *38*, 2897–2902.
(121) Wong, I. Y.; Gardel, M. L.; Reichman, D. R.; Weeks, E. R.; Valentine, M. T.; Bausch, A. R.; Weitz, D. A. Anomalous Diffusion Probes Microstructure Dynamics of Entangled F-Actin Networks. *Phys. Rev. Lett.* **2004**, *92*, 178101.
(122) Drazer, G.; Rosen, M.; Zanette, D. Anomalous Transport in Activated Carbon Porous Samples: Power-Law Trapping-Time Distributions. *Physica A* **2000**, *283*, 181–186.
(123) Bässler, H. Localized States and Electronic Transport in Single Component Organic Solids with Diagonal Disorder. *Phys. Status Solidi B* **1981**, *107*, 9–54.
(124) Frauenfelder, H.; Sligar, S. G.; Wolynes, P. G. The Energy Landscapes and Motions of Proteins. *Science* **1991**, *254*, 1598–1603.

(125) Kim, W. K.; Chudoba, R.; Milster, S.; Roa, R.; Kanduč, M.; Dzubiella, J. Tuning the Selective Permeability of Polydisperse Polymer Networks. *Soft Matter* **2020**, *16*, 8144–8154.
(126) Tokuyama, H.; Nakahata, Y.; Ban, T. Diffusion Coefficient of Solute in Heterogeneous and Macroporous Hydrogels and Its Correlation with the Effective Crosslinking Density. *J. Membr. Sci.* **2020**, *595*, 117533.
(127) Goodrich, C. P.; Brenner, M. P.; Ribbeck, K. Enhanced Diffusion by Binding to the Crosslinks of a Polymer Gel. *Nat. Commun.* **2018**, *9*, 4348.
(128) Lenzini, S.; Bargi, R.; Chung, G.; Shin, J.-W. Matrix Mechanics and Water Permeation Regulate Extracellular Vesicle Transport. *Nat. Nanotechnol.* **2020**, *15*, 217–223.
(129) Mardpour, S.; Ghanian, M. H.; Sadeghi-abandansari, H.; Mardpour, S.; Nazari, A.; Shekari, F.; Baharvand, H. Hydrogel-Mediated Sustained Systemic Delivery of Mesenchymal Stem Cell-Derived Extracellular Vesicles Improves Hepatic Regeneration in Chronic Liver Failure. *ACS Appl. Mater. Interfaces* **2019**, *11*, 37421–37433.
(130) Seo, Y.; Kim, H.-S.; Hong, I.-S. Stem Cell-Derived Extracellular Vesicles as Immunomodulatory Therapeutics. *Stem Cells Int.* **2019**, *2019*, 5126156.
(131) Meldolesi, J. Exosomes and Ectosomes in Intercellular Communication. *Curr. Biol.* **2018**, *28*, R435–R444.
(132) Fuhrmann, G. Diffusion and Transport of Extracellular Vesicles. *Nat. Nanotechnol.* **2020**, *15*, 168–169.
(133) Veening, J.; Barendregt, H. The Regulation of Brain States by Neuroactive Substances Distributed via the Cerebrospinal Fluid; a Review. *Cerebrospinal Fluid Res.* **2009**, *7*, 1–16.
(134) Lee, J. B.; Kim, D.-H.; Yoon, J.-K.; Park, D. B.; Kim, H.-S.; Shin, Y. M.; Baek, W.; Kang, M.-L.; Kim, H. J.; Sung, H.-J. Microchannel Network Hydrogel Induced Ischemic Blood Perfusion Connection. *Nat. Commun.* **2020**, *11*, 615.
(135) Cuchiara, M. P.; Gould, D. J.; McHale, M. K.; Dickinson, M. E.; West, J. L. Integration of Self -Assembled Microvascular Networks with Microfabricated PEG-Based Hydrogels. *Adv. Funct. Mater.* **2012**, *22*, 4511–4518.
(136) Lee, J. B.; Wang, X.; Faley, S.; Baer, B.; Balikov, D. A.; Sung, H.-J.; Bellan, L. M. Development of 3D Microvascular Networks Within Gelatin Hydrogels Using Thermoresponsive Sacrificial Microfibers. *Adv. Healthc. Mater.* **2016**, *5*, 781–785.
(137) Sawyer, S. W.; Shridhar, S. V.; Zhang, K.; Albrecht, L. D.; Filip, A. B.; Horton, J. A.; Soman, P. Perfusion Directed 3D Mineral Formation within Cell-Laden Hydrogels. *Biofabrication* **2018**, *10*, 035013.
(138) Contessi Negrini, N.; Bonnetier, M.; Giatsidis, G.; Orgill, D. P.; Farè, S.; Marelli, B. Tissue-Mimicking Gelatin Scaffolds by Alginate Sacrificial Templates for Adipose Tissue Engineering. *Acta Biomater.* **2019**, *87*, 61–75.
(139) Chen, T.; Buckley, M.; Cohen, I.; Bonassar, L.; Awad, H. A. Insights into Interstitial Flow, Shear Stress, and Mass Transport Effects on ECM Heterogeneity in Bioreactor-Cultivated Engineered Cartilage Hydrogels. *Biomech. Model Mechanobiol.* **2012**, *11*, 689–702.
(140) Katsuno, C.; Konda, A.; Urayama, K.; Takigawa, T.; Kidowaki, M.; Ito, K. Pressure-Responsive Polymer Membranes of Slide-Ring Gels with Movable Cross-Links. *Adv. Mater.* **2013**, *25*, 4636–4640.
(141) Zhao, X.; Kim, J.; Cezar, C. A.; Huebsch, N.; Lee, K.; Bouhadir, K.; Mooney, D. J. Active Scaffolds for On-Demand Drug and Cell Delivery. *Proc. Natl. Acad. Sci. U. S. A.* **2011**, *108*,

67.
(142) DiDomenico, C. D.; Xiang Wang, Z.; Bonassar, L. J. Cyclic Mechanical Loading Enhances Transport of Antibodies Into Articular Cartilage. *J. Biomech. Eng.* **2016**, *139*.
(143) Mauck, R. L.; Hung, C. T.; Ateshian, G. A. Modeling of Neutral Solute Transport in a Dynamically Loaded Porous Permeable Gel: Implications for Articular Cartilage Biosynthesis and Tissue Engineering. *J. Biomech. Eng.* **2003**, *125*, 602–614.
(144) DiDomenico, C. D.; Goodearl, A.; Yarilina, A.; Sun, V.; Mitra, S.; Sterman, A. S.; Bonassar, L. J. The Effect of Antibody Size and Mechanical Loading on Solute Diffusion Through the Articular Surface of Cartilage. *J. Biomech. Eng.* **2017**, *139*.
(145) Tate, M. L. K. "Whither Flows the Fluid in Bone?" An Osteocyte's Perspective. *Journal of Biomechanics* **2003**, *36*, 1409–1424.
(146) Ateshian, G. A. Mixture Theory for Modeling Biological Tissues: Illustrations from Articular Cartilage. In *Biomechanics: Trends in Modeling and Simulation*; Holzapfel, G. A., Ogden, R. W., Eds.; Studies in Mechanobiology, Tissue Engineering and Biomaterials; Springer International Publishing: Cham, 2017; pp 1–51.
(147) Huysmans, M.; Dassargues, A. Review of the Use of Péclet Numbers to Determine the Relative Importance of Advection and Diffusion in Low Permeability Environments. *Hydrogeol. J.* **2005**, *13*, 895–904.
(148) Fleury, M. E.; Boardman, K. C.; Swartz, M. A. Autologous Morphogen Gradients by Subtle Interstitial Flow and Matrix Interactions. *Biophys. J.* **2006**, *91*, 113–121.
(149) Johnston, S. T.; Deen, W. M. Hindered Convection of Ficoll and Proteins in Agarose Gels. *Ind. Eng. Chem. Res.* **2002**, *41*, 340–346.
(150) Brissová, M.; Petro, M.; Lacík, I.; Powers, A. C.; Wang, T. Evaluation of Microcapsule Permeability via Inverse Size Exclusion Chromatography. *Anal. Biochem.* **1996**, *242*, 104–111.
(151) Kosto, K. B.; Deen, W. M. Hindered Convection of Macromolecules in Hydrogels. *Biophys. J.* **2005**, *88*, 277–286.
(152) Reddy, S. T.; Berk, D. A.; Jain, R. K.; Swartz, M. A. A Sensitive in Vivo Model for Quantifying Interstitial Convective Transport of Injected Macromolecules and Nanoparticles. *J. Appl. Physiol.* **2006**, *101*, 1162–1169.
(153) Lieleg, O.; Ribbeck, K. Biological Hydrogels as Selective Diffusion Barriers. *Trends Cell Biol.* **2011**, *21*, 543–551.
(154) Englmeier, L.; Olivo, J. C.; Mattaj, I. W. Receptor-Mediated Substrate Translocation through the Nuclear Pore Complex without Nucleotide Triphosphate Hydrolysis. *Curr. Biol.* **1999**, *9*, 30–41.
(155) Ribbeck, K.; Kutay, U.; Paraskeva, E.; Görlich, D. The Translocation of Transportin–Cargo Complexes through Nuclear Pores Is Independent of Both Ran and Energy. *Curr. Biol.* **1999**, *9*, 47-S1.
(156) Ribbeck, K.; Görlich, D. Kinetic Analysis of Translocation through Nuclear Pore Complexes. *EMBO J.* **2001**, *20*, 1320–1330.
(157) Hansing, J.; Duke, J. R.; Fryman, E. B.; DeRouchey, J. E.; Netz, R. R. Particle Diffusion in Polymeric Hydrogels with Mixed Attractive and Repulsive Interactions. *Nano Lett.* **2018**, *18*, 5248–5256.

(158) Le Goas, M.; Testard, F.; Taché, O.; Debou, N.; Cambien, B.; Carrot, G.; Renault, J.-P. How Do Surface Properties of Nanoparticles Influence Their Diffusion in the Extracellular Matrix? A Model Study in Matrigel Using Polymer-Grafted Nanoparticles. *Langmuir* **2020**, *36*, 10460–10470.
(159) Goas, M. L.; Roussel, T.; Kalbazova, M.; Carrière, D.; Barruet, E.; Geertsen, V.; Fadda, G. C.; Testard, F.; Carrot, G.; Renault, J.-P. Combining Surface Chemistry Modification and in Situ Small-Angle Scattering Characterization to Understand and Optimize the Biological Behavior of Nanomedicines. *J. Mater. Chem. B* **2020**, *8*, 6438–6450.
(160) Villanueva, A.; Cañete, M.; Roca, A. G.; Calero, M.; Veintemillas-Verdaguer, S.; Serna, C. J.; Morales, M. del P.; Miranda, R. The Influence of Surface Functionalization on the Enhanced Internalization of Magnetic Nanoparticles in Cancer Cells. *Nanotechnology* **2009**, *20*, 115103.
(161) Zhang, Z.; Van Steendam, K.; Maji, S.; Balcaen, L.; Anoshkina, Y.; Zhang, Q.; Vanluchene, G.; De Rycke, R.; Van Haecke, F.; Deforce, D.; et al. Tailoring Cellular Uptake of Gold Nanoparticles Via the Hydrophilic-to-Hydrophobic Ratio of Their (Co)Polymer Coating. *Adv. Funct. Mater.* **2015**, *25*, 3433–3439.
(162) Sakiyama-Elbert, S. E. Incorporation of Heparin into Biomaterials. *Acta Biomater.* **2014**, *10*, 1581–1587.
(163) Lin, C. C.; Metters, A. T. Hydrogels in Controlled Release Formulations: Network Design and Mathematical Modeling. *Adv. Drug Deliv. Rev.* **2006**, *58*, 1379–1408.
(164) Matsuo, I.; Kimura-Yoshida, C. Extracellular Distribution of Diffusible Growth Factors Controlled by Heparan Sulfate Proteoglycans during Mammalian Embryogenesis. *Phil. Trans. R. Soc. B* **2014**, *369*, 20130545.
(165) Raman, R.; Venkataraman, G.; Ernst, S.; Sasisekharan, V.; Sasisekharan, R. Structural Specificity of Heparin Binding in the Fibroblast Growth Factor Family of Proteins. *Proc. Natl. Acad. Sci. U. S. A.* **2003**, *100*, 2357.
(166) Mitchell, A. C.; Briquez, P. S.; Hubbell, J. A.; Cochran, J. R. Engineering Growth Factors for Regenerative Medicine Applications. *Acta Biomater.* **2016**, *30*, 1–12.
(167) Thönes, S.; Rother, S.; Wippold, T.; Blaszkiewicz, J.; Balamurugan, K.; Moeller, S.; Ruiz-Gómez, G.; Schnabelrauch, M.; Scharnweber, D.; Saalbach, A.; et al. Hyaluronan/Collagen Hydrogels Containing Sulfated Hyaluronan Improve Wound Healing by Sustained Release of Heparin-Binding EGF-like Growth Factor. *Acta Biomater.* **2019**, *86*, 135–147.
(168) Garcia Abreu, J.; Coffinier, C.; Larraín, J.; Oelgeschläger, M.; De Robertis, E. M. Chordin-like CR Domains and the Regulation of Evolutionarily Conserved Extracellular Signaling Systems. *Gene* **2002**, *287*, 39–47.
(169) Wijelath, E. S.; Rahman, S.; Namekata, M.; Murray, J.; Nishimura, T.; Mostafavi-Pour, Z.; Patel, Y.; Suda, Y.; Humphries, M. J.; Sobel, M. Heparin-II Domain of Fibronectin Is a Vascular Endothelial Growth Factor-Binding Domain: Enhancement of VEGF Biological Activity by a Singular Growth Factor/Matrix Protein Synergism. *Circ. Res.* **2006**, *99*, 853–860.
(170) Sawicka, K. M.; Seeliger, M.; Musaev, T.; Macri, L. K.; Clark, R. A. F. Fibronectin Interaction and Enhancement of Growth Factors: Importance for Wound Healing. *Adv. Wound Care* **2015**, *4*, 469–478.

(171) Kim, S.-H.; Turnbull, J.; Guimond, S. Extracellular Matrix and Cell Signalling: The Dynamic Cooperation of Integrin, Proteoglycan and Growth Factor Receptor. *J. Endocrinol.* **2011**, *209*, 139–151.
(172) Lee, K.; Silva, E. A.; Mooney, D. J. Growth Factor Delivery-Based Tissue Engineering: General Approaches and a Review of Recent Developments. *J. R. Soc. Interface.* **2011**, *8*, 153–170.
(173) He, W.; Reaume, M.; Hennenfent, M.; Lee, B. P.; Rajachar, R. Biomimetic Hydrogels with Spatial- and Temporal-Controlled Chemical Cues for Tissue Engineering. *Biomater. Sci.* **2020**, *8*, 3248–3269.
(174) Yan, H. J.; Casalini, T.; Hulsart-Billström, G.; Wang, S.; Oommen, O. P.; Salvalaglio, M.; Larsson, S.; Hilborn, J.; Varghese, O. P. Synthetic Design of Growth Factor Sequestering Extracellular Matrix Mimetic Hydrogel for Promoting in Vivo Bone Formation. *Biomaterials* **2018**, *161*, 190–202.
(175) Lin, C. C.; Boyer, P. D.; Aimetti, A. A.; Anseth, K. S. Regulating MCP-1 Diffusion in Affinity Hydrogels for Enhancing Immuno-Isolation. *J. Control. Release* **2010**, *142*, 384–391.
(176) Freudenberg, U.; Atallah, P.; Limasale, Y. D. P.; Werner, C. Charge-Tuning of Glycosaminoglycan-Based Hydrogels to Program Cytokine Sequestration. *Faraday Discuss.* **2019**, *219*, 244–251.
(177) Atallah, P.; Schirmer, L.; Tsurkan, M.; Putra Limasale, Y. D.; Zimmermann, R.; Werner, C.; Freudenberg, U. In Situ-Forming, Cell-Instructive Hydrogels Based on Glycosaminoglycans with Varied Sulfation Patterns. *Biomaterials* **2018**, *181*, 227–239.
(178) Lieleg, O.; Baumgärtel, R. M.; Bausch, A. R. Selective Filtering of Particles by the Extracellular Matrix: An Electrostatic Bandpass. *Biophys J.* **2009**, *97*, 1569–1577.
(179) Prokopová-Kubinová, Š.; Vargová, L.; Tao, L.; Ulbrich, K.; Šubr, V.; Syková, E.; Nicholson, C. Poly[N-(2-Hydroxypropyl)Methacrylamide] Polymers Diffuse in Brain Extracellular Space with Same Tortuosity as Small Molecules. *Biophys. J.* **2001**, *80*, 542–548.
(180) Tang, S.; Habicht, A.; Li, S.; Seiffert, S.; Olsen, B. D. Self-Diffusion of Associating Star-Shaped Polymers. *Macromolecules* **2016**, *49*, 5599–5608.
(181) Ramirez, J.; Dursch, T. J.; Olsen, B. D. A Molecular Explanation for Anomalous Diffusion in Supramolecular Polymer Networks. *Macromolecules* **2018**, *51*, 2517–2525.
(182) Anderson, S. J.; Matsuda, C.; Garamella, J.; Peddireddy, K. R.; Robertson-Anderson, R. M.; McGorty, R. Filament Rigidity Vies with Mesh Size in Determining Anomalous Diffusion in Cytoskeleton. *Biomacromolecules* **2019**, *20*, 4380–4388.
(183) Regner, B. M.; Vučinić, D.; Domnisoru, C.; Bartol, T. M.; Hetzer, M. W.; Tartakovsky, D. M.; Sejnowski, T. J. Anomalous Diffusion of Single Particles in Cytoplasm. *Biophys. J.* **2013**, *104*, 1652–1660.
(184) Witten, J.; Ribbeck, K. The Particle in the Spider's Web: Transport through Biological Hydrogels. *Nanoscale* **2017**, *9*, 8080–8095.
(185) Fogelson, B.; Keener, J. P. Enhanced Nucleocytoplasmic Transport Due to Competition for Elastic Binding Sites. *Biophys. J.* **2018**, *115*, 108–116.
(186) Yang, Y. J.; Mai, D. J.; Dursch, T. J.; Olsen, B. D. Nucleopore-Inspired Polymer Hydrogels for Selective Biomolecular Transport. *Biomacromolecules* **2018**, *19*, 3905–3916.
(187) Yamamoto, U.; Carrillo, J.-M. Y.; Bocharova, V.; Sokolov, A. P.; Sumpter, B. G.; Schweizer, K. S. Theory and Simulation of Attractive Nanoparticle Transport in Polymer Melts.

Macromolecules **2018**, *51*, 2258–2267.
(188) Cu, Y.; Saltzman, W. M. Mathematical Modeling of Molecular Diffusion through Mucus. *Adv. Drug Deliv. Rev.* **2009**, *61*, 101–114.
(189) Bickel, T.; Bruinsma, R. The Nuclear Pore Complex Mystery and Anomalous Diffusion in Reversible Gels. *Biophys. J.* **2002**, *83*, 3079–3087.
(190) Fogelson, B.; Keener, J. P. Transport Facilitated by Rapid Binding to Elastic Tethers. *SIAM J. Appl. Math.* **2019**, *79*, 1405–1422.
(191) Maguire, L.; Stefferson, M.; Betterton, M. D.; Hough, L. E. Design Principles of Selective Transport through Biopolymer Barriers. *Phys. Rev. E* **2019**, *100*, 042414.
(192) Lalitha Sridhar, S.; Dunagin, J.; Koo, K.; Hough, L.; Vernerey, F. Enhanced Diffusion by Reversible Binding to Active Polymers. *Macromolecules* **2021.**
(193) Carroll, B.; Bocharova, V.; Carrillo, J.-M. Y.; Kisliuk, A.; Cheng, S.; Yamamoto, U.; Schweizer, K. S.; Sumpter, B. G.; Sokolov, A. P. Diffusion of Sticky Nanoparticles in a Polymer Melt: Crossover from Suppressed to Enhanced Transport. *Macromolecules* **2018**, *51*, 2268–2275.
(194) Kumar, P.; Theeyancheri, L.; Chaki, S.; Chakrabarti, R. Transport of Probe Particles in a Polymer Network: Effects of Probe Size, Network Rigidity and Probe–Polymer Interaction. *Soft Matter* **2019**, *15*, 8992–9002.
(195) Sprakel, J.; van der Gucht, J.; Cohen Stuart, M. A.; Besseling, N. A. M. Rouse Dynamics of Colloids Bound to Polymer Networks. *Phys. Rev. Lett.* **2007**, *99*, 208301.
(196) Tabatabaei, F.; Lenz, O.; Holm, C. Simulational Study of Anomalous Tracer Diffusion in Hydrogels. *Colloid Polym. Sci.* **2011**, *289*, 523–534.
(197) Saxton, M. J. A Biological Interpretation of Transient Anomalous Subdiffusion. I. Qualitative Model. *Biophys. J.* **2007**, *92*, 1178–1191.
(198) Lodge, A. S. Polymer Solutions and Melts: Viscosity, Diffusion, and Elasticity. *Ind. Eng. Chem. Res.* **1995**, *34*, 3355–3358.
(199) Hansing, J.; Netz, R. R. Particle Trapping Mechanisms Are Different in Spatially Ordered and Disordered Interacting Gels. *Biophys J.* **2018**, *114*, 2653–2664.
(200) Dowd, C. J.; Cooney, C. L.; Nugent, M. A. Heparan Sulfate Mediates BFGF Transport through Basement Membrane by Diffusion with Rapid Reversible Binding. *J. Biol. Chem.* **1999**, *274*, 5236–5244.
(201) Stylianopoulos, T.; Poh, M.-Z.; Insin, N.; Bawendi, M. G.; Fukumura, D.; Munn, L. L.; Jain, R. K. Diffusion of Particles in the Extracellular Matrix: The Effect of Repulsive Electrostatic Interactions. *Biophys. J.* **2010**, *99*, 1342–1349.
(202) Bonnans, C.; Chou, J.; Werb, Z. Remodelling the Extracellular Matrix in Development and Disease. *Nat. Rev. Mol. Cell Biol.* **2014**, *15*, 786–801.
(203) Patterson, J.; Hubbell, J. A. Enhanced Proteolytic Degradation of Molecularly Engineered PEG Hydrogels in Response to MMP-1 and MMP-2. *Biomaterials* **2010**, *31*, 7836–7845.
(204) Anderson, S. B.; Lin, C.-C.; Kuntzler, D. V.; Anseth, K. S. The Performance of Human Mesenchymal Stem Cells Encapsulated in Cell-Degradable Polymer-Peptide Hydrogels. *Biomaterials* **2011**, *32*, 3564–3574.
(205) Lutolf, M. P.; Raeber, G. P.; Zisch, A. H.; Tirelli, N.; Hubbell, J. A. Cell-Responsive Synthetic Hydrogels. *Adv. Mater.* **2003**, *15*, 888–892.

(206) Flynn, B. P.; Bhole, A. P.; Saeidi, N.; Liles, M.; DiMarzio, C. A.; Ruberti, J. W. Mechanical Strain Stabilizes Reconstituted Collagen Fibrils against Enzymatic Degradation by Mammalian Collagenase Matrix Metalloproteinase 8 (MMP-8). *PLOS ONE* **2010**, *5*, e12337.
(207) Lutolf, M. P.; Lauer-Fields, J. L.; Schmoekel, H. G.; Metters, A. T.; Weber, F. E.; Fields, G. B.; Hubbell, J. A. Synthetic Matrix Metalloproteinase-Sensitive Hydrogels for the Conduction of Tissue Regeneration: Engineering Cell-Invasion Characteristics. *Proc. Natl. Acad. Sci. U. S. A.* **2003**, *100*, 5413–5418.
(208) Skaalure, S. C.; Akalp, U.; Vernerey, F. J.; Bryant, S. J. Tuning Reaction and Diffusion Mediated Degradation of Enzyme-Sensitive Hydrogels. *Adv. Healthcare Mater.* **2016**, *5*, 432–438.
(209) Fields, G. B. The Rebirth of Matrix Metalloproteinase Inhibitors: Moving Beyond the Dogma. *Cells* **2019**, *8*, 984.
(210) Benjamin, M. M.; Khalil, R. A. Matrix Metalloproteinase Inhibitors as Investigative Tools in the Pathogenesis and Management of Vascular Disease. *Exp. Suppl.* **2012**, *103*, 209–279.
(211) Lalitha Sridhar, S.; Vernerey, F. Localized Enzymatic Degradation of Polymers: Physics and Scaling Laws. *Phys. Rev. Applied* **2018**, *9*, 031001.
(212) Lin, C. C.; Anseth, K. S. PEG Hydrogels for the Controlled Release of Biomolecules in Regenerative Medicine. *Pharm. Res.* **2009**, *26*, 631–643.
(213) Wood, M. D.; Borschel, G. H.; Sakiyama-Elbert, S. E. Controlled Release of Glial-Derived Neurotrophic Factor from Fibrin Matrices Containing an Affinity-Based Delivery System. *J. Biomed. Mater. Res. A* **2009**, *89A*, 909–918.
(214) Maddock, R. M. A.; Pollard, G. J.; Moreau, N. G.; Perry, J. J.; Race, P. R. Enzyme-Catalysed Polymer Cross-Linking: Biocatalytic Tools for Chemical Biology, Materials Science and Beyond. *Biopolymers* **2020**, *111*, e23390.
(215) Parsons, J. T.; Horwitz, A. R.; Schwartz, M. A. Cell Adhesion: Integrating Cytoskeletal Dynamics and Cellular Tension. *Nat. Rev. Mol. Cell Biol.* **2010**, *11*, 633–643.
(216) Bracher, M.; Bezuidenhout, D.; Lutolf, M. P.; Franz, T.; Sun, M.; Zilla, P.; Davies, N. H. Cell Specific Ingrowth Hydrogels. *Biomaterials* **2013**, *34*, 6797–6803.
(217) Tan, J. L.; Tien, J.; Pirone, D. M.; Gray, D. S.; Bhadriraju, K.; Chen, C. S. Cells Lying on a Bed of Microneedles: An Approach to Isolate Mechanical Force. *Proc. Natl. Acad. Sci. U. S. A.* **2003**, *100*, 1484–1489.
(218) Han, S. J.; Bielawski, K. S.; Ting, L. H.; Rodriguez, M. L.; Sniadecki, N. J. Decoupling Substrate Stiffness, Spread Area, and Micropost Density: A Close Spatial Relationship between Traction Forces and Focal Adhesions. *Biophysical Journal* **2012**, *103*, 640–648.
(219) Bell, E.; Ivarsson, B.; Merrill, C. Production of a Tissue-like Structure by Contraction of Collagen Lattices by Human Fibroblasts of Different Proliferative Potential in Vitro. *Proc. Natl. Acad. Sci. U. S. A.* **1979**, *76*, 1274–1278.
(220) Kobayashi, T.; Kim, H.; Liu, X.; Sugiura, H.; Kohyama, T.; Fang, Q.; Wen, F.-Q.; Abe, S.; Wang, X.; Atkinson, J. J.; et al. Matrix Metalloproteinase-9 Activates TGF-β and Stimulates Fibroblast Contraction of Collagen Gels. *Am. J. Physiol. Lung Cell Mol. Physiol.* **2014**, *306*, L1006–L1015.
(221) Hogrebe, N. J.; Reinhardt, J. W.; Tram, N. K.; Debski, A. C.; Agarwal, G.; Reilly, M. A.; Gooch, K. J. Independent Control of Matrix Adhesiveness and Stiffness within a 3D Self-

Assembling Peptide Hydrogel. *Acta Biomater.* **2018**, *70*, 110–119.
(222) Hogrebe, N. J.; Gooch, K. J. Direct Influence of Culture Dimensionality on Human Mesenchymal Stem Cell Differentiation at Various Matrix Stiffnesses Using a Fibrous Self-Assembling Peptide Hydrogel: Effect of Culture Dimensionality on HMSC Differentiation. *J. Biomed. Mater. Res.* **2016**, *104*, 2356–2368.
(223) Buitrago, J. O.; Patel, K. D.; El-Fiqi, A.; Lee, J.-H.; Kundu, B.; Lee, H.-H.; Kim, H.-W. Silk Fibroin/Collagen Protein Hybrid Cell-Encapsulating Hydrogels with Tunable Gelation and Improved Physical and Biological Properties. *Acta Biomater.* **2018**, *69*, 218–233.
(224) Di Caprio, N.; Bellas, E. Collagen Stiffness and Architecture Regulate Fibrotic Gene Expression in Engineered Adipose Tissue. *Adv. Biosys.* **2020**, *4*, 1900286.
(225) Liu, H.; Wu, M.; Jia, Y.; Niu, L.; Huang, G.; Xu, F. Control of Fibroblast Shape in Sequentially Formed 3D Hybrid Hydrogels Regulates Cellular Responses to Microenvironmental Cues. *NPG Asia Mater.* **2020**, *12*, 45.
(226) Cao, H.; Lee, M. K. H.; Yang, H.; Sze, S. K.; Tan, N. S.; Tay, C. Y. Mechanoregulation of Cancer-Associated Fibroblast Phenotype in Three-Dimensional Interpenetrating Hydrogel Networks. *Langmuir* **2019**, *35*, 7487–7495.
(227) Zhang, J.; Yang, H.; Abali, B. E.; Li, M.; Xia, Y.; Haag, R. Dynamic Mechanics-Modulated Hydrogels to Regulate the Differentiation of Stem-Cell Spheroids in Soft Microniches and Modeling of the Nonlinear Behavior. *Small* **2019**, *15*, 1901920.
(228) Scott, R. A.; Robinson, K. G.; Kiick, K. L.; Akins, R. E. Human Adventitial Fibroblast Phenotype Depends on the Progression of Changes in Substrate Stiffness. *Adv. Healthcare Mater.* **2020**, *9*, 1901593.
(229) Schweller, R. M.; West, J. L. Encoding Hydrogel Mechanics via Network Cross-Linking Structure. *ACS Biomater. Sci. Eng.* **2015**, *1*, 335–344.
(230) Wang, C.; Sinha, S.; Jiang, X.; Murphy, L.; Fitch, S.; Wilson, C.; Grant, G.; Yang, F. Matrix Stiffness Modulates Patient-Derived Glioblastoma Cell Fates in Three-Dimensional Hydrogels. *Tissue Eng. Part A* **2020**, ten.tea.2020.0110.
(231) Chaudhuri, O. Viscoelastic Hydrogels for 3D Cell Culture. *Biomater. Sci.* **2017**, *5*, 1480–1490.
(232) Teng, L.; Chen, Y.; Jia, Y.-G.; Ren, L. Supramolecular and Dynamic Covalent Hydrogel Scaffolds: From Gelation Chemistry to Enhanced Cell Retention and Cartilage Regeneration. *J. Mater. Chem. B* **2019**, *7*, 6705–6736.
(233) Dey, K.; Agnelli, S.; Sartore, L. Dynamic Freedom: Substrate Stress Relaxation Stimulates Cell Responses. *Biomater. Sci.* **2019**, *7*, 836–842.
(234) Ma, H.; Macdougall, L. J.; GonzalezRodriguez, A.; Schroeder, M. E.; Batan, D.; Weiss, R. M.; Anseth, K. S. Calcium Signaling Regulates Valvular Interstitial Cell Alignment and Myofibroblast Activation in Fast-Relaxing Boronate Hydrogels. *Macromol. Biosci.* **2020**, *20*, 2000268.
(235) Liu, A.; Wu, K.; Chen, S.; Wu, C.; Gao, D.; Chen, L.; Wei, D.; Luo, H.; Sun, J.; Fan, H. Tunable Fast Relaxation in Imine-Based Nanofibrillar Hydrogels Stimulates Cell Response through TRPV4 Activation. *Biomacromolecules* **2020**, *21*, 3745–3755.
(236) Silva, R.; Singh, R.; Sarker, B.; Papageorgiou, D. G.; Juhasz, J. A.; Roether, J. A.; Cicha, I.; Kaschta, J.; Schubert, D. W.; Chrissafis, K.; et al. Soft-Matrices Based on Silk Fibroin and Alginate for Tissue Engineering. *Int. J. Biol. Macromol.* **2016**, *93*, 1420–1431.

(237) Wei, Z.; Schnellmann, R.; Pruitt, H. C.; Gerecht, S. Hydrogel Network Dynamics Regulate Vascular Morphogenesis. *Cell Stem Cell* **2020**, *27*, 798–812.
(238) Roca-Cusachs, P.; Gauthier, N. C.; del Rio, A.; Sheetz, M. P. Clustering of 5 1 Integrins Determines Adhesion Strength Whereas v 3 and Talin Enable Mechanotransduction. *Proc. Natl. Acad. Sci. U. S. A.* **2009**, *106*, 16245–16250.
(239) Biggs, M. J. P.; Dalby, M. J. Focal Adhesions in Osteoneogenesis. *Proc. Inst. Mech. Eng. Pt. H J. Eng. Med.* **2010**, *224*, 1441–1453.
(240) Tamariz, E.; Grinnell, F. Modulation of Fibroblast Morphology and Adhesion during Collagen Matrix Remodeling. *Mol. Biol. Cell* **2002**, *13*, 3915–3929.
(241) Dallon, J. C.; Ehrlich, H. P. A Review of Fibroblast-Populated Collagen Lattices. *Wound Repair Regen.* **2008**, *16*, 472–479.
(242) Levental, I.; Georges, P. C.; Janmey, P. A. Soft Biological Materials and Their Impact on Cell Function. *Soft Matter* **2007**, *3*, 299–306.
(243) Wang, H.-B.; Dembo, M.; Wang, Y.-L. Substrate Flexibility Regulates Growth and Apoptosis of Normal but Not Transformed Cells. *Am. J. Physiol. Cell Physiol.* **2000**, *279*, C1345–C1350.
(244) Guo, W.; Frey, M. T.; Burnham, N. A.; Wang, Y. Substrate Rigidity Regulates the Formation and Maintenance of Tissues. *Biophys. J.* **2006**, *90*, 2213–2220.
(245) Solon, J.; Levental, I.; Sengupta, K.; Georges, P. C.; Janmey, P. A. Fibroblast Adaptation and Stiffness Matching to Soft Elastic Substrates. *Biophys. J.* **2007**, *93*, 4453–4461.
(246) Jacquemet, G.; Hamidi, H.; Ivaska, J. Filopodia in Cell Adhesion, 3D Migration and Cancer Cell Invasion. *Curr. Opin. Cell Biol.* **2015**, *36*, 23–31.
(247) Humphries, J. D.; Byron, A.; Humphries, M. J. Integrin Ligands at a Glance. *Journal of Cell Science* **2006**, *119*, 3901–3903.
(248) Kong, F.; García, A. J.; Mould, A. P.; Humphries, M. J.; Zhu, C. Demonstration of Catch Bonds between an Integrin and Its Ligand. *J. Cell Biol.* **2009**, *185*, 1275–1284.
(249) Paszek, M. J.; Boettiger, D.; Weaver, V. M.; Hammer, D. A. Integrin Clustering Is Driven by Mechanical Resistance from the Glycocalyx and the Substrate. *PLoS Comput. Biol.* **2009**, *5*, e1000604.
(250) Deshpande, V. S.; Mrksich, M.; McMeeking, R. M.; Evans, A. G. A Bio-Mechanical Model for Coupling Cell Contractility with Focal Adhesion Formation. *J. Mech. Phys. Solids* **2008**, *56*, 1484–1510.
(251) Balaban, N. Q.; Schwarz, U. S.; Riveline, D.; Goichberg, P.; Tzur, G.; Sabanay, I.; Mahalu, D.; Safran, S.; Bershadsky, A.; Addadi, L.; et al. Force and Focal Adhesion Assembly: A Close Relationship Studied Using Elastic Micropatterned Substrates. *Nat. Cell Biol.* **2001**, *3*, 466–472.
(252) Paszek, M. J.; Boettiger, D.; Weaver, V. M.; Hammer, D. A. Integrin Clustering Is Driven by Mechanical Resistance from the Glycocalyx and the Substrate. *PLOS Computational Biology* **2009**, *5*, e1000604.
(253) Deshpande, V.; Mrksich, M.; Mcmeeking, R.; Evans, A. A Bio-Mechanical Model for Coupling Cell Contractility with Focal Adhesion Formation. *Journal of the Mechanics and Physics of Solids* **2008**, *56*, 1484–1510.
(254) Ribeiro, A. J. S.; Denisin, A. K.; Wilson, R. E.; Pruitt, B. L. For Whom the Cells Pull: Hydrogel and Micropost Devices for Measuring Traction Forces. *Methods* **2016**, *94*, 51–64.

(255) Geng, Y.; Wang, Z. Review of Cellular Mechanotransduction on Micropost Substrates. *Med. Biol. Eng. Comput.* **2016**, *54*, 249–271.
(256) Zemel, A.; Safran, S. A. Active Self-Polarization of Contractile Cells in Asymmetrically Shaped Domains. *Phys. Rev. E* **2007**, *76*, 021905.
(257) Zemel, A.; Bischofs, I. B.; Safran, S. A. Active Elasticity of Gels with Contractile Cells. *Phys. Rev. Lett.* **2006**, *97*, 128103.
(258) Vernerey, F. J.; Akalp, U. Role of Catch Bonds in Actomyosin Mechanics and Cell Mechanosensitivity. *Phys. Rev. E* **2016**, *94*, 012403.
(259) Huxley, A. F. Muscle structure and theories of contraction. *Prog. Biophys. Biophys. Chem.* **1957**, *7*, 255–318.
(260) Guo, B.; Guilford, W. H. Mechanics of Actomyosin Bonds in Different Nucleotide States Are Tuned to Muscle Contraction. *Proc. Natl. Acad. Sci. U. S. A.* **2006**, *103*, 9844–9849.
(261) Capitanio, M.; Canepari, M.; Maffei, M.; Beneventi, D.; Monico, C.; Vanzi, F.; Bottinelli, R.; Pavone, F. S. Ultrafast Force-Clamp Spectroscopy of Single Molecules Reveals Load Dependence of Myosin Working Stroke. *Nat. Methods* **2012**, *9*, 1013–1019.
(262) Akalp, U.; Schnatwinkel, C.; Stoykovich, M. P.; Bryant, S. J.; Vernerey, F. J. Structural Modeling of Mechanosensitivity in Non-Muscle Cells: Multiscale Approach to Understand Cell Sensing. *ACS Biomater. Sci. Eng.* **2017**, *3*, 2934–2942.
(263) Ghibaudo, M.; Saez, A.; Trichet, L.; Xayaphoummine, A.; Browaeys, J.; Silberzan, P.; Buguin, A.; Ladoux, B. Traction Forces and Rigidity Sensing Regulate Cell Functions. *Soft Matter* **2008**, *4*, 1836.
(264) Vernerey, F. J.; Farsad, M. A Constrained Mixture Approach to Mechano-Sensing and Force Generation in Contractile Cells. *J. Mech. Behav. Biomed. Mater.* **2011**, *4*, 1683–1699.
(265) Farsad, M.; Vernerey, F. J. An XFEM-Based Numerical Strategy to Model Mechanical Interactions between Biological Cells and a Deformable Substrate: MODELING OF CELL-SUBSTRATE INTERACTIONS. *Int. J. Numer. Meth. Eng.* **2012**, *92*, 238–267.
(266) Foucard, L.; Vernerey, F. J. A Thermodynamical Model for Stress-Fiber Organization in Contractile Cells. *Appl. Phys. Lett.* **2012**, *100*, 013702.
(267) Deshpande, V. S.; McMeeking, R. M.; Evans, A. G. A Bio-Chemo-Mechanical Model for Cell Contractility. *Proc. Natl. Acad. Sci. U. S. A.* **2006**, *103*, 17065–17065.
(268) Hill, A. V. The Heat of Shortening and the Dynamic Constants of Muscle. *Proc. R. Soc. Lond. B Biol. Sci.* **1938**, *126*, 136–195.
(269) Deshpande, V. S.; McMeeking, R. M.; Evans, A. G. A Bio-Chemo-Mechanical Model for Cell Contractility. *PNAS* **2006**, *103*, 14015–14020.
(270) Pathak, A.; Deshpande, V. S.; McMeeking, R. M.; Evans, A. G. The Simulation of Stress Fibre and Focal Adhesion Development in Cells on Patterned Substrates. *J. R. Soc. Interface.* **2008**, *5*, 507–524.
(271) Guo, Y.; Du, S.; Quan, S.; Jiang, F.; Yang, C.; Li, J. Effects of Biophysical Cues of 3D Hydrogels on Mesenchymal Stem Cells Differentiation. *J. Cell Physiol.* **2020**, jcp.30042.
(272) Das, R. K.; Gocheva, V.; Hammink, R.; Zouani, O. F.; Rowan, A. E. Stress-Stiffening-Mediated Stem-Cell Commitment Switch in Soft Responsive Hydrogels. *Nature Mater.* **2016**, *15*, 318–325.

(273) Ferreira, S. A.; Motwani, M. S.; Faull, P. A.; Seymour, A. J.; Yu, T. T. L.; Enayati, M.; Taheem, D. K.; Salzlechner, C.; Haghighi, T.; Kania, E. M.; et al. Bi-Directional Cell-Pericellular Matrix Interactions Direct Stem Cell Fate. *Nat. Commun.* **2018**, *9*, 4049.
(274) Wang, N.; Naruse, K.; Stamenović, D.; Fredberg, J. J.; Mijailovich, S. M.; Tolić-Nørrelykke, I. M.; Polte, T.; Mannix, R.; Ingber, D. E. Mechanical Behavior in Living Cells Consistent with the Tensegrity Model. *Proc. Natl. Acad. Sci. U. S. A.* **2001**, *98*, 7765.
(275) Hamant, O.; Inoue, D.; Bouchez, D.; Dumais, J.; Mjolsness, E. Are Microtubules Tension Sensors? *Nat. Commun.* **2019**, *10*, 2360.
(276) Chan, C. E.; Odde, D. J. Traction Dynamics of Filopodia on Compliant Substrates. *Science* **2008**, *322*, 1687–1691.
(277) Gong, Z.; Szczesny, S. E.; Caliari, S. R.; Charrier, E. E.; Chaudhuri, O.; Cao, X.; Lin, Y.; Mauck, R. L.; Janmey, P. A.; Burdick, J. A.; et al. Matching Material and Cellular Timescales Maximizes Cell Spreading on Viscoelastic Substrates. *Proc. Natl. Acad. Sci. U. S. A.* **2018**, *115*, E2686–E2695.
(278) Peskin, C. S.; Odell, G. M.; Oster, G. F. Cellular Motions and Thermal Fluctuations: The Brownian Ratchet. *Biophys. J.* **1993**, *65*, 316–324.
(279) Mogilner, A.; Oster, G. Cell Motility Driven by Actin Polymerization. *Biophys. J.* **1996**, *71*, 3030–3045.
(280) Vernerey, F. J.; Farsad, M. A Mathematical Model of the Coupled Mechanisms of Cell Adhesion, Contraction and Spreading. *J. Math. Biol.* **2014**, *68*, 989–1022.
(281) Fang, Y.; Lai, K. W. C. Modeling the Mechanics of Cells in the Cell-Spreading Process Driven by Traction Forces. *Phys. Rev. E* **2016**, *93*, 042404.
(282) Fan, H.; Li, S. Modeling Microtubule Cytoskeleton via an Active Liquid Crystal Elastomer Model. *Comput. Mater. Sci.* **2015**, *96*, 559–566.
(283) Kassianidou, E.; Probst, D.; Jäger, J.; Lee, S.; Roguet, A.-L.; Schwarz, U. S.; Kumar, S. Extracellular Matrix Geometry and Initial Adhesive Position Determine Stress Fiber Network Organization during Cell Spreading. *Cell Rep.* **2019**, *27*, 1897-1909.e4.
(284) Albert, P. J.; Schwarz, U. S. Dynamics of Cell Shape and Forces on Micropatterned Substrates Predicted by a Cellular Potts Model. *Biophys. J.* **2014**, *106*, 2340–2352.
(285) Nourshargh, S.; Hordijk, P. L.; Sixt, M. Breaching Multiple Barriers: Leukocyte Motility through Venular Walls and the Interstitium. *Nat. Rev. Mol. Cell Biol.* **2010**, *11*, 366–378.
(286) Paul, C. D.; Mistriotis, P.; Konstantopoulos, K. Cancer Cell Motility: Lessons from Migration in Confined Spaces. *Nat. Rev. Cancer* **2017**, *17*, 131–140.
(287) Winkler, B.; Aranson, I. S.; Ziebert, F. Confinement and Substrate Topography Control Cell Migration in a 3D Computational Model. *Commun. Phys.* **2019**, *2*, 82.
(288) Wilson, S. L.; Wimpenny, I.; Ahearne, M.; Rauz, S.; El Haj, A. J.; Yang, Y. Chemical and Topographical Effects on Cell Differentiation and Matrix Elasticity in a Corneal Stromal Layer Model. *Adv. Funct. Mater.* **2012**, *22*, 3641–3649.
(289) Friedl, P.; Gilmour, D. Collective Cell Migration in Morphogenesis, Regeneration and Cancer. *Nat. Rev. Mol. Cell Biol.* **2009**, *10*, 445–457.
(290) Simpson, M. J.; Towne, C.; McElwain, D. L. S.; Upton, Z. Migration of Breast Cancer Cells: Understanding the Roles of Volume Exclusion and Cell-to-Cell Adhesion. *Phys. Rev. E Stat. Nonlin. Soft Matter Phys.* **2010**, *82*, 041901.

(291) Zhong, J.; Yang, Y.; Liao, L.; Zhang, C. Matrix Stiffness-Regulated Cellular Functions under Different Dimensionalities. *Biomater. Sci.* **2020**, *8*, 2734–2755.
(292) Oakes, P. W. Balancing Forces in Migration. *Curr. Opin. Cell Biol.* **2018**, *54*, 43–49.
(293) Wolf, K.; Müller, R.; Borgmann, S.; Bröcker, Eva.-B.; Friedl, P. Amoeboid Shape Change and Contact Guidance: T-Lymphocyte Crawling through Fibrillar Collagen Is Independent of Matrix Remodeling by MMPs and Other Proteases. *Blood* **2003**, *102*, 3262–3269.
(294) Friedl, P.; Weigelin, B. Interstitial Leukocyte Migration and Immune Function. *Nat. Immunol.* **2008**, *9*, 960–969.
(295) Wolf, K.; Wu, Y. I.; Liu, Y.; Geiger, J.; Tam, E.; Overall, C.; Stack, M. S.; Friedl, P. Multi-Step Pericellular Proteolysis Controls the Transition from Individual to Collective Cancer Cell Invasion. *Nat. Cell Biol.* **2007**, *9*, 893–904.
(296) Zaman, M. H.; Kamm, R. D.; Matsudaira, P.; Lauffenburger, D. A. Computational Model for Cell Migration in Three-Dimensional Matrices. *Biophys. J.* **2005**, *89*, 1389–1397.
(297) Mosiewicz, K. A.; Kolb, L.; van der Vlies, A. J.; Lutolf, M. P. Microscale Patterning of Hydrogel Stiffness through Light-Triggered Uncaging of Thiols. *Biomater. Sci.* **2014**, *2*, 1640–1651.
(298) Wang, M.; Yang, Y.; Han, L.; Han, S.; Liu, N.; Xu, F.; Li, F. Effect of Three-Dimensional ECM Stiffness on Cancer Cell Migration through Regulating Cell Volume Homeostasis. *Biochem. Biophys. Res. Commun.* **2020**, *528*, 459–465.
(299) Vasudevan, J.; Lim, C. T.; Fernandez, J. G. Cell Migration and Breast Cancer Metastasis in Biomimetic Extracellular Matrices with Independently Tunable Stiffness. *Adv. Funct. Mater.* **2020**, *30*, 2005383.
(300) Dubbin, K.; Robertson, C.; Hinckley, A.; Alvarado, J. A.; Gilmore, S. F.; Hynes, W. F.; Wheeler, E. K.; Moya, M. L. Macromolecular Gelatin Properties Affect Fibrin Microarchitecture and Tumor Spheroid Behavior in Fibrin-Gelatin Gels. *Biomaterials* **2020**, *250*, 120035.
(301) Daviran, M.; Catalano, J.; Schultz, K. M. Determining How Human Mesenchymal Stem Cells Change Their Degradation Strategy in Response to Microenvironmental Stiffness. *Biomacromolecules* **2020**, *21*, 3056–3068.
(302) Pelham, R. J.; Wang, Y. Cell Locomotion and Focal Adhesions Are Regulated by Substrate Flexibility. *Proc. Natl. Acad. Sci. U. S. A.* **1997**, *94*, 13661.
(303) Ruud, K. F.; Hiscox, W. C.; Yu, I.; Chen, R. K.; Li, W. Distinct Phenotypes of Cancer Cells on Tissue Matrix Gel. *Breast Cancer Res.* **2020**, *22*, 82.
(304) Tang, V. W. Collagen, Stiffness, and Adhesion: The Evolutionary Basis of Vertebrate Mechanobiology. *J. Mol. Cell Biol.* **2020**, *31*, 1823–1834.
(305) Anguiano, M.; Morales, X.; Castilla, C.; Pena, A. R.; Ederra, C.; Martínez, M.; Ariz, M.; Esparza, M.; Amaveda, H.; Mora, M.; et al. The Use of Mixed Collagen-Matrigel Matrices of Increasing Complexity Recapitulates the Biphasic Role of Cell Adhesion in Cancer Cell Migration: ECM Sensing, Remodeling and Forces at the Leading Edge of Cancer Invasion. *PLoS One* **2020**, *15*, e0220019.
(306) Ho, S. S.; Keown, A. T.; Addison, B.; Leach, J. K. Cell Migration and Bone Formation from Mesenchymal Stem Cell Spheroids in Alginate Hydrogels Are Regulated by Adhesive Ligand Density. *Biomacromolecules* **2017**, *18*, 4331–4340.

(307) He, Y. J.; Young, D. A.; Mededovic, M.; Li, K.; Li, C.; Tichauer, K.; Venerus, D.; Papavasiliou, G. Protease-Sensitive Hydrogel Biomaterials with Tunable Modulus and Adhesion Ligand Gradients for 3D Vascular Sprouting. *Biomacromolecules* **2018**, *19*, 4168–4181.
(308) Hung, B. P.; Harvestine, J. N.; Saiz, A. M.; Gonzalez-Fernandez, T.; Sahar, D. E.; Weiss, M. L.; Leach, J. K. Defining Hydrogel Properties to Instruct Lineage- and Cell-Specific Mesenchymal Differentiation. *Biomaterials* **2019**, *189*, 1–10.
(309) Haeger, A.; Wolf, K.; Zegers, M. M.; Friedl, P. Collective Cell Migration: Guidance Principles and Hierarchies. *Trends Cell Biol.* **2015**, *25*, 556–566.
(310) Borau, C.; Kamm, R. D.; García-Aznar, J. M. Mechano-Sensing and Cell Migration: A 3D Model Approach. *Phys. Biol.* **2011**, *8*, 066008.
(311) Schlüter, D. K.; Ramis-Conde, I.; Chaplain, M. A. J. Computational Modeling of Single-Cell Migration: The Leading Role of Extracellular Matrix Fibers. *Biophys. J.* **2012**, *103*, 1141–1151.
(312) Vincent, L. G.; Choi, Y. S.; Alonso-Latorre, B.; del Álamo, J. C.; Engler, A. J. Mesenchymal Stem Cell Durotaxis Depends on Substrate Stiffness Gradient Strength. *Biotechnol. J.* **2013**, *8*, 472–484.
(313) Shellard, A.; Mayor, R. All Roads Lead to Directional Cell Migration. *Trends Cell Biol.* **2020**, *30*, 852–868.
(314) Ebata, H.; Kidoaki, S. Avoiding Tensional Equilibrium in Cells Migrating on a Matrix with Cell-Scale Stiffness-Heterogeneity. *Biomaterials* **2021**, *274*, 120860.
(315) Sundararaghavan, H. G.; Monteiro, G. A.; Firestein, B. L.; Shreiber, D. I. Neurite Growth in 3D Collagen Gels with Gradients of Mechanical Properties. *Biotechnol. Bioeng.* **2009**, *102*, 632–643.
(316) Mason, B. N.; Starchenko, A.; Williams, R. M.; Bonassar, L. J.; Reinhart-King, C. A. Tuning Three-Dimensional Collagen Matrix Stiffness Independently of Collagen Concentration Modulates Endothelial Cell Behavior. *Acta Biomater.* **2013**, *9*, 4635–4644.
(317) Bordeleau, F.; Mason, B. N.; Lollis, E. M.; Mazzola, M.; Zanotelli, M. R.; Somasegar, S.; Califano, J. P.; Montague, C.; LaValley, D. J.; Huynh, J.; et al. Matrix Stiffening Promotes a Tumor Vasculature Phenotype. *Proc. Natl. Acad. Sci. U. S. A.* **2017**, *114*, 492–497.
(318) Kim, M.-C.; Silberberg, Y. R.; Abeyaratne, R.; Kamm, R. D.; Asada, H. H. Computational Modeling of Three-Dimensional ECM-Rigidity Sensing to Guide Directed Cell Migration. *Proc. Natl. Acad. Sci. U. S. A.* **2018**, *115*, E390–E399.
(319) Heck, T.; Vargas, D. A.; Smeets, B.; Ramon, H.; Van Liedekerke, P.; Van Oosterwyck, H. The Role of Actin Protrusion Dynamics in Cell Migration through a Degradable Viscoelastic Extracellular Matrix: Insights from a Computational Model. *PLoS Comput. Biol.* **2020**, *16*, e1007250.
(320) Dietrich, M.; Roy, H. L.; B. Brückner, D.; Engelke, H.; Zantl, R.; O. Rädler, J.; P. Broedersz, C. Guiding 3D Cell Migration in Deformed Synthetic Hydrogel Microstructures. *Soft Matter* **2018**, *14*, 2816–2826.
(321) Kim, M.-C.; Silberberg, Y. R.; Abeyaratne, R.; Kamm, R. D.; Asada, H. H. Computational Modeling of Three-Dimensional ECM-Rigidity Sensing to Guide Directed Cell Migration. *PNAS* **2018**, *115*, E390–E399.
(322) Ruprecht, V.; Wieser, S.; Callan-Jones, A.; Smutny, M.; Morita, H.; Sako, K.; Barone, V.; Ritsch-Marte, M.; Sixt, M.; Voituriez, R.; et al. Cortical Contractility Triggers a Stochastic

Switch to Fast Amoeboid Cell Motility. *Cell* **2015**, *160*, 673–685.
(323) Lin, C.; Tao, B.; Deng, Y.; He, Y.; Shen, X.; Wang, R.; Lu, L.; Peng, Z.; Xia, Z.; Cai, K. Matrix Promote Mesenchymal Stromal Cell Migration with Improved Deformation via Nuclear Stiffness Decrease. *Biomaterials* **2019**, *217*, 119300.
(324) Duan, Y.; Li, X.; Zuo, X.; Shen, T.; Yu, S.; Deng, L.; Gao, C. Migration of Endothelial Cells and Mesenchymal Stem Cells into Hyaluronic Acid Hydrogels with Different Moduli under Induction of Pro-Inflammatory Macrophages. *J. Mater. Chem. B* **2019**, *7*, 5478–5489.
(325) Hecht, I.; Levine, H.; Rappel, W.-J.; Ben-Jacob, E. "Self-Assisted" Amoeboid Navigation in Complex Environments. *PLOS ONE* **2011**, *6*, e21955.
(326) Moure, A.; Gomez, H. Phase-Field Model of Cellular Migration: Three-Dimensional Simulations in Fibrous Networks. *Comput. Methods Appl. Mech. Eng.* **2017**, *320*, 162–197.
(327) Campbell, E. J.; Bagchi, P. A Computational Model of Amoeboid Cell Motility in the Presence of Obstacles. *Soft Matter* **2018**, *14*, 5741–5763.
(328) Foucard, L.; Espinet, X.; Benet, E.; Vernerey, F. J. The Role of the Cortical Membrane in Cell Mechanics: Model and Simulation. In *Multiscale Simulations and Mechanics of Biological Materials*; Li, S., Qian, D., Eds.; John Wiley & Sons Ltd: Oxford, UK, 2013; pp 241–265.
(329) Lim, F. Y.; Koon, Y. L.; Chiam, K.-H. A Computational Model of Amoeboid Cell Migration. *Comput. Methods Biomech. Biomed. Engin.* **2013**, *16*, 1085–1095.
(330) Vernerey, F.; Shen, T. The Mechanics of Hydrogel Crawlers in Confined Environment. *J. R. Soc. Interface.* **2017**, *14*, 20170242.
(331) Thiery, J. P.; Acloque, H.; Huang, R. Y. J.; Nieto, M. A. Epithelial-Mesenchymal Transitions in Development and Disease. *Cell* **2009**, *139*, 871–890.
(332) Allen, S. C.; Widman, J. A.; Datta, A.; Suggs, L. J. Dynamic Extracellular Matrix Stiffening Induces a Phenotypic Transformation and a Migratory Shift in Epithelial Cells. *Integr. Biol. 12*, 161–174.
(333) Yamada, K. M.; Collins, J. W.; Cruz Walma, D. A.; Doyle, A. D.; Morales, S. G.; Lu, J.; Matsumoto, K.; Nazari, S. S.; Sekiguchi, R.; Shinsato, Y.; et al. Extracellular Matrix Dynamics in Cell Migration, Invasion and Tissue Morphogenesis. *Int. J. Exp. Path* **2019**, *100*, 144–152.
(334) Yamada, K. M.; Sixt, M. Mechanisms of 3D Cell Migration. *Nat. Rev. Mol. Cell Biol.* **2019**, *20*, 738–752.
(335) Zuo, X.; Zhang, H.; Zhou, T.; Duan, Y.; Shou, H.; Yu, S.; Gao, C. Spheroids of Endothelial Cells and Vascular Smooth Muscle Cells Promote Cell Migration in Hyaluronic Acid and Fibrinogen Composite Hydrogels. *Research* **2020**, *2020*, 1–15.
(336) Mrass, P.; Kinjyo, I.; Ng, L. G.; Reiner, S. L.; Puré, E.; Weninger, W. CD44 Mediates Successful Interstitial Navigation by Killer T Cells and Enables Efficient Antitumor Immunity. *Immunity* **2008**, *29*, 971–985.
(337) Dupré, L.; Houmadi, R.; Tang, C.; Rey-Barroso, J. T Lymphocyte Migration: An Action Movie Starring the Actin and Associated Actors. *Front. Immunol.* **2015**, *6*.
(338) Orgaz, J. L.; Pandya, P.; Dalmeida, R.; Karagiannis, P.; Sanchez-Laorden, B.; Viros, A.; Albrengues, J.; Nestle, F. O.; Ridley, A. J.; Gaggioli, C.; et al. Diverse Matrix

Metalloproteinase Functions Regulate Cancer Amoeboid Migration. *Nat. Commun.* **2014**, *5*, 4255.
(339) Ginzberg, M. B.; Kafri, R.; Kirschner, M. On Being the Right (Cell) Size. *Science* **2015**, *348*, 1245075–1245075.
(340) Boucrot, E.; Kirchhausen, T. Mammalian Cells Change Volume during Mitosis. *PLoS ONE* **2008**, *3*, e1477.
(341) Lloyd, A. C. The Regulation of Cell Size. *Cell* **2013**, *154*, 1194–1205.
(342) Wang, M.; Yang, Y.; Han, L.; Xu, F.; Li, F. Cell Mechanical Microenvironment for Cell Volume Regulation. *J. Cell Physiol.* **2020**, *235*, 4070–4081.
(343) Caliari, S. R.; Vega, S. L.; Kwon, M.; Soulas, E. M.; Burdick, J. A. Dimensionality and Spreading Influence MSC YAP/TAZ Signaling in Hydrogel Environments. *Biomaterials* **2016**, *103*, 314–323.
(344) Montagner, M.; Dupont, S. Mechanical Forces as Determinants of Disseminated Metastatic Cell Fate. *Cells* **2020**, *9*, 250.
(345) Virdi, J. K.; Pethe, P. Biomaterials Regulate Mechanosensors YAP/TAZ in Stem Cell Growth and Differentiation. *J. Tissue Eng. Regen. Med.* **2020**.
(346) Major, L. G.; Holle, A. W.; Young, J. L.; Hepburn, M. S.; Jeong, K.; Chin, I. L.; Sanderson, R. W.; Jeong, J. H.; Aman, Z. M.; Kennedy, B. F.; et al. Volume Adaptation Controls Stem Cell Mechanotransduction. *ACS Appl. Mater. Interfaces* **2019**, *11*, 45520–45530.
(347) Lee, H.; Stowers, R.; Chaudhuri, O. Volume Expansion and TRPV4 Activation Regulate Stem Cell Fate in Three-Dimensional Microenvironments. *Nat. Commun.* **2019**, *10*, 529.
(348) Wei, Q.; Holle, A.; Li, J.; Posa, F.; Biagioni, F.; Croci, O.; Benk, A. S.; Young, J.; Noureddine, F.; Deng, J.; et al. BMP-2 Signaling and Mechanotransduction Synergize to Drive Osteogenic Differentiation via YAP/TAZ. *Adv. Sci.* **2020**, *7*, 1902931.
(349) Nardone, G.; Oliver-De La Cruz, J.; Vrbsky, J.; Martini, C.; Pribyl, J.; Skládal, P.; Pešl, M.; Caluori, G.; Pagliari, S.; Martino, F.; et al. YAP Regulates Cell Mechanics by Controlling Focal Adhesion Assembly. *Nat. Commun.* **2017**, *8*, 15321.
(350) Heng, B. C.; Zhang, X.; Aubel, D.; Bai, Y.; Li, X.; Wei, Y.; Fussenegger, M.; Deng, X. Role of YAP/TAZ in Cell Lineage Fate Determination and Related Signaling Pathways. *Front. Cell Dev. Biol.* **2020**, *8*, 735.
(351) Lee, H.; Gu, L.; Mooney, D. J.; Levenston, M. E.; Chaudhuri, O. Mechanical Confinement Regulates Cartilage Matrix Formation by Chondrocytes. *Nature Mater.* **2017**, *16*, 1243–1251.
(352) Lee, K.; Chen, Y.; Li, X.; Wang, Y.; Kawazoe, N.; Yang, Y.; Chen, G. Solution Viscosity Regulates Chondrocyte Proliferation and Phenotype during 3D Culture. *J. Mater. Chem. B* **2019**, *7*, 7713–7722.
(353) Wei, Q.; Young, J.; Holle, A.; Li, J.; Bieback, K.; Inman, G.; Spatz, J. P.; Cavalcanti-Adam, E. A. Soft Hydrogels for Balancing Cell Proliferation and Differentiation. *ACS Biomater. Sci. Eng.* **2020**, *6*, 4687–4701.
(354) Tan, Y.; Huang, H.; Ayers, D. C.; Song, J. Modulating Viscoelasticity, Stiffness, and Degradation of Synthetic Cellular Niches via Stoichiometric Tuning of Covalent versus Dynamic Noncovalent Cross-Linking. *ACS Cent. Sci.* **2018**, *4*, 971–981.
(355) Chowdhuri, S.; Saha, A.; Pramanik, B.; Das, S.; Dowari, P.; Ukil, A.; Das, D. Smart Thixotropic Hydrogels by Disulfide-Linked Short Peptides for Effective Three-

Dimensional Cell Proliferation. *Langmuir* **2020**, *36*, 15450–15462.
(356) Boddupalli, A.; Bratlie, K. M. Second Harmonic Generation Microscopy of Collagen Organization in Tunable, Environmentally Responsive Alginate Hydrogels. *Biomater. Sci.* **2019**, *7*, 1188–1199.
(357) Kloxin, A. M.; Kloxin, C. J.; Bowman, C. N.; Anseth, K. S. Mechanical Properties of Cellularly Responsive Hydrogels and Their Experimental Determination. *Adv. Mater.* **2010**, *17*, 3484–3494.
(358) Bryant, S. J.; Anseth, K. S.; Lee, D. A.; Bader, D. L. Crosslinking Density Influences the Morphology of Chondrocytes Photo-Encapsulated in PEG Hydrogels. *J. Orthop. Res.* **2004**, *22*, 1143–1149.
(359) Zimberlin, J. A.; McManus, J. J.; Crosby, A. J. Cavitation Rheology of the Vitreous: Mechanical Properties of Biological Tissue. *Soft Matter* **2010**, *6*, 3632–3635.
(360) Zhu, J.; Li, T.; Cai, S.; Suo, Z. Snap-through Expansion of a Gas Bubble in an Elastomer. *J. Adhes.* **2011**, *87*, 466–481.
(361) Shen, T.; Long, R.; Vernerey, F. Computational Modeling of the Large Deformation and Flow of Viscoelastic Polymers. *Comput. Mech.* **2019**, *63*, 725–745.
(362) Dumont, S.; Mitchison, T. J. Force and Length in the Mitotic Spindle. *Curr. Biol.* **2009**, *19*, R749–R761.
(363) Nam, S.; Chaudhuri, O. Mitotic Cells Generate Protrusive Extracellular Forces to Divide in Three-Dimensional Microenvironments. *Nature Phys.* **2018**, *14*, 621–628.
(364) He, L.; Chen, W.; Wu, P.-H.; Jimenez, A.; Wong, B. S.; San, A.; Konstantopoulos, K.; Wirtz, D. Local 3D Matrix Confinement Determines Division Axis through Cell Shape. *Oncotarget* **2016**, *7*, 6994–7011.
(365) Sant, S.; Johnston, P. A. The Production of 3D Tumor Spheroids for Cancer Drug Discovery. *Drug Discov. Today Technol.* **2017**, *23*, 27–36.
(366) Li, Y.; Kumacheva, E. Hydrogel Microenvironments for Cancer Spheroid Growth and Drug Screening. *Sci. Adv.* **2018**, *4*, eaas8998.
(367) Jiang, T.; Munguia-Lopez, J. G.; Gu, K.; Bavoux, M. M.; Flores-Torres, S.; Kort-Mascort, J.; Grant, J.; Vijayakumar, S.; De Leon-Rodriguez, A.; Ehrlicher, A. J.; et al. Engineering Bioprintable Alginate/Gelatin Composite Hydrogels with Tunable Mechanical and Cell Adhesive Properties to Modulate Tumor Spheroid Growth Kinetics. *Biofabrication* **2019**, *12*, 015024.
(368) Taubenberger, A. V.; Girardo, S.; Träber, N.; Fischer-Friedrich, E.; Kräter, M.; Wagner, K.; Kurth, T.; Richter, I.; Haller, B.; Binner, M.; et al. 3D Microenvironment Stiffness Regulates Tumor Spheroid Growth and Mechanics via P21 and ROCK. *Adv. Biosys.* **2019**, *3*, 1900128.
(369) Li, Y.; Khuu, N.; Prince, E.; Tao, H.; Zhang, N.; Chen, Z.; Gevorkian, A.; McGuigan, A. P.; Kumacheva, E. Matrix Stiffness-Regulated Growth of Breast Tumor Spheroids and Their Response to Chemotherapy. *Biomacromolecules* **2020**, acs.biomac.0c01287.
(370) Lu, Y.-C.; Chu, T.; Hall, M. S.; Fu, D.-J.; Shi, Q.; Chiu, A.; An, D.; Wang, L.-H.; Pardo, Y.; Southard, T.; et al. Physical Confinement Induces Malignant Transformation in Mammary Epithelial Cells. *Biomaterials* **2019**, *217*, 119307.
(371) Liu, H.-Y.; Korc, M.; Lin, C.-C. Biomimetic and Enzyme-Responsive Dynamic Hydrogels for Studying Cell-Matrix Interactions in Pancreatic Ductal Adenocarcinoma. *Biomaterials*

2018, *160*, 24–36.
(372) Sivakumar, H.; Devarasetty, M.; Kram, D. E.; Strowd, R. E.; Skardal, A. Multi-Cell Type Glioblastoma Tumor Spheroids for Evaluating Sub-Population-Specific Drug Response. *Front. Bioeng. Biotechnol.* **2020**, *8*, 538663.
(373) Ashworth, J. C.; Thompson, J. L.; James, J. R.; Slater, C. E.; Pijuan-Galitó, S.; Lis-Slimak, K.; Holley, R. J.; Meade, K. A.; Thompson, A.; Arkill, K. P.; et al. Peptide Gels of Fully-Defined Composition and Mechanics for Probing Cell-Cell and Cell-Matrix Interactions in Vitro. *Matrix Biol.* **2020**, *85–86*, 15–33.
(374) Unal, D. B.; Caliari, S. R.; Lampe, K. J. 3D Hyaluronic Acid Hydrogels for Modeling Oligodendrocyte Progenitor Cell Behavior as a Function of Matrix Stiffness. *Biomacromolecules* **2020**, *21*, 4962–4971.
(375) Wu, S.; Xu, R.; Duan, B.; Jiang, P. Three-Dimensional Hyaluronic Acid Hydrogel-Based Models for in Vitro Human IPSC-Derived NPC Culture and Differentiation. *J. Mater. Chem. B* **2017**, *5*, 3870–3878.
(376) Shirinifard, A.; Gens, J. S.; Zaitlen, B. L.; Popławski, N. J.; Swat, M.; Glazier, J. A. 3D Multi-Cell Simulation of Tumor Growth and Angiogenesis. *PLOS ONE* **2009**, *4*, e7190.
(377) Liedekerke, P. V.; Neitsch, J.; Johann, T.; Alessandri, K.; Nassoy, P.; Drasdo, D. Quantitative Cell-Based Model Predicts Mechanical Stress Response of Growing Tumor Spheroids over Various Growth Conditions and Cell Lines. *PLOS Computational Biology* **2019**, *15*, e1006273.
(378) Ambrosi, D.; Mollica, F. The Role of Stress in the Growth of a Multicell Spheroid. *J. Math. Biol.* **2004**, *48*, 477–499.
(379) Rodriguez, E. K.; Hoger, A.; McCulloch, A. D. Stress-Dependent Finite Growth in Soft Elastic Tissues. *J. Biomech.* **1994**, *27*, 455–467.
(380) Wijeratne, P. A.; Vavourakis, V.; Hipwell, J. H.; Voutouri, C.; Papageorgis, P.; Stylianopoulos, T.; Evans, A.; Hawkes, D. J. Multiscale Modelling of Solid Tumour Growth: The Effect of Collagen Micromechanics. *Biomech. Model Mechanobiol.* **2016**, *15*, 1079–1090.
(381) Mills, K. L.; Kemkemer, R.; Rudraraju, S.; Garikipati, K. Elastic Free Energy Drives the Shape of Prevascular Solid Tumors. *PLoS ONE* **2014**, *9*, e103245.
(382) Mills, K. L.; Garikipati, K.; Kemkemer, R. Experimental Characterization of Tumor Spheroids for Studies of the Energetics of Tumor Growth: *Int. J. Mater. Res.* **2011**, *102*, 889–895.
(383) Dassios, G.; Kariotou, F.; Tsampas, M. N.; Sleeman, B. D. Mathematical Modelling of Avascular Ellipsoidal Tumour Growth. *Quart. Appl. Math.* **2012**, *70*, 1–24.
(384) Blondel, D.; Lutolf, M. P. Bioinspired Hydrogels for 3D Organoid Culture. *Chimia (aarau)* **2019**, *73*, 81–85.
(385) Magno, V.; Meinhardt, A.; Werner, C. Polymer Hydrogels to Guide Organotypic and Organoid Cultures. *Adv. Funct. Mater.* **2020**, *30*, 2000097.
(386) Liu, H.; Wang, Y.; Cui, K.; Guo, Y.; Zhang, X.; Qin, J. Advances in Hydrogels in Organoids and Organs-on-a-Chip. *Adv. Mater.* **2019**, *31*, 1902042.
(387) Kang, S.; Kim, D.; Lee, J.; Takayama, S.; Park, J. Y. Engineered Microsystems for Spheroid and Organoid Studies. *Adv. Healthcare Mater.* **2020**, 2001284.

(388) Matthys, O. B.; Silva, A. C.; McDevitt, T. C. Engineering Human Organoid Development Ex Vivo—Challenges and Opportunities. *Curr. Opin. Biomed. Eng.* **2020**, *13*, 160–167.
(389) Bratt-Leal, A. M.; Carpenedo, R. L.; McDevitt, T. C. Engineering the Embryoid Body Microenvironment to Direct Embryonic Stem Cell Differentiation. *Biotechnol. Progress* **2009**, *25*, 43–51.
(390) Li, Q.; Chow, K. L.; Chau, Y. Three-Dimensional Self-Assembling Peptide Matrix Enhances the Formation of Embryoid Bodies and Their Neuronal Differentiation: Formation of Embryoid Bodies and Neuronal Differentiation. *J. Biomed. Mater. Res.* **2014**, *102*, 1991–2000.
(391) Gjorevski, N.; Sachs, N.; Manfrin, A.; Giger, S.; Bragina, M. E.; Ordóñez-Morán, P.; Clevers, H.; Lutolf, M. P. Designer Matrices for Intestinal Stem Cell and Organoid Culture. *Nature* **2016**, *539*, 560–564.
(392) Cruz-Acuña, R.; Quirós, M.; Farkas, A. E.; Dedhia, P. H.; Huang, S.; Siuda, D.; García-Hernández, V.; Miller, A. J.; Spence, J. R.; Nusrat, A.; et al. Synthetic Hydrogels for Human Intestinal Organoid Generation and Colonic Wound Repair. *Nat. Cell Biol.* **2017**, *19*, 1326–1335.
(393) Lancaster, M. A.; Corsini, N. S.; Wolfinger, S.; Gustafson, E. H.; Phillips, A. W.; Burkard, T. R.; Otani, T.; Livesey, F. J.; Knoblich, J. A. Guided Self-Organization and Cortical Plate Formation in Human Brain Organoids. *Nat Biotechnol* **2017**, *35*, 659–666.
(394) Broguiere, N.; Isenmann, L.; Hirt, C.; Ringel, T.; Placzek, S.; Cavalli, E.; Ringnalda, F.; Villiger, L.; Züllig, R.; Lehmann, R.; et al. Growth of Epithelial Organoids in a Defined Hydrogel. *Adv. Mater.* **2018**, *30*, 1801621.
(395) Nowak, M.; Freudenberg, U.; Tsurkan, M. V.; Werner, C.; Levental, K. R. Modular GAG-Matrices to Promote Mammary Epithelial Morphogenesis in Vitro. *Biomaterials* **2017**, *112*, 20–30.
(396) Yavitt, F. M.; Brown, T. E.; Hushka, E. A.; Brown, M. E.; Gjorevski, N.; Dempsey, P. J.; Lutolf, M. P.; Anseth, K. S. The Effect of Thiol Structure on Allyl Sulfide Photodegradable Hydrogels and Their Application as a Degradable Scaffold for Organoid Passaging. *Adv. Mater.* **2020**, *32*, 1905366.
(397) Hushka, E. A.; Yavitt, F. M.; Brown, T. E.; Dempsey, P. J.; Anseth, K. S. Relaxation of Extracellular Matrix Forces Directs Crypt Formation and Architecture in Intestinal Organoids. *Adv. Healthcare Mater.* **2020**, *9*, 1901214.
(398) Montes-Olivas, S.; Marucci, L.; Homer, M. Mathematical Models of Organoid Cultures. *Front. Genet.* **2019**, *10*.
(399) Buske, P.; Przybilla, J.; Loeffler, M.; Sachs, N.; Sato, T.; Clevers, H.; Galle, J. On the Biomechanics of Stem Cell Niche Formation in the Gut - Modelling Growing Organoids: Modeling Intestinal Organoid Formation. *FEBS J.* **2012**, *279*, 3475–3487.
(400) Thalheim, T.; Quaas, M.; Herberg, M.; Braumann, U.-D.; Kerner, C.; Loeffler, M.; Aust, G.; Galle, J. Linking Stem Cell Function and Growth Pattern of Intestinal Organoids. *Dev. Biol.* **2018**, *433*, 254–261.
(401) Langlands, A. J.; Almet, A. A.; Appleton, P. L.; Newton, I. P.; Osborne, J. M.; Näthke, I. S. Paneth Cell-Rich Regions Separated by a Cluster of Lgr5+ Cells Initiate Crypt Fission in the Intestinal Stem Cell Niche. *PLoS Biol.* **2016**, *14*, e1002491.

(402) Almet, A. A.; Hughes, B. D.; Landman, K. A.; Näthke, I. S.; Osborne, J. M. A Multicellular Model of Intestinal Crypt Buckling and Fission. *Bull. Math. Biol.* **2018**, *80*, 335–359.
(403) Yan, H.; Konstorum, A.; Lowengrub, J. S. Three-Dimensional Spatiotemporal Modeling of Colon Cancer Organoids Reveals That Multimodal Control of Stem Cell Self-Renewal Is a Critical Determinant of Size and Shape in Early Stages of Tumor Growth. *Bull. Math. Biol.* **2018**, *80*, 1404–1433.
(404) Youssefpour, H.; Li, X.; Lander, A. D.; Lowengrub, J. S. Multispecies Model of Cell Lineages and Feedback Control in Solid Tumors. *J. Theor. Biol.* **2012**, *304*, 39–59.
(405) Wise, S. M.; Lowengrub, J. S.; Frieboes, H. B.; Cristini, V. Three-Dimensional Multispecies Nonlinear Tumor Growth--I Model and Numerical Method. *J. Theor. Biol.* **2008**, *253*, 524–543.
(406) Gao, X.; McDonald, J. T.; Hlatky, L.; Enderling, H. Acute and Fractionated Irradiation Differentially Modulate Glioma Stem Cell Division Kinetics. *Cancer Res.* **2013**, *73*, 1481–1490.
(407) Wisdom, K. M.; Indana, D.; Chou, P.-E.; Desai, R.; Kim, T.; Chaudhuri, O. Covalent Cross-Linking of Basement Membrane-like Matrices Physically Restricts Invasive Protrusions in Breast Cancer Cells. *Matrix Biol.* **2020**, *85–86*, 94–111.
(408) Arita, M.; Li, S.-W.; Kopen, G.; Adachi, E.; Jimenez, S. A.; Fertala, A. Skeletal Abnormalities and Ultrastructural Changes of Cartilage in Transgenic Mice Expressing a Collagen II Gene (COL2A1) with a Cys for Arg-Alpha1-519 Substitution. *Osteoarthr. Cartil.* **2002**, *10*, 808–815.
(409) Schneider, M. C.; Barnes, C. A.; Bryant, S. J. Characterization of the Chondrocyte Secretome in Photoclickable Poly(Ethylene Glycol) Hydrogels. *Biotechnol. Bioeng.* **2017.**
(410) Kiani, C.; Chen, L.; Wu, Y. J.; Yee, A. J.; Yang, B. B. Structure and Function of Aggrecan. *Cell Research* **2002**, *12*, 19–32.
(411) Nicodemus, G. D.; Skaalure, S. C.; Bryant, S. J. Gel Structure Has an Impact on Pericellular and Extracellular Matrix Deposition, Which Subsequently Alters Metabolic Activities in Chondrocyte-Laden PEG Hydrogels. *Acta. Biomater.* **2011**, *7*, 492–504.
(412) Reed, C. C.; Iozzo, R. V. The Role of Decorin in Collagen Fibrillogenesis and Skin Homeostasis. *Glycoconj J* **2002**, *19*, 249–255.
(413) Wiberg, C.; Klatt, A. R.; Wagener, R.; Paulsson, M.; Bateman, J. F.; Heinegård, D.; Mörgelin, M. Complexes of Matrilin-1 and Biglycan or Decorin Connect Collagen VI Microfibrils to Both Collagen II and Aggrecan. *J. Biol. Chem.* **2003**, *278*, 37698–37704.
(414) Loebel, C.; Kwon, M. Y.; Wang, C.; Han, L.; Mauck, R. L.; Burdick, J. A. Metabolic Labeling to Probe the Spatiotemporal Accumulation of Matrix at the Chondrocyte–Hydrogel Interface. *Adv. Funct. Mater.* **2020**, *30*, 1909802.
(415) Bryant, S. J.; Anseth, K. S. Hydrogel Properties Influence ECM Production by Chondrocytes Photoencapsulated in Poly(Ethylene Glycol) Hydrogels. *J. Biomed. Mater. Res.* **2002**, *59*, 63–72.
(416) Nicodemus, G. D.; Bryant, S. J. The Role of Hydrogel Structure and Dynamic Loading on Chondrocyte Gene Expression and Matrix Formation. *J. Biomech.* **2008**, *41*, 1528–1536.
(417) Rodriguez, E. K.; Hoger, A.; McCulloch, A. D. Stress-Dependent Finite Growth in Soft Elastic Tissues. *J Biomech* **1994**, *27*, 455–467.

(418) Humphrey, J. D.; Rajagopal, K. R. A Constrained Mixture Model for Growth and Remodeling of Soft Tissues. *Math. Models Methods Appl. Sci.* **2002**, *12*, 407–430.
(419) Skalak, R.; Dasgupta, G.; Moss, M.; Otten, E.; Dullumeijer, P.; Vilmann, H. Analytical Description of Growth. *J. Theor. Biol.* **1982**, *94*, 555–577.
(420) Garikipati, K.; Arruda, E. M.; Grosh, K.; Narayanan, H.; Calve, S. A Continuum Treatment of Growth in Biological Tissue: The Coupling of Mass Transport and Mechanics. *J. Mech. Phys. Solids* **2004**, *52*, 1595–1625.
(421) Sengers, B. G.; Van Donkelaar, C. C.; Oomens, C. W. J.; Baaijens, F. P. T. The Local Matrix Distribution and the Functional Development of Tissue Engineered Cartilage, a Finite Element Study. *Ann. Biomed. Eng.* **2004**, *32*, 1718–1727.
(422) Sridhar, S. L.; C. Schneider, M.; Chu, S.; Roucy, G. de; J. Bryant, S.; J. Vernerey, F. Heterogeneity Is Key to Hydrogel-Based Cartilage Tissue Regeneration. *Soft Matter* **2017**, *13*, 4841–4855.
(423) Trewenack, A. J.; Please, C. P.; Landman, K. A. A Continuum Model for the Development of Tissue-Engineered Cartilage around a Chondrocyte. *Math. Med. Biol.* **2009**, *26*, 241–262.
(424) Haider, M. A.; Olander, J. E.; Arnold, R. F.; Marous, D. R.; McLamb, A. J.; Thompson, K. C.; Woodruff, W. R.; Haugh, J. M. A Phenomenological Mixture Model for Biosynthesis and Linking of Cartilage Extracellular Matrix in Scaffolds Seeded with Chondrocytes. *Biomech. Model. Mechanobiol.* **2011**, *10*, 915–924.
(425) Wilson, C. G.; Bonassar, L. J.; Kohles, S. S. Modeling the Dynamic Composition of Engineered Cartilage. *Arch. Biochem. Biophys.* **2002**, *408*, 246–254.
(426) Dhote, V.; Vernerey, F. J. Mathematical Model of the Role of Degradation on Matrix Development in Hydrogel Scaffold. *Biomech. Model Mechanobiol.* **2014**, *13*, 167–183.
(427) Nemat-Nasser, S. North-Holland Series in Applied Mathematics and Mechanics (Book 37). In *Micromechanics: Overall Properties of Heterogeneous Materials*; Elsevier, 1999.
(428) Nicodemus, G. D.; Bryant, S. J. Cell Encapsulation in Biodegradable Hydrogels for Tissue Engineering Applications. *Tissue Eng. Part B Rev.* **2008**, *14*, 149–165.
(429) Neumann, A. J.; Quinn, T.; Bryant, S. J. Nondestructive Evaluation of a New Hydrolytically Degradable and Photo-Clickable PEG Hydrogel for Cartilage Tissue Engineering. *Acta Biomater.* **2016**, *39*, 1–11.
(430) Schneider, M. C.; Chu, S.; Sridhar, S. L.; de Roucy, G.; Vernerey, F. J.; Bryant, S. J. Local Heterogeneities Improve Matrix Connectivity in Degradable and Photoclickable Poly(Ethylene Glycol) Hydrogels for Applications in Tissue Engineering. *ACS Biomater. Sci. Eng.* **2017**, *3*, 2480–2492.
(431) Peng, S.; Liu, H.-X.; Ko, C.-Y.; Yang, S.-R.; Hung, W.-L.; Chu, I.-M. A Hydrolytically-Tunable Photocrosslinked PLA-PEG-PLA/PCL-PEG-PCL Dual-Component Hydrogel That Enhances Matrix Deposition of Encapsulated Chondrocytes: Photocrosslinked Dual-Component Hydrogel with Tunable Degradation for Tissue Engineering. *J. Tissue Eng. Regen. Med.* **2017**, *11*, 669–678.
(432) Cereceres, S.; Lan, Z.; Bryan, L.; Whitely, M.; Wilems, T.; Fabela, N.; Whitfield-Cargile, C.; Cosgriff-Hernandez, E. In Vivo Characterization of Poly(Ethylene Glycol) Hydrogels with Thio-β Esters. *Ann. Biomed. Eng.* **2020**, *48*, 953–967.

(433) Lueckgen, A.; Garske, D. S.; Ellinghaus, A.; Desai, R. M.; Stafford, A. G.; Mooney, D. J.; Duda, G. N.; Cipitria, A. Hydrolytically-Degradable Click-Crosslinked Alginate Hydrogels. *Biomaterials* **2018**, *181*, 189–198.
(434) Kroger, S. M.; Hill, L.; Jain, E.; Stock, A.; Bracher, P. J.; He, F.; Zustiak, S. P. Design of Hydrolytically Degradable Polyethylene Glycol Crosslinkers for Facile Control of Hydrogel Degradation. *Macromol. Biosci.* **2020**, *20*, 2000085.
(435) Flory, P. J. *Principles of Polymer Chemistry*; Cornell University Press, 1953.
(436) Katashima, T.; Kagami, R.; Chung, U.; Sakai, T. Similarity in Linear Viscoelastic Behaviors of Network Formation and Degradation Processes. *J. Soc. Rheol., Jpn* **2020**, *48*, 191–198.
(437) Aisenbrey, E. A.; Bryant, S. J. A MMP7-Sensitive Photoclickable Biomimetic Hydrogel for MSC Encapsulation towards Engineering Human Cartilage. *J. Biomed. Mater. Res. A* **2018**, *106*, 2344–2355.
(438) Lutolf, M. P.; Hubbell, J. A. Synthesis and Physicochemical Characterization of End-Linked Poly(Ethylene Glycol)-Co-Peptide Hydrogels Formed by Michael-Type Addition. *Biomacromolecules* **2003**, *4*, 713–722.
(439) Rogan, H.; Ilagan, F.; Yang, F. Comparing Single Cell Versus Pellet Encapsulation of Mesenchymal Stem Cells in Three-Dimensional Hydrogels for Cartilage Regeneration. *Tissue Eng. Part A* **2019**, *25*, 1404–1412.
(440) Kim, M.; Erickson, I. E.; Huang, A. H.; Garrity, S. T.; Mauck, R. L.; Steinberg, D. R. Donor Variation and Optimization of Human Mesenchymal Stem Cell Chondrogenesis in Hyaluronic Acid. *Tissue Eng. Part A* **2018**, *24*, 1693–1703.
(441) Schneider, M. C.; Sridhar, S. L.; Vernerey, F. J.; Bryant, S. J. Spatiotemporal Neocartilage Growth in Matrix-Metalloproteinase-Sensitive Poly(Ethylene Glycol) Hydrogels under Dynamic Compressive Loading: An Experimental and Computational Approach. *J. Mater. Chem. B* **2020**, *8*, 2775–2791.
(442) Carles-Carner, M.; Saleh, L. S.; Bryant, S. J. The Effects of Hydroxyapatite Nanoparticles Embedded in a MMP-Sensitive Photoclickable PEG Hydrogel on Encapsulated MC3T3-E1 Pre-Osteoblasts. *Biomed. Mater.* **2018**, *13*, 045009.
(443) Stevens, K. R.; Miller, J. S.; Blakely, B. L.; Chen, C. S.; Bhatia, S. N. Degradable Hydrogels Derived from PEG-diacrylamide for Hepatic Tissue Engineering. *J. Biomed. Mater. Res.* **2015**, *103*, 3331–3338.
(444) Cannon, W. B. Organization for Physiological Homeostasis. *Physiol. Rev.* **1929**, *9*, 399–431.
(445) Roberts, J. J.; Nicodemus, G. D.; Greenwald, E. C.; Bryant, S. J. Degradation Improves Tissue Formation in (Un)Loaded Chondrocyte-Laden Hydrogels. *Clin. Orthop. Relat. Res.* **2011**, *469*, 2725–2734.
(446) Chu, S.; Maples, M. M.; Bryant, S. J. Cell Encapsulation Spatially Alters Crosslink Density of Poly(Ethylene Glycol) Hydrogels Formed from Free-Radical Polymerizations. *Acta. Biomater.* **2020**, *109*, 37–50.
(447) Chu, S.; Sridhar, S. L.; Akalp, U.; Skaalure, S. C.; Vernerey, F. J.; Bryant, S. J. Understanding the Spatiotemporal Degradation Behavior of Aggrecanase-Sensitive Poly(Ethylene Glycol) Hydrogels for Use in Cartilage Tissue Engineering. *Tissue Eng. Part A* **2017**, *23*, 795–810.

(448) Roberts, J. J.; Bryant, S. J. Comparison of Photopolymerizable Thiol-Ene PEG and Acrylate-Based PEG Hydrogels for Cartilage Development. *Biomaterials* **2013**, *34*, 9969–9979.
(449) Vernerey, F. J.; Bryant, S. The Role of Percolation in Hydrogel-Based Tissue Engineering and Bioprinting. *Curr. Opin. Biomed. Eng.* **2020.**
(450) Aharony, A. *Introduction to Percolation Theory : Second Edition*; Taylor & Francis, 2018.
(451) Skaalure, S. C.; Dimson, S. O.; Pennington, A. M.; Bryant, S. J. Semi-Interpenetrating Networks of Hyaluronic Acid in Degradable PEG Hydrogels for Cartilage Tissue Engineering. *Acta. Biomater.* **2014**, *10*, 3409–3920.
(452) Walker, C.; Mojares, E.; del Río Hernández, A. Role of Extracellular Matrix in Development and Cancer Progression. *Int. J. Mol. Sci.* **2018**, *19*, 3028.
(453) Poltavets, V.; Kochetkova, M.; Pitson, S. M.; Samuel, M. S. The Role of the Extracellular Matrix and Its Molecular and Cellular Regulators in Cancer Cell Plasticity. *Front. Oncol.* **2018**, *8*, 431.

Table of Contents (TOC) graphic